



TAMPEREEN TEKNILLINEN YLIOPISTO  
TAMPERE UNIVERSITY OF TECHNOLOGY

Fikret Emre Kapucu

**Methods to Enhance Information Extraction from  
Microelectrode Array Measurements of Neuronal  
Networks**



Julkaisu 1438 • Publication 1438

Tampere 2016

Tampereen teknillinen yliopisto. Julkaisu 1438  
Tampere University of Technology. Publication 1438

Fikret Emre Kapucu

## **Methods to Enhance Information Extraction from Microelectrode Array Measurements of Neuronal Networks**

Thesis for the degree of Doctor of Science in Technology to be presented with due permission for public examination and criticism in Sähköotalo Building, Auditorium S3, at Tampere University of Technology, on the 30<sup>th</sup> of November 2016, at 12 noon.

Tampereen teknillinen yliopisto - Tampere University of Technology  
Tampere 2016

ISBN 978-952-15-3857-5 (printed)  
ISBN 978-952-15-3862-9 (PDF)  
ISSN 1459-2045

## Abstract

For the last couple of decades, hand-in-hand progresses in stem-cell technologies and culturing neuronal cells together with advances in microelectrode array (MEA) technology have enabled more efficient biological models. Thus, understanding the neuronal behavior in general or realizing some particular disease model by studying neuronal responses to pharmacological or neurotoxic assays has become more achievable.

Moreover, with the widespread practical usage of MEA technology, a vast amount of new types of data has been collected to be analyzed. Conventionally, MEA data from neuronal networks have been analyzed, e.g., with the methods using predefined parameters and suitable for analyzing only specific neuronal behaviors or by considering only a portion of the data such as extracted extracellular action potentials (EAPs). Therefore, in addition to the current analysis methods, novel methods and newly acquired measures are needed to understand the new models. In fact, we hypothesized that existing measurement data carry a lot more information than is considered at present. In this thesis, we proposed novel methods and measures to increase the information which we can extract from MEA recordings; thus, we hope these to contribute to better understanding of neuronal behaviors and interactions.

Firstly, to analyze firing properties of neuronal ensembles, we developed a method which identifies bursts based on spiking behavior of recordings; thus, the method is feasible for the cultures with variable firing dynamics. The developed method was also designed to process a large amount of data automatically for statistical justification. Therefore, we increased the analysis power in the subsequent analyses in comparison to the existing burst detection methods which are using pre-defined and strict definitions.

Subsequently, we proposed novel metrics to evaluate and quantify the information content of the bursts. Entropy-based measures were employed for quantifying bursts according to their self-similarity and spectral uniformity. We showed that different types of bursts can be distinguished using entropy-based measures. Also, the joint analysis of bursts and action potential waveforms were proposed to obtain a novel type of information, i.e., spike type compositions of bursts. We presented that the spike type compositions of bursts would change under different pharmacological applications.

In addition, we developed a novel method to calculate synchronization between neuronal ensembles by evaluating their time variant spectral distributions: For

that, we assessed correlations of the spectral entropy (CorSE). We showed that CorSE was able to estimate synchronicity by studying both local field potentials (LFPs) and extracellular action potentials (EAPs); thus, we could contribute to understanding synchronicity between neuronal ensembles which also don't exhibit detectable EAPs.

In conclusion, motivated by the recent popularity of MEA usage in the neuroscience field, we developed novel and enhanced methods to derive new types of information. We showed that by using our developed methods one could extract additional information from MEA recordings. As a result, the proposed methods and metrics would enhance the analysis efficiency of the microelectrode array measurement based studies and provide different viewpoints for the analyses. The derived novel information would contribute to interpreting neuronal signals recorded from a single or multiple recording locations. Consequently, methods presented in this thesis are important complements to the existing methods to understand neuronal behavior and population-wise neuronal interactions.

## Preface

The research presented in this thesis has been carried out during 2010 to 2016 at the former Department of Biomedical Engineering, and Department of Electronics and Communication Engineering, BioMediTech, Tampere University of Technology, Tampere, Finland.

Firstly, I would like to express my gratitude to my supervisor, Prof. Jari Hyttinen, for his support and guidance throughout my research. I would like to especially thank my co-supervisor and office-mate, Dr. Jarno Tanskanen, for his guidance, support and invaluable discussions during my entire research and for his friendship at work. I sincerely thank Dr. Jarno Mikkonen for his collaboration, fruitful discussions and his kind hosting during our visits to University of Jyväskylä.

I owe special thanks to the reviewers Docent Markku Penttonen and Dr. Günther Zeck for their careful examination and constructive reviews of my thesis.

I would like to thank my former and current colleagues and staff from the former Ragnar Granit Institute, Department of Biomedical Engineering, and Department of Electronics and Communication Engineering, Dr. Baran Aydoğan, Dr. Alper Cömert, Markus Hannula, Nathaniel Narra Girish and Dr. Narayan Subramaniam for the friendly working atmosphere and for joyful coffee break discussions. I am especially thankful to Inkeri Välikki for her contributions to my research and sharing the toughness of trying and learning new things in cell culturing laboratory. I also sincerely thank Julia Johansson for her assistance in cell culturing and usage of laboratory equipment. I am grateful to the former Ragnar Granit Institute members for their collaboration and contributions to my research. For the same, I would particularly would like to thank Docent Susanna Narkilahti, the head of Neuro Group, BioMediTech, and her group members Dr. Laura Ylä-Outinen and Meeri Mäkinen.

I would like to express my special thanks to Soile Lönnqvist and Tuija Grek for helping me on all the practical issues during my research.

The works in this thesis were supported by the 3DNeuroN project in the European Unions Seventh Framework Programme, Future and Emerging Technologies, grant agreement no. 296590; by the Academy of Finland under the project Bio-integrated Software Development for Adaptive Sensor Networks, project number 278882; and by the Human Spare Parts Project funded by TekesThe Finnish Funding Agency for Innovation. I am deeply grateful to Finnish Cultural Foundation, and Ella and Georg Ehrnrooth Foundation for the personal grants supporting my research. Additionally, I would like to thank Dr. Francois Christophe and Prof. Tommi

Mikkonen for giving me the opportunity to work together with them for the project Bio-integrated Software Development for Adaptive Sensor Networks and opening new viewpoints in my research.

I warmly thank all my friends, especially my friends in Tampere from Turkey for being around and being part of my life in Finland.

I cannot express my gratitude to my family, my father Fuat, my mother Cemile, my brother Utku, my sister-in-law Hare and my niece Deniz for all their unconditional support and existence in my life.

Finally, I thank to my dear wife, Talvi for being the color and meaning of my life and my daughter, Ilta for making me forget every other challenge in my life with her wonderful existence. Nothing would be important without your love.

Fikret Emre Kapucu  
Tampere, 18 October 2016



## LIST OF PUBLICATIONS

This thesis is written based on the following five original publications of the author. Publications are referred to as “Publication X” in the text, where X is the number of the publication. All publications are printed with permission from the publishers.

**Publication I:** F. E. Kapucu, J. M. Tanskanen, J. E. Mikkonen, L. Ylä-Outinen, S. Narkilahti, and J. A. Hyttinen. Burst analysis tool for developing neuronal networks exhibiting highly varying action potential dynamics. *Frontiers in Computational Neuroscience*, 6:38, 2012.

**Publication II:** F. E. Kapucu, J. E. Mikkonen, J. M. Tanskanen, and J. A. Hyttinen. Quantification and automatized adaptive detection of in vivo and in vitro neuronal bursts based on signal complexity. In *Proceedings of the 37th Annual International Conference of the IEEE Engineering in Medicine and Biology Society (EMBC), Milan, Aug. 2015.*, pp. 4729-4732. IEEE, 2015.

**Publication III:** F. E. Kapucu, M. E.- L. Mäkinen , J. M. Tanskanen, L. Ylä-Outinen, S. Narkilahti, and J. A. Hyttinen. Joint analysis of extracellular spike waveforms and neuronal network bursts. *Journal of Neuroscience Methods*, 259:143-155, 2016.

**Publication IV:** , F. E. Kapucu, J. E. Mikkonen, J. M. Tanskanen, and J. A. Hyttinen. Analyzing the feasibility of time correlated spectral entropy for the assessment of neuronal synchrony, In *Proceedings of the 38th Annual International Conference of the IEEE Engineering in Medicine and Biology Society (EMBC), Orlando(FL), Aug. 2016.*, pp. 1595-1598. IEEE, 2016.

**Publication V:** F. E. Kapucu, I. Vornanen, J. E. Mikkonen, C. Leone, K. Lenk, J. M. A. Tanskanen, and J. A. K. Hyttinen. Spectral entropy based neuronal network synchronization analysis based on microelectrode array measurements, *Frontiers in Computational Neuroscience*, 10:112, 2016.

## AUTHOR'S CONTRIBUTIONS

The author's contributions to each article are as follows:

**Publication I:** The author developed the algorithm, implemented codes, and analyzed data in Matlab. All the figures in the publication were produced and the manuscript was written by the author.

**Publication II:** The author implemented codes for computing the spectral and sample entropy, employed his own developed automatic burst detection algorithm, and analyzed the data. The manuscript was mainly written by the author.

**Publication III:** The author developed the joint analysis tool and implemented codes. Pharmacological experiments obtained by co-authors and suitable data were selected by the author. The figures in the publication were mainly produced and manuscript was mostly written by the author.

**Publication IV:** The author developed the proposed algorithm, implemented the codes, and tested the method in Matlab. The manuscript was written mainly by the author.

**Publication V:** The author developed the proposed algorithm, implemented the codes, made toy model simulations, and analyzed the data. The author took active part in mouse cortical cell culturing and MEA recordings. The manuscript was written and figures were produced mainly by the author.



<b>List of Publications</b>	<b>i</b>
<b>Author's Contributions</b>	<b>iii</b>
<b>Glossary</b>	<b>vii</b>
<b>1 Introduction</b>	<b>1</b>
<b>2 Background</b>	<b>7</b>
2.1 Bioelectric activity and neuronal electrophysiology . . . . .	7
2.2 MEA recordings . . . . .	9
2.2.1 Recorded signal . . . . .	11
2.3 MEA signal analysis . . . . .	14
2.3.1 Analyses based on spike information . . . . .	15
2.3.2 Analyses based on complete electrophysiological recordings .	20
<b>3 Materials and methods</b>	<b>23</b>
3.1 Neuronal cultures and the experiments performed . . . . .	23
3.1.1 Stem cell-derived neurons . . . . .	24
3.1.2 Rat and mouse cortical neurons . . . . .	25
3.1.3 Rat hippocampus . . . . .	26
3.2 Microelectrode array recordings . . . . .	26
3.3 Simulations . . . . .	27
3.4 Signal analysis methods . . . . .	28
3.4.1 Methods employed for evaluating spiking behavior . . . . .	29

3.4.2	Methods developed for evaluating spiking behavior . . . . .	30
3.4.3	Methods employed for evaluating the information content of neuronal bursts . . . . .	34
3.4.4	Employed neuronal network analysis methods . . . . .	37
3.4.5	Developed entropy-based neuronal network analysis method .	39
<b>4</b>	<b>Results</b>	<b>41</b>
4.1	Adaptive burst detection . . . . .	41
4.2	Spike behavior and information content during bursts . . . . .	45
4.3	Spectral entropy-based synchrony analysis . . . . .	51
<b>5</b>	<b>Discussions</b>	<b>59</b>
<b>6</b>	<b>Conclusions</b>	<b>67</b>
	<b>References</b>	<b>69</b>
	<b>Original Publications</b>	<b>81</b>

### Abbreviations in text

AP	action potential
CA1	cornu ammonis region 1
CA3	cornu ammonis region 3
cES	corrected event synchrony
CMA	cumulative moving average
CorSE	correlated spectral entropy
DG	dentate gyrus
DIV	days <i>in vitro</i>
EAP	extracellular action potential
ES	event synchrony
eSTD	spike detection based on estimated background noise
FFT	fast Fourier transform
HDMEA	high density microelectrode array
hESC	human embryonic stem cells
IAP	intracellular action potential
IQR	interquartile range
ISI	inter-spike interval
LFP	local field potential
logISIH	logarithmic inter-spike interval histogram
MEA	microelectrode array

MI	mutual information
PGC	partial Granger causality
SE	spectral entropy
SmpE	sample entropy
SNR	signal-to-noise ratio
STD	spike detection based on standard deviation
TE	transfer entropy
WGN	white Gaussian noise

## Mathematical abbreviations and symbols

$\alpha_1$	factor for burst spikes
$\alpha_2$	factor for burst-related spikes
$\oslash$	diameter
<i>CH</i>	cumulative histogram
<i>CMA</i>	cumulative moving average
<i>CorSE</i>	correlated spectral entropy
<i>H</i>	Shannon entropy
<i>MI</i>	mutual information
<i>Q</i>	event synchrony
<i>S</i>	spectral entropy
$S_{\text{norm}}$	normalized spectral entropy
<i>SmpE</i>	sample entropy
<i>TE</i>	transfer entropy

# CHAPTER 1

## INTRODUCTION

Neuroscience has been searching for answers to the functioning of neurons and neuronal systems for decades. While technology is advancing, new methods arise to gather new types of information on neuronal functioning, and consequently more opportunities arise to understand and treat neurological diseases. On the other hand, the amount of knowledge gathered so far is not adequate for solving major problems of neuroscience yet. Despite the large amount of collected data, the information obtained is still limited since reasonable amount of information in the measurement data is not completely revealed. This has actually been stated as one of the seven challenges by Markram (2013) as the necessity of increasing the information which we can extract from experiments. Hypothetically, measurement data carry a lot more information than we are obtaining with current methods. Such information, which potentially exists in the currently attainable data, would be essential, e.g., for answering important problems of neuroscience or finding cures for currently untreatable diseases.

In fact, despite the technological advances, neurodegenerative diseases are regarded as the silent epidemic of the 21st century. Stroke and heart diseases have been the top two largest causes of death, and stroke alone is the leading cause of long-term disability in the world according to the World Health Organization (The top 10 causes of death, World Health Organization fact sheet no:310, WHO). Traumatic events such as spinal cord injuries and brain insults affect especially the population of young adults, leading to drastic disabilities, and need long-term rehabilitation and use of various health care services, including lifelong institutional

accommodation. Also, neurological disorders, such as epilepsy, affect millions of people and increase the risk of death (Vos et al., 2015). Currently, novel stem cell technologies provide hope that repairing damaged neuronal tissues due to accidents and many diseases might become a reality in the near future. However, understanding neuronal systems and behavior is crucial in the search for treatment of neurodegenerative diseases.

Together with the biological advances, cultured neuronal cells are very effective to use as a model for studying the central nervous system, in particular the brain. Such biological models provide a more flexible environment for the applications used in, e.g., drug discovery, personalized medicine, and developing functional organs. Besides, recent developments in microelectrode array (MEA) technology enable studying the electrophysiological properties of neuronal cells, including the characteristics of their connections and interaction with each other from early stages of their development. Thus, current developments in MEA technology with the widespread practical usage in studying developing neuronal cell cultures produced new types of data which we could not obtain previously. In fact, recent MEA systems provide alternative ways to collect data at different spatial resolutions and thus provide a new type of data, potentially carrying information on population and cellular interactions (Obien et al., 2014). The acquired neuroelectrophysiological information from cultures with highly plastic neuronal networks demands novel methods, and using MEAs could enhance the interpretation and understanding of neuronal behavior. With the increasing growth of using MEAs and studies on developing neuronal cells, newer research questions are elevated.

In summary, there is a call to extract new information for studying developing neuronal cell cultures, and in this thesis we propose novel tools and novel metrics for such analysis. Accordingly, the main motivation of this thesis work can be summarized as:

- Deriving new metrics by developing novel methods: Developing new methods to acquire new metrics for analyzing the activity of neuronal cells and developing novel methods to understand the functionality of the cells and cell networks.
- Obtaining novel information by using existing methods: Using new ways to employ methods which were previously practiced in neuroscience or other disciplines to gather novel information from neuronal cell cultures.

The thesis aims to find specific solutions for some existing research questions

in this area. The contributions of the thesis to these research questions can be grouped under three categories:

1. Identification of action potential (AP), i.e., spike, firing properties from new culturing paradigms such as networks developed from stem cell based neurons.

*Research question:* APs have been widely studied by means of their waveforms and firing characteristics, where different definitions of AP bursts were also made (Legendy and Salcman, 1985; Chiappalone et al., 2005; Mazzoni et al., 2007; Pasquale et al., 2010). However, the existing definitions of bursts are not well suited for the new type of data obtained from highly variable developing neuronal cultures. Previously, a large amount of spike data from, e.g., stem cell derived neuronal networks would be considered as data without any bursts and removed from further analysis by existing algorithms. *How would we define and assess burst activity for highly variable neuronal networks without using any predefined criteria?* Moreover, although the effects of the overall spike activity on network bursting have been studied previously (Harris et al., 2001), the potential relations between AP waveforms and their participation to burst activity, i.e. network activity, have not been studied sufficiently. *Can we obtain novel information by analyzing spike type compositions of bursts?*

*Aims of the thesis to contribute to the research question:*

- We aim to develop a method to detect bursts by utilizing the dynamics of the studied signal, so that bursts which are not detected previously can be analyzed. The burst detection method also needs to operate with minimal user intervention to increase objectivity. Thus, an automatic algorithm which enables the analysis of large data for statistical justification is preferable (Publication I).
- We aim to develop a method to study single unit and network activity simultaneously by means of spike waveforms and bursts. Consequently, we would reveal any potential relations between AP waveforms and their participation in network activity (Publication III).

*Biological applications:* Hypothetically, detecting bursts based on the dynamics of the studied signal instead of pre-defined criteria would enable electrophysiological characterization of developing neuronal cultures. For such cultures, because of the variability in the spike firing dynamics, an adaptive

and automatic analysis process is required to minimize user intervention and increase time efficiency. Thus, by utilizing an adaptive burst detection algorithm, bursts with different metrics or different spike type compositions can be classified, for example, for the assessment of neuronal response to the pharmacological or neurotoxicological experiments, as in Johnstone et al. (2010), as well as for tracking network development, as in Wagenaar et al. (2006).

2. Investigation of population activity and neuronal interactions in developing neuronal networks.

*Research question:* Population activity of neurons has been intensively studied in the literature. Bursts are one of the most commonly used markers for network activity (Kandel and Spencer, 1961; Connors et al., 1982; Wagenaar et al., 2006) and are also utilized for the assessment of neuronal responses. Parameters calculated from bursts are commonly used as features for classifying them (Johnstone et al., 2010; Mack et al., 2014). For example, according to Johnstone et al. (2010), different drugs have specific affects on different burst parameters but not on all. Thus, hypothetically, parameters/metrics to quantify/classify bursts based on new type of information in addition to the conventionally used ones would enrich the information and are highly required (Johnstone et al., 2010). *Would information theory based metrics be beneficial to quantify and classify bursts?*

*Aims of the thesis to contribute to the research question:*

- We aim to quantify detected neuronal bursts by using their information content (Publication II).

*Biological applications:* We hypothesize that metrics based on the information theory would reveal additional features of the bursts; accordingly, providing additional features would enhance the efficiency of burst classification. Such enhancement would have potential advantages in practical fields where the response of neuronal networks is commonly assessed by the changes in burst activity, e.g., neurotoxicology studies.

3. Analysis of the synchronous network activity in developing cultures.

*Research question:* Synchronicity has been studied for neuronal populations to analyze simultaneous network activity. Generally, neuronal events such as APs and bursts have been assessed for calculating network synchrony

(Quiroga et al., 2002; Garofalo et al., 2009; Ito et al., 2011), or alternatively phase or frequency coupling in some specific frequency bands have been analyzed (Ginter Jr et al., 2005). Local field potentials (LFPs) in the recordings are totally omitted by event-based synchrony measures, and performances of event detection methods have crucial influence on sequential analysis procedures (Obien et al., 2014). There is a call for methods which calculate network synchrony by taking LFPs also into consideration and depending less on the performances of event detection methods. *How could we analyze network synchrony by taking EAPs and LFPs into account for the neuronal networks whose effective bandwidths were not well defined?*

*Aims of the thesis to contribute to the research question:*

- We aim to develop an algorithm to estimate network synchrony which depends less on the performances of event detection methods and takes LFPs also into consideration (Publication IV and V).

*Biological applications:* Changes in the synchronization and accordingly functional connectivity are assessed to obtain information on neuronal plasticity. Also external manipulations or spontaneous developments of neuronal networks need to be assessed without omitting the large amount of LFP data, which is currently usually considered as biological noise. Thus, for such studies, methods considering also LFPs would be beneficial.

In conclusion, we are inspired by the recent calls in neuroscience with the increased usage of MEA technologies in the field. Hence, we developed novel and enhanced data analysis methods to extract the new information hypothetically carried by the existing data. We applied the new methods on various types of *in vivo* and *in vitro* neuronal cell cultures, which were obtained with MEA recordings, and ended up successfully gaining the hypothesized information.



In this chapter, the basics of neuronal electrophysiology are explained to provide background information on the data which was studied in this thesis. Next, we summarize how MEA technology is being used currently, what kind of potential information MEA data contain, and what are the sources influencing the recorded data. Finally, commonly used data analysis procedures for MEA recordings are presented with the required enhancements or novelties to make these methods produce more information and also more feasible for the analysis of developing neuronal cultures.

## 2.1 Bioelectric activity and neuronal electrophysiology

Neurons are electrically active also at rest, where there is a potential difference between the intracellular and extracellular medium originated from different concentrations of ions. In a resting state, the inside of the neuron is negative relative to the outside, and this causes a voltage difference called *transmembrane potential* which is around  $-65$  mV. The most evident activity of a neuronal cell, i.e., AP, occurs when the transmembrane potential reaches a threshold. This process can be initiated with the arrival of a stimulus to the cell: a stimulus is first received by the dendrites of a nerve cell. This causes the  $Na^+$  channels to open;  $Na^+$  influx drives the interior of the cell membrane, making the inside of the cell more positive. Because of this change, the  $K^+$  ions are pushed out through the non-gated

$K^+$  ion channels, which are much slower to open. With the  $K^+$  channels open, the membrane begins to repolarize first back to its resting potential and later to hyperpolarization. After hyperpolarization, active  $Na^+/K^+$  pumps bring the membrane back to its resting state once more (Hall and Guyton, 2011). This whole process is reflected as an AP waveform to the electrophysiological recording.

Neuronal electrophysiology includes different techniques for measuring electrical activity of neurons, and the measured information varies depending on the location and the characteristics of the measurement electrode. For example, if the above mentioned process is measured extracellularly, i.e., extracellular AP (EAP), then initially in the waveform there will be a large decay on the negative side followed by a small positive peak, unlike in intracellular AP (IAP) (Henze et al., 2000). In this thesis work, we merely concentrated on mesoscale extracellular measurements which will be discussed later.

EAPs are generally tens to hundreds of microvolts in amplitude and less than 2 ms in duration (Buzsáki et al., 2012). EAPs, which are also referred to as “spikes” in this work, can be identified when the source is in the vicinity of the electrodes (up to  $\approx 100\mu m$  according to Egert et al. (2002) and up to  $\approx 140\mu m$  according to Henze et al. (2000)). AP polarities are also affected by the electrode positions; according to Egert et al. (2002), electrodes close to the somatic area have a better chance for spike detection, and spikes are negative in polarity close to the soma and positive in the dendritic tree. Gold et al. (2006) also proposed that varied composition of ionic currents in different cells can alter the features of the EAP.

Electrode size also influences the electrical data measured. If the electrode is small enough and located close enough to a single cell, it would enable recording of APs from a single cell (single-unit recording) (Humphrey and Schmidt, 1990) or, depending on the placement, it may record the spike activity of several nearby cells simultaneously (multi-unit recording). On the other hand, with the increase of electrode size, the amplitudes of APs are averaged with smaller amplitude signals originating from nearby sources since larger electrodes collect the net activity of several cells which are observed as local field potentials (LFPs). LFPs are more challenging than APs to interpret (Einevoll et al., 2013), where any biological structure with an excitable cell membrane, i.e., spine, dendrite, soma, axon, or axon terminal and any sort of transmembrane current has contributions on the extracellular field. Briefly, the main contributions on the extracellular field are summarized in Buzsáki et al. (2012) as synaptic activities, fast action potentials, calcium spikes, intrinsic currents, hyperpolarizations after spikes, gap junctions, neuron-glia interactions, and ephaptic effects. Particularly APs, although they are

not always detectable extracellularly, have important implications on LFPs.

Several studies, which are extensively reviewed in Buzsáki et al. (2012), address interrelations between the spike activity and frequency relations of LFPs: Briefly, increased spiking produces a broad frequency spectrum in LFPs. Increased power in the higher frequency bands (over 100 Hz) is associated with an increased and synchronized spike firing. The power in high frequency components of LFPs increases with spatially dense cell bodies, and their effective area is limited to shorter distances. LFP components other than spike-related membrane voltage fluctuations, i.e., postsynaptic potentials and membrane voltage fluctuations, have influence on high frequency power as well. There can be phase lock between high and low frequency components where phase locked neurons generate mostly extracellular rhythmic currents, and the high frequency power of LFPs has indirect influence on firing of neurons.

In conclusion, the bioelectric activity of neuronal cells is the main target for information gathering in MEA measurements. Biological signals in the vicinity of a recording electrode are the most essential component forming EAPs and LFPs; however, a notable amount of background signals from further biological sources is contributed to LFPs as well. For example, signals originating from, e.g., EAPs of distant cells, ionic sub-threshold activity of nearby cells, or neurites contribute to LFPs but are generally accepted as biological noise since it is challenging to interpret most of these signals (Obien et al., 2014). Thus, it is crucial to know the abilities and limitations of the measurement setup and the equipment before further analysis is done to be able to interpret accurately what is recorded by MEAs and also to avoid losing information as much as possible.

## 2.2 MEA recordings

The first works with MEAs were introduced starting from the early 1970s by Thomas et al. (1972), Wise and Angell (1975), Gross et al. (1977), and Pine (1980); however, developments in information technology, microelectronics, and material sciences gave a boost to MEA development and consequently to MEA-based studies starting from the second half of the 1990s. MEAs are basically designed for recording mesoscale extracellular electrophysiology, which consists of LFPs and EAPs (Obien et al., 2014). During the time, MEAs have been developed to answer the needs of *in vivo* and *in vitro* studies; and they have been designed accordingly.

For *in vivo* studies, implantable MEAs have been fabricated by using three common techniques: microwires, micro-machined arrays, and flexible arrays (Cheung,

2007; Ghane-Motlagh et al., 2013). Briefly, microwires are advantageous for deep brain recordings. They were mainly designed to focus on individual neurons, but an array of microwires allows multi-neural recordings as well. On the other hand, accurate location of the electrode tips relative to each other is challenging because of the bending of the wires during implantation (Ghane-Motlagh et al., 2013). Silicon based micro-machined MEAs come in two specific models: silicon-based multi-shaft arrays, i.e., Michigan arrays (Fig. 2.1A), and silicon-based multi-needle arrays, i.e., Utah arrays (Fig. 2.1B). Michigan arrays allow recording from multiple depths along the shaft and to keep the distance between electrodes fixed, which makes them advantageous compared to microwires. Utah arrays have silicon needles isolated from each other, where the recording is obtained from the tips of these needles (Ghane-Motlagh et al., 2013). Utah arrays are mostly designed to be implanted in cerebral cortex or peripheral nerves (Normann, 2007). Flexible arrays allow electrodes to be placed on the surface of the brain in a less invasive way, which also reduces chronic tissue inflammation. On the other hand, their flexible structure may cause difficulties during implantation (Ghane-Motlagh et al., 2013).

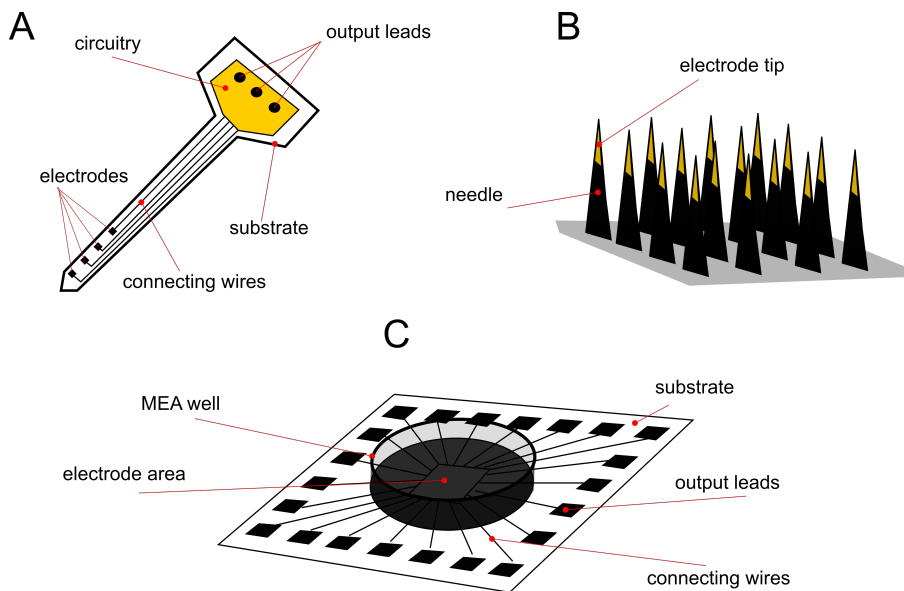


**Figure 2.1:** Simplified illustrations of some commonly used MEA designs for *in vivo* and *in vitro* recordings. MEA components are not in scale, and the numbers of electrodes are for illustration only. (A) Michigan and (B) Utah arrays for *in vivo* recordings. (C) Planar MEA in a well for *in vitro* recordings.

For *in vitro* studies, MEAs can be used for example for tissue slices or dissociated cell cultures (Fig. 2.1C). Planar MEAs have been commonly used to record

neuronal activity extracellularly. MEAs with electrode diameter of 10 to 30  $\mu m$  and an inter-electrode distance of 100 to 500  $\mu m$  have been found beneficial for studying local neuronal activity and population interactions (Obien et al., 2014). There are also different designs to improve the electrode-tissue contact with perforation. For such MEAs, tissue slices are pulled by negative pressure applied through the openings in the substrate to position the slice on the electrodes and improve signal quality, as in Gonzalez-Sulser et al. (2012). Recently, ultra-small electrodes in nanometer scale are also being used to record intracellular activity, including subthreshold signals by penetrating the cell membrane (cf. Spira and Hai (2013)). These electrodes can be structured as three-dimensional silicon nanowires (Robinson et al., 2013) or gold mushrooms (Hai et al., 2009). Another important development is the number of electrodes and their spatial distribution on MEAs. Initially, the number of electrodes on MEAs was limited to tens, and the distances between electrodes were tens of micrometers. Later, advances in field effect transistor and particularly complementary metal oxide semiconductor-based active electrodes also initiated the development of high density MEAs (HDMEAs) (Berdondini et al., 2001), which enabled the assessment of neuronal activity at sub-cellular resolutions. Currently, thousands of electrodes are on HDMEAs, and the distances between electrodes are less than 20 $\mu m$ . Together with MEA technology, *in vitro* studies provide a better access compared to *in vivo* models in terms of electrical stimulation and pharmacological or neurotoxicological manipulation (Wagenaar et al., 2006). Moreover, engaging MEAs with *in vitro* cultures enable studying the fundamental features of network activities, e.g., plasticity, learning, pharmacological testing, and models of epilepsy.

### 2.2.1 Recorded signal

Biological signals are the main target of MEA recordings. However, signals recorded by MEAs have contributions from different sources other than the biological ones as well. Starting from neurons and until the recording device, several parameters have an effect on the observed signal (Obien et al., 2014). Fig. 2.2 illustrates this process.

#### Effects of source and extracellular medium

Extracellular medium is generally assumed as resistive (ohmic), homogeneous and isotropic for simple models. A signal recorded at one point is basically the linear sum of the current sources which are inversely weighted with the distance between

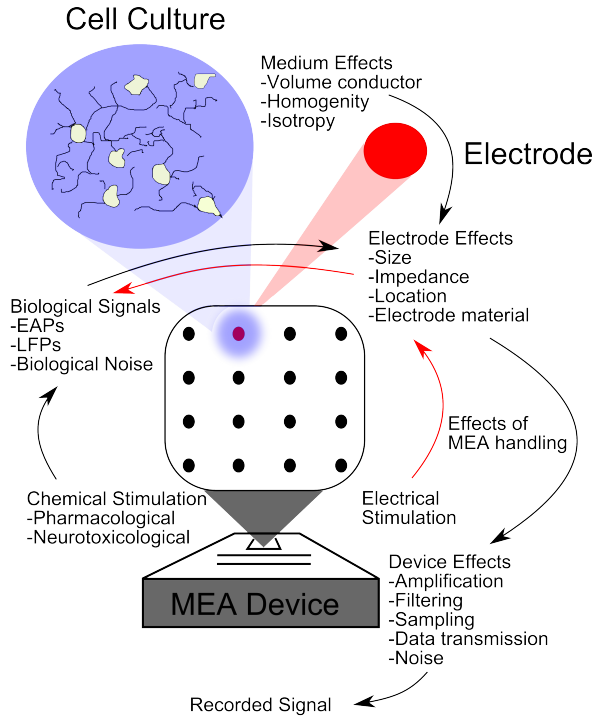


**Figure 2.2:** Parameters affecting the signal recorded with MEAs

the recording point and the source locations (Nicholson and Freeman, 1975). Consequently, signs, shapes, and amplitudes are strongly dependent on the electrode and the source positions (Einevoll et al., 2013). The following equation gives a single point current source for the potential at an electrode,  $V_e$ , and thus explains the importance of electrode distance to the source.

$$V_e = \frac{I}{4\pi\sigma r}, \quad (2.1)$$

where  $I$  is the current,  $\sigma$  is the conductivity of the medium, and  $r$  is the distance between the recording point and the source point. The equation can be written as a volume integration of all transmembrane currents,

$$V(r_e) = \frac{1}{4\pi\sigma} \iiint_V \frac{c_r}{|r_e - r_0|} d^3r. \quad (2.2)$$

Here,  $r_e$  and  $r_0$  are the positions of the electrode and the source respectively,  $c_r$  is the current source density, and the triple integral states volume integration of all transmembrane currents (Nicholson and Freeman, 1975). Consequently, the

equation explains the importance of the size of the electrode on the measured signal. The averaging effect can easily be read from (2.2) for large electrodes.

Another effect of the extracellular space is the widely observed frequency-dependent filtering which causes low-pass filtering of EAPs. Low-pass filtering occurs not only in a non-homogeneous medium, i.e., a medium consisting of compositions of a complex aggregate of fluids and the existence of different cell bodies, but also in a purely ohmic and homogeneous medium. Spatial separation of correlated current sources and ionic diffusions cause such low-pass filtering effects (Pettersen and Einevoll, 2008).

### **Effects of electrode size and impedance**

Beside the electrode positions and distances to the source, electrode size and impedance have critical influence on the recorded signals as well. For the electrodes, (2.2) should be solved for the multiple locations on the electrode surface and should be averaged. Although larger electrodes have larger averaging effects, they have lower impedance, which improves the signal-to-noise ratio, and larger effective area to detect signals. On the other hand, even though the smaller electrodes have higher electrode noise, with the recent developments of HDMEA technology and with active electrodes it is possible to record the desired information with a high spatial resolution and with smaller effective electrode capacitance, which reduces the attenuation of the signal (Obien et al., 2014).

The size of the MEAs used in this thesis are suitable for recording single-unit activity, multi-unit activity and LFPs; however, the averaging effect as well as overlapping spike activity was observed on the analyzed recordings. Such a measurement system is not as feasible as HDMEAs for the analysis of single neurons and their interactions (cf. Franke et al. (2012)). On the other hand, the recorded signal includes information on local population activity, which enables us to analyze local networks, i.e., sub-populations and interrelations of these sub-populations whether they are parts of a bigger neuronal network or not.

### **Effects of device hardware and settings**

Other effects from the device hardware which includes an amplifier, filters, AC/DC converters, and data transmission have also direct influence on the recorded signal, which should be taken into account while designing the measurement and analysis setups (cf. Obien et al. (2014)).

## 2.3 MEA signal analysis

Generally, according to the desired information from the analyzed biological sources, the experimental setup is designed and recordings are obtained. Consequently, during the signal analysis of the recorded data, analysis procedures are also selected depending on the desired information, i.e., the objective of the study. Fig. 2.3 summarizes the analysis procedures and resulting information based on data collected with MEA recordings particular to this thesis. Only the methods related to the work done in the thesis are described in this section.

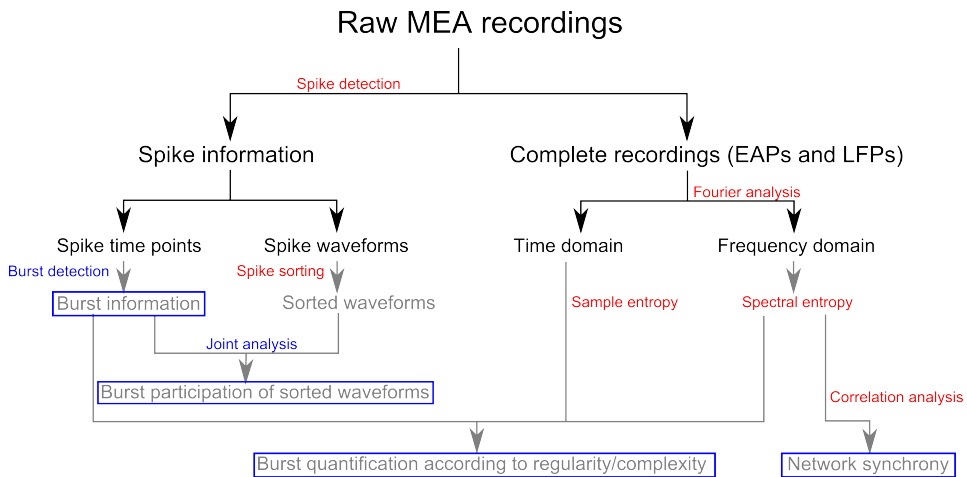


**Figure 2.3:** Analysis procedures and resulting information based on acquired data from MEA recordings. Labels written in red are the employed analysis methods and blue are the developed analysis methods in this thesis. Text written in gray indicates the resulting information, whereas the gray text in blue boxes denotes enhanced or new types of information.

Typically, initial data obtained from MEA recordings are analyzed either by extracting EAPs from the raw recordings to obtain spike information (spike time points and spike waveform cutouts) or with complete electrophysiological signal which includes EAPs and LFPs together. Analyses which are described in this thesis are practiced on both spike information and complete electrophysiological signal. In the following sections, the general practices and outcomes for both types of data are explained with the applications in the literature as well as with the required developments and novelties to the current analysis procedures.

### 2.3.1 Analyses based on spike information

Assessment of signals from neuronal recordings based on spike firing information is very common in neuronal studies. Spike firing behavior reflects the activity of neuronal cells by means of EAPs, and for such analysis spike time points should be obtained initially. To obtain merely spike information, i.e., spike time points and spike waveforms, EAPs should be separated from background signal. LFPs are considered as biological noise for this procedure (Obien et al., 2014). This particular step is called spike detection.

#### Spike Detection

Spike detection may be applied on raw or filtered signals. Even though the bounds between the unit activity (300–6000 Hz) and the LFP ( $< 600$  Hz) are not set clearly (Gibson et al., 2012), filtering, e.g., with a bandpass filter of 300–3000 Hz, is adequate to sufficiently attenuate LFP components of the signal (Quiroga et al., 2004).

Amplitude thresholding is the most common spike detection method, since it is very simple and computationally efficient; however, several different spike detection methods are also used. Amplitude thresholding is usually applied at a multiple of noise level, e.g., 5 times of the baseline noise level, calculated as root mean square of the zero-mean signal, i.e., standard deviation (herein, STD) or multiple of an estimated background noise (herein, eSTD). Median is also used instead of mean to eliminate outliers (Quiroga et al., 2004). Tanskanen et al. (2015) also proposed an objective method for selecting the threshold by using amplitude histograms. Other proposed spike detection methods utilize template matching (Kim and McNames, 2007), for example, or define some parameters for spikes, such as the duration of spikes and the interval between two spikes, for more precise detection (Maccione et al., 2009). On-line and off-line usability is an important factor for some studies, whereas it was not taken into account as an important criterion for the studies in this thesis. We worked on both on-line and off-line detected spikes.

Since spike detection is the first and foremost step of any EAP-based analysis, the spike detection accuracy has critical influence on further analysis and thus on the quality of the research. The differences resulting from different spike detection algorithms are expected to change the results of the subsequent analyses. Thus, analyses which critically depend on accurate spike detection, such as network synchrony assessment, should either take the quality of the spike detection into account or not depend solely on the detection of spikes. Spike detection results in two main

outcomes for additional analysis: spike time points and spike cutouts, i.e., spike waveforms.

### **Spike activity: Information and analysis methods based on spike time points**

Spike activity is generally observed by means of spike time series, i.e., spike time points. Spike time points are commonly used to assess the firing characteristics of single cells or networks by deriving metrics such as inter-spike intervals (ISIs), firing rate, firing behaviors (e.g., spike bursts, spike trains) (Johnstone et al., 2010; Novellino et al., 2011; Uchida et al., 2012) or to assess network relations by means of causal relations or synchrony (Wagenaar et al., 2006; Garofalo et al., 2009; Maccione et al., 2012).

Different neuronal behaviors based on spike firing frequencies have been observed very early in the field (Connors et al., 1982). Spike time points also provide different information in a neuronal network where neurons are interacting intensely. ISI reflects the type of firing behavior in neuronal networks, where frequent firing of several neurons is observed in an orchestrated manner (Kandel and Spencer, 1961; Connors et al., 1982; Gray and McCormick, 1996). This kind of short episode of intense firing is called a burst. Bursts are important informational content which are not only reflecting the network plasticity but also influencing it (Lisman, 1997; Massobrio et al., 2015). Several studies previously suggested that neuronal cultures exhibit more bursts in their late development stages (Ichikawa et al., 1993; Maeda et al., 1995; Kamioka et al., 1996; Wagenaar et al., 2006). Robinson et al. (1993) showed that synchronized bursts in the cortex are dependent on glutamatergic synaptic activity, indicating that neuronal populations are forming large-scale excitatory networks. Consequently, bursts are noted as markers for developed neuronal networks and are an important information source for evaluating synchronized activity.

ISIs are widely used to analyze firing characteristics of neuronal cells and networks. Since calculating ISIs is simple and computationally efficient, it is also employed to define bursts by applying a clear-cut threshold for the maximum ISI in a burst (Chiappalone et al., 2005; Wagenaar et al., 2006; Mazzoni et al., 2007). This technique is usually practiced by making also an assumption to define the minimum number of spikes in a burst. Additionally, an ISI histogram reflects the general firing characteristics of the neuronal recording. A histogram of ISIs can be easily formed after spike detection by counting the spikes and binning them

according to intervals between spikes. Although ISI histograms are capable of representing some characteristics of the firing activities, it is usually challenging to interpret them in their raw form. Alternatively, ISI histograms have been calculated previously in logarithmic scale (logISIH), which would reveal the differences between firing characteristics of individual firing and synchronous firing, i.e., bursts Selinger et al. (2007); Pasquale et al. (2010). On the other hand, in most of the cases, individual firing and bursts are not easily distinguishable from logISIH either.

Despite the general consensus that bursts are important markers of network activity, definition of bursts highly varies between different studies. Several studies have been using fixed thresholds to define, e.g., the maximum ISIs between spikes in a burst or the number of spikes which a burst should include (Chiappalone et al., 2005; Wagenaar et al., 2006). Some utilized more adaptive parameters which are derived from the analyzed recordings, such as thresholds calculated from logISIH or average ISI (Mazzoni et al., 2007; Selinger et al., 2007; Pasquale et al., 2010). However, some of these adaptive methods were using fixed parameters as well (Pasquale et al., 2010). In developing cultures, bursts should be considered without any predefined criteria. In fact, previously, developing cultures were analyzed and different types of bursts were observed (Wagenaar et al., 2006). Even though maturing networks, particularly stem cell derived neuronal cultures, were not widely available previously, some recent studies show that such neuronal cultures also exhibit not only very dynamic firing but also highly varying bursting behavior (Heikkilä et al., 2009). Indeed, bursts lasting from milliseconds to seconds and bursts which are formed by a few spikes to tens of spikes are seen very frequently for such networks (Heikkilä et al., 2009; Kapucu et al., 2012) (see Fig. 4.1). Consequently, previously defined thresholds and parameters may not be feasible for the assessment of bursting in maturing cultures.

Generally, spike time point information is processed as binary data where 1s represent spike activity and 0s represent no activity. Such binary data have been widely analyzed as time series in the information technology field. Consequently, algorithms widely used for analyzing the information content of any time series are also potentially feasible for the analysis of the information content of neuronal recordings. Previously, such neuronal data have been widely analyzed to assess the information content, and the challenges and principles were also defined in Quiroga and Panzeri (2009). The information content of time series is analyzed essentially by means of entropy which was first described by Shannon (1948). After that, different entropy algorithms have been derived to study the information content of time series. Briefly, entropy is a measure of unpredictability of the information

content. Entropy-based methods enable studying the complexity or uncertainty of the neuronal behavior (Burggren and Monticino, 2005; Monticino, 2007) or the network relations by means of information transfer between different neuronal populations or different locations in a neuronal system (Garofalo et al., 2009; Ito et al., 2011).

In conclusion, information based on spike time points obtained from extracellular recordings have been utilized commonly for analyzing firing behaviors as well as for the assessment of network relations. However, enhancing conventional methods or developing novel methods for the acquired neuronal data is necessary. For example, to better understand the evolution of information transfer in developing neuronal networks, conventional methods used in information technology, e.g., methods based on the entropy concept, have great potential for the assessment of developing neuronal cultures (Quiroga and Panzeri, 2013). Also, the high variance of the collected data from maturing neuronal cells requires more adaptive methods for the analysis since in such cases the conventional methods have a tendency to ignore a considerable amount of data. Adaptive detection of bursts without any pre-defined criteria as well as non-parametric quantification of bursts allow analyzing highly varying network behaviors. Additionally, adaptively defined bursts can be characterized further according to desired metrics or again non-parametrically. It is essential to obtain these metrics for the analysis of the network responses to different treatments, e.g., drugs, toxins, or chemicals (Bal-Price et al., 2010; Äänismaa et al., 2011; Defranchi et al., 2011; Hogberg et al., 2011). Metrics should be obtained by using large data pools, and these data pools should be formed by an analysis tool which has no bias for a certain type of network behavior; naturally, this would not be feasible using methods with pre-defined or biased parameters.

### **Spike waveforms: Information and analysis methods based on spike waveforms**

Representative spike waveforms of neuronal recordings are mainly obtained via spike sorting. Already for a couple of decades, spike sorting algorithms have been utilized in various neuronal studies such as in epileptic seizure studies (Truccolo et al., 2011), brain computer interface development (Santhanam et al., 2006), and in developmental neuroscience (Sun et al., 2010). It is an important technique to separate the single unit activity, where principally electrodes record EAPs from multiple neurons in their vicinity. Spike sorting classifies spikes into classes corresponding to different neuronal AP waveforms, where ideally each waveform represents signals

from individual neurons (Gibson et al., 2012).

On the other hand, there are limitations on the number of neurons which can be detected by a single electrode (Pedreira et al., 2012). Principally, an initial feature extraction from stored spike waveforms and then an effective clustering, which enables separating distinct features from each other, is needed for spike sorting. Fig. 2.4 summarizes the required steps for a standard spike sorting algorithm. Briefly, after obtaining EAPs from raw recordings by spike detection, spikes can be sorted according to their waveforms. For that spike features which represent the spike waveform classes are extracted first; this step is called feature extraction and can be parametric or nonparametric. Next, a dimension reduction procedure reduces the number of features to obtain ideally only the features which can separate different spike types and eliminates the features dominated by noise. In other words, the extracted features are reduced to keep the most distinctive features for different spikes. Finally, clusters are calculated in a way that ideally each cluster will be formed by the same types of spikes which are different from other clusters' spikes. For feature extraction, principle component analysis and wavelet-based methods are commonly used (Gibson et al., 2012), and for clustering, e.g.,  $k$ -means clustering is commonly employed. In practice, it is not always possible to obtain clear-cut clusters for spike waveforms. Thus, as a common practice in spike analysis, spike waveform cut-outs are sorted, and the waveforms in each resulting class or cluster averaged to obtain the representative spike waveform types (Gibson et al., 2012). The clustering step of the spike sorting algorithm still needs an accurate and fully unsupervised method, which still remains a largely open question (Quiroga and Panzeri, 2013). There are several spike sorting algorithms in the field (see Gibson et al. (2012) for more details and performance evaluation of previously proposed methods).

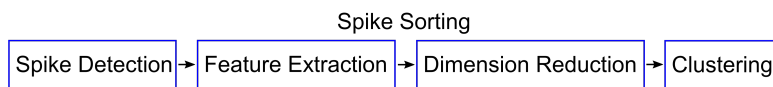


**Figure 2.4:** Employed steps for a standard spike sorting algorithm.

Recent developments in HDMEA technology enable recordings in which signals from an individual neuron may be recorded by multiple electrodes which results in improved spike sorting and spatial information (Franke et al., 2012; Obien et al., 2014). However, in most of the MEA recordings in the literature, no precise information is available about the number of cells located in the vicinity of the electrode; thus, average spike waveforms would represent not the single unit activities but the

averages of multi-unit activities (from several neurons) which are clustered together. Especially for the frequently firing neuronal populations such as in bursts, overlapping spikes from different neuronal sources make the sorting more challenging (Quiroga et al., 2004; Wild et al., 2012). In summary, even though spike sorting is challenging, it is required for isolating or identifying single neuronal cell activities in a population (Buzsáki, 2004).

Single neuron activity and its relation with the general network activity is another topic for deriving necessary information on neuronal behavior and information transfer. Some previous studies analyze the relationship between single spike firing and network bursting, e.g., Harris et al. (2001) showed that conditions that cause high firing rates do not necessarily produce high bursting in pyramidal cells. Also, Fee et al. (1996) and Stratton et al. (2012) analyzed the changes in spike waveforms with different firing rates. However, to our knowledge, there has not been any study analyzing spike waveforms and network bursting simultaneously, which would extend our knowledge on bursts.

### **2.3.2 Analyses based on complete electrophysiological recordings**

Electrophysiological recordings consist of several components of biological signals and noise which were summarized in section 2.2.1. Consequently, working with complete data has advantages in keeping comprehensive information which allows broader analysis if necessary; on the other hand, the pile of different signal components makes interpretation challenging. Thus, filtering out the undesired components for a better analysis and interpretation is very common; however, filtering signal components strongly depends on the required information, pre-made assumptions, or previously obtained knowledge on the studied subject. For example, while studying EEG, well defined EEG rhythms, i.e., alpha, beta, gamma, delta, theta, and mu, can be extracted from the recording by filtering, and then the interrelations between different rhythms can be assessed (Steriade et al., 1993). Such analysis, which is common for EEG studies, is not always feasible for neuronal cultures, particularly for developing dissociated cultures, which are more primitive comparing to the human brain and have large variability between experiments. However, sub-threshold activities would also consist of important information for developing cultures. In fact, according to Shoham et al. (2006), in some brain areas, 90% of the neurons are not spiking or just firing occasionally; thus, synaptic potentials from such neurons would include a great deal of information. Buzsáki

et al. (2012) also indicate that synaptic activity contributes to LFPs and is often the most important source of extracellular current flow. Currents from many individual compartments must be simultaneous to form a measurable signal, and such activity is most easily achieved for relatively slow events, such as synaptic currents. Additionally, as the contribution of neuronal activity in the measured signal decreases with increasing distance of the source from the electrode, there would be a large amount of neuronal information from distant EAPs buried in the LFPs.

While working with complete data, we can analyze not only EAPs but also LFPs in the assessment of neuronal cells or networks. Analyzing LFPs also allows studying the frequency spectrum of other signal components than EAPs in the recordings. Sometimes working on the frequency domain reveals different viewpoints; e.g., the distribution of spectral energy reveals the changes in the network connectivity as in Tibau et al. (2013). Spectral information is also beneficial for deriving and comparing the parameters and metrics for neuronal bursts. In the past years, neuronal bursts in MEA studies have been assessed and classified with respect to several parameters mostly based on spike information such as burst duration, burst amplitude, ISI, and inter-burst interval (Grattarola et al., 2001; Keefer et al., 2001; Wagenaar et al., 2006). New metrics based on entire recorded signals or frequency dynamics of the recorded signal in addition to spike information would provide additional and enhanced information where conventional ones can not quantify the analyzed network in a similar way.

Network relations have especially influential effects on LFPs (Buzsáki et al., 2012); thus, analyzing synchronicity, causality, phase and frequency coupling, or tracking defined rhythms reveal pathways for the assessment of network connectivity (Salinas and Sejnowski, 2001; Ginter Jr et al., 2005; Buehlmann and Deco, 2010; Battaglia et al., 2012). Unlike binary analysis based on detected events such as spike time points, spectral analysis is not widely applied for the cultured cells on MEAs. Although there are studies showing that *in vitro* brain slices would repeat the cortical oscillations (Compte et al., 2008) or that *in vitro* dissociated rat cortical cultures can be analyzed by means of EEG sleep-wake rhythms (Colombi et al., 2016), the effective bandwidths in cell cultures were not defined as well as in brain studies. Inter-culture variability and high plasticity (Biffi et al., 2013) as well as a lack of supplementary mechanisms seen *in vivo* (cf. Colombi et al. (2016)) make such analysis more challenging *in vitro*. On the other hand, for the studies where spike information is challenging to obtain, e.g., with low-amplitude spikes hidden in high-level background signal, or if the user wants to avoid conflicts between different spike detection algorithms, working on the spectrum could provide a good

alternative. Briefly, analyzing spectral features of developing neuronal networks is promising, and novel methods are required for assessing network synchrony of highly plastic networks without well defined rhythms.

In conclusion, recent developments in MEA technology enable us to acquire data which potentially have more information than the current analysis methods reveal. Whether the analysis depends on merely spike information or complete recordings, to answer the related research questions we need to obtain more information from the data at hand. In this thesis, we addressed some of these research questions by enhancing the existing methods or proposing novel ones; consequently, we increased the information or acquired new types of information from the obtainable data.

# CHAPTER 3

## MATERIALS AND METHODS

In this section, we first give brief information on the cell cultures, MEA recordings, and simulations used for this thesis. Then, we define the signal analysis methods which were employed and developed in this thesis.

### 3.1 Neuronal cultures and the experiments performed

The signal analysis methods studied in this thesis were employed on various types of *in vivo* and *in vitro* neuronal cells. Fig. 3.1 shows the used cell cultures and corresponding publications included in this thesis. Beside recording spontaneous electrophysiological activity, pharmacological manipulation and electrical stimulation were also experimented with for some cell types. Cell culturing, cell experiments, and electrophysiological recordings of stem cell-derived neuronal cells, rat cortical cells, and rat hippocampus were performed by different laboratories, whereas mouse cortical cell culturing and recordings were carried out by the author of this thesis.

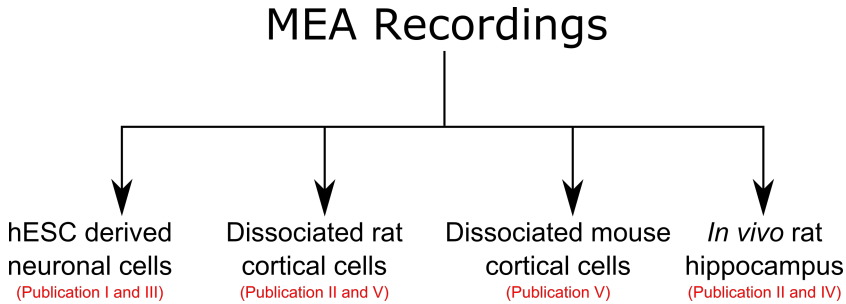


**Figure 3.1:** Sources of MEA data used in the publications in this thesis.

### 3.1.1 Stem cell-derived neurons

Human embryonic stem cells (hESCs) were differentiated into neuronal cells<sup>1</sup>. Briefly, the neural differentiation was performed by dissecting hESC colonies into small clusters, and these clusters were cultured in suspension (see details in Sundberg et al. (2009) and similarly in Lappalainen et al. (2010)) till they formed hESC-derived neural aggregates in approximately 4 to 5 weeks. Before plating the cells, MEA dishes were coated with polyethylenimine (0.05% solution, Sigma-Aldrich, St. Louis, MO, USA) and subsequently with human laminin (20  $\mu\text{g}/\text{ml}$ , Sigma-Aldrich). Then, pieces of hESC-derived neural aggregates were dissected from neurospheres (10–15 small aggregates with 50,000–150,000 cells in total) and placed on the electrode area of the MEA dishes. Culture medium containing basic fibroblast growth factor (4 ng/ml, FGF, Sigma-Aldrich) and brain-derived growth factor (5 ng/ml, BDNF, Gibco Invitrogen, Carlsbad, CA, USA or Peprotech, Rocky Hill, NJ, USA) was replaced three times a week. All the MEAs with cells were kept in an incubator (+37°C, 5% CO<sub>2</sub>, 95% air) prior to and between recordings.

Pharmacological experiments were also performed on stem cell-derived neuronal cultures for the data used in Publication III. The experiment was performed in 7 phases. MEA data was recorded in the beginning before any manipulations and at each phase immediately after pharmacological manipulation or wash:

1. Baseline.
2. First wash with fresh medium: to observe the effects of immediate medium change.

---

<sup>1</sup>The University of Tampere has ethical approval from the Pirkanmaa Hospital District to derivate, culture, and differentiate hESC (Skottman, R05116) and permission from the National Authority for Medicolegal Affairs (1426/32/300/05) to conduct human stem cell research.

3. CNQX (20  $\mu\text{mol}$ , AMPA/kainate receptor antagonist 6-cyano-7-nitroquinoxaline-2,3-dione, Abcam): to block AMPA/kainate mediated signaling.
4. CNQX (20  $\mu\text{mol}$ , Abcam) + D-AP5 (30  $\mu\text{mol}$ , D(-)-2-amino-5-phosphonopentanoic acid, Abcam) AMPA/kainate and NMDA receptor antagonist; to block glutamatergic signaling.
5. Second wash with fresh medium.
6. GABA (100  $\mu\text{mol}$ , Sigma): to enhance GABAergic signaling.
7. Bicuculline (30  $\mu\text{mol}$ , GABAA antagonist bicuculline methiobromide, Sigma): to inhibit GABAergic signaling.

### 3.1.2 Rat and mouse cortical neurons

Data from rat cortical cells were collected previously for another study (Weihberger et al., 2013). Rat cortical cells were obtained from newborn Wistar rats<sup>2</sup>. Briefly, the prefrontal cortical tissue was dissected after decapitation. The tissue was dissociated into neuronal cells and cultured on MEAs which were previously coated with polyethylenimine (Sigma-Aldrich, St. Louis, MO). Culture medium containing minimum essential media supplemented with 5% heat-inactivated horse serum, 0.5 mM l-glutamine, and 20 mM glucose (Gibco Invitrogen, Life Technologies, Grand Island, NY) was replaced twice a week. Neuronal density was approximately 1250 neurons/ $\text{mm}^2$  after the first day *in vitro* (DIV). All the MEAs with cells were kept in an incubator (+37°C, 5% CO<sub>2</sub>, 95% air).

Commercially available mouse cortical cells were purchased (A15586, Gibco, Thermo Fisher). According to the supplier, mouse cortical neurons were isolated and cryopreserved from C57BL/6 embryonic day-17 mice. The viability, i.e., neuronal purity, was declared in the range of 50–80% by the supplier. Purchased cells were sowed as droplets on MEAs which were previously coated with poly-L-lysine and subsequently laminin. The number of cells per MEA was varied between 20,000 and 40,000. Culture medium containing GlutaMAX (2.5 ml/l) and B27 (20 ml/l) was replaced three times a week. All the MEAs with cells were kept in an incubator (+37°C, 5% CO<sub>2</sub>, 95% air) prior to and between recordings.

---

<sup>2</sup>Animal treatment was according to the Freiburg University (Freiburg, Germany) and German guidelines on the use of animals in research.

### 3.1.3 Rat hippocampus

The *in vivo* experiments were performed on anesthetized rats<sup>3</sup> (Mikkonen and Penttonen, 2005). Briefly, anesthetized rats were placed in a stereotaxic instrument and holes were drilled on the skull above the target structures. The location of the hippocampus, and thus the probe, was estimated based on *cornu ammonis* region 1 (CA1) pyramidal cell firing patterns to antidromical stimulation of the commissural efferents of the contralateral *cornu ammonis* region 3 (CA3). The data were collected previously for other research (Mikkonen and Penttonen, 2005) and also used for Publications II and IV.

We used three consecutive recordings for Publications II and IV. Particularly for Publication IV, before analyzing the whole data, we created a toy dataset from three consecutive recordings by selecting two neighboring channels per each recording (a total of six channels from three consecutive recordings). The toy dataset was used to test the proposed method initially. Channels from the same recordings were named the with same variable names, i.e.,  $(X1, X2)$ ,  $(Y1, Y2)$ , and  $(Z1, Z2)$ , and expected to exhibit higher correlations.

## 3.2 Microelectrode array recordings

*In vitro* electrophysiological recordings in this thesis were obtained by using single-well (200/30iR-Ti-gr, MCS) and 6-well (60-6wellMEA200/30iR-Ti-rcr) MEAs with electrode diameter 30  $\mu\text{m}$  and inter-electrode distance 200  $\mu\text{m}$ . Reference electrodes are embedded internally, where a 6-well MEA has nine electrodes per well (with a grid of  $3 \times 3$ ) including one reference electrode, and a single-well MEA has fifty-nine electrodes and one reference electrode (with a grid of  $8 \times 8$  without any electrodes in the corners). The signals from the MEAs were amplified with a pre-amplifier MEA 1060-Inv-BC (Multi Channel Systems MCS GmbH, Reutlingen, Germany, MCS) and analog-filtered and amplified with a filter amplifier FA60S-BC (MCS) (bandwidth: 1 Hz – 8 kHz, total gain: 1100). For all the recordings, the culture temperature was maintained at  $+37^\circ\text{C}$  using a TC02 temperature controller (MCS) during the measurements.

In Publication I, the cell seeding area in the MEA was used as standard, which is 20 mm in diameter as well as also restricted to be  $\varnothing$  4 mm to reduce the amount of cells needed and to guide the cells to grow on the top of the electrode area.

---

<sup>3</sup>The experimental procedures involving animal models followed the international guidelines on the ethical use of experimental animals and were approved by the Provincial Government of Eastern Finland (approval number 99-61).

In Publications II and IV, a silicon probe (courtesy of the University of Michigan Center for Neural Communication Technology, MI, USA) was used with sixteen electrodes on one shank and  $100\ \mu\text{m}$  distance between the electrodes. Two of the topmost electrodes (channels 15 and 16) of the probe were not used due to setup design and recording apparatus restrictions. The probe was lowered into the hippocampus, and the electrophysiological signals were recorded. During a measurement session, stimulation described in Mikkonen and Penttonen (2005) was repeated every ten minutes. The data were collected previously for other research. The full description of the experimental setup can be found in Mikkonen and Penttonen (2005).

### 3.3 Simulations

In addition to the recorded MEA data, we validate the developed method also with simulations in Publication V. For that, first, we setup a toy model based on the idea that the neuronal activity could be defined as the sum of oscillations of different neuronal units contributing to the signaling in a time window (see (Montgomery Jr, 2014) for *Sine* wave representation of LFPs). The neuronal unit activity (EAPs) and the average activity of neuronal ensembles (LFPs) in a population was assumed as cardinal *Sine*, i.e., *Sinc* waves and oscillations of *Sine* respectively. Consequently, the population activity in a time window was defined as the sum of these activities in that corresponding time. The model is simulated for three populations (Fig. 3.2), two of which had neuronal ensembles always active together (populations 1 and 2), so the same number of neuronal ensembles was contributing to the signaling in a time window (fully synchronized populations), but the third population (population 3) had the contribution of a different number of neuronal ensembles (not synchronized). The number of neuronal ensembles contributing to population activity is quasi-randomly selected. For the applications, we tested the algorithm with five different  $P_{EAPs/LFPs}$ : 0%, 10%, 20%, 50%, and 100%, where  $P_{EAPs/LFPs}$  is calculated as:

$$P_{EAPs/LFPs} = \frac{P_{EAPs}}{P_{EAPs}P_{LFPs}} \times 100, \quad (3.1)$$

where  $P_{EAPs}$  and  $P_{LFPs}$  is the total estimated power for the signals generated as *Sinc* and *Sine* functions respectively.

We also created simulated data from integrate-and-fire model-based neuronal networks with known connectivity levels for validation. For that, two populations were simulated each having 50 neurons (40 excitatory and 10 inhibitory). Each

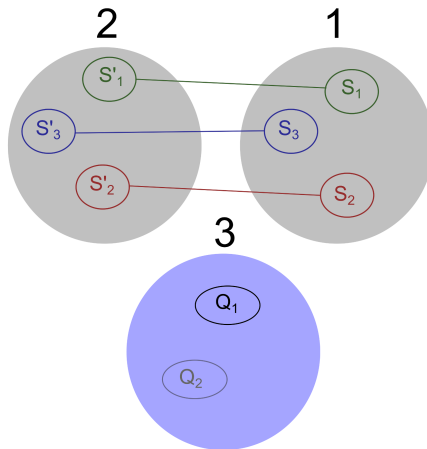


**Figure 3.2:** A toy model of three populations. Populations 1 and 2 are fully synchronized, where each neuronal ensemble in one of these populations activates another neuronal ensemble in the other population. Population 3 is not synchronized with the other populations. Signals generated from neuronal ensembles belonging to population 1, 2 and 3 are  $S$ ,  $S'$  and  $Q$  respectively and which were defined as *Sinc* waves or *Sine* oscillations depending on the simulation setup.

population is internally connected fully without autapses, and they are connected to each other with the defined connectivity level, i.e., 0%, 10%, 20%, 50%, and 100%. Here, the percentages give the probabilities for one neuron to connect to another neuron in the other population. One hundred pairs of populations were simulated for each connectivity level. From the time stamps, artificial MEA recordings are constructed to simulate raw MEA recordings by first calculating the population activity and then applying a *Sinc* kernel to obtain a continuous function based on the simulated spike time stamps similar to Nawrot et al. (1999); Blanche and Swindale (2006). Basically, *Sinc* signals, peaking in spike time points, were summed to generate an artificial signal. Artificial LFPs and white Gaussian noise (WGN) were also added to evaluate the method with different levels of noise and signal power.

### 3.4 Signal analysis methods

The used signal analysis methods can be classified in three subsections: methods evaluating spiking behavior, methods evaluating information content of neuronal bursts, and finally methods for neuronal network analysis. In the following sections, the methods of each class from the literature which are used in this thesis are

explained and followed by the descriptions of the methods developed in this thesis.

### 3.4.1 Methods employed for evaluating spiking behavior

Evaluating ISIs of a spike time series provides information on spike firing dynamics of the analyzed neuronal activity. Thus, average ISI or the calculated ISI threshold from an ISI histogram have been widely employed for neuronal burst detection in the literature. On the other hand, to analyze the single unit activity, spike sorting is essentially used to classify the spike waveforms into clusters. In this thesis, we employed a method to detect bursts by utilizing ISI histograms in logarithmic scale, i.e., logISIH (Selinger et al., 2007; Pasquale et al., 2010), and a commonly used spike sorting algorithm, Waveclus, to sort the spike waveforms. The employed algorithms are explained below.

**logISIH:** The method is based on plotting ISI histograms using a logarithmic instead of linear scale. In the algorithm, the ISI threshold is selected at the point where intra-burst ISIs are most clearly separable from inter-burst ISIs. Clear separation is indicated by the distinct principal and secondary peaks formed in the logarithmic histogram representing intra- and inter-burst ISIs respectively. For that, a so called *void* parameter is calculated and further evaluated with a predefined threshold. The *void* parameter is defined as:

$$void = 1 - \frac{g(\text{minimum})}{\sqrt{g(\text{peak}_1)g(\text{peak}_2)}}, \quad (3.2)$$

where  $g$  is the distribution of  $\ln(ISI)$ . Accordingly, the *void* parameter takes values between 0 and 1. If it is 0, two peaks cannot be separated from each other, and 1 means that they can be separated perfectly. Usually a threshold for the value of *void* is predefined (Pasquale et al., 2010).

**Spike sorting:** We used the Waveclus algorithm for spike sorting (Quiroga et al., 2004). A brief description of the algorithm is given below:

After spike detection, Waveclus utilizes Haar wavelets for feature extraction. Then, the number of features is reduced to ten. For this task, the Kolmogorov-Smirnov test is employed which is able to distinguish distributions of wavelet coefficients from the normal distribution; thus, ten distributions which are least close to the unimodal normal distribution are retained for clustering. For the clustering, the Waveclus algorithm uses a type of nearest neighbor algorithm, where nearest neighbors are a group of points whose local density is higher than a certain value. The algorithm used by Waveclus is called superparamagnetic clustering, where nearest neighbor interactions depend on one parameter called *temperature*.

The term *temperature* is used as an analogy with mechanics from where the term is taken: shortly, in low temperatures all the points are clustered together, whereas in high temperatures there are many small clusters; however, in the superparamagnetic phase there are middle-sized clusters where the algorithm cuts the clusters automatically. Finally, spike waveforms are separated into different classes.

### 3.4.2 Methods developed for evaluating spiking behavior

We evaluated spiking behavior of neuronal cultures in terms of single-unit activity observed as spikes and synchronous network activity manifested as bursts. Firstly, we developed a method to detect bursts adaptively based on the spiking behavior of recordings (Publication I). Next, we proposed simultaneous analysis of spike waveforms and bursts for the assessment of spike type compositions of bursts (Publication III).

#### Adaptive neuronal burst detection

Neuronal recordings showing burst activity exhibit similar characteristics on their ISI histograms (Christodoulou and Bugmann, 2001): first forming a peak and then gradual decay. Such behavior has been associated usually with a Poisson distribution with different means (Chen et al., 2009). Therefore, we used *skewness*, which is a measure quantifying asymmetry, to detect differently behaving bursts (e.g., bursts with different intra-burst ISIs). Asymmetrical behavior of the ISI distribution reflects the characteristics of different bursts (Fig. 3.3).

For a unimodal distribution, skewness is positive when the distribution spreads out more to the right of the mean than to the left. In other words, for the positively skewed distribution the tail of the distribution is longer on the right side, and vice versa. The skewness of the normal or any other purely symmetric distribution is zero (Fig. 3.4).

Skewness,  $s$ , is calculated as:

$$s = \frac{\frac{1}{n} \sum_{i=1}^n (x_i - \bar{x})^3}{\left( \sqrt{\frac{1}{n} \sum_{i=1}^n (x_i - \bar{x})^2} \right)^3}, \quad (3.3)$$

where  $x$  is a data vector of length  $n$  samples, and  $\bar{x}$  is its mean. For a Poisson distribution, skewness is equal to  $\lambda^{-\frac{1}{2}}$ , where  $\lambda$  is the mean of the distribution. Then it can also be seen that with an increasing mean, skewness decreases exponentially, and the distribution looks more similar to a Gaussian distribution.

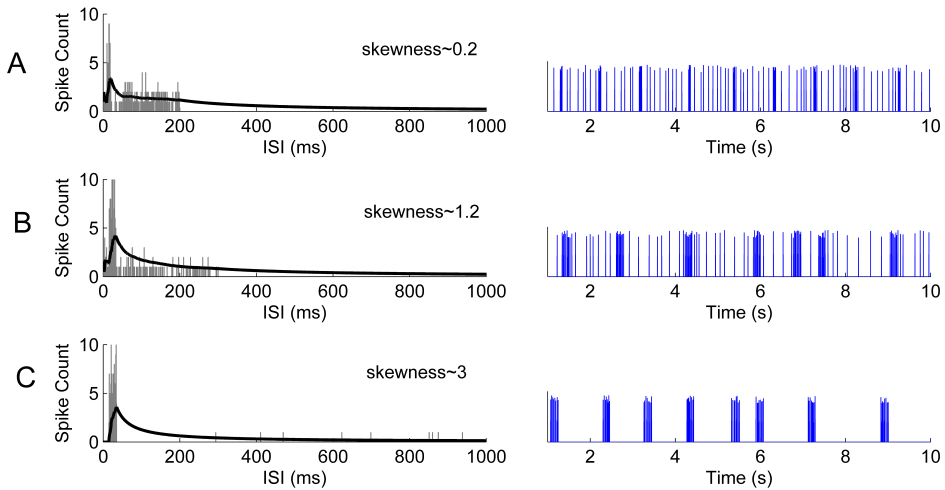


**Figure 3.3:** Simulation of bursts with different spiking behaviors. Right-hand panels present the spike activity in time (blue), and left-hand panels present the corresponding ISI histogram (gray) and the calculated CMA (black). (Figure modified from the figure originally published in Publication 1).

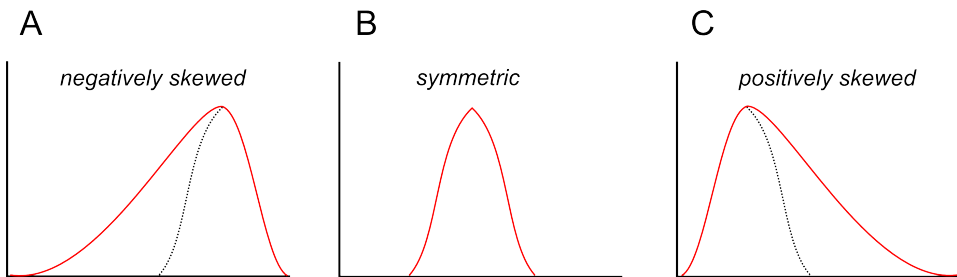


**Figure 3.4:** An illustration of distributions with different skewness values: (A) A negatively skewed distribution, (B) symmetric distribution with skewness equal to zero, and (C) a positively skewed distribution. The dotted line represents the normal distribution to illustrate the asymmetry of the distribution better.

Before employing the algorithm, spikes are detected with a threshold according to the standard deviation of the signal noise level. In the proposed algorithm, after computing ISI histograms, skewness of the histograms is calculated initially. Calculated skewnesses of ISI histograms are stored to be used for the calculation of the ISI threshold for the putative bursts. Then, the cumulative moving average (CMA) of the ISIs is calculated. The CMA gives the marginal change on the average count of spikes up until the current ISI value; thus, it is calculated as a function of ISI bins as follows:

Let  $y_i$  be the spike count in the  $i$ th ISI bin, where  $i = 1, \dots, N$ , with  $N$  being the total number of ISI bins. The value of the cumulative sum,  $CH_I$ , of the histogram at the  $I$ th ISI bin,  $I \leq N$ , is defined as

$$CH_I = \sum_{i=1}^I y_i. \quad (3.4)$$

The corresponding  $CMA$  is given by

$$CMA_I = \frac{1}{I} \sum_{i=1}^I y_i, \quad (3.5)$$

whose maximum,  $CMA_m$ , is reached at the  $m$ th ISI bin, and

$$m = \arg \max_{k=1, \dots, N} \left( \frac{1}{k} \sum_{i=1}^k y_i \right). \quad (3.6)$$

This point represents the maximum that the average spike count reaches; in other words, for the ISI values beyond this point, the average count starts decreasing. This can be used as a critical point for calculating thresholds of intra-burst ISIs. In fact, for the recordings containing burst patterns, intra-burst ISIs of bursts should be shorter than the ISIs of individual spikes that don't belong to a burst. On the other hand, as we showed in Fig. 3.4, bursts with different ISIs have different skewnesses, and skewness should also be considered for the threshold calculation. Thus, we define a tolerance  $\alpha$  and set the threshold to  $\alpha \cdot CMA_m$ , where  $0 < \alpha < 1$ . Here,  $\alpha$  is selected according to the skewness of the ISI histogram. Additionally, we consider pre-burst spikes and burst tails (burst-related spikes) as in the literature (Wang and Hatton, 2005; Wagenaar et al., 2006) and include them in the bursts. We assume that individual spikes are located in the tail of the histogram, whereas burst spikes are located in the vicinity of  $CMA_m$ . Consequently, burst-related spikes are located in the histogram between ISIs of intra-burst spikes and ISIs of individual spikes. According to this, we defined two parameters:  $\alpha_1$  for the bursts and  $\alpha_2$  for the burst-related spikes, with  $\alpha_1 > \alpha_2$ . The  $\alpha$  values are obtained empirically to enable automatization of the method (Table 3.1).

**Table 3.1:** Alpha values for corresponding skewnesses.

	$s < 1$	$1 \leq s < 4$	$4 \leq s < 9$	$9 \leq s$
$\alpha_1$	1	0.7	0.5	0.3
$\alpha_2$	0.5	0.5	0.3	0.1

Finally, denoting the ISI at  $CMA_m$  by  $x_m$ , the ISI threshold  $x_t > x_m$  for burst detection is found at the mid-time point of the ISI bin for which the value of the CMA curve is closest to  $\alpha \cdot CMA_m$ . This step is first realized for burst spikes and then repeated for burst-related spikes (Fig. 3.5). ISI thresholds  $x_{t1}$  and  $x_{t2}$  are calculated for burst spikes and burst-related spikes respectively. After detecting the putative burst and burst-related spikes, the burst-related spikes which are not following or followed by a burst are omitted. Also, the bursts which are closer to each other than the threshold calculated for the burst-related spikes, i.e.,  $\alpha_2 \cdot CMA_m$ , are merged together. This step also corrects erroneous burst spike detections and misses caused by ISI variance inside bursts and is especially advantageous for the analysis of maturing networks, which frequently have high ISI variance.

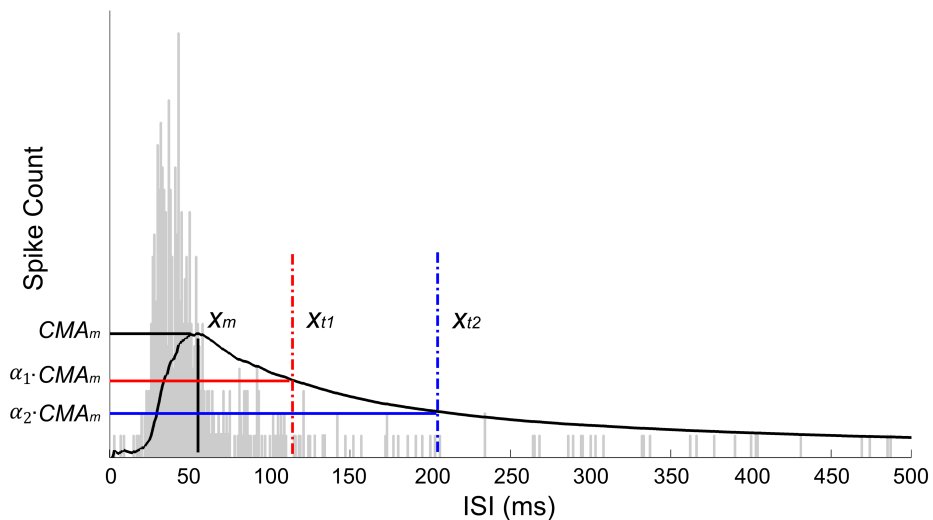


**Figure 3.5:** Calculation of burst threshold (red vertical line) and burst-related spikes threshold (blue vertical line) via CMA curve (black line) of the ISI histogram (gray bars).  $\alpha$  coefficients used for skewness values are given in Table 3.1. ISI thresholds  $x_{t1}$  and  $x_{t2}$  are calculated for burst spikes and burst-related spikes respectively.

### Joint analysis of neuronal bursts and sorted EAPs

From the current knowledge in the literature (Fee et al., 1996; Harris et al., 2001; Stratton et al., 2012), we can hypothesize that an increase in the activity of a spike type with a unique waveform would not guarantee a higher probability of its participation in bursts. Thus, a method to jointly assess the spike waveforms and bursts would derive novel information about the contribution of the individual neurons

to the network activity. Such information can be utilized for analyzing neuronal response to external manipulations such as pharmaceuticals or neurotoxins as we suggested in Publication III.

In Publication III, as the final outcome of spike sorting and burst detection, spike types and burst start and end time points were obtained. To analyze the spike type compositions of the bursts, a joint analysis method based on the simultaneous assessment of spike waveforms and neuronal bursts was developed (Fig. 3.6). This was motivated by the need to observe how bursts were modified by pharmacological manipulation. Representative average waveforms are selected as spike types based on the results of the analysis of the first phase of the pharmacological experiment. Waveforms obtained in the subsequent experiment phases are classified based on correlations between the waveforms and the selected spike types. If there were conflicts with the average and standard deviation waveform correlations, then the newly occurred spike was labeled with a new type and also considered as a new representative spike type in the later steps. As the final outcome, the developed method reveals the spike type compositions of the bursts.

### 3.4.3 Methods employed for evaluating the information content of neuronal bursts

As it was mentioned previously, entropy was introduced by Shannon (1948) as an information theoretical context to evaluate information content. The term *Shannon entropy*,  $H$ , is used as a measure of uncertainty and defined for time series as

$$H = - \sum_i p_i \log p_i, \quad (3.7)$$

where  $p_i$  is the probability that an amplitude value occurs in the  $i$ th amplitude bin and is given by the probability distribution function of the time series. Similarly for SE,  $S$  is calculated from the normalized power spectrum for the frequencies  $[f_1, \dots, f_k, \dots, f_K]$ :

$$S = \sum_{f_k=f_1}^{f_K} P(f_k) \log \left( \frac{1}{P(f_k)} \right). \quad (3.8)$$

Then, SE is normalized to reside between 1 and 0 as

$$S_{\text{norm}} = \frac{S}{\log K}. \quad (3.9)$$

SE is a measure of how uniformly the power of the signal is distributed across the considered frequencies. A broadband signal has higher entropy than a narrowband

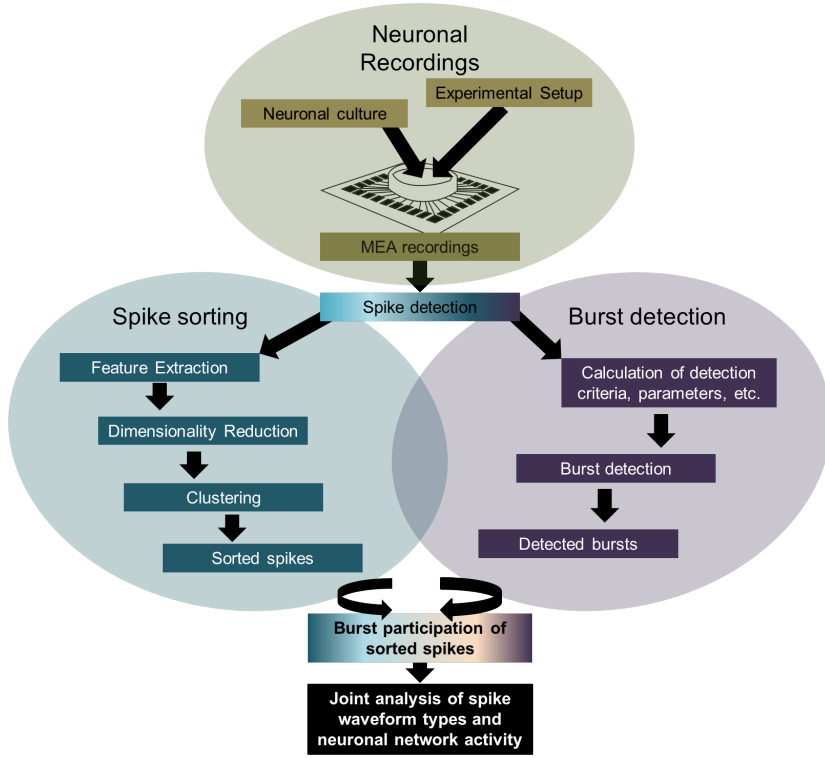


**Figure 3.6:** Illustration of joint analysis of spike waveforms and neuronal bursts. The analysis results with the participation of the spikes of different types observed in bursts. In Publication III, the spike sorting by Quiroga et al. (2004) and burst detection by Kapucu et al. (2012) were employed. (Adapted from Publication III.)

signal of equal total energy (Semmlow and Griffel, 2014). Thus, it is an effective algorithm to distinguish the signals with different frequency distributions.

Entropy of time series can be evaluated also by means of self-similarity. Sample entropy (SmpE) measures the conditional probability that a time series repeating itself for  $m$  points will also repeat itself for  $m + 1$  points. SmpE is calculated for a time series of length  $n$  as follows: Firstly,  $(n - m + 1)$  vectors of length  $m$  are formed to be  $X_m(i) = (x_i, x_{i+1}, \dots, x_{i+m-1})$ , where  $m$  is the embedding dimension. Thereafter, the probability that any other vector is similar to  $X_m(i)$  is calculated with a distance function  $d[X_m(i), X_m(j)]$ ,  $i \neq j$  as

$$C_i(r) = \frac{\text{number of } j \text{ where } d[X_m(i), X_m(j)] \leq r}{n - m + 1}, \quad (3.10)$$

where  $r$  is the similarity criterion. This process is explained in Fig. 3.7 more

illustratively. Then the average probability of vector pairs of length  $m$  is

$$\Phi(n, m, r) = \frac{1}{n - m} \sum_1^{n-m} C_i(r). \quad (3.11)$$

Finally, SmpE is estimated as

$$\text{SmpE}(n, m, r) = -\ln \frac{\Phi(n, m + 1, r)}{\Phi(n, m, r)}. \quad (3.12)$$

In the work described in this thesis, we implemented SmpE by using the publicly available Matlab code (Sample Entropy Source Code; Lee, 2012).

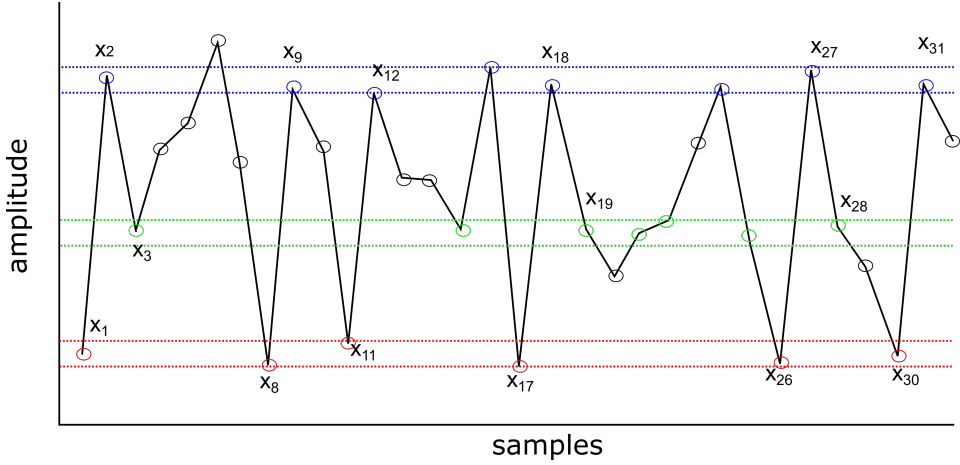


**Figure 3.7:** An exemplary time series with samples  $x_1, \dots, x_{32}$  to illustrate probability calculations for SmpE. Vector length for the example was  $m = 2$ , and the similarity criterion,  $r$ , was illustrated around data points  $x_1$ ,  $x_2$ , and  $x_3$  as  $x_1 \pm r$ ,  $x_2 \pm r$ , and  $x_3 \pm r$  respectively. Two data points are considered to be of the same amplitude if their amplitude difference is less than or equal to  $r$ . In other words, all data points circled in red, blue, and green are considered as having the same amplitude with  $x_1$ ,  $x_2$ , and  $x_3$  respectively; data points circled in black are different. According to the SmpE calculation with  $m = 2$ , starting from the first index, the vectors equal to the pair  $(x_1, x_2)$  are  $(x_8, x_9)$ ,  $(x_{11}, x_{12})$ ,  $(x_{17}, x_{18})$ ,  $(x_{26}, x_{27})$ , and  $(x_{30}, x_{31})$ ; whereas for  $m + 1$ , only  $(x_{17}, x_{18}, x_{19})$  and  $(x_{26}, x_{27}, x_{28})$  are equal to  $(x_1, x_2, x_3)$ . Therefore, in this case, the number of sequences matching the two-component template sequences is 5, and the number of sequences matching the three-component template sequence is 2. These calculations are repeated for the next two-component and three-component template sequences, which are  $(x_2, x_3)$  and  $(x_2, x_3, x_4)$  respectively. Then, this procedure is done for all other possible sequences up to  $(x_{30}, x_{31})$ . Finally, the natural logarithm of the ratio between the total number of repeated two-component sequences and the total number of repeated three-component sequences gives us the SmpE after multiplying the calculated number with a negative sign.

## Quantifying neuronal bursts according to their information content

We quantified neuronal bursts by calculating sample and spectral entropy values between the start and end points of the bursts which were determined by an automated adaptive burst detection algorithm (Publication II). Briefly, SmpE measures self-similarity of bursts, whereas SE of bursts gives the uniformity of spectral distributions during bursting. Consequently, both measures can quantify bursts with respect to the intra-burst variability and enable further classification of bursts with respect to the experimental set up.

The analysis is conducted in the following three steps:

1. Automatic burst detection with the adaptive burst detection algorithm, CMA.
2. Burst start and end times are determined by the first and last spikes.
3. Calculating spectral and sample entropies: SEs and SmpEs are calculated for the signal sections between burst start and end times and stored for further analysis.

For rat hippocampal recordings classification was done with respect to the recording sequence to observe possible changes between three sequential recordings. Medians of the entropy values of bursts for each recording sequence were calculated along with the interquartile ranges (IQRs). Additionally, a colormap for rat cortical cell recordings from a 60-channel MEA was formed to illustrate the median entropy values of bursts in separate channels so that the spatial distributions of classified bursts could be observed.

### 3.4.4 Employed neuronal network analysis methods

Neuronal synchrony can be expressed as the simultaneous activity of neuronal ensembles. Several methods are employed to analyze the synchronous activity of neuronal populations. One of the most common methods is evaluating simultaneous occurrences of spikes (Quiroga et al., 2002) or temporal occurrences of neuronal bursts in a time window (Selinger et al., 2004; Zwanenburg et al., 2012). Other methods quantify frequency and phase correlations between specific frequency bands (Palva et al., 2005).

Among the methods which assess neuronal network synchrony, methods which analyze network information transfer deserve to be mentioned separately. Such methods, e.g., mutual information (MI), transfer entropy (TE), evaluate connectivity or synchronicity based on the mutual dependence of analyzed time series.

They have been most commonly employed on spike time point data; however, there are also studies in which, e.g., TE was employed for complete data including LFPs (Ma et al., 2013). We employed TE and MI as well as event synchrony (ES) methods (Quiroga et al., 2002) in Publication V.

The methods employed in the literature can be briefly described as follows:

**ES:** The algorithm measures synchronicity based on the quasi-simultaneous appearance of events (Quiroga et al., 2002). As an initial step, the algorithm defines the maximum time period  $\tau_{i,j}$  between two consecutive spikes from the time series  $\mathbf{x}$  and  $\mathbf{y}$ , so that the two spikes occurring at times  $t_i^x$  and  $t_j^y$  in signals  $\mathbf{x}$  and  $\mathbf{y}$  respectively—where  $i$  and  $j$  are spike indexes—can be considered simultaneous by calculating the local spike appearances:

$$\tau_{i,j} = \frac{\min \{t_{i+1}^x - t_i^x, t_i^x - t_{i-1}^x, t_{j+1}^y - t_j^y, t_j^y - t_{j-1}^y\}}{2}. \quad (3.13)$$

Then, the number of times a spike appears in  $\mathbf{x}$  after a spike appears in  $\mathbf{y}$  according to the calculated  $\tau_{i,j}$  is denoted with  $C_{x|y}$  and defined as

$$C_{x|y} = \sum_{i=1}^{M_x} \sum_{j=1}^{M_y} J_{i,j}, \quad (3.14)$$

where  $M_x$  and  $M_y$  are the total numbers of events for  $\mathbf{x}$  and  $\mathbf{y}$  respectively, and

$$J_{i,j} = \begin{cases} 1 & \text{if } 0 < t_i^x - t_j^y < \tau_{i,j}, \\ \frac{1}{2} & \text{if } t_i^x = t_j^y, \\ 0 & \text{else.} \end{cases} \quad (3.15)$$

Finally, synchronization is calculated as

$$Q = \frac{C_{x|y} + C_{y|x}}{\sqrt{M_x M_y}}. \quad (3.16)$$

The source code for the ES method is available online (ES Source Code; Kreuz, 2015). The algorithm originally does not have a condition on the minimum number of events to be synchronized; therefore, a time series with even one simultaneous detectable event is considered as fully synchronized by the algorithm. Thus, for the MEA recordings we added the homemade criterion (minimum of 50 spikes per 300 s), as in Publication I and Publication III. This allows for eliminating unjustified synchronizations which could be caused by coincidentally appearing rare events in very sparsely firing channels. We named the modified algorithm corrected ES (cES).

**MI:** The method considers both single and joint probabilities of two time series  $x$  and  $y$  (Gray, 1990).

$$MI_{xy} = \sum_{e_i^y \in y} \sum_{e_i^x \in x} p(e_i^x, e_i^y) \log \left( \frac{p(e_i^x, e_i^y)}{p(e_i^x)p(e_i^y)} \right), \quad (3.17)$$

where  $e_i^x$  and  $e_i^y$  are single events in the signals  $x$  and  $y$  respectively, with  $i$  being the event index,  $p(e_i^x, e_i^y)$  is the joint probability density function, and  $p(e_i^x)$  and  $p(e_i^y)$  are the single probabilities. Mutual information is a symmetric measure, i.e.,  $MI_{xy} = MI_{yx}$ . The analysis was made by using the freely available tool (Brown et al., 2012).

**TE:** The method extends the concept of MI to conditional properties by considering the history of the information (Schreiber, 2000). In other words,  $TE_{y \rightarrow x}$  measures the increase in predictability of the future and the past of  $x$  once  $y$  is known. Then, TE is calculated as

$$TE_{y \rightarrow x} = \sum_{e_i^x, e_i^y} p(e_{i+1}^x, e_i^x, e_i^y) \log \left( \frac{p(e_{i+1}^x | e_i^x, e_i^y)}{p(e_{i+1}^x | e_i^x)} \right), \quad (3.18)$$

where  $p(e_{i+1}^x | e_i^x)$  denotes the conditional probability of observing the state  $e_{i+1}^x$  after  $e_i^x$ . TE was calculated for 1 ms signal bins with delays up to three bins (3.19), and the maximum value of TE was considered as given in Ito et al. (2011).

$$TE_{y \rightarrow x} = \sum_{e_i^x, e_i^y} p(e_{i+1}^x, e_i^x, e_{i+1-d}^y) \log \left( \frac{p(e_{i+1}^x | e_i^x, e_{i+1-d}^y)}{p(e_{i+1}^x | e_i^x)} \right), \quad (3.19)$$

where  $d$  is the time delay.

### 3.4.5 Developed entropy-based neuronal network analysis method

After having observed the capabilities of the entropy-based methods for quantifying neuronal behavior (Publication II), we hypothesized that the synchronized neuronal behavior could be reflected in the correlations of entropy measures. Particularly SE could be a promising tool because of its computationally efficient nature, since it is based on fast Fourier transform (FFT) (Semmlow and Griffel, 2014), and because it does not depend on accurate spike detection. We evaluate the correlations of time variant spectral entropies (CorSE) for the analysis of synchronicity as follows (Publications IV and V):

SE was calculated according to (3.8) and normalized using (3.9) for each consecutive time window. Time window in Publications IV and V was selected to be

0.5 s with 50% overlap. As a result, time variant SE signals were obtained. Finally, the degree of common temporal changes in SE signals of different recordings was assessed with sample cross-correlations. Cross-covariance,  $C_{S_x S_y}(t, t + \tau)$ , of SE signals  $S_x$  and  $S_y$  describes how well the SE of signal  $y$  at time  $t + \tau$  is correlated with the SE of signal  $x$  at time  $t$ . Cross-covariance at lag  $l = 0$  was calculated as

$$C_{S_x S_y} = \frac{1}{N} \sum_{i=1}^N ((S_{x,i} - \bar{S}_x)(S_{y,i} - \bar{S}_y)), \quad (3.20)$$

where  $\bar{S}_x$  and  $\bar{S}_y$  are the sample means of the corresponding SE signals and  $N$  is the number of time windows in which SEs were calculated. The cross-correlation  $r_{S_x S_y}$  at  $l = 0$  was estimated as

$$r_{S_x S_y} = \frac{C_{S_x S_y}}{\sigma_{S_x} \sigma_{S_y}}, \quad (3.21)$$

where  $\sigma_{S_x}$  and  $\sigma_{S_y}$  are the standard deviations of the corresponding SEs.  $r_{S_x S_y}$  was used as the measure of the level of synchronization, and  $CorSE_{xy} = r_{S_x S_y}$ .

In Publication IV, we estimated synchrony between the recorded locations of rat hippocampus by using a multielectrode probe. First, CorSE was tested with the toy dataset explained in section 3.1.3. Next, the level of synchrony between hippocampal regions was estimated. We provided the information on the locations of the electrodes from the previous works done (Finnerty and Jefferys, 1993; Mikkonen and Penttonen, 2005). Consequently, an interrelation map of three consecutive recordings was formed. In Publication IV, the data were also analyzed with a widely used causality algorithm, partial Granger causality (PGC) (Guo et al., 2008; Luo et al., 2013), for joint evaluation. Granger causality basically describes that  $X$  Granger causes  $Y$  if a prediction error of the future values of  $Y$  made by considering the past values of  $Y$  and the past values of  $X$  together is less than the prediction error made considering only the past values of  $Y$ . PGC extends Granger causality with the existence of common exogenous inputs and latent variables driven by  $Z$ . The corresponding causality algorithm tool which we employed is available online (Granger Causality GUI; Luo, 2015).

Further validation of CorSE was realized with simulations (see section 3.3 for details) and a larger dataset obtained from rat and mouse cortical cells (see section 3.1.2 for details) in Publication V. Data from rat cortical cells were used for evaluating two MEA cultures with different spiking activities and for comparison of the CorSE with three different event synchrony-based methods, which are ES, TE, and MI. Also the data from mouse cortical recordings were analyzed for different measurement days, and their network development was evaluated by using CorSE.

In this chapter, we present the results of the published methods to demonstrate their contributions to the main aims of this thesis. First, the results of the adaptive burst detection algorithm are given. Next, the results of the assessment of spiking behavior and information content of the bursts are presented, and the novel obtainable information, i.e., the spike type composition of bursts and entropy-based measures, respectively, are demonstrated. Finally, we present the results of spectral entropy-based synchrony analysis developments.

## 4.1 Adaptive burst detection

Here, we present the results of detecting bursts in data acquired from hESC-derived neuronal cultures and compare them to the results of the methods described earlier in the thesis. First, we present the variability in spike firing activities of hESC-derived neuronal cultures (Fig. 4.1). Next, to illustrate the problematics and the ISI histograms, two types of data with different burst behaviors are shown in Fig. 4.2, where it can be seen that the logISIH (Pasquale et al., 2010) was able to find well the burst spikes for some kinds of data (Fig. 4.2A), while there also exist data in which logISIH cannot find bursts (Fig. 4.2B), although they clearly exist based on visual observation of the spike time point data. In Fig. 4.2A, the results of logISIH with different thresholds are shown along with the results of the CMA method; the results are seen to be comparable. In the case in Fig. 4.2B, logISIH did not work, and the results are shown for traditional burst detection methods

with different fixed burst defining parameters and for the CMA method; it can be seen that the CMA method produced results better in agreement with visual assessment of the spike time point data. According to our experience, the kind of data seen in Fig. 4.2B is not rare among data measured from hESC-derived neuronal cultures. The most-encountered cases are shown in Fig. 4.3 from which it is clear that there are usually no separable principal and secondary peaks in the logarithmic ISI histograms.

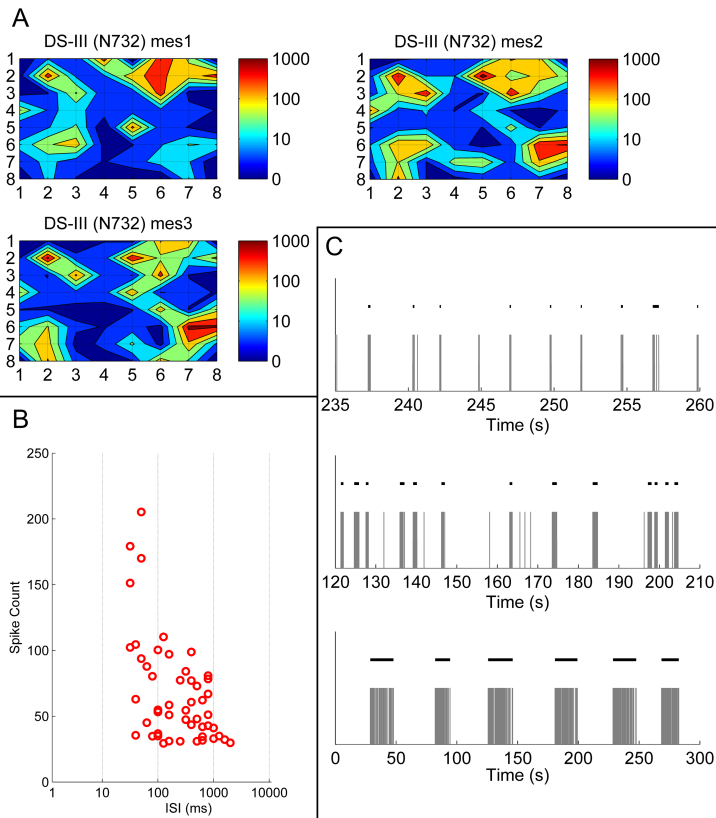


**Figure 4.1:** (A) Colormaps of the spike activities for the measurements obtained from maturing neuronal culture in 22 days (mes1), 27 days (mes2), and 29 days (mes3) *in vitro* (DIV). The corners of the grids represent electrode locations, where the different colors are coded for the number of recorded spikes from corresponding electrodes. (B) Principal peak locations of the calculated logarithmic ISI histograms from different channels of different neuronal cultures. (C) Examples of bursts observed from hESC-derived neuronal recordings showing different firing statistics. (Figure modified from the figures originally published in Publication I.)

To demonstrate that the selection of the burst detection method truly matters to the analysis, the effects of the different methods on the numbers of MEA channels

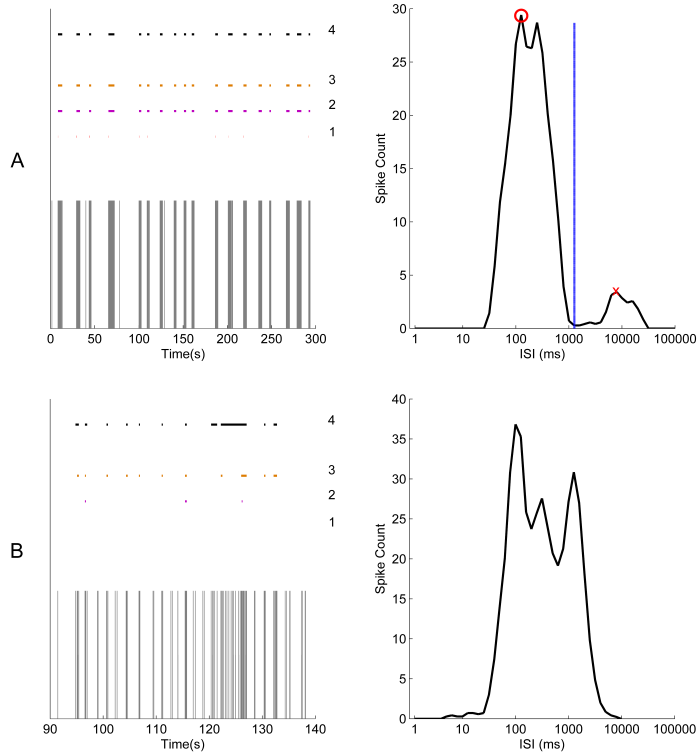


**Figure 4.2:** Exemplary spike time point signals with different burst behaviors (left-hand panels), their burst detection results (left-hand panels), and logarithmic ISI histograms (right-hand panels). (A) Logarithmic ISI histogram (black solid line) which has two well separated peaks: a principle peak (red circle) and a secondary peak (red cross). The minimum point between peaks is found at 1259 ms (blue line). Burst detection results of the logISIH method by employing a pre-defined intra-burst threshold for finding principle peaks at 100, 200, and 1000 ms are labeled in the left-hand panel as 1, 2, and 3 respectively. The result of the CMA algorithm is labeled as 4. (B) Logarithmic histogram (black solid line) which does not have well separated peaks. Burst detection results by employing a threshold for intra-burst spikes of 100 ms with at least 10 spikes in a burst, 100 ms with at least three spikes, and 200 ms with at least three spikes are labeled in the left hand panel as 1, 2, and 3 respectively. The result of the CMA algorithm is labeled as 4. (Figure modified from the figures originally published in Publication 1.)

exhibiting bursts found in our data are presented in Table 4.1. It is clear from Table 4.1 that the amount of data available for subsequent burst analysis is dictated by the selected method. Here only data exhibiting sufficient spiking activity was analyzed, i.e., only the recordings from every channel from all measurement days and all data sets which exhibited over 50 spikes at least in one of the measurements of approximately 300 s were utilized.

The CMA algorithm was applied also on recordings with different ISI histogram

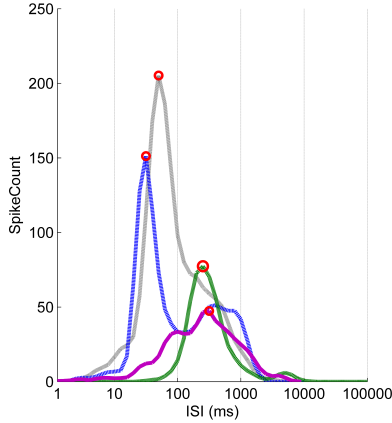


**Figure 4.3:** The logarithmic ISI histograms and their principal peak locations for the data selected to illustrate the different commonly encountered cases. Histograms with two well separated peaks (blue and green), with only one peak and no local extrema (gray), and with local extrema which cannot be separated well (purple) are typical for ISIs of hESC-derived neuronal recordings. (Figure modified from the figures originally published in Publication I.)

**Table 4.1:** The number of burst-exhibiting channels found by different methods. Five different data sets (Data 1, Data 2, Data 3, Data 4 and Data 5) were used from 27 MEAs (see Publication I).

		Data 1	Data 2	Data 3	Data 4	Data 5
Number of recordings with over 50 spikes/Total number of recordings		12/18	47/93	76/117	14/27	41/86
Numbers and percentages of burst-exhibiting channels found by different burst detection algorithms	CMA algorithm***	7 (39%)	57 (61%)	78 (67%)	13 (48%)	46 (53%)
	logISIH(100ms threshold)*	6 (33%)	13 (14%)	49 (42%)	10 (37%)	16 (19%)
	10 spikes with $ISI < 100\text{ms}^*$	1 (6%)	0 (0%)	9 (8%)	1 (4%)	1 (1%)
	5 spikes with $ISI < 100\text{ms}^{**}$	3 (17%)	6 (6%)	28 (24%)	2 (7%)	5 (6%)
	3 spikes with $ISI < 100\text{ms}^{**}$	8 (44%)	18 (19%)	55 (47%)	10 (37%)	18 (21%)
	3 spikes with $ISI < 200\text{ms}^{**}$	12 (67%)	32 (34%)	64 (55%)	13 (48%)	27 (31%)
	logISIH(200ms threshold)**	12 (67%)	28 (30%)	57 (49%)	12( 44%)	24 (28%)

\* Previously proposed burst detection method.

\*\* Methods modified from previously proposed burst detection methods.

\*\*\* Novel burst detection method.

skewnesses and for different types of data to observe its performance (Fig. 4.4). As a result of the CMA algorithm, bursts of different types were detected and thus available from the different experimental setups for further analysis.

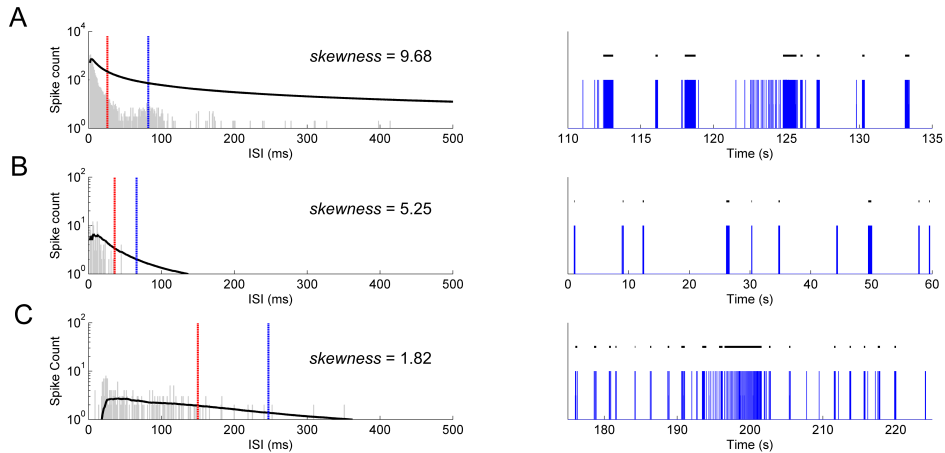


**Figure 4.4:** Burst detection results of the CMA algorithm for differently behaving networks. Recordings shown in the right panels of (A), (B), and (C) exhibit different skewness values. The ISI histograms (gray bars), CMA curves (black lines), and the thresholds for the burst and burst-related spikes (red and blue respectively) are shown in the left panels. Skewness values are given along with the histograms. A logarithmic scale is used for the vertical axis for a better visualization. Detected bursts are labeled with black lines (right panel). (A) Recording from a mouse cortical culture. (B) Recording from a rat cortical culture. (C) Recording from a hESC-derived neuronal cell culture.

## 4.2 Spike behavior and information content during bursts

Here, the results of burst analysis are presented for analyzing both the spike type compositions (Publication III) and the information content of the bursts (Publication II). For the burst spike type composition analysis, bursts were detected adaptively as proposed in Publication I and described in section 3.4.2.

### Analysis of spike type compositions of bursts

Spike type compositions of bursts were analyzed from the data recorded from hESC-derived neuronal cell cultures during a multi-phase pharmacological study. After spike sorting, the individual spikes were classified resulting in four different spike types, denoted as Spike-I, Spike-II, Spike-III, and Spike-IV, which are shown in Fig. 4.5 for the different phases of the pharmacological experiment. Then the joint analysis proposed in Publication III described in section 3.4.2 was employed. Fig. 4.6 presents the results obtained from one channel of MEA: burst information and individual spike activities are presented as well as contributions of different

spike types to the bursts.

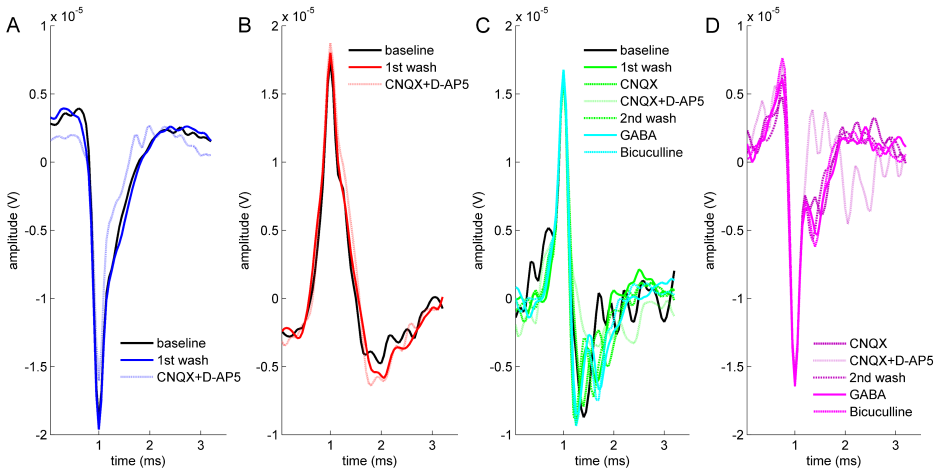


**Figure 4.5:** The average spike waveforms for each phase of the pharmacological experiment. (A) Spike-I, (B) Spike-II, (C) Spike-III, (D) Spike-IV. (*Reprinted from Publication III, with permission from Elsevier.*)

To demonstrate the results of the joint analysis, for example, spike type compositions of bursts seen in the baseline and spike type compositions under CNQX + D-AP5 application can be compared. Baseline bursts were composed merely of spikes of types Spike-I and II (Fig. 4.6E), whereas in the later phase of the experiment, i.e., under CNQX + D-AP5 application, the bursts were composed mostly of spikes of type Spike-II, and the second wash nearly abolished bursting (Fig. 4.6B-D). However, the results were totally different under the influence of GABA and subsequently bicuculline: The bursts were composed merely of spikes of types Spike-III and Spike-IV. Thus, the joint analysis of spike types and bursts (Fig. 4.6E and F) provided more information on the network effects of pharmacological treatment than the traditional burst analysis alone (Fig. 4.6B-D).

To emphasize the new information given by the proposed joint analysis more apparently, for example, in Fig. 4.6A it is seen that after the first wash, there was an obvious decrease in the occurrence of Spike-I type spikes and a slight decrease in the number of Spike-II type spikes, whereas simultaneously the number of bursts more than doubled compared to the baseline (Fig. 4.6B). Accordingly, for the same experiment phase, the joint analysis results in Fig. 4.6E show a notable increase in the burst participation of Spike-I type spikes and a slight increase in the burst participation of Spike-II type spikes. Collaborative findings can be observed in the percentage amounts of the spikes of these types appearing in bursts compared to

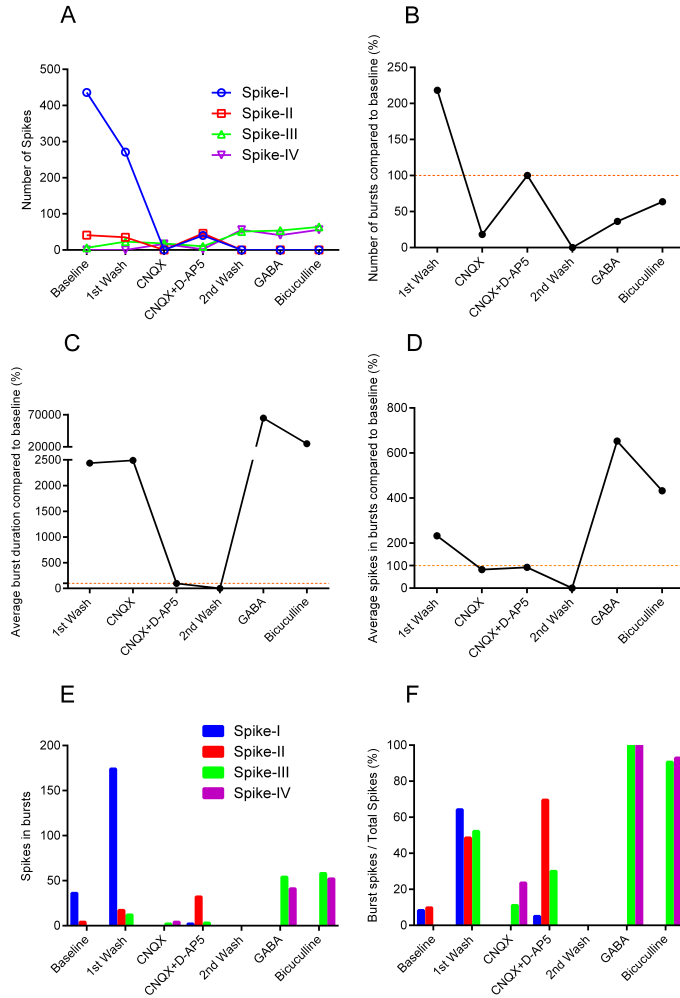


**Figure 4.6:** The results of the traditional spike and burst analysis (A-D) and the joint analysis (E and F) at all phases of the pharmacological experiment for one MEA channel. Orange dashed lines in panels (B-D) present the level of baseline values. (A) The numbers of different types of spikes. (B) The relative numbers of bursts. (C) The relative average durations of bursts. (D) The relative average numbers of spikes in a burst. (E) The numbers of spikes of each type in bursts. (F) The numbers of each type of spikes in bursts relative to the total numbers of spikes. The relative quantities are with respect to the corresponding values at the respective baselines. The spike types: Spike-I (blue), Spike-II (red), Spike-III (green), Spike-IV (purple). (*Modified from Publication III, with permission from Elsevier.*)

the total spike counts (Fig. 4.6F). This information on the changes in the burst participation of the different types of spikes cannot be obtained by the traditional analysis results in Fig. 4.6B-D.

Also, new information provided by the joint analysis can be shown by observing the activity in Fig. 4.6A after the CNQX + D-AP5 application when the number of Spike-II type spikes recovered to the approximately same level as it was at the baseline. Spike-I type spikes also recovered approximately to the same level as Spike-II type spikes, remaining still at a lower count than at the baseline, however. For the same phase of the experiment, the number of bursts, average burst durations, and the average numbers of spikes in bursts were close to what they had been at the baseline (Fig. 4.6B-D respectively). At this point of the experiment, the joint analysis results in Fig. 4.6E demonstrate that the bursts were mostly composed of Spike-II type spikes, whereas at the baseline, the burst spikes had been mainly Spike-I type spikes. Briefly, although the traditional burst characteristics (Fig. 4.6B-D) were approximately the same at the baseline and after the CNQX + D-AP5 application, the joint analysis exposed that the main spike type composition was different between these two experiment phases. This information on the burst composition change cannot be obtained from the results of the traditional analyses in Fig. 4.6A and B, but only with the proposed joint analysis. In conclusion, the results showed that the novel joint analysis method would provide new information on the contents of bursts that we could not obtain by only using traditional burst analysis methods.

## Information content-based burst analysis

Bursts were also analyzed based on their information content quantified with different entropy measures: The results of SE-based analysis represented the quantified spectral uniformity of the bursts, whereas SmpE quantified their self-similarity. Fig. 4.7A presents a recording of 20 s from which bursts were detected with automated burst detection and the corresponding entropies, SmpE and SE, were calculated for every 0.5 s with 50% overlapping. In Fig. 4.7A, SmpE gives different entropy values for the two different bursts around the 70th time bin, whereas SE is approximately the same for both bursts according to visual observation of Fig. 4.7A. However, another sample recording is illustrated in Fig. 4.7B, where SE values are different for the differently behaving bursts as well.

The entropy values obtained from nine bursts detected from an exemplary 200 s recording (Fig. 4.8A) are shown in Fig. 4.8B. The normalized entropy values are

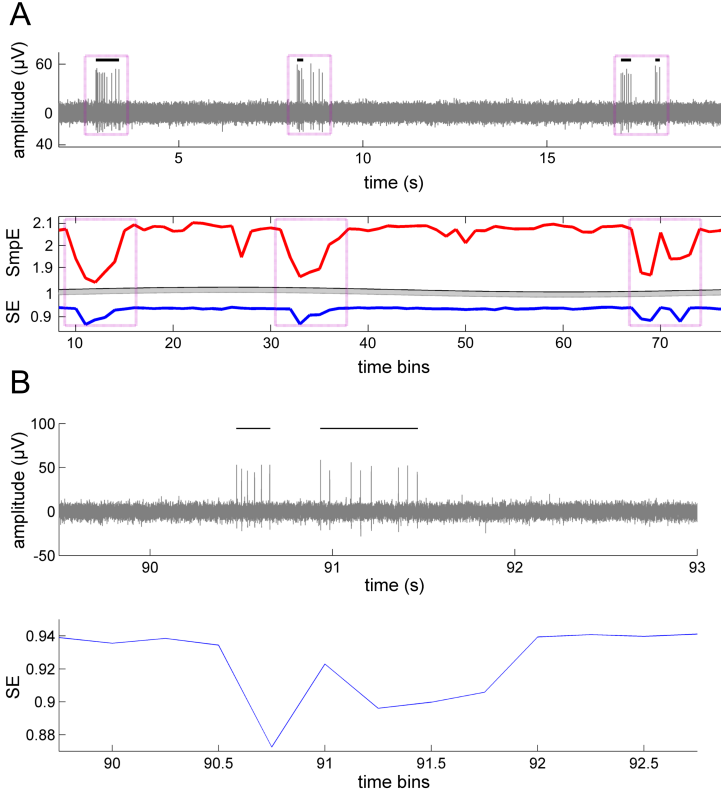


**Figure 4.7:** (A) A signal with bursts detected with the automatized burst detection algorithm. Bursts are labeled with black horizontal lines above the signal. SmpE (red) and SE (blue) values in the lower panel were calculated for the signal seen in the upper panel using 0.5 s long 50% overlapped bins. (B) A short sequence from a neuronal recording with the detected bursts (upper panel) and the time variant SE signal calculated from the recording (lower panel). (*Modified from Publications II and IV, with permission from IEEE.*)

shown along with the normalized burst parameters (Fig. 4.8B) for the nine bursts detected from this recording. The SmpE values for these bursts seem to correlate with the burst durations and the number of spikes in these bursts, whereas no such correlation can be observed for the SE values.

Spatial distributions of burst SEs and SmpEs are illustrated in Fig. 4.9 for a MEA recording of a rat cortical cell culture. Briefly, the medians of the entropy values were calculated from the bursts and presented in colormaps. Although the SE and SmpE values are different, the results from both entropies indicate that the maximum values are at the electrodes (2, 4) and (8, 7). In Fig. 4.9, similar to Fig. 4.8B, the differences between the bursts were more pronounced based on

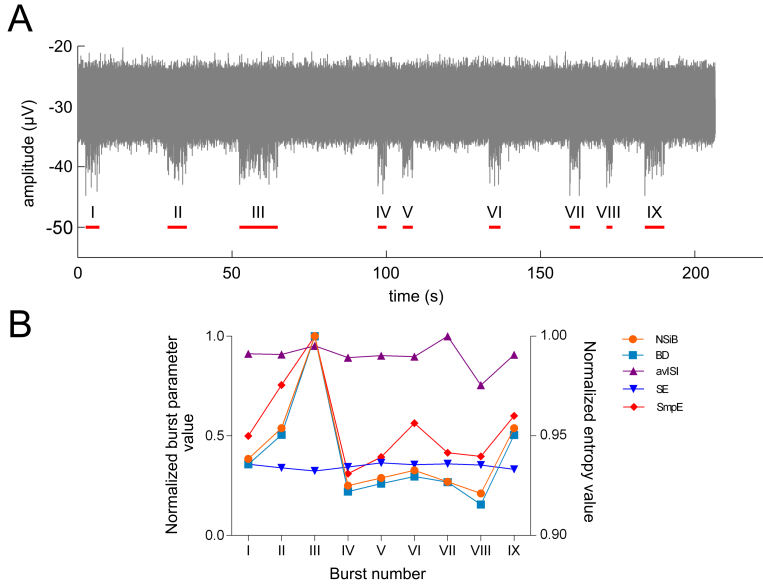


**Figure 4.8:** (A) A signal with the bursts detected with the automatized burst detection algorithm. The detected bursts are labeled with red lines. (B) SmpE (red) and SE (blue) values calculated for the nine bursts see in panel (A). Entropy values and burst parameters are normalized between 0 and 1. Burst durations (BD), the number of spikes in bursts (NSiB), and average ISI (avISI) are shown for the same nine bursts. Horizontal axis labeling in (B) identifies the bursts as numbered in (A). (*Modified from Publication II, with permission from IEEE.*)

the SmpE values than the SE values. Additionally, the spatial analysis of the *in vitro* experiments showed that channels with high median SE and SmpE values (Fig. 4.9) had neighboring channels with higher SE or SmpE values than on the MEA in general.

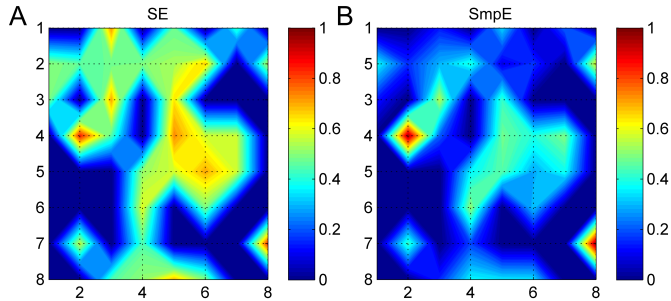


**Figure 4.9:** (A) Colormaps of the medians of the (A) SE and (B) SmpE values calculated for every burst from each channel of a 60-channel MEA. The grid intersections indicate the locations of the electrodes with the exception of the corners where there were no electrodes. (*Reprinted from Publication II, with permission from IEEE.*)

In conclusion, the results showed that entropy-based measures, particularly SmpE, could quantify bursts with different features, such as number of spikes, and durations. On the other hand, SmpE and SE are both feasible for quantifying bursts from different channels for spatial analysis.

### 4.3 Spectral entropy-based synchrony analysis

In Fig. 4.10, the ability of SE to locate the types of bursts is illustrated: ones that are composed of very high-amplitude spikes (over  $100\mu\text{V}$ ) (Fig. 4.10A) and the other that are mostly buried inside background noise (Fig. 4.10A and B). Synchronized bursting is shown inside red dotted boxes based on visual examination. This is an exemplary result of the use of SE in detecting possibly synchronized channels; the results indicate that a SE signal could present characteristics of the recording without depending greatly on the burst or background noise amplitudes.

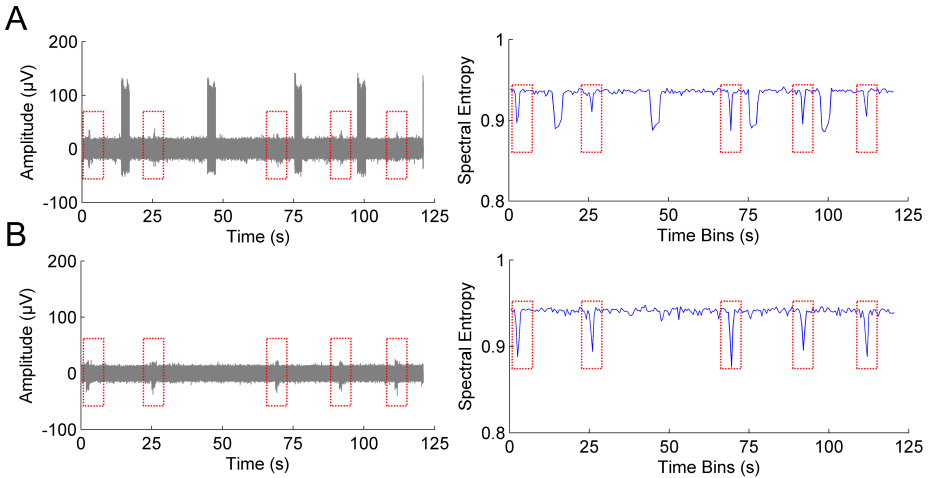


**Figure 4.10:** Exemplary 120 s long recordings from two neighboring MEA channels along with their corresponding time variant SE signals. (A) A MEA signal channel with two different types of activity: one with higher amplitudes and the other buried in background noise. (B) A MEA signal from a channel adjacent to that seen in (A) with lower amplitude spike bursts. The red boxes indicate the synchronized bursts based on visual examination.

The feasibility of the CorSE was first shown in Fig. 4.11 with a small toy data set extracted from rat hippocampal recordings as explained in section 3.1.3. CorSE distinguished the channels with higher correlated SEs from the neighboring channels of the same recording sequence as expected (Fig. 4.11A), and the results correlated with the causalities calculated using PGC for the same toy data set

(Fig. 4.11B).

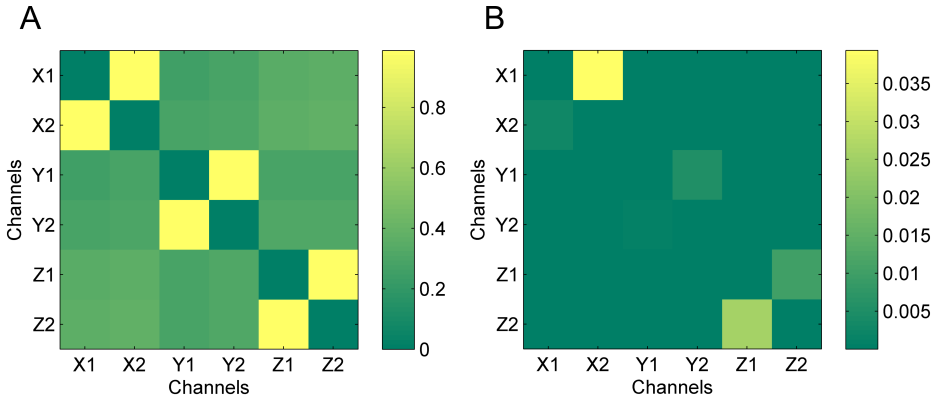


**Figure 4.11:** (A) Correlation results for the small data set calculated based on time variant SEs. (B) PGCs for the same data set. Channels from the same recordings are named with the same variable names, i.e.,  $(X1, X2)$ ,  $(Y1, Y2)$ , and  $(Z1, Z2)$ . (Reprinted from Publication IV, with permission from IEEE.)

Additionally, complete rat hippocampal recordings of fourteen channels from three sequential Michigan probe recordings were analyzed, and interrelation maps were plotted according to the CorSE values (Fig. 4.12), where only the relations with  $CorSE > 0.8$  are shown, with the relations with  $CorSE > 0.9$  indicated by red or blue as also shown on the measurement probe illustrations (Fig. 4.12A-C). The probe and electrode locations in the hippocampus are illustrated in Fig. 4.12D. In each measurement (Fig. 4.12A-C), two different groups were identified based on the strongest relations ( $CorSE > 0.9$ ). However, these two strong groups also had weaker relations with each other. Actually, the interrelation maps (Fig. 4.12A-C) clearly indicate two separate connected groups which correspond to the anatomical regions CA1 and CA3 of the hippocampus (Fig. 4.12D). Additionally, the analysis revealed that the strongly connected group in the CA3 region was expanding as the experiment proceeded, which was probably due to the effects of electrical stimulation during the experiment. Briefly, the strongest groups in the map ( $CorSE > 0.9$ ) were seen to expand, and the weaker correlations ( $CorSE < 0.9$ ) were also seen to get stronger.

Further validation of the method was realized with simulations and a larger dataset. Accordingly, we employed the CorSE on three populations of the toy model, 1, 2, and 3, as explained in section 3.3 and shown in Fig. 3.2. Results were considered successful if and only if the correlation between the synchronized populations ( $CorSE_{(1,2)}$ ) was higher than the correlations between each of those

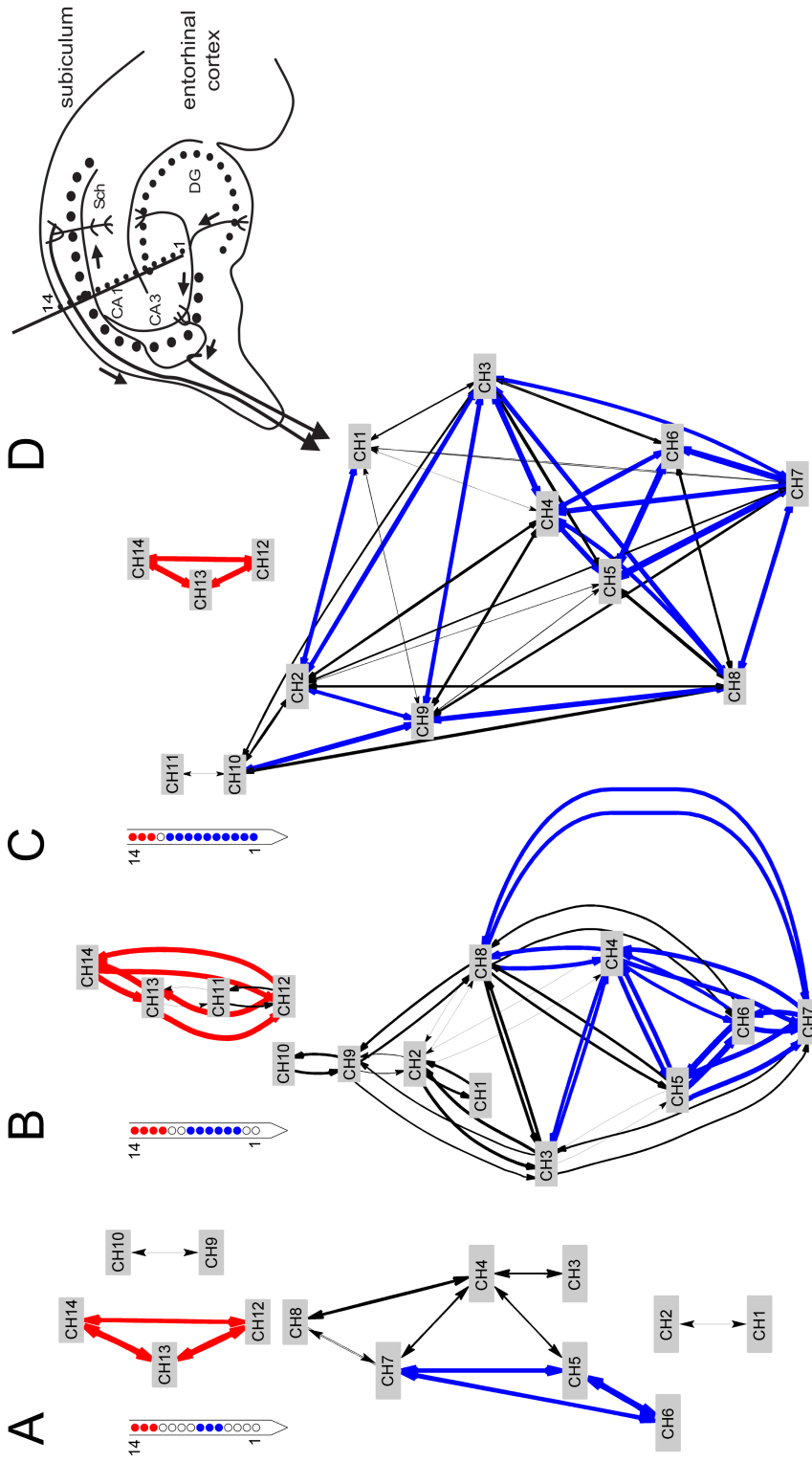


**Figure 4.12:** (A)-(C) The interrelation maps based on the stronger correlations ( $CorSE > 0.8$ ) found in the three sequential *in vivo* measurements by CorSE. Line width indicates correlation strength. The strongest correlations ( $CorSE > 0.9$ ) are indicated by blue or red, and the corresponding electrodes with the same colors on the schematic illustrations of the electrode shafts. The results for one measurement are presented in each panel (A)-(C). (D) A schematic illustration of the rat hippocampus with the locations of channels 1 and 14 with the hippocampal regions indicated (Sch-Schaffer collaterals, DG-dentate gyrus). (Reprinted from *Publication IV*, with permission from *IEEE*.)

and the third population ( $CorSE_{(1,3)}$  and  $CorSE_{(2,3)}$ ) (Table 4.2). CorSE was successful for this task.

**Table 4.2:** The results of the analysis of the signals from the toy model with different EAP-LFP power ratios. Successful detection of synchronized populations is observed when  $CorSE_{(1,2)} > CorSE_{(1,3)}$  and  $CorSE_{(1,2)} > CorSE_{(2,3)}$  simultaneously, i.e., when CorSE of the connected populations is higher than the CorSE of both unconnected population pairs

Ratio of EAP-LFP power	Number of successes/1000 simulations
$P_{EAPs/LFPs} \approx 100\%$ (only EAPs)	998
$P_{EAPs/LFPs} \approx 50\%$	979
$P_{EAPs/LFPs} \approx 20\%$	971
$P_{EAPs/LFPs} \approx 10\%$	967
$P_{EAPs/LFPs} \approx 0\%$ (only LFPs)	995

Next, we evaluated synchronization according to the different connectivity levels simulated with integrate-and-fire model-based networks. The results were also compared with the other considered algorithms that were previously explained in section 3.4.4. Fig. 4.13A presents the synchronizations calculated from the artificial recordings with only EAPs. All the algorithms distinguished the different levels of connectivity except for the connectivity strengths of 50% and 100% where CorSE was the only method showing an increase in the synchrony when connectivity increased from 50% and 100%.

The results from combinations of EAPs and LFPs with different EAP and LFP power ratios for the two connected populations can be seen in Fig. 4.13B and C. Spike detection rates decreased with the increasing power of LFPs (see Publication V), which greatly affected the performances of the algorithms which depended on spike detection. With the added artificial LFPs, the synchronizations assessed with event-based algorithms were significantly decreased. Also, the correlation between the increased level of connectivity and the increased synchrony was not always retained. The results indicate that spike detection performance has a strong influence on the synchronicity results of the event-based algorithms as expected. On the contrary, although the synchrony values of the artificial recordings measured with CorSE changed with the superimposed LFPs, correlation between the increased synchrony and the increased level of connectivity was to some extent preserved. Fig. 4.13D and E show the synchronicities calculated from the recordings

with EAPs and added WGN. Adding WGN greatly decreased the synchronization detected by the event based algorithms. On the other hand, to compare, cES presented better performance in distinguishing the relation between the increasing levels of connectivity and synchronization. CorSE cannot distinguish the different levels of connectivity especially with the lower signal-to-noise ratio (SNR); however, was still able to distinguish the unconnected populations (0% level connectivity) from the connected populations.

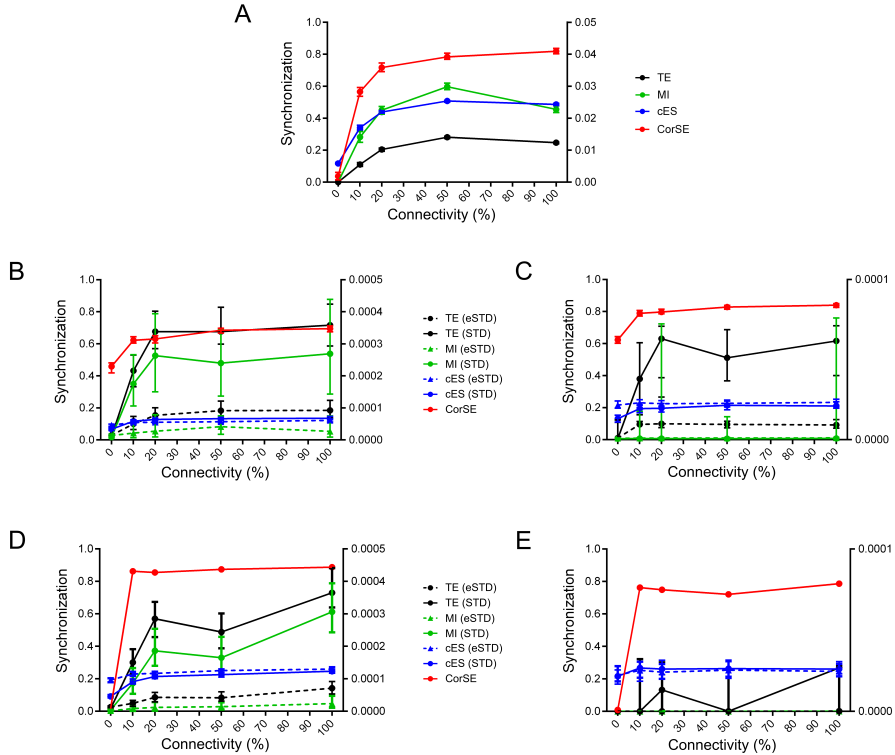


**Figure 4.13:** The synchronizations calculated by the CorSE (red) and cES (blue) methods from the artificial recordings with only EAPs (left vertical axis). The synchronizations calculated by the TE (black) and MI (green) methods from the artificial recordings with only EAPs (right vertical axis). For the event-based methods, the line types indicate the spike detection method used: STD (solid) and eSTD (dashed). (A) The synchronizations calculated with only EAPs. (B) The synchronizations calculated with both EAPs and LFPs with  $P_{EAPs/LFPs} \approx 50\%$  for one population and  $P_{EAPs/LFPs} \approx 20\%$  for the other. (C) The synchronizations calculated with both EAPs and LFPs with  $P_{EAPs/LFPs} \approx 20\%$  for both populations. (D) Synchronizations calculated with EAP and added WGN with  $SNR = 50\%$ . (E) Synchronizations calculated with EAP and added WGN with  $SNR = 20\%$ . (Reprinted from Publication V.)

More results are presented in Publication V regarding the performances of

CorSE and the other compared algorithms for the analysis of real MEA data obtained from rat cortical neuronal cultures.

Finally, we evaluated the performance of CorSE on MEA recordings collected from mouse cortical neuronal cell cultures. Fig. 4.14 presents the development of an *in vitro* neuronal network between the 13th and 29th DIV. Pairwise channels which have  $CorSE > 0.5$  are used to illustrate the network. The first links were seen on the 13th DIV, and then the network gradually expanded while also synchrony between all the channels got stronger: the strongest synchronizations in the network were measured on the 22nd DIV (Fig. 4.14). The mean values of synchronizations between all the channels (1770 links in total) are calculated and presented for the measurement days in Fig. 4.15. The mean values of all synchronizations were also correlated with the number of synchronizations greater than 0.5; in other words, the overall network synchrony followed the same trend with the synchronizations calculated from channel pairs with  $CorSE > 0.5$ . Synchrony between some channels varies for different measurement days. A noteworthy example for such a case is seen following the development from the 25th DIV as a smaller network appeared, disappeared, and reappeared (Fig. 4.14). Choosing an arbitrary synchrony value, i.e.,  $CorSE > 0.5$ , and applying it as a clear-cut threshold would affect the temporary appearance and disappearance of some channels in the network development map in Fig. 4.14; however, the results calculated using the arbitrarily chosen threshold also correlated with the overall network behavior (Fig. 4.15). Moreover, the overall network development seen in Fig. 4.14 and Fig. 4.15 could be considered biologically plausible during the entire experiment.

In conclusion, the results show that by using CorSE the synchrony of different types of neuronal networks can be assessed without facing the shortcomings of event-based methods resulting from possible poor event, e.g., spike, detection performance.

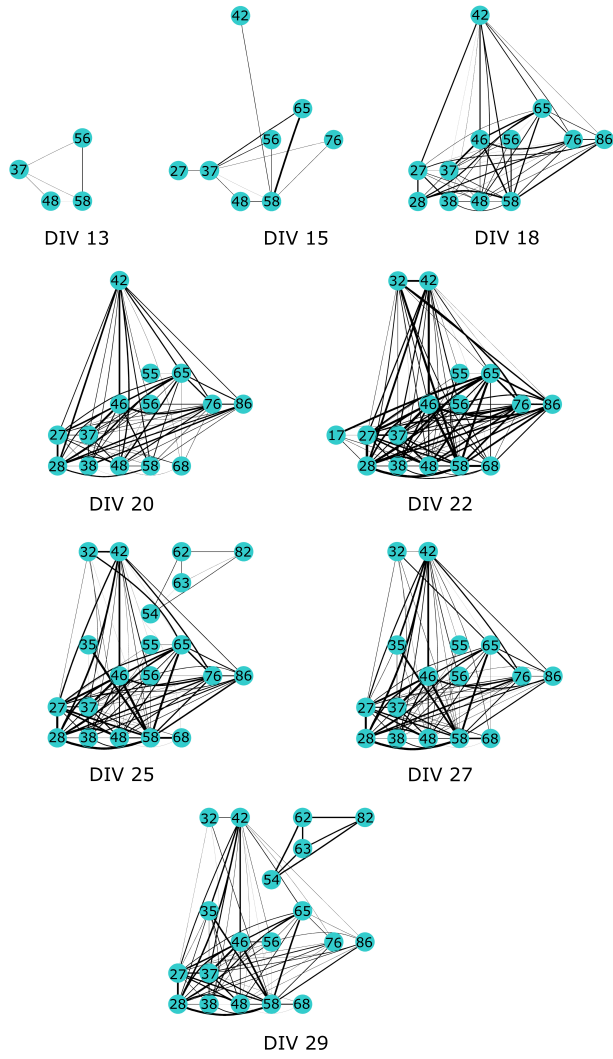


**Figure 4.14:** The development of a network in cultured mouse cortical cells between the 13th and 29th DIV determined using CorSE. Channels with synchronizations  $CorSE > 0.5$  are taken to constitute the network. (Reprinted from Publication V.)

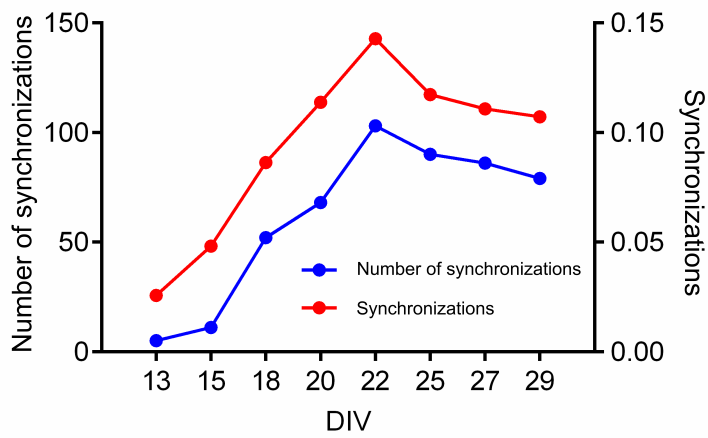


**Figure 4.15:** The synchronizations between all the channels and the numbers of synchronizations with  $CorSE > 0.5$  for a developing mouse cortical cell culture. The mean values of the synchronizations between all channels (1770 links in total) (red) along with the numbers of synchronizations (blue) with  $CorSE > 0.5$  are presented with respect to the DIV. (*Reprinted from Publication V.*)

To describe the entire content of the work done in a nutshell: First, we aimed to detect neuronal bursts without any predefined or fixed criteria. Then, we proposed metrics to quantify the adaptively detected bursts and also devised a novel analysis method to jointly study detected bursts and their spike types. Finally, we proposed a synchronicity algorithm to evaluate the interrelations of the population activities.

In our first work (Publication I), the research question resulted from the previously employed different definitions of AP bursts. Our results showed that it was not feasible to employ a predefined fixed burst criteria on the recordings which exhibited different firing behaviors such as hESC-derived neuronal cells. We were initially motivated particularly by the behavior and the problematic analysis of functional neural networks of hESC-derived neuronal cells, but our adaptive burst detection algorithm, i.e., CMA, is applicable to any neuronal cell recording (cf. Fig. 4.4). We compared CMA with existing methods in Publication I. Methods which we employed in Publication I for comparison were using fixed ISI thresholds, e.g., as in Chiappalone et al. (2005), or adaptive algorithms, e.g., logISIH (Pasquale et al., 2010) for burst detection. In addition to Publication I, Cotterill et al. (2016) compared CMA with other adaptive methods such as logISIH (Pasquale et al., 2010), ISI Rank Threshold (Hennig et al., 2011), Poisson Surprise (Legendy and Salcman, 1985), Rank Surprise (Gourévitch and Eggermont, 2007), Robust Gaussian Surprise (Ko et al., 2012), Hidden Semi-Markov Model (Tokdar et al., 2010), and MaxInterval method (Neuroexplorer manual, NEX Technologies). According to the comparisons by Cotterill et al. (2016), and in Publication I, CMA is prefer-

able among the other burst detection methods for the cases where one can not set appropriate burst detection parameters or distinguish between inter- and intra-burst ISIs. According to our experiences, such conditions are frequently observable for developing neuronal cell cultures.

We also showed that one can increase the amount of burst data for subsequent analyses by using the CMA algorithm. The actual advantage of the CMA algorithm was exposed for the data which likely contained bursts not detectable by the traditional methods, e.g., hESC-derived neuronal cell cultures. Table 4.1 presents how much burst data could be extracted by using the CMA algorithm and other methods. To clarify, the results presented in Table 4.1 are not concerned with the superiority of any detection algorithm by means of accuracy but demonstrate the ability of the CMA to produce more results for further evaluation. Since the bursts were defined without any predefined limitations comparable to the conventional criteria, the accuracy was considered more as an issue of statistical consistency. In other words, the parameters obtained from falsely detected bursts were expected to be seen as outliers while analyzing the parameters derived from adaptively detected bursts. Also, adding limitations and criteria after burst detection (post hoc screening) is always possible for the studies which desire to assess certain types of bursts. Consequently, freely defined bursting behavior enables studying the bursts with different parametric values. On the other hand, the major limitation of CMA was stated by Cotterill et al. (2016) as its tendency to erroneously detect a large amount of bursting activity in sparsely bursting spike trains. Cotterill et al. (2016) indicated, as we had proposed in Publication I, that post hoc screening and restricting the max ISI to within a biologically plausible range would be needed to solve this issue.

In Publication III, we proposed a novel analysis method for studying the single units of the neuronal network activity. We applied our method to analyze the chemical modification of neuronal networks. For that, bursts were studied jointly with their spike type compositions, providing a new view to the bursts, and a new kind of information, i.e., **the spike type compositions of the burst** or, in other words, **burst participations of different types of spikes**, was obtained. The proposed method was applied on data from hESC-derived neuronal cultures during a pharmacological experiment.

Briefly, such analysis provides an information gain similar to that of observing a string of letters formed from the alphabet of the size equal to the number of the spike types plus one (each letter corresponding to a spike type and a symbol '0' to denote 'no waveform') vs. a binary string ('1' corresponding to a de-

tected spike). For example, in a recording with three detected non-overlapping spike waveform types denoted A, B, and C, e.g., a burst would be observed as ‘00A0B0000A0CC’, whereas the same burst will be observed with only spike detection as ‘0010100001011’ (for the example here, only a few 0s are shown). The information gain would then result from the information content of the burst accordingly. For the binary alphabet with equal symbol probabilities, the information content is  $\log_2 2 = 1$  bit per symbol, whereas an alphabet of size four with equal symbol probabilities results in the information content of  $\log_2 4 = 2$  bits per symbol (Shannon, 1948). Certainly, spike sorting alone provides the same amount of information per spike waveform, but with the proposed joint analysis this information is extracted specifically for each burst. For a real MEA recording, the probability of an occurrence of the ‘no waveform’ symbol is much larger than that of a symbol denoting a spike; thus, the information contents of the spike symbols are larger than in the example, but the principal difference between the two approaches remains. Consequently, the information gain achievable through the analyses of the spike type waveforms themselves, their changes, and their occurrences in time, compared to the analysis of mere time stamps of the burst spikes, depends on the following neurobiological analysis, and the associated information gain is not simply formally quantifiable.

Since the analysis method is based on the joint application of spike sorting and burst detection, any weaknesses of the employed spike sorting and burst detection algorithms will be reflected in the final result. Generally, the effect of overlapping spikes during frequent spike activity (here bursts) on the spike sorting algorithms is crucial (Lewicki, 1998; Quiroga et al., 2004; Wild et al., 2012). The results should be evaluated with the effects of overlapping spikes in mind. In our case, in Publication III, spike sorting was used to cluster average waveforms from multi-units, and representative waveforms were utilized for the assessment of the neuronal responses to external manipulation. Thus, average waveforms would represent the general activity of the neurons near the electrode, and overlapping spikes could be averaged out if the number of spikes was high enough. In fact, according to our results, even though the effects of overlapping could be seen in our analysis, they did not have major effects on our results nor changed our overall conclusions.

Another issue which was encountered in Publication III is the effect of high variability during the analysis of pooled data which consist of all the electrodes in a well. Such analysis done with pooled data naturally does not provide information from single units or more local sub-populations but more on general behaviors of the network. Alternatively, to benefit from the proposed joint analysis in future

studies, single channel-based joint analysis employed in Publication III can be expanded to analyze the entire MEA. For that, each channel can be analyzed separately, and corroborative results from different channels can be assessed to draw overall conclusions. However, expanding the analysis to the entire culture requires developing a valid method where localized information can be employed to reveal the spatial distributions of the different types of spikes composing the bursts. This analysis technique would be promising, e.g., for tracking spike waveforms and their network participations. For such cases, HDMEA measurements would be more promising since the spatial resolution is high enough to be able to record the same spike activity with multiple electrodes.

In summary, the proposed joint analysis reveals information on the burst activity which is not obtainable by the traditional analysis alone. On the other hand, investigating the actual biological sources of the newly acquired information via joint analysis requires detailed studies with in-depth neuronal network analysis providing information on the sources of spike waveforms, including information on active neuronal types and cell compartments.

Joint analysis was not the only method we proposed to enhance the information obtained from neuronal bursts. We also proposed evaluating the information content of the bursts to obtain new metrics by applying different entropy measures. Reliable metrics to quantify or classify bursts, in addition to the conventionally used ones, would enrich the information and be highly desirable (Johnstone et al., 2010). In addition to the adaptive detection of bursts, which enables detecting bursts of different types, a further classification could be done according to the desired parameters. We showed that self-similarity (quantified by SmpE) and spectral uniformity (quantified by SE) are promising metrics for such classification. In Publication II, the entropy-based measures calculated different features of the bursts. For our data, both entropy measures were good at reflecting the changes in neuronal recordings during bursts. In particular, SmpE was more sensitive to the burst duration and the number of spikes in bursts and produced more distinct values for the presumably different kinds of bursts compared to SE. We also compared entropy based metrics with the conventionally used metrics, i.e., burst duration, number of spikes in bursts, and average ISIs, e.g., as used by Keefer et al. (2001), and Hayar and Ennis (2007). SmpE would also reflect features similar to conventional burst parameters, such as burst duration, number of spikes in bursts, and average ISIs in bursts, at least in some cases (Fig. 4.8). These results would actually indicate that different features from the same burst would correlate according to the data type analyzed. Thus, every distinct feature which can be obtained from the data would

initially increase the dimension of clustering and potentially classification efficiency. However, a larger data set or preferably a specifically tailored experimental setup would be needed to reveal the real potential of entropy-based measures.

In addition to quantify bursts, entropy-based measures would be assessed spatially to reveal network relations. Fig. 4.9 showed that there were similarities between the burst entropies of neighboring locations; thus, interrelations between the bursts of nearby channels can be assessed by means of entropy measures. We also showed that such sort of spatial relations can also be revealed by time variant SE signals (Fig. 4.10) and is studied further in Publication IV.

In Publication IV, we have studied the spatial functional interrelation based on the correlations of entropy measures in time. For that, *in vivo* rat hippocampal recordings were analyzed. The experimental setup used provides good demonstration data since the neuronal pathways in the hippocampus are known (Amaral and Witter, 1989; Mikkonen and Penttonen, 2005), providing expected connectivity. Correlations over a threshold were tracked to assess the time courses of the interrelations. The results showed a clear interrelation between the CA1 and CA3 regions of the hippocampus; moreover, the synchronization became stronger during the stimulation experiment particularly in the CA3 network, which was probably due to the effects of electrical stimulation (see section 3.1.3 for the experimental setup). Even though we did not validate the results of the proposed method in this study with biological controls, the causality algorithm also provided corroborative results with the proposed method, especially with the toy data. Although Publication IV showed that CorSE has potential to assess neuronal interrelations, the justification of the method that was sought after came with known neuronal networks and simulated data in the subsequent publication.

In Publication V, CorSE was justified for the assessment of synchrony with simulations and a larger data set obtained from rat and mouse cortical cell cultures. Initially, a simple computational model was created where neuronal activity was defined in terms of the number of oscillations equal to the number of neuronal ensembles participating in the population activity. In such a model, neuronal synchrony between populations was defined as simultaneous activity of neuronal ensembles in a simple way: When a number of neuronal ensembles activated in a population, the same number of neuronal ensembles also activated in the other population, since the model assumed that all neuronal ensembles in one population were connected to ensembles in the other population. As a result, CorSE showed over 96% success in distinguishing the fully synchronized populations from the unsynchronized population in this simple model. Additional simulations were also

made based on computational integrate-and-fire model neuronal networks. CorSE was employed on the data produced with the model and statistically validated. The model was formed based on the assumption that an increase in neuronal synchrony correlated with an increase in neuronal connectivity.

We also compared CorSE with other algorithms, i.e., cES (modified version of ES (Quiroga et al., 2002)), MI (Gray, 1990) and TE (Schreiber, 2000). The results indicated that CorSE and other event-based methods could distinguish the different levels of connectivity by estimating the synchrony between populations. On the other hand, the main advantage of CorSE over the event-based methods was revealed while working on synchronized LFPs and when EAPs did not exist or could not be detected accurately. In such cases, by using CorSE, the level of synchrony was somewhat preserved, and the correlation between the increasing synchrony and connectivity was still distinguishable to some extent. Simulations also showed that even with increasing noise it was still possible to distinguish between the connected and unconnected populations with CorSE, even though the level of connectivity strength was not distinguishable anymore. Thus, CorSE is an advantageous tool for the cases where one could not rely on the accuracy of spike detection.

In summary, we validated CorSE with simulation models and demonstrated its applicability with real recordings. For example, CorSE was successfully employed in the assessment of mouse cortical cell network development *in vitro*. The method exposed network development by calculating synchrony values and detecting functional connectivity using a fixed synchrony threshold with respect to the measurement days. Overall synchrony values for the same days were also calculated to illustrate the consistency of the results obtained by applying a fixed threshold. To interpret the results correctly, we should note that CorSE does not analyze causal relations or indirect connectivity. For such analyses, multivariate methods which are also estimating causal relations would be more effective. Here we studied bivariate synchrony between populations and proposed a simple and fast tool for analyzing overall network relations. CorSE was derived to reveal these relations automatically. Since the algorithm is based on FFT and sample cross-correlation, it is very straightforward and fast; thus, it would be a very efficient tool for fast analysis of neuronal networks. It could also be employed as an online analysis tool, e.g., to observe the acute effects of electrical or chemical stimulations similar to what is used in the anesthesia depth screening monitors (Viertiö-Oja et al., 2004).

The methods developed and the metrics proposed in this thesis contribute the information extraction from the neuronal recordings obtained by MEAs. We have

compared our analysis methods and proposed metrics with the previously available methods and metrics, respectively. Only the novel joint spike sorting and burst detection based analysis, proposed in Publication III, was not compared with previously available methods; since the proposed method extracts new kind of information, and thus there were no methods to which to compare. Thus, the joint analysis method in Publication III was evaluated with spike sorting and burst detection results separately. Based on the results, the methods and metrics developed in this thesis provide advantageous data analysis possibilities also in specific cases in excess to the existing methods: For example: CMA is preferable when one can not set appropriate burst detection parameters or distinct between inter- and intra-burst ISIs (cf. Cotterill et al. (2016) and Publication I). CorSE is advantageous for the cases, where one would like to take LFPs into account and not depend only on the EAP detection (cf. Publication V). However, I believe that there is no "perfect" method suitable for all the conditions; thus, our methods and metrics would provide additional value enhancing the information extraction in addition to the existing methods for some studies in the field of neuroscience.



We aimed to develop new analysis methods and metrics to enhance the information which can be obtained from MEA measurements of neuronal networks, especially developing neuronal networks such as hESC-derived neuronal cultures. Increasing our information on neuronal networks is crucial to understanding how neuronal systems work and, hopefully, in time also to contributing to our knowledge of the nervous system through the enhancement of the analysis power for *in vivo* and *in vitro* experiments, such as screening of pharmacological assays, or the development of stem cell-based neuronal networks. With this work, we particularly contribute to solving the research questions associated with the spiking behavior of neuronal networks, the information content of neuronal bursts, and functional neuronal network connectivity.

Based on the results presented in this thesis, the following can be concluded:

- The problems associated with using predefined fixed burst thresholds can be eliminated using the proposed adaptive burst detection algorithm (Publication I). The method increases the analysis power when working with neuronal networks with highly varying AP dynamics. In addition, the amount of burst-exhibiting data available for subsequent analyses can be increased by using the proposed method.
- The joint analysis of EAP waveforms and detected bursts provides us novel information, i.e., the spike type compositions of bursts. In Publication III, it was shown that such information was not obtainable by analyzing spike

waveform types or different burst parameters. The obtained information can be especially utilized to track changes in the network behavior.

- The entropy-based measures, SE and SmpE, can be used to quantify or classify bursts. Self-similarity and spectral uniformity reveal differently behaving bursts; however, their efficiency depends on the data as demonstrated in Publication II.
- We showed that synchronization in a neuronal network can be assessed by calculating the correlations of time variant SE signals. By using CorSE, we can overcome the shortcomings of event-based synchronicity measures caused by poor event detection. The proposed method can be used for the fast or even online assessment of the neuronal network development or changes in the functional connectivity.

In this thesis, we proposed methods and metrics to enhance the currently obtainable information from microelectrode array measurements. We justified the methods with different types of *in vivo* and *in vitro* neuronal networks. In conclusion, we showed our original hypothesis that MEA measurements contain information in excess to that analyzable with current methods to be true. Accordingly, the proposed methods and metrics would improve the analysis efficiency and open up new perspectives in the studies that use microelectrode array recordings. On the other hand, in addition to the works presented in this thesis, we believe that there is still much work to be done in order to extract all the information that the MEA measurements potentially carry.

## REFERENCES

- ES Source Code. <http://wwold.fi.isc.cnr.it/users/thomas.kreuz/Source-Code/Event-Sync.html>. Accessed: 12.05.2016.
- Sample entropy source code. [http://se.mathworks.com/matlabcentral/fileexchange/35784-sample-entropy?s\\_tid=srchtitle](http://se.mathworks.com/matlabcentral/fileexchange/35784-sample-entropy?s_tid=srchtitle). Accessed: 17.05.2016.
- Granger Causality GUI. [www.dcs.warwick.ac.uk/~feng/causality.html](http://www.dcs.warwick.ac.uk/~feng/causality.html). Accessed: 18.05.2016.
- Neuroexplorer manual, Nex Technologies . <http://www.neuroexplorer.com/downloadspage/>. Accessed: 14.10.2016.
- The top 10 causes of death, world health organization fact sheet n310. <http://www.who.int/mediacentre/factsheets/fs310/en/>. Accessed: 10.4.2015.
- R. Äänismaa, J. E. Mikkonen, L. Ylä-Outinen, and S. Narkilahti. Human pluripotent stem cell-derived neuronal networks: their electrical functionality and usability for modelling and toxicology. In *Methodological Advances in the Culture, Manipulation and Utilization of Embryonic Stem Cells for Basic and Practical Applications*. INTECH Open Access Publisher, 2011.
- D. Amaral and M. Witter. The three-dimensional organization of the hippocampal formation: a review of anatomical data. *Neuroscience*, 31(3):571–591, 1989.
- A. K. Bal-Price, H. T. Hogberg, L. Buzanska, P. Lenas, E. van Vliet, and T. Hartung. In vitro developmental neurotoxicity (dnt) testing: relevant models and endpoints. *Neurotoxicology*, 31(5):545–554, 2010.

- D. Battaglia, A. Witt, F. Wolf, and T. Geisel. Dynamic effective connectivity of inter-areal brain circuits. *PLoS Computational Biology*, 8(3):e1002438, 2012.
- L. Berdondini, T. Overstolz, N. De Rooij, M. Koudelka-Hep, M. Wany, and P. Seitz. High-density microelectrode arrays for electrophysiological activity imaging of neuronal networks. In *Proceedings of the 8th IEEE International Conference on Electronics, Circuits and Systems, Malta, Sept. 2001.*, volume 3, pages 1239–1242. IEEE, 2001.
- E. Biffi, G. Regalia, A. Menegon, G. Ferrigno, and A. Pedrocchi. The influence of neuronal density and maturation on network activity of hippocampal cell cultures: a methodological study. *PLoS One*, 8(12):e83899, 2013.
- T. J. Blanche and N. V. Swindale. Nyquist interpolation improves neuron yield in multiunit recordings. *Journal of neuroscience methods*, 155(1):81–91, 2006.
- G. Brown, A. Pocock, M.-J. Zhao, and M. Luján. Conditional likelihood maximisation: a unifying framework for information theoretic feature selection. *The Journal of Machine Learning Research*, 13(1):27–66, 2012.
- A. Buehlmann and G. Deco. Optimal information transfer in the cortex through synchronization. *PLoS Computational Biology*, 6(9):e1000934, 2010.
- W. Burggren and M. Monticino. Assessing physiological complexity. *Journal of Experimental Biology*, 208(17):3221–3232, 2005.
- G. Buzsáki. Large-scale recording of neuronal ensembles. *Nature Neuroscience*, 7(5):446–451, 2004.
- G. Buzsáki, C. A. Anastassiou, and C. Koch. The origin of extracellular fields and currentseeg, ecog, lfp and spikes. *Nature Reviews Neuroscience*, 13(6):407–420, 2012.
- L. Chen, Y. Deng, W. Luo, Z. Wang, and S. Zeng. Detection of bursts in neuronal spike trains by the mean inter-spike interval method. *Progress in Natural Science*, 19(2):229–235, 2009.
- K. C. Cheung. Implantable microscale neural interfaces. *Biomedical Microdevices*, 9(6):923–938, 2007.
- M. Chiappalone, A. Novellino, I. Vajda, A. Vato, S. Martinoia, and J. van Pelt. Burst detection algorithms for the analysis of spatio-temporal patterns in cortical networks of neurons. *Neurocomputing*, 65:653–662, 2005.

- C. Christodoulou and G. Bugmann. Coefficient of variation vs. mean interspike interval curves: What do they tell us about the brain? *Neurocomputing*, 38: 1141–1149, 2001.
- I. Colombi, F. Tinarelli, V. Pasquale, V. Tucci, and M. Chiappalone. A simplified in vitro experimental model encompasses the essential features of sleep. *Frontiers in Neuroscience*, 10, 2016.
- A. Compte, R. Reig, V. F. Descalzo, M. A. Harvey, G. D. Puccini, and M. V. Sanchez-Vives. Spontaneous high-frequency (1080 hz) oscillations during up states in the cerebral cortex in vitro. *The Journal of Neuroscience*, 28(51): 13828–13844, 2008.
- B. Connors, M. Gutnick, and D. Prince. Electrophysiological properties of neocortical neurons in vitro. *Journal of Neurophysiology*, 48(6):1302–1320, 1982.
- E. Cotterill, P. Charlesworth, C. W. Thomas, O. Paulsen, and S. J. Eglén. A comparison of computational methods for detecting bursts in neuronal spike trains and their application to human stem cell-derived neuronal networks. *Journal of Neurophysiology*, pages jn-00093, 2016.
- E. Defranchi, A. Novellino, M. Whelan, S. Vogel, T. Ramirez, B. Van Ravenzwaay, and R. Landsiedel. Feasibility assessment of micro-electrode chip assay as a method of detecting neurotoxicity in vitro. *Frontiers in Neuroengineering*, 4, 2011.
- U. Egert, D. Heck, and A. Aertsen. Two-dimensional monitoring of spiking networks in acute brain slices. *Experimental Brain Research*, 142(2):268–274, 2002.
- G. T. Einevoll, C. Kayser, N. K. Logothetis, and S. Panzeri. Modelling and analysis of local field potentials for studying the function of cortical circuits. *Nature Reviews Neuroscience*, 14(11):770–785, 2013.
- M. S. Fee, P. P. Mitra, and D. Kleinfeld. Variability of extracellular spike waveforms of cortical neurons. *Journal of Neurophysiology*, 76(6):3823–3833, 1996.
- G. Finnerty and J. Jefferys. Functional connectivity from ca3 to the ipsilateral and contralateral cal in the rat dorsal hippocampus. *Neuroscience*, 56(1):101–108, 1993.
- F. Franke, D. Jäckel, J. Dragas, J. Müller, M. Radivojevic, D. Bakkum, and A. Hierlemann. High-density microelectrode array recordings and real-time spike sorting

- for closed-loop experiments: an emerging technology to study neural plasticity. *Frontiers in Neural Circuits*, 6, 2012.
- M. Garofalo, T. Nieuw, P. Massobrio, and S. Martinoia. Evaluation of the performance of information theory-based methods and cross-correlation to estimate the functional connectivity in cortical networks. *PloS One*, 4(8):e6482, 2009.
- B. Ghane-Motlagh, M. Sawan, et al. Design and implementation challenges of microelectrode arrays: a review. *Materials Sciences and Applications*, 4(08):483, 2013.
- S. Gibson, J. W. Judy, and D. Markovic. Spike sorting. *IEEE Signal Processing Magazine*, 29(1):124, 2012.
- J. Ginter Jr, K. Blinowska, M. Kamin, P. Durka, G. Pfurtscheller, C. Neuper, et al. Propagation of eeg activity in the beta and gamma band during movement imagery in humans. *Methods of Information in Medicine*, 44(1):106–113, 2005.
- C. Gold, D. A. Henze, C. Koch, and G. Buzsáki. On the origin of the extracellular action potential waveform: a modeling study. *Journal of Neurophysiology*, 95(5): 3113–3128, 2006.
- A. Gonzalez-Sulser, J. Wang, B. N. Queenan, M. Avoli, S. Vicini, and R. Dzakpasu. Hippocampal neuron firing and local field potentials in the in vitro 4-aminopyridine epilepsy model. *Journal of Neurophysiology*, 108(9):2568–2580, 2012.
- B. Gourévitch and J. J. Eggermont. A nonparametric approach for detection of bursts in spike trains. *Journal of Neuroscience Methods*, 160(2):349–358, 2007.
- M. Grattarola, M. Chiappalone, F. Davide, S. Martinoia, M. Tedesco, N. Rosso, and A. Vato. Burst analysis of chemically stimulated spinal cord neuronal networks cultured on microelectrode arrays. In *Proceedings of the 23rd Annual International Conference of the IEEE Engineering in Medicine and Biology Society, Oct. 2001.*, volume 1, pages 729–732. IEEE, 2001.
- C. M. Gray and D. A. McCormick. Chattering cells: superficial pyramidal neurons contributing to the generation of synchronous oscillations in the visual cortex. *Science*, 274(5284):109–113, 1996.
- R. M. Gray. *Entropy and Information*. Springer, 1990.

- G. Gross, E. Rieske, G. Kreutzberg, and A. Meyer. A new fixed-array multi-microelectrode system designed for long-term monitoring of extracellular single unit neuronal activity in vitro. *Neuroscience Letters*, 6(2):101–105, 1977.
- S. Guo, A. K. Seth, K. M. Kendrick, C. Zhou, and J. Feng. Partial granger causality-eliminating exogenous inputs and latent variables. *Journal of Neuroscience Methods*, 172(1):79–93, 2008.
- A. Hai, A. Dormann, J. Shappir, S. Yitzchaik, C. Bartic, G. Borghs, J. Langedijk, and M. E. Spira. Spine-shaped gold protrusions improve the adherence and electrical coupling of neurons with the surface of micro-electronic devices. *Journal of The Royal Society Interface*, page rsif20090087, 2009.
- J. E. Hall and A. C. Guyton. *Textbook of Medical Physiology*. Saunders, 2011.
- K. D. Harris, H. Hirase, X. Leinekugel, D. A. Henze, and G. Buzsáki. Temporal interaction between single spikes and complex spike bursts in hippocampal pyramidal cells. *Neuron*, 32(1):141–149, 2001.
- A. Hayar and M. Ennis. Endogenous gaba and glutamate finely tune the bursting of olfactory bulb external tufted cells. *Journal of Neurophysiology*, 98(2):1052–1056, 2007.
- T. J. Heikkilä, L. Ylä-Outinen, J. M. Tanskanen, R. S. Lappalainen, H. Skottman, R. Suuronen, J. E. Mikkonen, J. A. Hyttinen, and S. Narkilahti. Human embryonic stem cell-derived neuronal cells form spontaneously active neuronal networks in vitro. *Experimental Neurology*, 218(1):109–116, 2009.
- M. H. Hennig, J. Grady, J. van Coppenhagen, and E. Sernagor. Age-dependent homeostatic plasticity of gabaergic signaling in developing retinal networks. *The Journal of Neuroscience*, 31(34):12159–12164, 2011.
- D. A. Henze, Z. Borhegyi, J. Csicsvari, A. Mamiya, K. D. Harris, and G. Buzsáki. Intracellular features predicted by extracellular recordings in the hippocampus in vivo. *Journal of Neurophysiology*, 84(1):390–400, 2000.
- H. T. Hogberg, T. Sobanski, A. Novellino, M. Whelan, D. G. Weiss, and A. K. Bal-Price. Application of micro-electrode arrays (meas) as an emerging technology for developmental neurotoxicity: evaluation of domoic acid-induced effects in primary cultures of rat cortical neurons. *Neurotoxicology*, 32(1):158–168, 2011.

- D. R. Humphrey and E. M. Schmidt. *Extracellular Single-Unit Recording Methods*, pages 1–64. Humana Press, Totowa, NJ, 1990. ISBN 978-1-59259-620-1.
- M. Ichikawa, K. Muramoto, K. Kobayashi, M. Kawahara, and Y. Kuroda. Formation and maturation of synapses in primary cultures of rat cerebral cortical cells: an electron microscopic study. *Neuroscience Research*, 16(2):95–103, 1993.
- S. Ito, M. E. Hansen, R. Heiland, A. Lumsdaine, A. M. Litke, and J. M. Beggs. Extending transfer entropy improves identification of effective connectivity in a spiking cortical network model. *PloS One*, 6(11):e27431, 2011.
- A. F. Johnstone, G. W. Gross, D. G. Weiss, O. H.-U. Schroeder, A. Gramowski, and T. J. Shafer. Microelectrode arrays: a physiologically based neurotoxicity testing platform for the 21st century. *Neurotoxicology*, 31(4):331–350, 2010.
- H. Kamioka, E. Maeda, Y. Jimbo, H. P. Robinson, and A. Kawana. Spontaneous periodic synchronized bursting during formation of mature patterns of connections in cortical cultures. *Neuroscience Letters*, 206(2):109–112, 1996.
- E. Kandel and W. Spencer. Electrophysiology of hippocampal neurons: Ii. afterpotentials and repetitive firing. *Journal of Neurophysiology*, 24(3):243–259, 1961.
- F. E. Kapucu, J. M. Tanskanen, J. E. Mikkonen, L. Ylä-Outinen, S. Narkilahti, and J. A. Hyttinen. Burst analysis tool for developing neuronal networks exhibiting highly varying action potential dynamics. *Frontiers in Computational Neuroscience*, 6:38, 2012.
- E. W. Keefer, A. Gramowski, D. A. Stenger, J. J. Pancrazio, and G. W. Gross. Characterization of acute neurotoxic effects of trimethylolpropane phosphate via neuronal network biosensors. *Biosensors and Bioelectronics*, 16(7):513–525, 2001.
- S. Kim and J. McNames. Automatic spike detection based on adaptive template matching for extracellular neural recordings. *Journal of Neuroscience Methods*, 165(2):165–174, 2007.
- D. Ko, C. Wilson, C. Lobb, and C. Paladini. Detection of bursts and pauses in spike trains. *Journal of Neuroscience Methods*, 211(1):145–158, 2012.
- R. S. Lappalainen, M. Salomäki, L. Ylä-Outinen, T. J. Heikkilä, J. A. Hyttinen, H. Pihlajamäki, R. Suuronen, H. Skottman, and S. Narkilahti. Similarly derived and cultured hesc lines show variation in their developmental potential towards neuronal cells in long-term culture. *Regenerative Medicine*, 5(5):749–762, 2010.

- C. R. Legendy and M. Salcman. Bursts and recurrences of bursts in the spike trains of spontaneously active striate cortex neurons. *Journal of Neurophysiology*, 53(4):926–939, 1985. ISSN 0022-3077.
- M. S. Lewicki. A review of methods for spike sorting: the detection and classification of neural action potentials. *Network: Computation in Neural Systems*, 9(4):R53–R78, 1998.
- J. E. Lisman. Bursts as a unit of neural information: making unreliable synapses reliable. *Trends in Neurosciences*, 20(1):38–43, 1997.
- Q. Luo, W. Lu, W. Cheng, P. A. Valdes-Sosa, X. Wen, M. Ding, and J. Feng. Spatio-temporal granger causality: A new framework. *NeuroImage*, 79:241–263, 2013.
- C. Ma, X. Pan, R. Wang, and M. Sakagami. Estimating causal interaction between prefrontal cortex and striatum by transfer entropy. *Cognitive Neurodynamics*, 7(3):253–261, 2013.
- A. Maccione, M. Gandolfo, P. Massobrio, A. Novellino, S. Martinoia, and M. Chiappalone. A novel algorithm for precise identification of spikes in extracellularly recorded neuronal signals. *Journal of Neuroscience Methods*, 177(1):241–249, 2009.
- A. Maccione, M. Garofalo, T. Nieuw, M. Tedesco, L. Berdondini, and S. Martinoia. Multiscale functional connectivity estimation on low-density neuronal cultures recorded by high-density cmos micro electrode arrays. *Journal of Neuroscience Methods*, 207(2):161–171, 2012.
- C. M. Mack, B. J. Lin, J. D. Turner, A. F. Johnstone, L. D. Burgoon, and T. J. Shafer. Burst and principal components analyses of {MEA} data for 16 chemicals describe at least three effects classes. *NeuroToxicology*, 40:75 – 85, 2014. ISSN 0161-813X.
- E. Maeda, H. Robinson, and A. Kawana. The mechanisms of generation and propagation of synchronized bursting in developing networks of cortical neurons. *The Journal of Neuroscience*, 15(10):6834–6845, 1995.
- H. Markram. Seven challenges for neuroscience. *Functional Neurology*, 28(3):145–151, 2013.

- P. Massobrio, J. Tessadori, M. Chiappalone, and M. Ghirardi. In vitro studies of neuronal networks and synaptic plasticity in invertebrates and in mammals using multielectrode arrays. *Neural Plasticity*, 2015, 2015.
- A. Mazzoni, F. D. Broccard, E. Garcia-Perez, P. Bonifazi, M. E. Ruaro, and V. Torre. On the dynamics of the spontaneous activity in neuronal networks. *PloS One*, 2(5):e439, 2007.
- J. Mikkonen and M. Penttonen. Frequency bands and spatiotemporal dynamics of  $\beta$  burst stimulation induced afterdischarges in hippocampus in vivo. *Neuroscience*, 130(1):239–247, 2005.
- E. B. Montgomery Jr. *Intraoperative Neurophysiological Monitoring for Deep Brain Stimulation: Principles, Practice and Cases*. Oxford University Press, 2014.
- M. G. Monticino. *Determining Properties of Synaptic Structure in a Neural Network Through Spike Train Analysis*. PhD thesis, University of North Texas, 2007.
- M. Nawrot, A. Aertsen, and S. Rotter. Single-trial estimation of neuronal firing rates: from single-neuron spike trains to population activity. *Journal of neuroscience methods*, 94(1):81–92, 1999.
- C. Nicholson and J. A. Freeman. Theory of current source-density analysis and determination of conductivity tensor for anuran cerebellum. *Journal of Neurophysiology*, 38(2):356–368, 1975.
- R. A. Normann. Technology insight: future neuroprosthetic therapies for disorders of the nervous system. *Nature Clinical Practice Neurology*, 3(8):444–452, 2007.
- A. Novellino, B. Scelfo, T. Palosaari, A. Price, T. Sobanski, T. J. Shafer, A. F. Johnstone, G. W. Gross, A. Gramowski, O. Schroeder, et al. Development of micro-electrode array based tests for neurotoxicity: assessment of interlaboratory reproducibility with neuroactive chemicals. *Frontiers in Neuroengineering*, 4, 2011.
- M. E. J. Obien, K. Deligkaris, T. Bullmann, D. J. Bakkum, and U. Frey. Revealing neuronal function through microelectrode array recordings. *Frontiers in Neuroscience*, 8, 2014.
- J. M. Palva, S. Palva, and K. Kaila. Phase synchrony among neuronal oscillations in the human cortex. *The Journal of Neuroscience*, 25(15):3962–3972, 2005.

- V. Pasquale, S. Martinoia, and M. Chiappalone. A self-adapting approach for the detection of bursts and network bursts in neuronal cultures. *Journal of Computational Neuroscience*, 29(1-2):213–229, 2010.
- C. Pedreira, J. Martinez, M. J. Ison, and R. Q. Quiroga. How many neurons can we see with current spike sorting algorithms? *Journal of Neuroscience Methods*, 211(1):58–65, 2012.
- K. H. Pettersen and G. T. Einevoll. Amplitude variability and extracellular low-pass filtering of neuronal spikes. *Biophysical Journal*, 94(3):784–802, 2008.
- J. Pine. Recording action potentials from cultured neurons with extracellular microcircuit electrodes. *Journal of Neuroscience Methods*, 2(1):19–31, 1980.
- R. Quiroga, Z. Nadasdy, and Y. Ben-Shaul. Unsupervised spike detection and sorting with wavelets and superparamagnetic clustering. *Neural Computation*, 16(8):1661–1687, 2004.
- R. Q. Quiroga and S. Panzeri. Extracting information from neuronal populations: information theory and decoding approaches. *Nature Reviews Neuroscience*, 10(3):173–185, 2009.
- R. Q. Quiroga and S. Panzeri. *Principles of neural coding*. CRC Press, 2013.
- R. Q. Quiroga, T. Kreuz, and P. Grassberger. Event synchronization: a simple and fast method to measure synchronicity and time delay patterns. *Physical Review E*, 66(4):041904, 2002.
- H. Robinson, M. Kawahara, Y. Jimbo, K. Torimitsu, Y. Kuroda, and A. Kawana. Periodic synchronized bursting and intracellular calcium transients elicited by low magnesium in cultured cortical neurons. *Journal of Neurophysiology*, 70(4):1606–1616, 1993.
- J. T. Robinson, M. Jorgolli, and H. Park. Nanowire electrodes for high-density stimulation and measurement of neural circuits. 2013.
- E. Salinas and T. J. Sejnowski. Correlated neuronal activity and the flow of neural information. *Nature Reviews Neuroscience*, 2(8):539–550, 2001.
- G. Santhanam, S. I. Ryu, M. Y. Byron, A. Afshar, and K. V. Shenoy. A high-performance brain–computer interface. *Nature*, 442(7099):195–198, 2006.

- T. Schreiber. Measuring information transfer. *Physical Review Letters*, 85(2):461, 2000.
- J. V. Selinger, J. J. Pancrazio, and G. W. Gross. Measuring synchronization in neuronal networks for biosensor applications. *Biosensors and Bioelectronics*, 19(7):675–683, 2004.
- J. V. Selinger, N. V. Kulagina, T. J. O’Shaughnessy, W. Ma, and J. J. Pancrazio. Methods for characterizing interspike intervals and identifying bursts in neuronal activity. *Journal of Neuroscience Methods*, 162(1):64–71, 2007.
- J. L. Semmlow and B. Griffel. *Biosignal and medical image processing*. CRC press, 2014.
- C. E. Shannon. A mathematical theory of communication. *The Bell System Technical Journal*, 27(4):623–656, Oct 1948.
- S. Shoham, D. H. OConnor, and R. Segev. How silent is the brain: is there a dark matter problem in neuroscience? *Journal of Comparative Physiology A*, 192(8):777–784, 2006.
- M. E. Spira and A. Hai. Multi-electrode array technologies for neuroscience and cardiology. *Nature nanotechnology*, 8(2):83–94, 2013.
- M. Steriade, A. Nuñez, and F. Amzica. Intracellular analysis of relations between the slow (<1 hz) neocortical oscillation and other sleep rhythms of the electroencephalogram. *The Journal of Neuroscience*, 13(8):3266–3283, 1993.
- P. Stratton, A. Cheung, J. Wiles, E. Kiyatkin, P. Sah, and F. Windels. Action potential waveform variability limits multi-unit separation in freely behaving rats. *PloS One*, 7(6):e38482, 2012.
- J.-J. Sun, W. Kilb, and H. J. Luhmann. Self-organization of repetitive spike patterns in developing neuronal networks in vitro. *European Journal of Neuroscience*, 32(8):1289–1299, 2010.
- M. Sundberg, L. Jansson, J. Ketolainen, H. Pihlajamäki, R. Suuronen, H. Skottman, J. Inzunza, O. Hovatta, and S. Narkilahti. Cd marker expression profiles of human embryonic stem cells and their neural derivatives, determined using flow-cytometric analysis, reveal a novel cd marker for exclusion of pluripotent stem cells. *Stem Cell Research*, 2(2):113–124, 2009.

- J. Tanskanen, F. E. Kapucu, and J. A. Hyttinen. On the threshold based neuronal spike detection, and an objective criterion for setting the threshold. In *Proceedings of the 7th International IEEE/EMBS Conference on Neural Engineering (NER)*, Montpellier, Apr. 2015., pages 1016–1019. IEEE, 2015.
- C. Thomas, P. Springer, G. Loeb, Y. Berwald-Netter, and L. Okun. A miniature microelectrode array to monitor the bioelectric activity of cultured cells. *Experimental Cell Research*, 74(1):61–66, 1972.
- E. Tibau, M. Valencia, and J. Soriano. Identification of neuronal network properties from the spectral analysis of calcium imaging signals in neuronal cultures. *Frontiers in neural circuits*, 7:199, 2013.
- S. Tokdar, P. Xi, R. C. Kelly, and R. E. Kass. Detection of bursts in extracellular spike trains using hidden semi-markov point process models. *Journal of Computational Neuroscience*, 29(1-2):203–212, 2010.
- W. Truccolo, J. A. Donoghue, L. R. Hochberg, E. N. Eskandar, J. R. Madsen, W. S. Anderson, E. N. Brown, E. Halgren, and S. S. Cash. Single-neuron dynamics in human focal epilepsy. *Nature Neuroscience*, 14(5):635–641, 2011.
- T. Uchida, S. Suzuki, Y. Hirano, D. Ito, M. Nagayama, and K. Gohara. Xenon-induced inhibition of synchronized bursts in a rat cortical neuronal network. *Neuroscience*, 214:149–158, 2012.
- H. Viertio-Oja, V. Maja, M. Särkelä, P. Talja, N. Tenkanen, H. Tolvanen-Laakso, M. Paloheimo, A. Vakkuri, A. Yli-Hankala, and P. Meriläinen. Description of the entropy algorithm as applied in the datex-ohmeda  $s/5$  entropy module. *Acta Anaesthesiologica Scandinavica*, 48(2):154–161, 2004.
- T. Vos, R. M. Barber, B. Bell, A. Bertozzi-Villa, S. Biryukov, I. Bolliger, F. Charlson, A. Davis, L. Degenhardt, D. Dicker, et al. Global, regional, and national incidence, prevalence, and years lived with disability for 301 acute and chronic diseases and injuries in 188 countries, 1990–2013: a systematic analysis for the global burden of disease study 2013. *The Lancet*, 386(9995):743–800, 2015.
- D. A. Wagenaar, J. Pine, and S. M. Potter. An extremely rich repertoire of bursting patterns during the development of cortical cultures. *BMC Neuroscience*, 7(1):11, 2006.
- Y.-F. Wang and G. I. Hatton. Burst firing of oxytocin neurons in male rat hypothalamic slices. *Brain Research*, 1032(1):36–43, 2005.

- O. Weihberger, S. Okujeni, J. E. Mikkonen, and U. Egert. Quantitative examination of stimulus-response relations in cortical networks in vitro. *Journal of Neurophysiology*, 109(7):1764–1774, 2013.
- J. Wild, Z. Prekopcsak, T. Sieger, D. Novak, and R. Jech. Performance comparison of extracellular spike sorting algorithms for single-channel recordings. *Journal of Neuroscience Methods*, 203(2):369–376, 2012.
- K. D. Wise and J. Angell. A low-capacitance multielectrode probe for use in extracellular neurophysiology. *IEEE Transactions on Biomedical Engineering*, (3):212–219, 1975.
- A. Zwanenburg, E. Meijer, W. Jennekens, C. van Pul, B. Kramer, and P. Andriessen. Automatic detection of burst synchrony in preterm infants. In *Proceedings of the annual international conference of the IEEE Engineering in medicine and biology society (EMBC), San Diego, CA, Aug.-Sept. 2012.*, pages 4720–4723. IEEE, 2012.

ORIGINAL PUBLICATIONS



Kapucu F.E., Tanskanen J.M.A., Mikkonen J.E., Ylä-Outinen L., Narkilahti S.,  
Hyttinen J.A.K.

**Burst analysis tool for developing neuronal networks exhibiting highly  
varying action potential dynamics.**

*Frontiers in Computational Neuroscience, 6:38, 2012.*

Open access. Authors retain the copyright to this publication.





# Burst analysis tool for developing neuronal networks exhibiting highly varying action potential dynamics

Fikret E. Kapucu<sup>1,2</sup>, Jarmo M. A. Tanskanen<sup>1,2</sup>, Jarmo E. Mikkonen<sup>3</sup>, Laura Ylä-Outinen<sup>2,4</sup>, Susanna Narkilahti<sup>2,4</sup> and Jari A. K. Hyttinen<sup>1,2\*</sup>

<sup>1</sup> Department of Biomedical Engineering, Tampere University of Technology, Tampere, Finland

<sup>2</sup> Institute of Biosciences and Medical Technology, Tampere, Finland

<sup>3</sup> Department of Psychology, University of Jyväskylä, Jyväskylä, Finland

<sup>4</sup> NeuroGroup, Institute of Biomedical Technology, University of Tampere and Tampere University Hospital, Tampere, Finland

## Edited by:

Misha Tsodyks, Weizmann Institute of Science, Israel

## Reviewed by:

Antonio Novellino, ETT S.R.L., Italy

Jason Weick, University of Wisconsin-Madison, USA

Wisconsin-Madison, USA

## \*Correspondence:

Jari A. K. Hyttinen, Department of Biomedical Engineering, Tampere University of Technology, P. O. Box 692, FI-33101 Tampere, Finland.  
e-mail: jari.hyttinen@tut.fi

In this paper we propose a firing statistics based neuronal network burst detection algorithm for neuronal networks exhibiting highly variable action potential dynamics. Electrical activity of neuronal networks is generally analyzed by the occurrences of spikes and bursts both in time and space. Commonly accepted analysis tools employ burst detection algorithms based on predefined criteria. However, maturing neuronal networks, such as those originating from human embryonic stem cells (hESCs), exhibit highly variable network structure and time-varying dynamics. To explore the developing burst/spike activities of such networks, we propose a burst detection algorithm which utilizes the firing statistics based on interspike interval (ISI) histograms. Moreover, the algorithm calculates ISI thresholds for burst spikes as well as for pre-burst spikes and burst tails by evaluating the cumulative moving average (CMA) and skewness of the ISI histogram. Because of the adaptive nature of the proposed algorithm, its analysis power is not limited by the type of neuronal cell network at hand. We demonstrate the functionality of our algorithm with two different types of microelectrode array (MEA) data recorded from spontaneously active hESC-derived neuronal cell networks. The same data was also analyzed by two commonly employed burst detection algorithms and the differences in burst detection results are illustrated. The results demonstrate that our method is both adaptive to the firing statistics of the network and yields successful burst detection from the data. In conclusion, the proposed method is a potential tool for analyzing of hESC-derived neuronal cell networks and thus can be utilized in studies aiming to understand the development and functioning of human neuronal networks and as an analysis tool for *in vitro* drug screening and neurotoxicity assays.

**Keywords:** spike trains, action potential bursts, burst analysis, hESCs, human embryonic stem cells, developing neuronal networks, MEA, microelectrode array

## INTRODUCTION

In this paper we study methods to assess the bursting behavior of developing human neuronal networks. Previously, it has been shown that human embryonic stem cell (hESC)-derived neuronal cells are functional at single cell level (Carpenter et al., 2001; Erceg et al., 2008; Lai et al., 2008; Daadi et al., 2009; Bissonnette et al., 2011; Kim et al., 2011) and can form spontaneously functional neuronal networks (Heikkilä et al., 2009). Compared to the more widely studied *in vitro* neuronal networks, that is, rodent primary cultures, it seems that networking mechanisms and behavior of hESC-derived neurons are more variable in their statistics from individual spikes to bursts (Heikkilä et al., 2009). This calls for new methods for the assessment of network development and functioning, since traditional burst detection algorithms are not in general capable of capturing the bursts and related features of such networks.

To assess the functioning of neuronal networks in their different developmental stages and to observe their responses to

different drugs, toxins, and chemicals, substrate integrated microelectrode arrays (MEAs) provide an *in vitro* platform to monitor the firing patterns and the network activity (Gross et al., 1977; Pine, 1980; Wagenaar et al., 2006; Illes et al., 2007; Heikkilä et al., 2009; Ylä-Outinen et al., 2010). Neuronal activity is normally described either by single cell firing called spikes or actual network activity manifested by more or less regular occurring short episodes of intense firing called bursts (Kandel and Spencer, 1961; Connors et al., 1982; Gray and McCormick, 1996). In this type of network activity, neurons are interacting and firing in an orchestrated manner. It is suggested that bursts reflect and influence the plasticity mechanisms and could be used for assessment of network activity (Lisman, 1997). It has been shown, for example, that cultured networks of rat cortical neurons exhibit a significant increase in spontaneous bursting during the development of new synapses and networks (Ichikawa et al., 1993; Maeda et al., 1995; Kamioka et al., 1996). Thus, analysis of bursting behavior is a way to assess the developing neuronal network properties.

Even though bursting is a very fundamental property of the neuronal networks, the definitions of bursts and burst detection methods, however, differ between studies. Some define bursts according to interspike interval (ISI) thresholds and the numbers of spikes in bursts which are set by visual inspection, such as utilizing a fixed ISI of 100 ms and a minimum number of 10 spikes in bursts (Chiappalone et al., 2005), or again utilizing a fixed ISI and a minimum number of spikes in bursts which are chosen according to experimental conditions and differentiate bursts from other activity based on the slopes in time-spike number curves (Turnbull et al., 2005). Others utilize calculated average ISIs of the measurements (Mazzoni et al., 2007), average firing rates and alternatively a fixed ISI threshold of 100 ms (Wagenaar et al., 2006), or logarithmic histogram of ISIs to calculate an ISI threshold for detecting bursts (Selinger et al., 2007; Pasquale et al., 2010). These methods, except that by Turnbull et al. (2005), are focused on analyzing the activity of neurons extracted from rat central nervous system such as rat cortical neurons (Chiappalone et al., 2005; Wagenaar et al., 2006; Pasquale et al., 2010) and rat hippocampal neurons (Mazzoni et al., 2007). Thus, they may be tuned to the type of the analyzed network. In the developing networks, the spiking and bursting may behave differently as the network is formed by active neuronal movement, process formation, and synaptic modulation. In fact, beside the frequent occurrence of “primitive” bursts which are formed by a few spikes, we also observed bursts with tens of spikes and bursts lasting from milliseconds to seconds while studying maturing hESC-derived neuronal networks (Heikkilä et al., 2009). The earlier mentioned most widely applied burst detection and burst analysis methods, however, ignore the primitive and unstable spike train and burst activity of hESC-derived neuronal networks. The spike trains or bursts of such networks are in this paper defined to be “unstable” if their statistics such as the number of spikes forming bursts, ISIs inside and between bursts, burst durations, etc., highly vary.

In addition to the need for an applicable burst detection method for developing neuronal networks, it is necessary to obtain characterization measures for the practical analysis of the responses of the networks to different treatments, drugs, toxins, or chemicals. Several parameters such as overall spiking activity, burst frequency, and duration can be used in activity characterization (Bal-Price et al., 2010; Äänismaa et al., 2011; Defranchi et al., 2011; Hogberg et al., 2011). These parameters can be obtained from large data pools by an analysis tool which has no bias for a certain type of analyzed networks, such as fixed burst parameters, e.g., ISI or the number of spikes in bursts. Thus there is a need for methods that provide these parameters also intrinsically from developing networks.

Here, we propose a burst detection method without any a priori fixed burst criteria, and demonstrate its applicability with maturing hESC-derived neuronal networks. To demonstrate the need for such methods we illustrate the dynamic nature of hESC-derived neuronal networks during maturation by spike activity maps for different measurement days. Thereafter, we shortly review the existing burst detection methods and compare their performances in the analysis of hESC-derived neuronal network recordings. We compare the applicability of the

methods, and finally discuss potential uses of the hereby proposed method in assessing the characteristics of various neuronal networks.

## MATERIALS AND METHODS

### CELL CULTURES

hESCs [cell line Regea 08/023, passages 36 (used in dataset-I), 42 (used in datasets-II and -III), 44 (used in dataset-IV), and 60 (used in dataset-V)] were differentiated into neuronal cells using the previously published method (Sundberg et al., 2009; Lappalainen et al., 2010) and plated on MEAs as described in Heikkilä et al. (2009). Briefly, 10–15 small aggregates dissected from neurospheres (50,000–150,000 cells in total) were plated on MEA dishes coated with polyethyleneimine (0.05% solution, Sigma-Aldrich, St. Louis, MO, USA) and subsequently with human laminin (20 µg/ml, Sigma-Aldrich). Medium containing basic fibroblast growth factor (4 ng/ml, FGF, Sigma-Aldrich) and brain-derived growth factor (5 ng/ml, BDNF, Gibco Invitrogen, Carlsbad, CA, USA or Peprotech, Rocky Hill, NJ, USA) was replaced three times a week. The cell seeding area in the MEA was either the normal, that is, 20 mm in diameter or the area was restricted to Ø 4 mm to reduce the amount of cells needed and to guide the cells to grow on top of the electrode area.

All the MEAs with cells were kept in an incubator (+37°C, 5% CO<sub>2</sub>, 95% air) prior to and between recordings. All recordings were made using MEAs and equipment's purchased from Multi Channel Systems MCS GmbH (MCS, Reutlingen, Germany). hESC experiments were performed in the Institute of Biomedical Technology (University of Tampere, Tampere, Finland) that has the approval from the Ethics Committee of the Pirkanmaa Hospital District to culture the hESC lines.

### ELECTROPHYSIOLOGICAL RECORDINGS

Electrical activities were recorded using MEAs with square arrays of 59 substrate-embedded titanium nitride microelectrodes (30 µm in diameter, 200 µm inter-electrode distance, model: 200/30iR-Ti-gr, MCS) and internal embedded reference electrodes. Signals were sampled at 20 kHz, and stored to a standard PC using the MC\_Rack software (MCS). The culture temperature was maintained at +37°C using a TC02 temperature controller (MCS) during the measurements. Recordings were visually inspected for artifacts and the measurements or channels likely to contain artifacts were excluded from the further analysis. In this paper, for demonstrating the proposed analysis methods, we opted for the analysis of artifact free data only. Spike detection was carried out online by setting an amplitude threshold at six times the standard deviation of the signal noise level and the spike time stamps and spike waveform cutouts were stored in the MC Rack software.

For method validation, we utilized five different data sets (Ds-I, Ds-II, Ds-III, Ds-IV, Ds-V) that altogether contained measured data from 27 MEAs (each containing 59 electrodes referred to hereafter as channels or ch). Each MEA was measured altogether three times (mes1, mes2, and mes3) and each measurement lasted approximately 300 s. The first measurement day was chosen according to the criteria that at least 10% of the channels in a MEA were active and in active channels at least 100 spikes

were found during the recording period. The first measurement day (mes1) varied between 6 and 22 days of culturing in MEA. Thereafter, the developing networks were measured at 4–7 days after the first measurement (mes2), and the third measurement day (mes3) was 2–4 days after the second measurement day (Table 1).

### SPIKE ACTIVITY COLORMAPS

To observe how dynamic the firing was during the maturation process of hESC-derived neurons, a spike activity map (colormap) of all 59 channels for different measurement days were formed. In our colormaps, MEA channels are represented as an  $8 \times 8$  matrix and the layout of the MEA matches the colormap matrix elements spatially. Since a MEA has 60 channels (including the reference channel), the corner elements of the colormap matrix have no values. Thus, the color shown in the corners of the subfigures of Figure 1 is set based on values interpolated from the neighboring channels.

At first, spikes were counted separately for the different measurement days, yielding the total spike counts of each measurement for every MEA channel. Secondly, the logarithms of these spike counts were calculated to be able to show a wide range of values in the same colormap, and the values were mapped to color, the colors were interpolated between the channels, and the colormaps were contoured.

### ISI AND ISI HISTOGRAM BASED BURST DEFINITIONS

Time intervals between consecutive spikes, i.e., ISIs are very commonly used in the analysis of neuronal recordings. ISI has also been used as one of criteria to detect the burst activity in some reported algorithms (Chiappalone et al., 2005; Wagenaar et al., 2006; Mazzoni et al., 2007). In these algorithms, an ISI threshold is selected or calculated and a fixed number of consecutive spikes (three, four, or ten, depending on the algorithm) with ISIs less than the selected threshold are considered burst spikes. On the other hand, an ISI histogram can be easily formed after spike detection by counting the spikes and time binning ISIs. It can be calculated for, e.g., each channel, recording, measurement day or complete dataset. Although ISI histograms are capable of representing some characteristics of the firing activities, it is usually not rewarding to analyze them alone. Gradual decay in the ISI histogram, forming a tail after the peak of the ISI histogram and fluctuations of local extrema (local minima and maxima) are common observations in ISI histograms. The analysis of such histogram behavior is a promising method for network analysis, although some aspects of network characteristics are not easily observable in raw ISI histograms.

### LOGARITHMIC INTERSPIKE INTERVAL HISTOGRAM (logISIH) ALGORITHM

One of the alternative solutions for analyzing ISI histograms is plotting the logarithmic ISI instead of plain ISI, which was proposed previously by Selinger et al. (2007) and employed in rat cortical cell measurement analysis by Pasquale et al. (2010). The method is based on plotting ISI histograms using logarithmic instead of linear scale. In the algorithm, ISI threshold is selected at the point where intra-burst ISI is most clearly separated from inter-burst ISI. Clear separation is indicated by the distinct principal and secondary peaks formed in the logarithmic histogram representing intra and inter-burst ISIs, respectively (see Figure 7A). Parameter “void,” which is described in detail by Selinger et al. (2007), is calculated to assess this separation. In logISIH algorithm, if the ISI threshold is lower than 100 ms, bursts are detected only according to this threshold; otherwise a fixed ISI threshold of 100 ms is employed in finding *burst cores* and the calculated threshold is employed to detect *burst boundary spikes*. Complete detected bursts are formed by combining the detected *burst cores* with the boundary spikes adjacent to each burst core. The algorithm has strict rules such as the occurrence of the first peak (principal peak) in the ISI histogram, which represents intra-burst ISIs, within a defined time window (here 100 ms). Recordings should have at least one peak at an ISI less than 100 ms in their logarithmic ISI histograms. In the case where the logarithmic histograms of the recordings have no good separation between inter-burst and intra-burst ISIs or there is no principal peak before 100 ms, another strict burst definition is employed, such as requiring 10 spikes in a row which have ISIs less than 100 ms, as in the study by Chiappalone et al. (2005). As a result, this algorithm was not very suitable for the analysis of our data as bursts with 10 or more spikes are hardly available. To make the algorithm more comparable to our algorithm and applicable to our data, we modified the algorithm to consider three spikes in a row instead of 10.

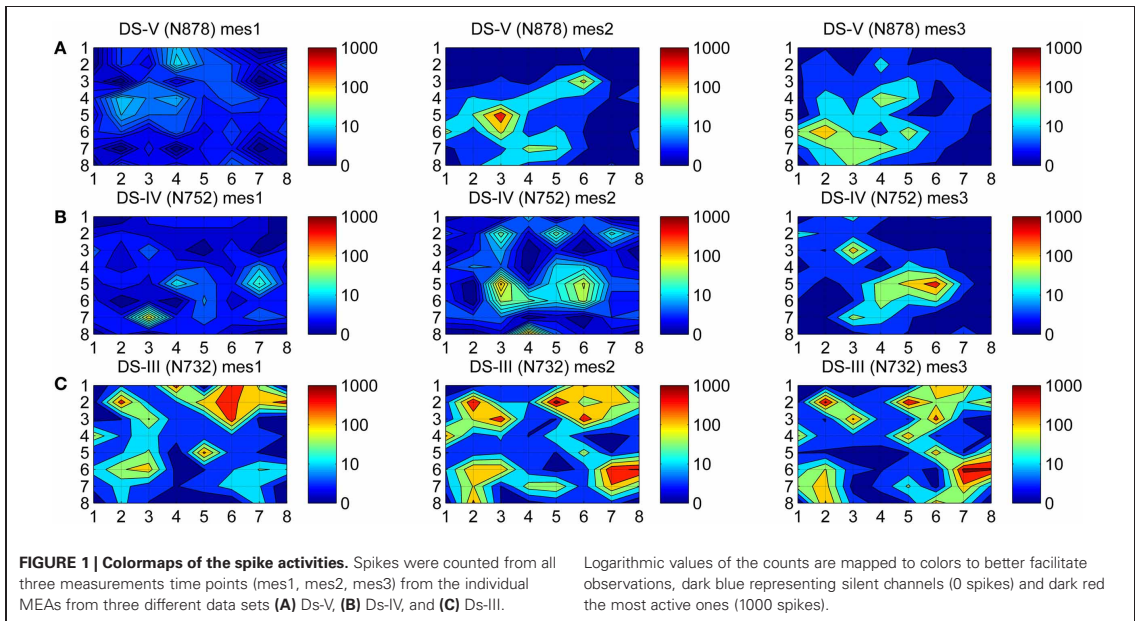
### CUMULATIVE MOVING AVERAGE METHOD FOR DETECTING BURSTS

For analyzing the recordings for which no clear separation can be observed between the inter- and intra-burst ISIs, like the majority of the recordings obtained from maturing hESCs (see Figure 8A), we propose an adaptive method based on the cumulative moving average (CMA) of the ISI histogram. As an alternative for analyzing the raw ISI histogram, CMA of the ISI histogram allows us to observe the cumulative average spike count up to a particular ISI. Generally, CMA of a data series smoothens short term fluctuations and highlights long term trends. In our particular case, CMA of the ISI histogram provides us the general change

**Table 1 | The measurement days and the number of included MEAs for different data sets.**

	Ds-I (7 MEAs)	Ds-II (6 MEAs)	Ds-III (7 MEAs)	Ds-IV (6 MEAs)	Ds-V (6 MEAs)
mes1 (days after plating)	20	7	22	6	10
mes2 (days after plating)	25	11	27	12	17
mes3 (days after plating)	28*	15	29	15	20

\* Analysis based on six MEAs instead of seven.



in the trend of the ISI histogram, and allows us to define an ISI value which we can use as a threshold to define the bursts in a particular recording. Thus, without considering any local changes we can identify the ISIs at which critical changes occur, i.e., the ISI at which the average spike count starts decreasing. The proposed algorithm has no strictly fixed parameters that would render any particular types of neuronal network behaviors not analyzable. Thus, every recording is evaluated based on its inner dynamics and bursts are detected for further network analyzes and characterization.

The proposed CMA algorithm was implemented in Matlab environment for post recording analysis and consists of the steps described in the following three subchapters.

**Calculating ISI threshold for burst like patterns**

Let  $y_i, i = 1, \dots, N$ , with  $N$  the total number of ISI bins, be the spike count in the  $i$ th ISI bin. The value of the cumulative sum of the histogram  $CH_I$  at the  $I$ th,  $I \leq N$ , ISI bin is defined as

$$CH_I = \sum_{i=1}^I y_i \tag{1}$$

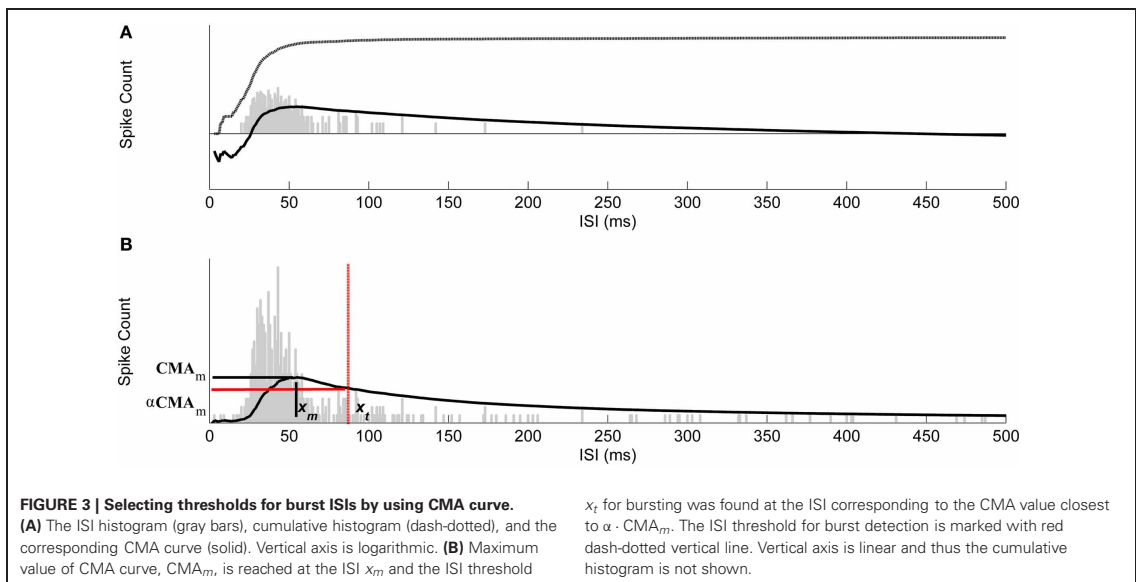
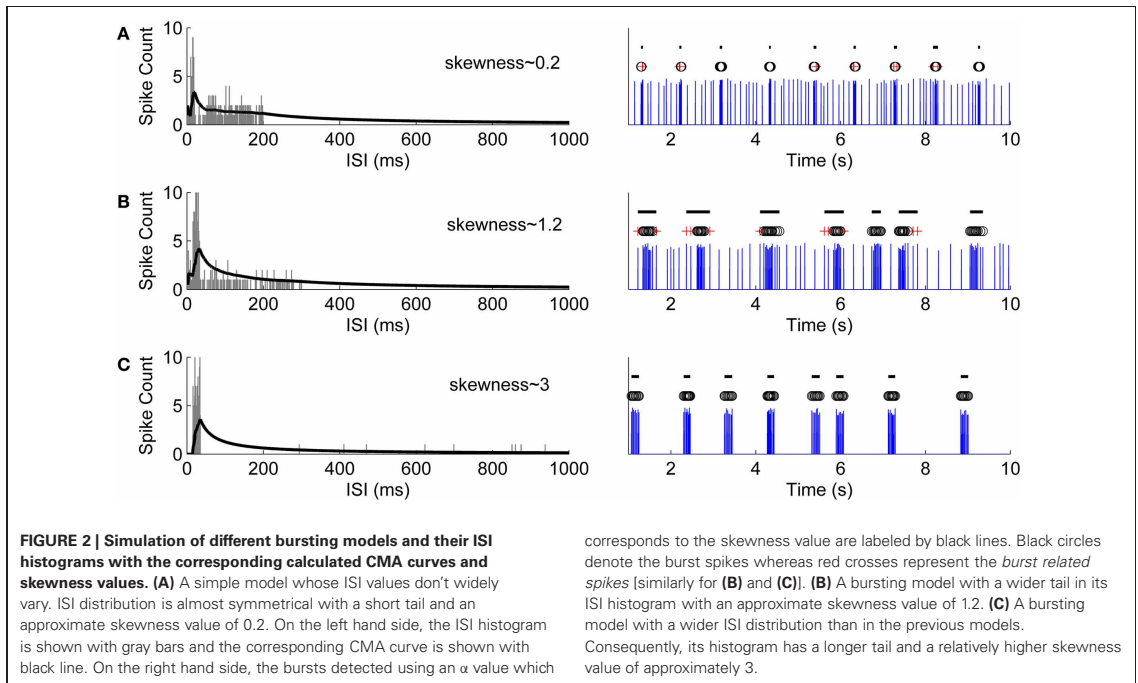
The corresponding CMA is given by

$$CMA_I = \frac{1}{I} \sum_{i=1}^I y_i \tag{2}$$

whose maximum,  $CMA_m$ , is reached at the  $m$ th ISI bin, and

$$m = \arg \max_{k=1, \dots, N} \left( \frac{1}{k} \sum_{i=1}^k y_i \right) \tag{3}$$

This point represents the maximum that the average spike count reaches. ISI threshold for defining a burst might, for example, be selected at this maximum point after which CMA begins to decrease. However, adding a tolerance to this maximum, i.e., selecting the actual ISI threshold as  $\alpha \cdot CMA_m$ , where  $0 < \alpha < 1$ , strengthens the burst detection. Here,  $\alpha$  is selected according to the ISI behavior of the ISI histogram. Generally, the ISI histogram of a burst containing recording and its CMA curve exhibit a peak at lower ISI values and a tail at higher ISI values. Intra-burst ISIs are expected to be in the neighborhood of the peak because of the fact that intra-burst spikes are shorter than the ISIs of individual spikes which don't belong to a burst. If they exist, individual spikes are located in the tail of the histogram, whereas *burst tails* or *pre-burst spikes* (*burst related spikes*) are located in the histogram between ISIs of intra-burst spikes and ISIs of individual spikes. For a simple bursting model, in which ISI values do not widely vary, ISI values will form an almost symmetrical distribution with a short tail, i.e., the skewness of the distribution is approximately zero, and most of the burst spikes are expected to be located in the vicinity of  $CMA_m$  (c.f., **Figure 2A**). Thus, we can define two parameters:  $\alpha_1$  which can be set close to one, and for the *burst related spikes*  $\alpha_2 < \alpha_1$ . However, for most of the burst models ISI histograms lean to the right with a tail, i.e., they are positively skewed. In these cases, ISI values have large variance, and also the tail of the ISI histogram contains intra-burst ISIs (c.f., **Figures 2B,C**). Longer the tail, more skewed the histogram, and the smaller  $\alpha$  can be set not to miss the intra-burst ISIs in the tail. Denoting the ISI at  $CMA_m$  (3) by  $x_m$ , the ISI threshold  $x_t, x_t > x_m$ , for burst detection is found at the mid time point of the ISI bin for which the value of the CMA curve is the closest to  $\alpha \cdot CMA_m$ .



In **Figure 3**, CMA of the ISI histogram and the calculation of the threshold are illustrated. After calculating the threshold, burst detection is employed, here with the requirement of at least three spikes in a row (triplet) with ISIs below the calculated ISI threshold. We consider that extracellular burst means more event

than one, as also noted by Lisman (1997) and Izhikevich et al. (2003), thus we concentrated on triplets to be sure for this study. However, also two spikes in a row (duplet) instead of a triplet can be accommodated in the algorithm's if the user prefers this option.

### Calculating ISI threshold for burst related spikes

The term *burst related spikes* is used here for defining the *burst tails* or *pre-burst spikes* which are located in the neighborhood of bursts and are an essential part of the bursting behavior. In a previous study, changes in the firing activity before and after bursts were observed and analyzed (Wang and Hatton, 2005). Burst tails have also been studied and utilized in classifying bursting behaviors (Wagenaar et al., 2006). It is common to observe the *burst related spikes* in our recordings as well. To calculate ISI threshold for the *burst related spikes* with  $\alpha_2$ , the first step of the CMA algorithm is repeated. After detecting the potential *burst related spikes*, the ones which are not following or followed by a burst are omitted.

To automatically select  $\alpha$  values, we can form a scale of  $\alpha$  values with the corresponding skewness values. This relationship is depicted in **Figure 4** with  $\alpha_1$  values used for detecting burst spikes and  $\alpha_2$  values used for detecting *burst related spikes*. The scale was formed by experimenting with the relation of  $\alpha$  and skewness for our recordings.

### Extending bursts with the burst related spikes and merging close bursts

The *burst related spikes* are included in their neighboring bursts in this step. Also, the bursts which are closer to each other than the threshold calculated in the second step are merged together. This step also corrects erroneous burst spike detections and misses caused by ISI variance inside bursts and is especially advantageous for the analysis of maturing networks, which frequently have high ISI variance and consist of both bursts and individual spikes. **Figure 5** demonstrates data with high intra-burst ISI variability. Black circles are detected burst spikes whereas red crosses are the detected *burst related spikes* after the first step of CMA algorithm, whereas black lines indicate bursts after the extending and merging process. In **Figure 5**, the burst around the 50th second has an intra-burst ISI variability of approximately 600 ms and the *burst related spikes* are detected during the burst. Extending bursts to the *burst related spikes* and merging close bursts, we get the satisfactorily detected burst marked with black line instead of the erroneously detected two separate bursts.

### ANALYSIS OF THE DETECTED BURSTS

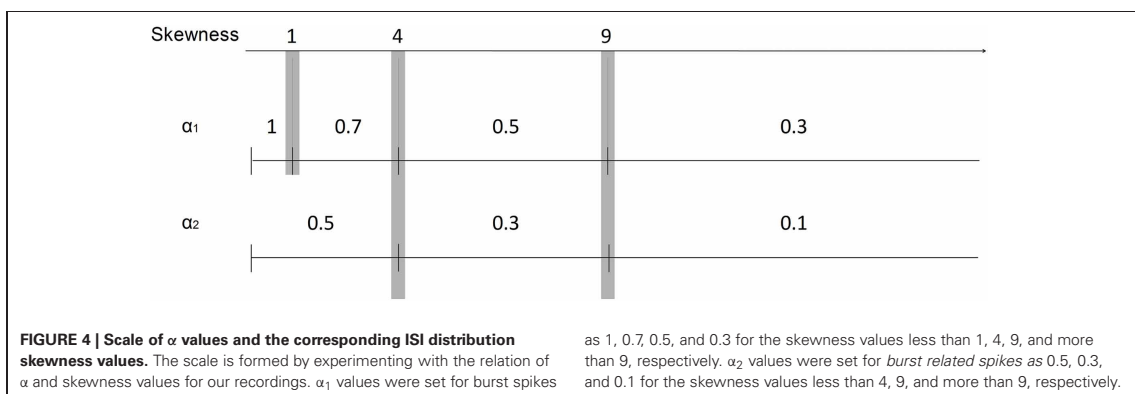
After detecting the bursts by CMA algorithm, all the bursts from five data sets were pooled according to their measurement days. Additionally, we pooled the bursts according cell seeding area size on the MEAs. For analyzing the bursts, we calculated three parameters from the detected bursts for each channel: average burst duration (ABD), total number of bursts detected (TNB), and average number of spikes per burst (ASpB). The relations of these parameters were plotted for different measurement days to analyze the changes during the development.

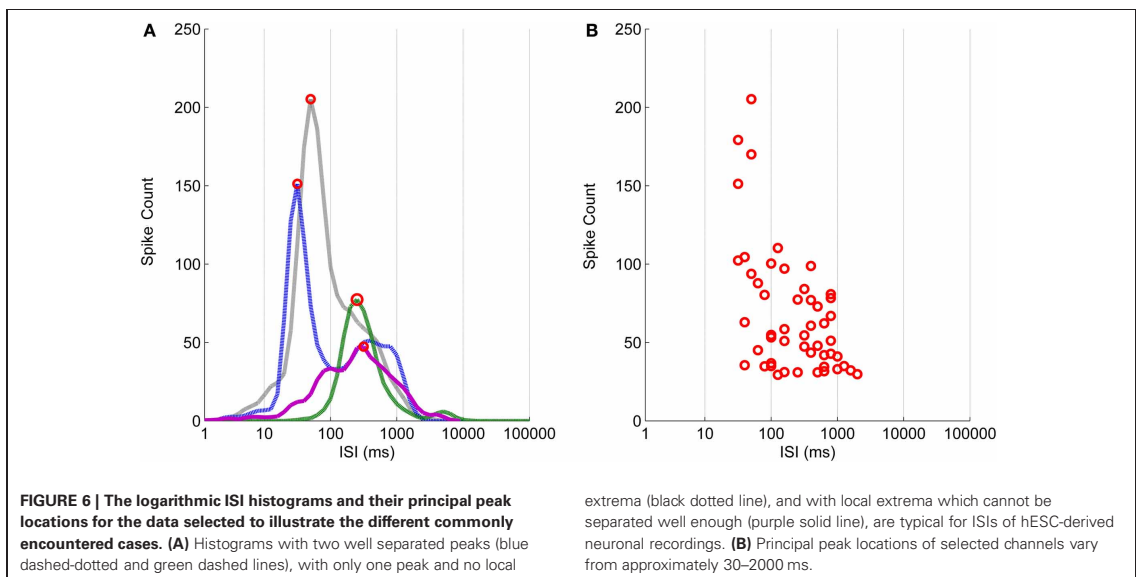
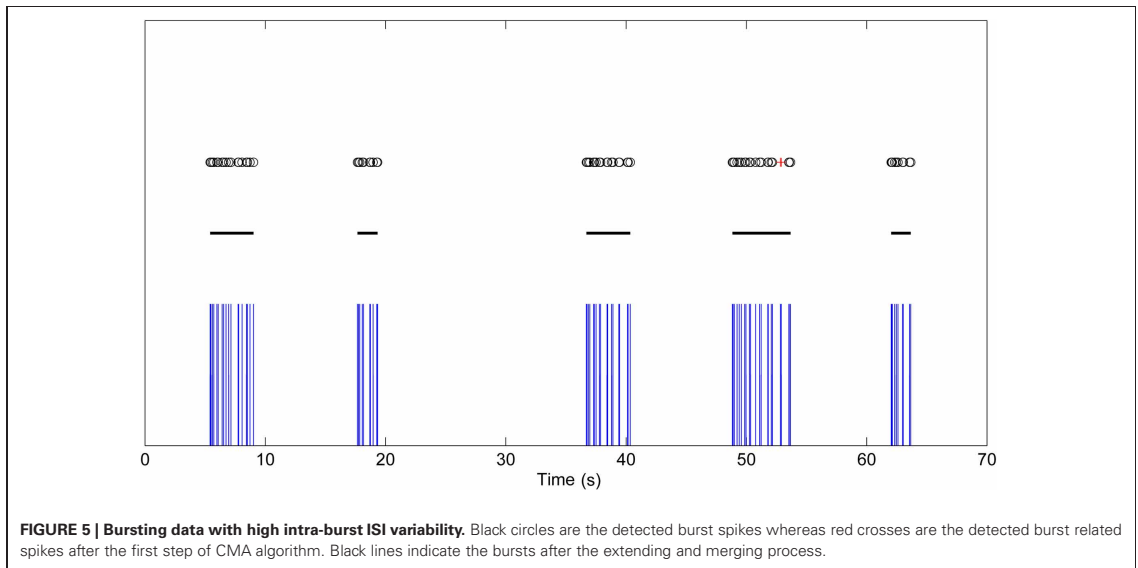
### RESULTS

A colormap which shows the spike activities is a useful tool for viewing the channel dynamics of hESC-derived neurons during the maturation process. The activity colormaps for the three measurement days (mes1, mes2, and mes3) of three MEAs (N732, N752, and N878) from three data sets (Ds-III, Ds-IV, and Ds-V) are presented in **Figure 1**. The dynamics of the networks can be observed from the fading and rising of the firing activities in time.

Before proceeding to compare the burst detection results using the previously published methods (Chiappalone et al., 2005; Pasquale et al., 2010) and our method, we investigated if it was appropriate to set one fixed threshold to define intra-burst ISIs for the burst detection algorithms. Since the principal peak in a logarithmic histogram represents mostly the intra-burst ISI values as mentioned earlier, the principal peak ISI values of our recordings were calculated to observe the feasibility of using a fixed threshold as in previously published algorithms.

In **Figure 6** are shown the logarithmic ISI histograms of the selected active channels whose principal peaks of the logarithmic histograms include at least 30 spikes to make the three different common types of logarithmic ISI histogram trends found in hESC-derived neuronal recordings clearly observable. Histograms with two well separated peaks, with only one peak and no local extrema, and with local extrema which cannot be separated well enough are typical in our recordings. **Figure 6A** demonstrates that both the principal ISI values and the histogram shape may be greatly varying. To further show the variability of the ISI value of the peak, logarithmic ISI histograms for all of the channels from every recording were calculated and the locations

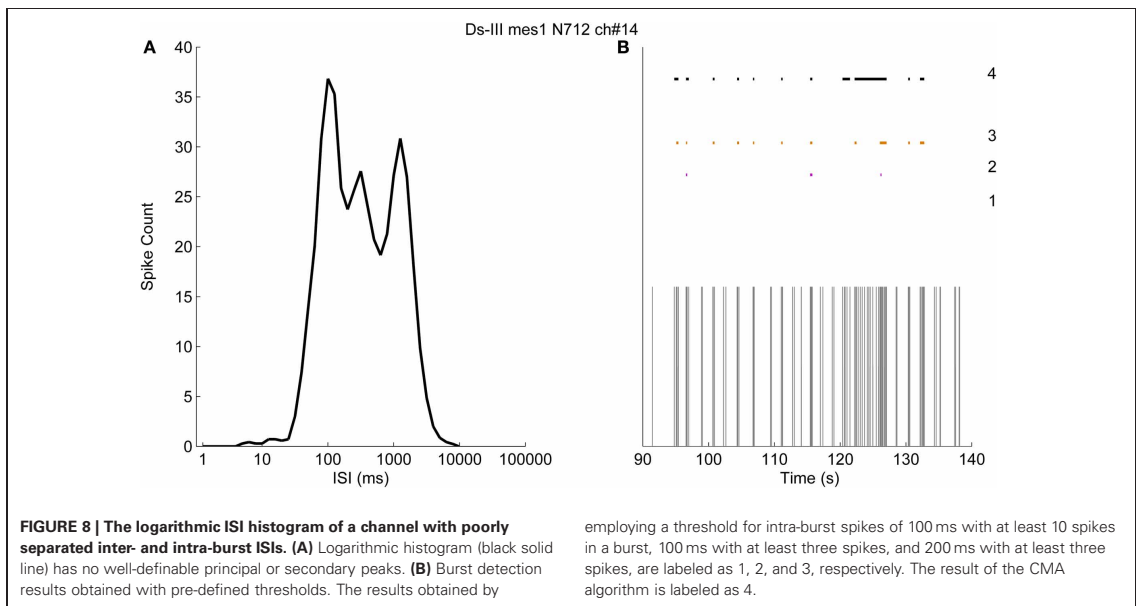
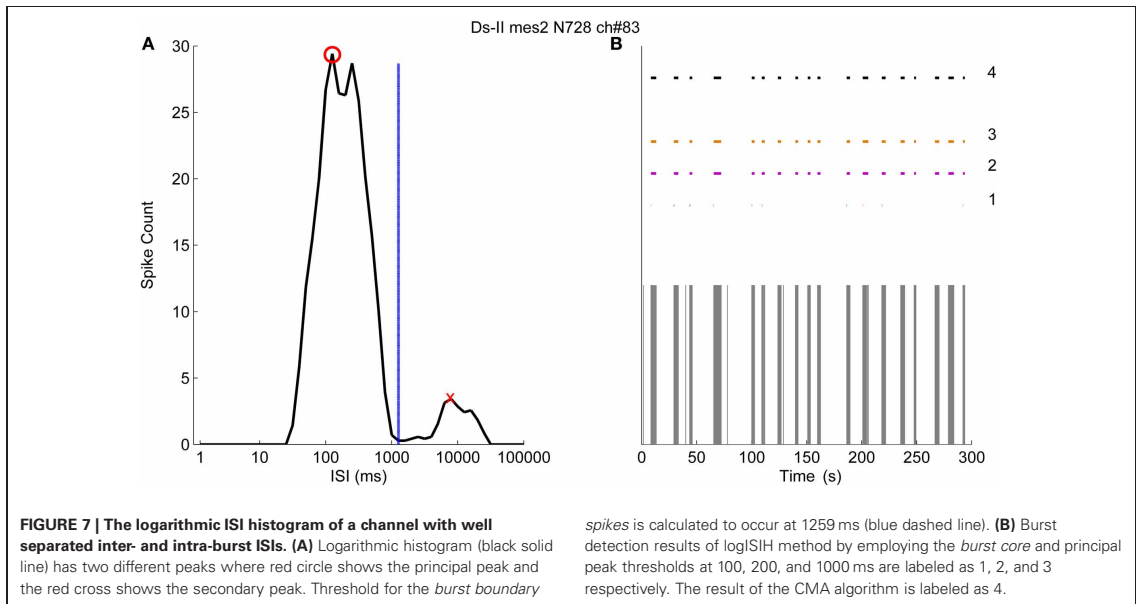




of the principal peaks consisting of the minimum of 30 spikes are shown in **Figure 6B**. The peak locations have an approximate ISI range from 30 to 2000 ms.

**Figure 7A** demonstrates the logarithmic ISI histogram of the data from one channel of a MEA (MEA N728, Ds-II, mes2) which exhibits clearly separated bursts shown in **Figure 7B**. In the case shown in **Figure 7**, it can be seen that the principal peak (red circle) and the secondary peak (red cross) are well separated and the ISI threshold for the *burst boundary spikes* is calculated at 1259 ms

(blue dashed line). On the other hand, the location of the principal peak is almost at the proposed threshold for the *burst cores* at 100 ms. Accordingly, we experimented with the ISI thresholds for the *burst cores* at 100, 200, and also at 1000 ms, which seems more rational when observing the **Figure 7A**. The burst detection results labeled with “1” in **Figure 7B** represent the results by the logISIH algorithm with the threshold ISI of 100 ms as also previously shown (Pasquale et al., 2010). The results obtained by changing the threshold to 200 ms for the principal peak locations



and for the *burst cores* are shown labeled “2.” The results obtained by changing ISI threshold for the *burst cores* from 100 to 1000 ms and also changing the threshold for the principal peak locations to 1000 ms are shown labeled “3.” The results given by our CMA algorithm are shown labeled “4” in **Figure 7B**. Skewness of the ISI distribution was in this case found to be 4.7, which corresponds to  $\alpha_1 = 0.5$  and  $\alpha_2 = 0.3$ .

**Figure 8A** shows an example of logarithmic ISI histogram of a recording in which the bursts are not clearly separable. As can be seen, results cannot be obtained by logSIH algorithm since the required criterion for the separation cannot be satisfied. Instead, we used fixed ISI threshold values and fixed number of burst spikes as the criteria to compare the methods. In **Figure 8B**, 50 s of the recording and the results are shown to better observe the burst

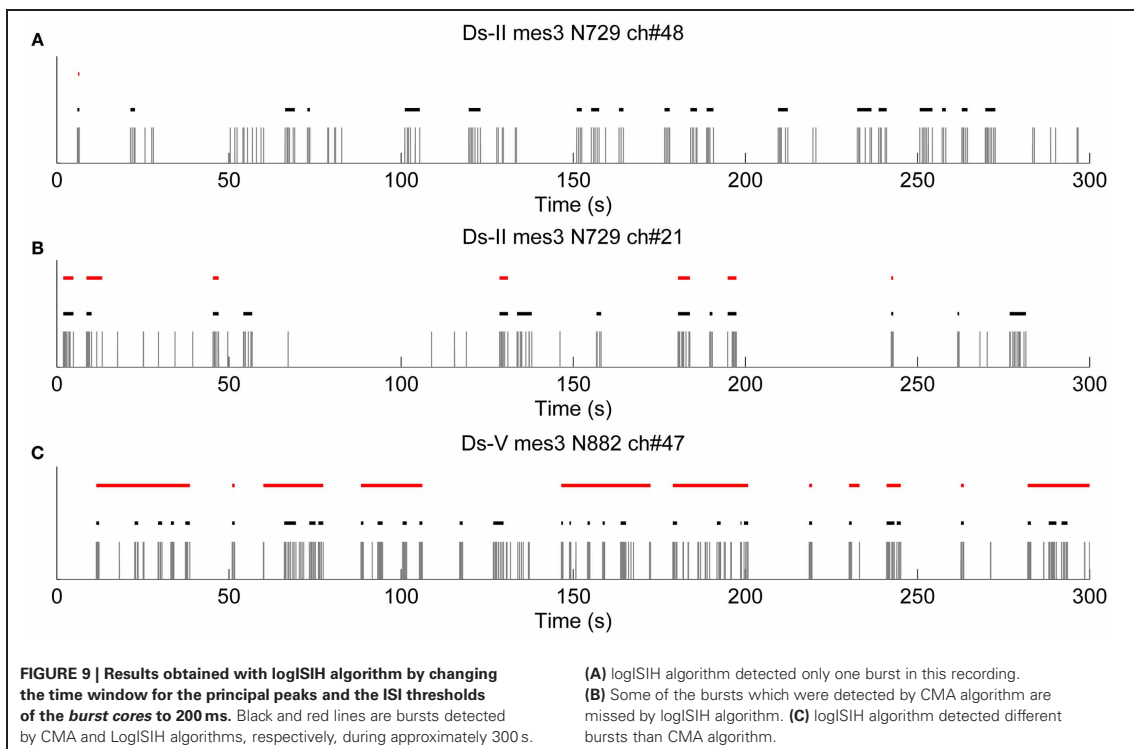
detection results. The results labeled from “1” to “3” in **Figure 8B** represent the algorithm with 100 ms intra-burst ISI threshold and the minimum of 10 spikes for detecting bursts (Chiappalone et al., 2005) and its modified versions alike in **Figure 7**. The algorithm with the criteria of 100 ms intra-burst ISI threshold and the minimum three of spikes in a burst is labeled with “2,” whereas the algorithm with 200 ms intra-burst ISI threshold with the minimum of three spikes is labeled with “3.” The result of CMA algorithm for this recording is labeled with “4.” In this case skewness of the ISI distribution is found to be 2.7, which corresponds to  $\alpha_1 = 0.7$  and  $\alpha_2 = 0.5$ .

Further results obtained with logISIH algorithm by changing its parameters for testing its applicability for analyzing our recordings are shown in **Figure 9**. For this case, the time window for principal peaks and ISI threshold for *burst cores* was set at 200 ms, which is different from that proposed by Pasquale et al. (2010). As seen in **Figure 9A**, logISIH algorithm with the fixed ISI threshold of 200 ms does not detect more than one burst in this data. This is because the principal peak of the logarithmic histogram for this data is beyond the ISI of 200 ms. In comparison, our method succeeds in finding bursts in this data (**Figure 9A**). In **Figure 9B** is shown a case in which some of the bursts correctly found by our method are missed by the logISIH algorithm, whereas in case shown in **Figure 9C**, the burst detection results between the algorithms are different. For the cases shown in **Figures 9A,B**, the algorithm proposed in this paper is

clearly advantageous over the logISIH algorithm. For the case shown in **Figure 9C**, the selection of the preferable algorithm depends on the desired subsequent analysis.

We analyzed the usability of the CMA algorithm further with recordings from differently behaving hESC-derived neuronal networks. Recordings shown in **Figures 10A–C** have different skewness values of their ISI distributions. As seen from **Figures 10A–C**, the longer the tail of the ISI histogram, the bigger the skewness value, which also indicates higher variance of the ISI values. **Figure 10A** presents a recording which has closely located ISI values and naturally almost symmetrical ISI distribution with skewness of one. Accordingly, burst detection ISI threshold is set at the peak of CMA curve. On the other hand, the recordings presented in **Figures 10B,C** have more positively skewed ISI distributions with increasing variance of the ISI values, and accordingly ISI thresholds are calculated with smaller  $\alpha$  values with the result of setting the detection threshold further away to the right from the peak of the CMA curve.

We also tested the usability of the methods with a larger amount of data to demonstrate how much of the data is produced for further burst analysis by different methods without considering whether the burst detection was true or false. Simply, if a burst detection algorithm doesn't detect any bursts in a recording, that recording is not included in the further analysis and vice versa. Thus, we applied all the algorithms on a collection of data sets consisting of MEA channels which potentially exhibited bursts.



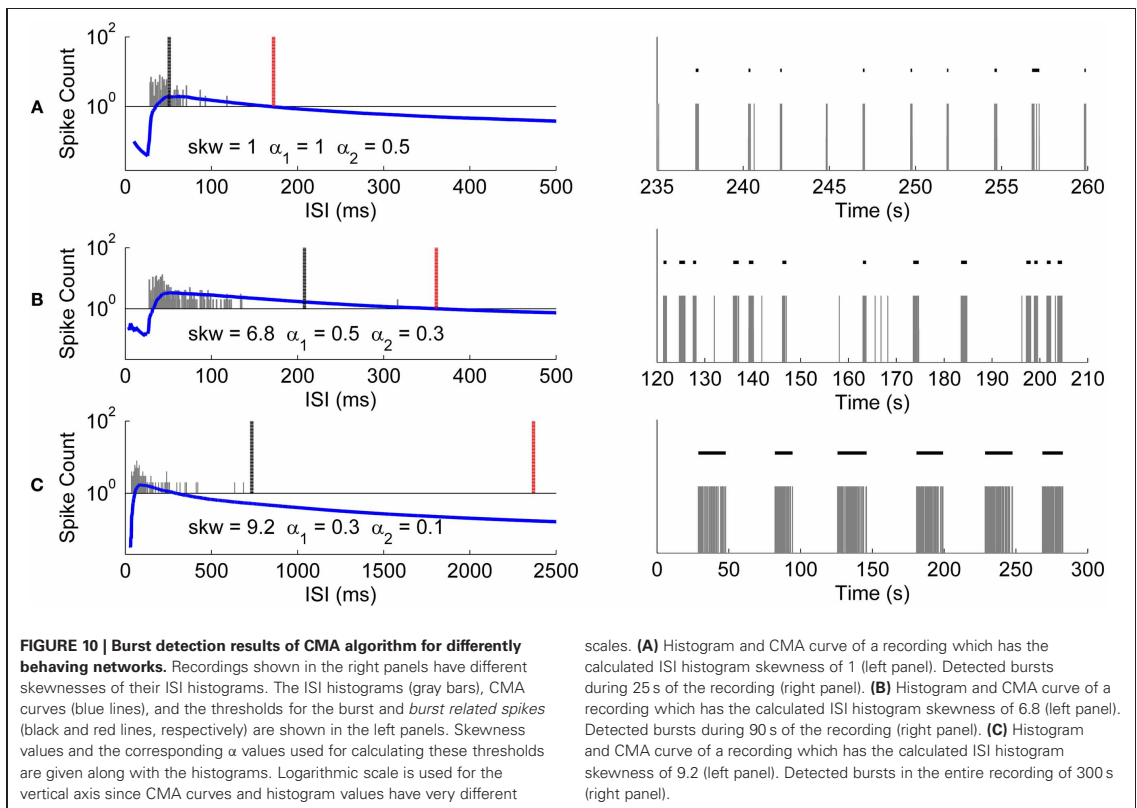


**Table 2 | The number of burst containing channels which are found by different methods.**

		Ds-I	Ds-II	Ds-III	Ds-IV	Ds-V
<b>Number of recordings with over 50 spikes/Total number of recordings</b>		<b>12/18</b>	<b>47/93</b>	<b>76/117</b>	<b>14/27</b>	<b>41/86</b>
<b>Number of burst containing channels found by different burst detection algorithms and criteria</b>	CMA algorithm	7 (39%)	57 (61%)	78 (67%)	13 (48%)	46 (53%)
	logSIH (100 ms threshold)*	6 (33%)	13 (14%)	49 (42%)	10 (37%)	16 (19%)
	Ten spikes with ISI < 100 ms*	1 (6%)	0 (0%)	9 (8%)	1 (4%)	1 (1%)
	Five spikes with ISI < 100 ms**	3 (17%)	6 (6%)	28 (24%)	2 (7%)	5 (6%)
	Three spikes with ISI < 100 ms**	8 (44%)	18 (19%)	55 (47%)	10 (37%)	18 (21%)
	Three spikes with ISI < 200 ms**	12 (67%)	32 (34%)	64 (55%)	13 (48%)	27 (31%)
	logSIH (200 ms threshold)**	12 (67%)	28 (30%)	57 (49%)	12 (44%)	24 (28%)

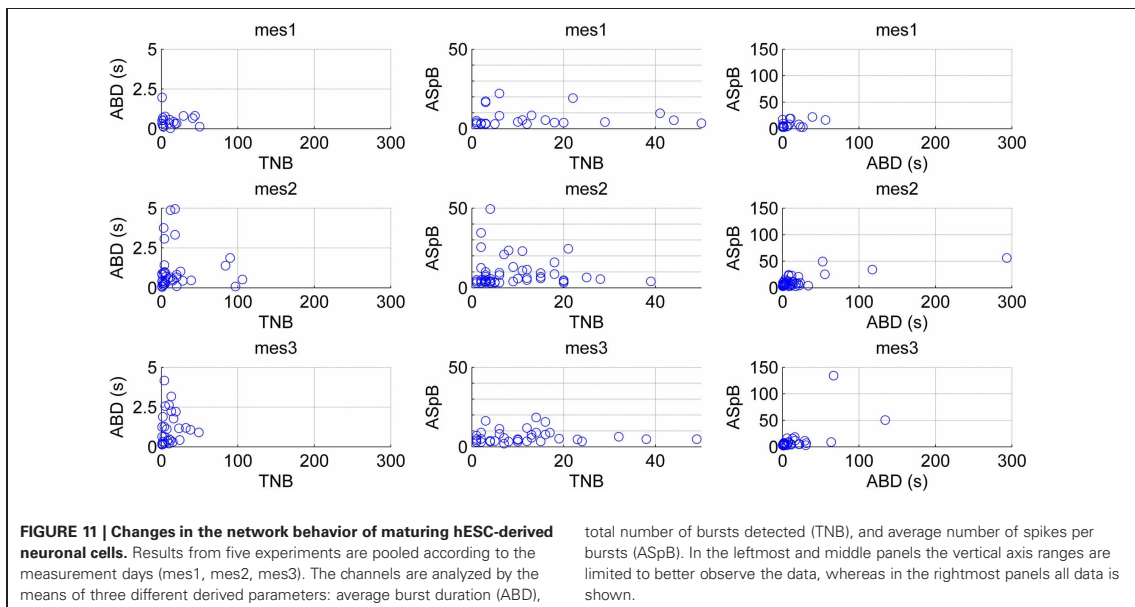
\* Previously proposed burst detection method.

\*\* Methods modified from previously proposed burst detection methods by changing burst criteria parameters to further investigate the usability of these methods for analysis of hESC-derived neuronal cell recordings.

Data from channels from all measurement days and all data sets which exhibit over 50 spikes at least in one of the measurements of approximately 300 s were chosen for a test. For example, if a channel exhibits over 50 spikes in the second measurement day, then the same channel data from the first and third measurement days are also chosen for the test without considering how many spikes they contain. In **Table 2** are given the numbers of channels

in which the burst were detected. Percentage values represent the ratio of detected bursts containing channels to total number of recordings tested.

In addition to success of the algorithm demonstrated in **Figures 7** and **8**, **Table 2** points out that we can increase the number of channels to be further analyzed by employing our CMA algorithm, which means extracting more burst or burst-like



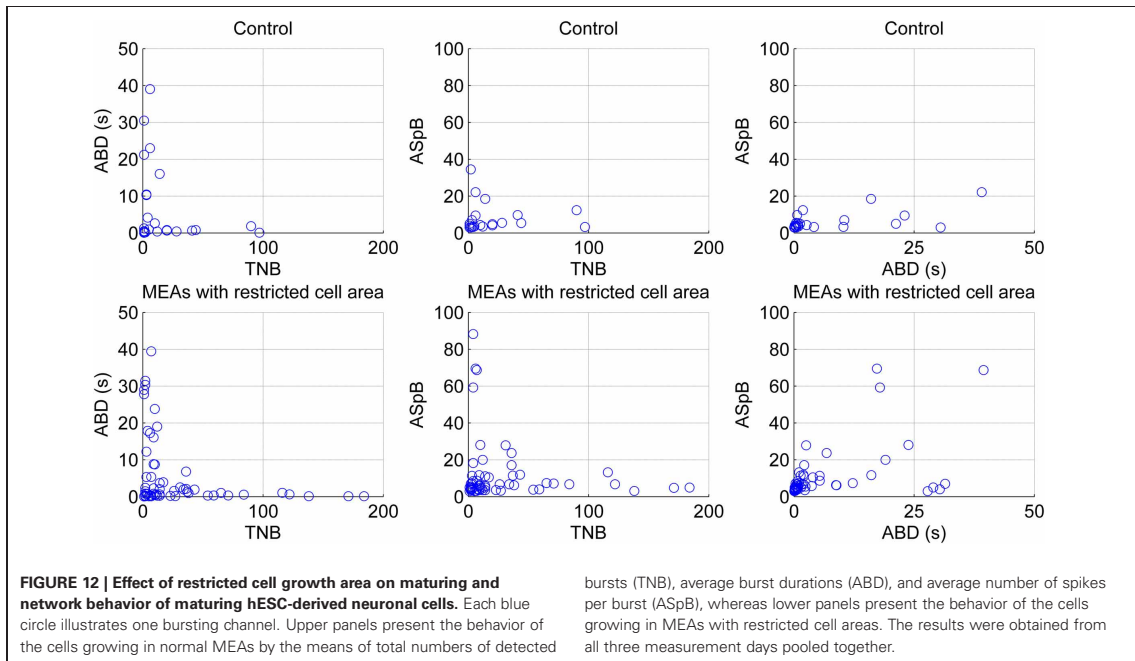
data for the subsequent analysis. As seen from **Table 2**, CMA algorithm works well in comparisons with the other tested algorithms and their variants. In **Table 2**, the methods with three spikes with  $ISI < 200$  ms and logISIH with 200 ms threshold did not yield satisfactory results. **Figure 9** shows an example of this comparison for three different channels, comparing logISIH algorithm with modified burst detection criteria of intra-burst ISI threshold of 200 ms with at least three spikes in a burst and our CMA algorithm. The results demonstrate that even though logISIH algorithm with modified parameters detects bursts (c.f., **Table 2**), this does not necessarily mean that the burst detection is satisfactory for further analysis since some burst event may be missed (**Figures 9A,B**) or differently detected (**Figure 9C**).

The CMA algorithm can be used to assess the developing network with regard to different types of MEAs and cultures as well. To demonstrate this, we pooled all the spontaneous recordings from five data sets according to the measurement days and plotted the relations of the calculated parameters ABD, TNB, and ASpB. **Figure 11** shows the results for all three measurement time points with each channel represented by one blue circle. The number of burst containing channels increased after the first measurement day. The numbers of burst containing channels for mes1, mes2, and mes3 were 28, 60 and 50, respectively. Despite of the small dataset available, we were able to observe changes by simply analyzing the ABD vs. TNB panels for all three measurement days in **Figure 11**, where the values for up to ABD of 5 s are demonstrated for a better view. We can conclude that majority of ABDs increased for second and third measurement days compared to first measurement day. The ABD values for mes1, mes2, and mes3 were found to be 7.7, 14, and 10.9 s, respectively. The ASpB values increased as well, and were 7, 9.4, and 9.3 spikes per bursts for the three measurement days, respectively. Increase in ASpB

values can be seen from ASpB vs. TNB panels for all three measurement days. The values for up to 50 spikes are shown in the ASpB vs. TNB panels of **Figure 11** for more in detail observations. Also, the effects of restricted cell growth area on the development of the network were assessed: the number of bursting channels increased with the restricted cell growth area. The total number of burst containing channels was 28 in 10 normal MEAs, whereas the total number was 63 measured from three MEAs with restricted cell growth area. ASpB and TNB values for those active channels increased as well for the MEAs which had restricted cell growth areas (**Figure 12**). Average number of bursts per channel was calculated to be 16.6 and 27.1 bursts for normal MEAs and MEAs with restricted cell growth areas, respectively, and the average spikes per burst were calculated to be 11.9 and 23.4 spikes, respectively. The relations between these three parameters give us an idea about changes in the bursting behavior during network development: as expected, increasing number of bursts is seen during development, as is the increase in the ASpB.

## DISCUSSION

As hESC-derived neuronal cells can generate spontaneously functional networks *in vitro* (Heikkilä et al., 2009), analyzing their bursting behaviors is essential to understand the development and functioning of human neuronal networks *in vitro*, and thus to strive to analyze the development of connections in these rather primitive networks with implications to the understanding of brain function. As we show in this paper, hESC-derived neuronal cells exhibit extremely time varying trends, and changing spiking trends can be observed as various types of burst-like patterns that are dynamically changing during the maturation of the cells and networks. Different burst definitions have been proposed previously, which mainly use fixed criteria, or as in



Wagenaar et al. (2006), employ a detection algorithm based on channel synchrony. As seen in **Figure 1**, developing active hESC-derived networks change their firing trends often. For such networks, in which the spatial synchronicity is changing rapidly, taking synchronicity as the primary criterion for bursting may not always be fruitful. Thus, synchronicity is not in the scope of this paper but for future studies, taking synchronicity into account would provide additional outcomes. For example, for the networks where bursts have tendencies to fire synchronously, bursts would be considered as individual events or clusters and neuronal network maturity can be assessed by analyzing IBIs instead of bursts itself (Tateno et al., 2002).

Another observation of variable neuronal network behavior is the irrationality of applying predefined fixed burst definition parameters. Classical parameters used for the burst detection and analysis, i.e., the number of spikes in bursts and burst durations (Harris et al., 2001; Tam, 2002; Kepecs and Lisman, 2004; Chiappalone et al., 2005), are often neither useful nor preferable for analysis of the developing networks. A previous study using intracellular recordings demonstrated the presence of singlet and duplet spikes that occur upon burst mediated depolarization (Weick et al., 2011). However for their study, hESC-derived neuroepithelial aggregates were added on a slice rather than grown as an entity. Also the temperature of their experiments (room temperature, 21–23°C) may have resulted in different results as our experiments were carried out in 37°C. Cooling from 34 to 21°C has been shown to remove network synchronization in rat hippocampal slices (Javedan et al., 2002). Furthermore, since extracellularly detected bursts require synchronization of large network of neurons, we consider that extracellular burst means

more than one spike (Lisman, 1997; Izhikevich et al., 2003), and at least duplets or triplets should be evaluated as bursts. Here, we propose that other detection parameters should not restrict the burst. This can be realized by extracting the parameters from statistics of the firing networks. It is possible that some of the maturing cells that still are incapable of emitting several spikes are omitted from our bursting criteria. However, multiple recordings of the same culture would reveal if such a neuronal assemble is later detected by the algorithm. Let us also note that cellular network activity manifested only in local field potentials (Kelly et al., 2010) could be utilized to improve network burst analysis, but is naturally ignored by our purely action potential based analysis. **Figure 6** demonstrates the problems with the analysis of developing networks if a priori defining ISI threshold boundaries as suggested previously (Harris et al., 2001; Kepecs and Lisman, 2004; Chiappalone et al., 2005; Pasquale et al., 2010). It can be seen that the major concentrations of intra-burst ISIs represented by the principal peaks appear in a wide range of approximately from 30 to 2000 ms. We could find a well behaving predetermined threshold by experimenting with various threshold values, but this is not very practical and the results would be sporadic. Our CMA algorithm is based on our motivation to detect burst like activities according to the assessment of the dynamics of the data itself. It provides us means to assess the developing networks with irregular and evolving dynamics.

With CMA algorithm the skewness and skewness based factor  $\alpha$ , can be used in analyzing the network behavior. Skewness of ISI distributions has been considered, for example, also in conjunction with the assessment of different neuronal and network models, e.g., by Hosaka et al. (2006). The relation of  $\alpha$  and

skewness is assessed in this paper by observing the relationship at a few discrete values of  $\alpha$  and skewness. Since only a limited number of values of the skewness and  $\alpha$  were tested, in some cases, different  $\alpha$  values may produce better results than the  $\alpha$ 's employed here. The set of values employed here simplifies the detection algorithm and more importantly still results in satisfactory performance of our algorithm. For future studies,  $\alpha$  and skewness may be utilized more extensively to describe network behaviors. Further, CMA also enables considering burst pre-spiking and burst tails as part of the analysis while considering dynamic network behavior and data.

A drawback of the CMA algorithm is that since it is devised to point out any “noteworthy” burst like events in the recordings, it may detect bursts erroneously in certain conditions, especially when applied on rarely spiking data with no bursts or on very active channels with very frequent nonstop spiking. Such kind of erroneous detections can be seen in the analysis of outliers and can be excluded by, e.g., simple cluster analysis, filtering, or thresholding. In our data, an example of a rare spiking channel which fires approximately 50 spikes in 300 s was detected as a single burst. The plot for this burst is seen as an outlier in **Figure 11** in the rightmost panel for the second measurement day. It can be seen as an extraordinary behavior among the usual bursts which forms a cluster in lower values in the same panel. If needed, exclusion of this outlier and focusing only on common bursting behavior for the subsequent analysis is a simple task by using a threshold of for instance 50 spikes for ASpB and 5 s for ABD values in this example. In fact, in closer observation, **Figure 11** demonstrates the increase in ABD and ASpB values as well as increase in the number of burst containing channels after the first measurement day. This is supported by the calculated average values for these parameters as well. Effect of cell growth area is shown in **Figure 12**. Increase in the average number of bursts per channels and ASpB is evident in **Figure 12** and confirmed by numerical analysis results. It seems that the restricted cell growth area results in faster network development since the number of burst containing channels increased as well in comparison with the control MEAs (**Figure 12**).

logSIH algorithm is excellent in detecting the bursting behavior especially for very frequent firing networks which have a good separation of inter-burst ISIs from intra-burst ISIs. Thus, it would be effective for detecting burst like activities of matured dynamic hESC-derived neurons. For developing networks the predefined boundaries limit its usability and, further, the logarithmic ISI

distribution of developing non-matured networks is not usually analyzable with this method as was the case for our data. In this paper we have quite freely utilized the concept of bursting behavior and enabled our parameters to go well above the commonly applied thresholds (Harris et al., 2001; Kepecs and Lisman, 2004; Chiappalone et al., 2005). As developing hESC-derived neuronal cell networks have not been available earlier, we feel that we should more openly think about the dynamics of the developing networks and at least study the concept of bursting more freely than before. Especially the logSIH and CMA algorithms provide ways to do so. Also, recurrence quantification analysis, which was proposed by Novellino and Zaldivar (2010) for analyzing and screening the changes in the neuronal activity especially for networks having slow dynamics, could be promising for hESC-derived neurons since slow dynamics in electrophysiological recordings can be observed in the early days of network development (Heikkilä et al., 2009) and the dynamics are demonstrated, e.g., by spiking/bursting frequency, inter-burst intervals, number of spikes per bursts. Additionally, a novel spike detection algorithm, e.g., by Maccione et al. (2009), could be combined with our method to yield enhanced analysis instead of the basic spike detection algorithm we used in this study.

In this paper, we were particularly motivated by the behavior and the problematic analysis of functional neural networks of hESC-derived neuronal cells and proposed a new burst detection and analysis method capable of the analysis of data measured from such networks. Our method provides enhanced analysis power to understand the development and functioning of neuronal networks, thus hopefully in time also contributing to our knowledge of the brain and towards the development of safe and functional neuronal stem cell based cures. Moreover, the proposed analysis method could be employed in developing new *in vitro* tests for drug screening and neurotoxicity assays.

## ACKNOWLEDGMENTS

This study was funded by Academy of Finland (decisions number 122947, 122959, 123233, and 135220), BioneXt Tampere, and Competitive Research Funding of Pirkanmaa Hospital District. Research of Fikret E. Kapucu was supported by Finnish Cultural Foundation and Ella and Georg Ehrnrooth Foundation. We want to acknowledge the personnel of Stem Cell Unit of Institute of Biomedical Technology, Tampere, Finland, for the support in stem cell research.

## REFERENCES

- Äänismaa, R., Ylä-Outinen, L., Mikkonen, J. E., and Narkilahti, S. (2011). “Human pluripotent stem cell-derived neuronal networks: their electrical functionality and usability for modelling and toxicology,” in *Methodological Advances in the Culture, Manipulation and Utilization of Embryonic Stem Cells for Basic and Practical Applications*, ed C. Atwood (Rijeka, Croatia: InTech), 459–472.
- Bal-Price, A. K., Hogberg, H. T., Buzanska, L., Lenas, P., van Vliet, E., and Hartung, T. (2010). *In vitro* developmental neurotoxicity (DNT) testing: relevant models and endpoints. *Neurotoxicology* 31, 545–554.
- Bissonnette, C. J., Lyass, L., Bhattacharyya, B. J., Belmadani, A., Miller, R. J., and Kessler, J. A. (2011). The controlled generation of functional basal forebrain cholinergic neurons from human embryonic stem cells. *Stem Cells* 29, 802–811.
- Carpenter, M. K., Inokuma, M. S., Denham, J., Mujitaba, T., Chiu, C. P., and Rao, M. S. (2001). Enrichment of neurons and neural precursors from human embryonic stem cells. *Exp. Neurol.* 172, 383–397.
- Chiappalone, M., Novellino, A., Vajda, I., Vato, A., Martinoia, S., and van Pelt, J. (2005). Burst detection algorithms for the analysis of spatio-temporal patterns in cortical networks of neurons. *Neurocomputing* 65–66, 653–662.
- Connors, B. W., Gutnick, M. J., and Prince, D. A. (1982). Electrophysiological properties of neocortical neurons *in vitro*. *J. Neurophysiol.* 48, 1302–1320.
- Daadi, M. M., Li, Z., Arac, A., Grueter, B. A., Sofilos, M., Malenka, R. C., Wu, J. C., and Steinberg, G. K. (2009). Molecular and magnetic resonance imaging of human

- embryonic stem cell-derived neural stem cell grafts in ischemic rat brain. *Mol. Ther.* 17, 1282–1291.
- Defranchi, E., Novellino, A., Whelan, M., Vogel, S., Ramirez, T., van Ravenzwaay, B., and Landsiedel, R. (2011). Feasibility assessment of micro-electrode chip assay as a method of detecting neurotoxicity *in vitro*. *Front. Neuroeng.* 4:6. doi: 10.3389/fneng.2011.00006
- Erceg, S., Láinez, S., Ronaghi, M., Stojkovic, P., Pérez-Aragó, M. A., Moreno-Manzano, V., Moreno-Palauques, R., Planells-Cases, R., and Stojkovic, M. (2008). Differentiation of human embryonic stem cells to regional specific neural precursors in chemically defined medium conditions. *PLoS ONE* 3:e2122. doi: 10.1371/journal.pone.0002122
- Gray, C. M., and McCormick, D. A. (1996). Chattering cells: superficial pyramidal neurons contributing to the generation of synchronous oscillations in the visual cortex. *Science* 274, 109–113.
- Gross, G. W., Rieske, E., Kreuzberg, G. W., and Meyer, A. (1977). A new fixed-array multi-microelectrode system designed for long-term monitoring of extracellular single unit neuronal activity *in vitro*. *Neurosci. Lett.* 6, 101–105.
- Harris, K. D., Hirase, H., Leinekugel, X., Henze, D. A., and Buzsáki, G. (2001). Temporal interaction between single spikes and complex spike bursts in hippocampal pyramidal cells. *Neuron* 32, 141–149.
- Heikkilä, T., Ylä-Outinen, L., Tanskanen, J. M. A., Lappalainen, R. S., Skottman, H., Suuronen, R., Mikkonen, J. E., Hyttinen, J. A., and Narkilahti, S. (2009). Human embryonic stem cell-derived neuronal cells form spontaneously active neuronal networks *in vitro*. *Exp. Neurol.* 218, 109–116.
- Hogberg, H. T., Sobanski, T., Novellino, A., Whelan, M., Weiss, D. G., and Bal-Price, A. K. (2011). Application of micro-electrode arrays (MEAs) as an emerging technology for developmental neurotoxicity: evaluation of domoic acid-induced effects in primary cultures of rat cortical neurons. *Neurotoxicology* 32, 158–168.
- Hosaka, R., Sakai, Y., Ikeguchi, T., and Yoshizawa, S. (2006). BvP neurons exhibit a larger variety in statistics of inter-spike intervals than LIF neurons. *J. Phys. Soc. Jpn.* 75, 124007.
- Ichikawa, M., Muramoto, K., Kobayashi, K., Kawahara, M., and Kuroda, Y. (1993). Formation and maturation of synapses in primary cultures of rat cerebral cortical cells: an electron microscopic study. *Neurosci. Res.* 16, 95–103.
- Illes, S., Fleischer, W., Siebler, M., Hartung, H. P., and Dihné, M. (2007). Development and pharmacological modulation of embryonic stem cell-derived neuronal network activity. *Exp. Neurol.* 207, 171–176.
- Izhikevich, E. M., Desai, N. S., Walcott, E. C., and Hoppensteadt, F. C. (2003). Bursts as a unit of neuronal information: selective communication via resonance. *Trends Neurosci.* 26, 161–167.
- Javedan, S. P., Fisher, R. S., Eder, H. G., Smith, K., and Wu, J. (2002). Cooling abolishes neuronal network synchronization in rat hippocampal slices. *Epilepsia* 43, 574–580.
- Kamioka, H., Maeda, E., Jimbo, Y., Robinson, H. P., and Kawana, A. (1996). Spontaneous periodic synchronized bursting during formation of mature patterns of connections in cortical cultures. *Neurosci. Lett.* 206, 109–112.
- Kandel, E. R., and Spencer, W. A. (1961). Electrophysiology of hippocampal neurons. II. Afterpotentials and repetitive firing. *J. Neurophysiol.* 24, 243–259.
- Kelly, R. C., Smith, M. A., Kass, R. E., and Lee, T. S. (2010). Local field potentials indicate network state and account for neuronal response variability. *J. Comput. Neurosci.* 29, 567–579.
- Kepecs, A., and Lisman, J. (2004). How to read a burst duration code. *Neurocomputing* 58–60, 1–6.
- Kim, J. E., O'Sullivan, M. L., Sanchez, C. A., Hwang, M., Israel, M. A., Brennand, K., Deerinck, T. J., Goldstein, L. S., Gage, F. H., Ellisman, M. H., and Ghosh, A. (2011). Investigating synapse formation and function using human pluripotent stem cell-derived neurons. *Proc. Natl. Acad. Sci. U.S.A.* 108, 3005–3010.
- Lai, B., Mao, X. O., Greenberg, D. A., and Jin, K. (2008). Endothelium-induced proliferation and electrophysiological differentiation of human embryonic stem cell-derived neuronal precursors. *Stem Cells Dev.* 17, 565–572.
- Lappalainen, R. S., Salomäki, M., Ylä-Outinen, L., Heikkilä, T. J., Hyttinen, J. A., Pihlajamäki, H., Suuronen, R., Skottman, H., and Narkilahti, S. (2010). Similarly derived and cultured hESC lines show variation in their developmental potential towards neuronal cells in long-term culture. *Regen. Med.* 5, 749–762.
- Lisman, J. E. (1997). Bursts as a unit of neural information: making unreliable synapses reliable. *Trends Neurosci.* 20, 38–43.
- Maccione, A., Gandolfo, M., Massobrio, P., Novellino, A., Martinoia, S., and Chiappalone, M. (2009). A novel algorithm for precise identification of spikes in extracellularly recorded neuronal signals. *J. Neurosci. Methods* 177, 241–249.
- Maeda, E., Robinson, H. P., and Kawana, A. (1995). The mechanisms of generation and propagation of synchronized bursting in developing networks of cortical neurons. *J. Neurosci.* 15, 6834–6845.
- Mazzoni, A., Broccard, F. D., Garcia-Perez, E., Bonifazi, P., Ruaro, M. E., and Torre, V. (2007). On the dynamics of the spontaneous activity in neuronal networks. *PLoS ONE* 2:e439. doi: 10.1371/journal.pone.0000439
- Novellino, A., and Zaldivar, J.-M. (2010). Recurrence quantification analysis of spontaneous electrophysiological activity during development: characterization of *in vitro* neuronal networks cultured on multi electrode array chips. *Adv. Artif. Intell.* 2010, 10.
- Pasquale, V., Martinoia, S., and Chiappalone, M. (2010). A self-adapting approach for the detection of bursts and network bursts in neuronal cultures. *J. Comput. Neurosci.* 29, 219–229.
- Pine, J. (1980). Recording action potentials from cultured neurons with extracellular microcircuit electrodes. *J. Neurosci. Methods* 2, 19–31.
- Selinger, J. V., Kulagina, N. V., O'Shaughnessy, T. J., Ma, W., and Pancrazio, J. J. (2007). Methods for characterizing interspike intervals and identifying bursts in neural activity. *J. Neurosci. Methods* 162, 64–71.
- Sundberg, M., Jansson, L., Ketolainen, J., Pihlajamäki, H., Suuronen, R., Skottman, H., Inzunza, J., Hovatta, O., and Narkilahti, S. (2009). CD marker expression profiles of human embryonic stem cells and their neural derivatives, determined using flow cytometric analysis, reveal a novel CD marker for exclusion of pluripotent stem cells. *Stem Cell Res.* 2, 113–124.
- Tam, D. C. (2002). An alternate burst analysis for detecting intraburst firings based on inter-burst periods. *Neurocomputing* 44–46, 1155–1159.
- Tateno, T., Kawana, A., and Jimbo, Y. (2002). Analytical characterization of spontaneous firing in networks of developing rat cultured cortical neurons. *Phys. Rev. E Stat. Nonlin. Soft Matter Phys.* 65, 051924.
- Turnbull, L., Dian, E., and Gross, G. (2005). The string method of burst identification in neuronal spike trains. *J. Neurosci. Methods* 145, 23–35.
- Wagenaar, D. A., Pine, J., and Potter, S. M. (2006). An extremely rich repertoire of bursting patterns during the development of cortical cultures. *BMC Neurosci.* 7, 11.
- Wang, Y. F., and Hatton, G. I. (2005). Burst firing of oxytocin neurons in male rat hypothalamic slices. *Brain Res.* 1032, 36–43.
- Weick, J. P., Liu, Y., and Zhang, S.-C. (2011). Human embryonic stem cell-derived neurons adopt and regulate the activity of an established neuronal network. *Proc. Natl. Acad. Sci. U.S.A.* 108, 20189–20194.
- Ylä-Outinen, L., Heikkilä, J., Skottman, H., Suuronen, R., Äänismaa, R., and Narkilahti, S. (2010). Human cell-based micro electrode array platform for studying neurotoxicity. *Front. Neuroeng.* 3:111. doi: 10.3389/fneng.2010.00111

**Conflict of Interest Statement:** The authors declare that the research was conducted in the absence of any commercial or financial relationships that could be construed as a potential conflict of interest.

Received: 21 March 2012; accepted: 30 May 2012; published online: 19 June 2012.

Citation: Kapucu FE, Tanskanen JMA, Mikkonen JE, Ylä-Outinen L, Narkilahti S and Hyttinen JAK (2012) Burst analysis tool for developing neuronal networks exhibiting highly varying action potential dynamics. *Front. Comput. Neurosci.* 6:38. doi: 10.3389/fncom.2012.00038

Copyright © 2012 Kapucu, Tanskanen, Mikkonen, Ylä-Outinen, Narkilahti and Hyttinen. This is an open-access article distributed under the terms of the Creative Commons Attribution Non Commercial License, which permits non-commercial use, distribution, and reproduction in other forums, provided the original authors and source are credited.

Kapucu F.E., Mikkonen J.E., Tanskanen J.M.A., Hyttinen J.A.K.

**Quantification and automatized adaptive detection of in vivo and in vitro neuronal bursts based on signal complexity.**

*In Proceedings of the 37th Annual International Conference of the IEEE Engineering in Medicine and Biology Society (EMBC), Milan, Aug.2015, pp. 4729-4732. IEEE, 2015.*

©2015 IEEE. Reprinted, with permission, from Kapucu F.E., Mikkonen J.E., Tanskanen J.M.A., Hyttinen J.A.K., Quantification and automatized adaptive detection of in vivo and in vitro neuronal bursts based on signal complexity, In Proceedings of the 37th Annual International Conference of the IEEE Engineering in Medicine and Biology Society (EMBC), Aug, 2015.



# Quantification and Automatized Adaptive Detection of *in Vivo* and *in Vitro* Neuronal Bursts Based on Signal Complexity\*

Fikret E. Kapucu, Jarno E. Mikkonen, Jarno M. A. Tanskanen, *Member, IEEE*, and  
Jari A. K. Hyttinen, *Member, IEEE*

**Abstract**— In this paper, we propose employing entropy values to quantify action potential bursts in electrophysiological measurements from the brain and neuronal cultures. Conventionally in the electrophysiological signal analysis, bursts are quantified by means of conventional measures such as their durations, and number of spikes in bursts. Here our main aim is to devise metrics for burst quantification to provide for enhanced burst characterization. Entropy is a widely employed measure to quantify regularity/complexity of time series. Specifically, we investigate the applicability and differences of spectral entropy and sample entropy in the quantification of bursts in *in vivo* rat hippocampal measurements and in *in vitro* dissociated rat cortical cell culture measurement done with microelectrode arrays. For the task, an automatized and adaptive burst detection method is also utilized. Whereas the employed metrics are known from other applications, they are rarely employed in the assessment of burst in electrophysiological field potential measurements. Our results show that the proposed metrics are potential for the task at hand.

## I. INTRODUCTION

Neuronal activity is generally expressed by action potentials, i.e., neuronal spikes. In an ensemble of neuronal cells neurons are interacting and sometimes firing spikes in an orchestrated manner. These short episodes of intense firing are called bursts [1,2,3]. It has been known that bursts reflect and influence the plasticity mechanisms and network activity [4]. Moreover, it has been shown that network communication also depends on the nature of the bursts. For example, according to Izhikevich et al. [5], selective communication exists depending on interspike frequencies in the bursts as a presynaptic cell can selectively influence some postsynaptic targets, but not others. This indicates that bursts with different firing dynamics have different effects on neuronal communications.

In the past years, neuronal bursts *in vitro* or *in vivo* have been assessed and classified with respect to several parameters such as burst duration, interspike amplitude, interspike interval (ISI), and power spectrum [6,7,8]. Similar

\* The works of F. E. Kapucu and J. M. A. Tanskanen have been supported by the 3DNeuroN project in the European Union's Seventh Framework Programme, Future and Emerging Technologies, grant agreement n°296590.

F. E. Kapucu (e-mail: fikret.kapucu@tut.fi, tel.: +358 40 849 0023), J. M. A. Tanskanen (e-mail: jarno.m.tanskanen@tut.fi), and J. A. K. Hyttinen (e-mail: jari.hyttinen@tut.fi) are with Tampere University of Technology, Department of Electronics and Communications Engineering, Computational Biophysics and Imaging Group, BioMediTech, 33520 Tampere, Finland.

J. E. Mikkonen (e-mail: jarno.e.mikkonen@jyu.fi) is with University of Jyväskylä, Department of Psychology, Oscillatory Brain Research Group, 40014 University of Jyväskylä, Finland.

parameters have been used to emphasize the effects of, for example, pharmaceuticals [9], neurotoxins [10], and gene expressions [11]. A noteworthy study for classifying EEG bursts related to applied anesthetic agent was presented by Lipping et al. [12]. In that study spectral entropy (SE) and sample entropy (SmE) were employed. Bursts were identified manually by authors. An earlier study on EEG indicated that also the lengths of bursts as well as periods of burst suppression provide clear classification of bursts confirming to the patient groups [13]. Prior to the analysis, non-biased and adaptive detection of bursts is crucial for EEG and local field potential measurements alike. Moreover, analyzing larger sets of data with high numbers of bursts with greatly varying dynamics [14], such as those encountered in long-term measurements of developing neuronal networks, calls for automatized burst detection algorithms.

In this paper, we propose a method for quantifying neuronal bursts with calculated entropy values with the start and end points of the bursts were marked by an automatized adaptive burst detection algorithm. We first show how SE and SmE values can be used in quantifying bursts with different dynamics. We demonstrate our method by analyzing the bursts in *in vivo* hippocampal recordings from anesthetized rats and in *in vitro* dissociated rat cortical cells on microelectrode arrays (MEAs).

## II. EXPERIMENTAL TEST DATA

The *in vivo* experiments were performed on anaesthetized rats. Detailed description of the experimental setup has been described in [15] along with the ethical approval information. Briefly, anaesthetized rats were placed in a stereotaxic instrument and holes were drilled on the skull above the target structures. A silicon probe (courtesy of University of Michigan Center for Neural Communication Technology, MI, USA) was used with 16 electrodes on one shank and 100  $\mu\text{m}$  distance between the electrodes. Two of the top most electrodes (channels 15 and 16) of the probe were not used due to setup design and recording apparatus restrictions. The probe was lowered into hippocampus and electrophysiological signals were recorded. Here, we analyzed three consecutive recordings from one rat to provide a proof of concept.

The *in vitro* experiments were performed on dissociated rat cortical cells which were plated on MEAs. Detailed description of the experimental setup has been described in [16] along with the statement of the ethical conduction of the research. Briefly, cells were taken from prefrontal cortical tissue of Wistar rats and sowed randomly on a MEA plate with 60 TiN electrodes of 30  $\mu\text{m}$  in diameter and 200  $\mu\text{m}$  interelectrode distances on an 8x8 rectangular grid with

corner electrodes missing (Multi Channel Systems, Reutlingen, Germany) for culturing. Cell density was approximately 1250 cells/mm<sup>2</sup>. After four weeks of culturing, electrophysiological data were recorded. For the proof of concept, we here analyzed one minute of a recording from one MEA.

Both the *in vivo* and *in vitro* data were collected previously for other research, e.g. for [15] and [16], respectively.

### III. METHODS

The analysis was conducted in the following three steps:

- Automatized detection using an adaptive burst detection algorithm.
- Calculating spectral and sample entropies for detected bursts.
- For the *in vivo* data, group the entropy values with respect to the experimental design, and calculate the medians along with the 1st and 3rd quartiles to obtain interquartile ranges (IQRs).
- For the *in vitro* data, calculate the medians of the entropy values for the detected bursts for each MEA channel and form color maps for better spatial assessment of quantified bursts.

#### A. Adaptive automatized burst selection

Burst detection algorithm used in this study was devised previously by Kapucu et al. [14]. Briefly, ISI histograms of the recordings to be analyzed were formed, and cumulative moving averages (CMA) of the histograms were calculated as

$$CMA_l = \frac{1}{l} \sum_{i=1}^l y_i, \quad (1)$$

where  $y_i, i = 1, \dots, N$  is the spike count in the  $i$ th ISI bin with  $N$  the total number of ISI bins. The maximum value of  $CMA, CMA_m$  is reached at the  $m$ th ISI bin

$$m = \underset{m = 1, \dots, N}{\arg \max} \left( \frac{1}{m} \sum_{i=1}^m y_i \right). \quad (2)$$

Thereafter, two separate thresholds were calculated for burst spikes and burst related spikes by multiplying  $CMA_m$  with a skewness depended factor  $0 < \alpha < 1$ . The ISI threshold  $x_t, x_t > x_m$  for burst detection was found at the mid time point of the ISI bin for which the value of the CMA curve was the closest to  $\alpha CMA_m$ . Burst spikes and burst related spikes were merged to mark the bursts. In this study we used the same  $\alpha$  values suggested in Kapucu et al. [14].

#### B. Spectral Entropy based measure

SE is basically the application of Shannon's entropy algorithm on power spectrum. Shannon entropy is based on the summation of probability density function (PDF) values within a time window, whereas SE is the sum of PDF values within a frequency range. We employed SE as described by Vertiö-Oja et al. [17].

Power spectra of the previously detected bursts were calculated, and the power spectra were normalized with a constant  $C_n$  in the frequency range  $[f_1, f_2]$  where SE  $S$  was calculated so that the normalized power spectrum  $P_n(f_i)$  was equal to 1.

$$\sum_{f_i=f_1}^{f_2} P_n(f_i) = C_n \sum_{f_i=f_1}^{f_2} P(f_i) = 1 \quad (3)$$

SE  $S_N$  was calculated from the normalized power spectrum and normalized with  $\log(N[f_1, f_2])$  to reside within  $0 < S_N < 1$ , where  $N[f_1, f_2]$  is the total number of frequency components in the frequency range  $[f_1, f_2]$ .

$$S_N = \frac{1}{\log(N[f_1, f_2])} \sum_{f_i=f_1}^{f_2} P_n(f_i) \log\left(\frac{1}{P_n(f_i)}\right) \quad (4)$$

We calculated spectral entropies in the Nyquist range, since the effective bandwidths of the studied signals were not known, especially for the *in vitro* data.

#### C. Sample Entropy based measure

The SmE [18] employed was a modified form of the approximate entropy, which was previously introduced by Pincus [19]. The main difference between the two entropies is that SmE does not include self-matching, and according to a previous study, SmE is less sensitive to changes in data length [20].

SmE was calculated for the signal  $s$  of length  $N$  samples as follows:  $(N - m + 1)$  vectors of length  $m$  were formed:  $X(i) = (s(i), s(i + 1), \dots, s(i + m - 1))$ , where  $m$  is the embedding dimension. Thereafter, the probability that any other vector is similar to  $X(i)$  was calculated as

$$C_i(r) = \frac{\text{number of } j \text{ where } d(X(i), X(j)) \leq r}{n - m + 1}, \quad (5)$$

where  $d(X(i), X(j))$  is defined as the maximum absolute difference between the vectors  $X(i)$  and  $X(j)$ , and  $r$  is the filtering level. Average probability was calculated as

$$\Phi(N, m, r) = \frac{1}{N - m} \sum_{i=1}^{N - m} C_i(r), \quad (6)$$

and the SmE was obtained as

$$SmE(N, m, r) = -\ln \frac{\Phi(N, m + 1, r)}{\Phi(N, m, r)}. \quad (7)$$

Following the common practice, we set  $r$  to 0.2 times the standard deviation, and the embedding dimension  $m = 2$ .

#### D. Statistical calculation

Calculated values for spectral entropies were listed for different experiment points: for *in vivo* data, the SE values of all the bursts from 14 channels were pooled for the three consecutive experiments, and for the *in vitro* data, the same was done for each recording channel.

Next, the median values together with the 25<sup>th</sup> and 75<sup>th</sup> percentiles were calculated for each experimental point and results were plotted for comparisons.

## IV. RESULTS

First, we demonstrate the capabilities of the two described entropy algorithms on quantifying the automatically detected neuronal bursts. Fig. 1 shows how SmE and spectral entropies change in the existence of bursts for the *in vitro* MEA recordings, and that the bursts with different interspike properties, seen in the upper panel, resulted in different SE and SmE values.

Fig. 2 illustrates the proposed bursts quantification. The example was calculated from nine separate bursts automatically detected in a 200 s long MEA recording. The

bursts have different durations and the numbers of spikes, but not very varying ISIs. Fig. 2 shows the changes in the above mentioned burst values, as well as how well they are quantified with entropy measures. As it can be seen from Fig. 2B and C, SmE reflects the changes in burst duration and the number of spikes in bursts, whereas these do not have significant effects on SE.

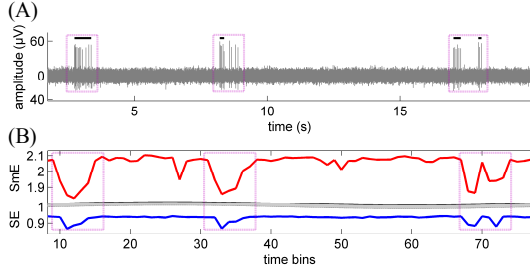


Figure 1. (A) A signal with bursts detected with automatized burst detection algorithm. Bursts are labeled with black horizontal lines above the signal. (B) SmE (red) and SE (blue) values (lower panel) calculated for the signal seen in the upper panel using 0.5 s long 50% overlapped bins. The three purple boxes in (A) indicate the changes during bursts.

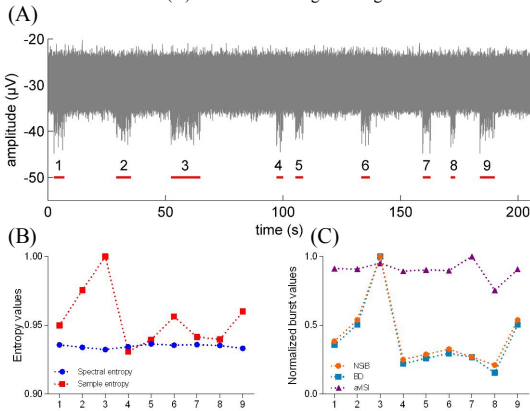


Figure 2. (A) A signal with the bursts detected with the automatized burst detection algorithm. The detected bursts are labeled with red lines. (B) SmE (red) and SE (blue) values calculated for the nine bursts seen in the upper panel. Entropy values are normalized between 0 and 1 for a better visual comparison. (C) Burst durations (BD), number of spikes in bursts (NSiB), and average ISI (avISI) are shown for the same nine bursts. Horizontal axis labeling in (B) and (C) identifies the bursts as numbered in (A).

Finally, we demonstrated our method on quantifying the automatically detected bursts from *in vivo* and *in vitro* experiments. Fig. 3 shows the medians and IQRs of the entropy values calculated for the bursts in the entire three measurements from rat hippocampus. Considering the overall bursting (Fig. 3) in these measurements, both entropy measures exhibit similar behavior. This could be expected, since the state of an anesthetized rat does not change by the means of bursts, and on the other hand, the entropy values show some variance as indicated by the IQRs in Fig. 3.

The results of spatial characteristic of the complex measures *in vitro* data are shown in Fig. 4. Although the SE and SmE values are different, results from both entropies indicate that the maximum values are at the electrodes 24 and

87. Also, both entropy based burst quantification results revealed similar spatial entropy value patterns (Fig. 4). In Fig. 4, as also in Fig. 2B, the differences between the bursts were more pronounced based on the SmE values than indicated by the SE values.

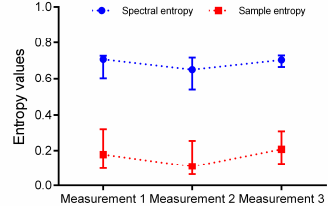


Figure 3. SE (blue) and SmE (red) calculated for the bursts of the *in vitro* data. The numbers of the analyzed bursts were 426, 1244 and 1464 for the measurement 1, 2, and 3, respectively. The whiskers indicate the 1<sup>st</sup> and 3<sup>rd</sup> quartiles.

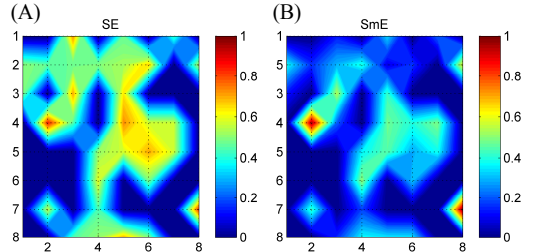


Figure 4. Colormaps of the medians of the (A) SE and (B) SmE values calculated for every burst from each channel of a 60-channel MEA. The grid intersections indicate the locations of the electrodes, except that there were no electrodes at the corners of the figures.

## V. CONCLUSIONS AND DISCUSSION

We showed that entropy measures, specifically SE and SmE, can be used for quantifying neuronal bursts for *in vivo* and *in vitro* studies, alike seen in the example in Fig. 2. Working with an automatized adaptive burst detection algorithm, quantification could be applied on large data sets to obtain statistically significant results. Here, our aim was to introduce and demonstrate the SE and SmE based burst quantification, providing a proof of concept.

We observed that there are differences between the employed entropy measures. In our particular case, SmE was more sensitive to the burst duration and the number of spikes in bursts, and produced more distinct values for the presumably different kinds of bursts compared to SE. On the other hand, both entropy measures were good at reflecting the changes in neuronal recordings during bursts. As entropies are measures of regularity/complexity of signals, which information is not provided by the conventional burst metrics, the information they provide is complimentary to the conventional burst quantification information. Further studies are warranted to investigate the actual meaning of the entropy values from the point of view of the neuronal network function; the real potential of the SE can be revealed with the use of appropriate data where there are differences in the regularity of spectra of the bursts.

The spatial analysis of *in vitro* experiments showed that channels with high overall SE and SmE values (Fig. 4) had neighboring channels with higher SE or SmE values than on the MEA in general. This could have been due to the spatial neuronal synchrony, possibly indicating functional connectivity.

Based on SE and SmE, burst classification and further characterization may be attempted. For future studies, the proposed methods could also be useful in assessing the existence of functionally different neuronal networks manifested by bursts with different entropy values. In conclusion, we find both SE and SmE potential for quantifying action potential bursts.

#### REFERENCES

- [1] B. W. Connors, M. J. Gutnick, and D. A. Prince, "Electrophysiological properties of neocortical neurons in vitro," *J. Neurophysiol.*, vol. 48, pp. 1302–1320, 1982. Available: <http://jn.physiology.org/content/48/6/1302>
- [2] C. M. Gray and D. A. McCormick, "Chattering cells: superficial pyramidal neurons contributing to the generation of synchronous oscillations in the visual cortex," *Science*, vol. 274, pp. 109–113, 1996. DOI:10.1126/science.274.5284.109
- [3] E. R. Kandel and W. A. Spencer, "Electrophysiology of hippocampal neurons. II. After-potentials and repetitive firing," *J. Neurophysiol.*, vol. 24, pp. 243–259, 1961. Available: <http://jn.physiology.org/content/24/3/243>
- [4] J. E. Lisman, "Bursts as a unit of neural information: making unreliable synapses reliable," *Trends Neurosci.*, vol. 20, pp. 38–43, 1997. Available: <http://www.sciencedirect.com/science/article/pii/S0166223696100709>
- [5] E. M. Izhikevich, N.S. Desai, E. C. Walcott, and F. C. Hoppensteadt, "Bursts as a unit of neuronal information: selective communication via resonance," *Trends Neurosci.*, vol. 26, pp. 161–167, 2003. Available: <http://www.sciencedirect.com/science/article/pii/S0166223603000341>
- [6] D. A. Wagenaar, J. Pine, and S. M. Potter, "An extremely rich repertoire of bursting patterns during the development of cortical cultures," *BMC Neuroscience*, vol. 7, no. 11, 2006. DOI: 10.1186/1471-2202-7-11.
- [7] R. A. J. van Elburg and A. van Ooyen, "A new measure for bursting," *Neurocomputing*, vol. 58–60, pp. 497–502, 2004. DOI:10.1016/j.neucom.2004.01.086
- [8] W. Bair, C. Koch, W. Newsome, and K. Britten, "Power spectrum analysis of bursting cells in area MT in the behaving monkey," *J. Neurosci.*, vol. 14, pp. 2870–2892, 1994. Available: <http://www.jneurosci.org/content/14/5/2870>
- [9] A. Hayar and M. Ennis, "Endogenous GABA and glutamate finely tune the bursting of olfactory bulb external tufted cells," *J. Neurophysiol.*, vol. 98, pp. 1052–1056, 2007. DOI: 10.1152/jn.01214.2006
- [10] E. W. Keefer, A. Gramowski, D. A. Stenger, J. J. Pancrazio and G. W. Gross, "Characterization of acute neurotoxic effects of trimethylolpropane phosphate via neuronal network biosensors," *Biosens. Bioelectron.*, vol. 16, pp. 513–525, 2001. Available: <http://www.sciencedirect.com/science/article/pii/S0956566301001658>
- [11] M. A. Clifford, J. K. Kanwal, R. Dzakpasu, and M. J. Donoghue, "EphA4 expression promotes network activity and spine maturation in cortical neuronal cultures," *Neural Development*, vol. 6, no. 21, 2011. DOI:10.1186/1749-8104-6-21.
- [12] T. Lipping, J. Stålnacke, E. Olejarczyk, R. Marciniak, and V. Jääntti, "Classification of EEG Bursts in deep sevoflurane, desflurane and isoflurane anesthesia using AR-modeling and entropy measures," in *Prof. 2013 35th Ann. Int. Conf. IEEE Eng. in Medicine and Biology Soc.*, pp. 5083–5086, Osaka, Japan, 2013. DOI: 10.1109/EMBC.2013.6610691
- [13] T. Lipping, V. Jääntti, A. Yli-Hankala, and K. Hartikainen, "Adaptive segmentation of burst-suppression pattern in isoflurane and enflurane anesthesia," *International Journal of Clinical Monitoring and Computing*, vol. 12, pp.161–167, 1995. DOI:10.1007/BF02332690
- [14] F. E. Kapucu, J. M. A. Tanskanen, J. E. Mikkonen, L. Ylä-Outinen, S. Narkilahti, and J. A. K. Hyttinen, "Burst analysis tool for developing neuronal networks exhibiting highly varying action potential dynamics," *Front. Comput. Neurosci.*, vol. 6, no. 38, 2012. DOI: 10.3389/fncom.2012.00038.
- [15] J. E. Mikkonen and M. Penttonen, "Frequency bands and spatiotemporal dynamics of beta burst stimulation induced afterdischarges in hippocampus in vivo," *Neurosci.*, vol. 130, pp.239–247, 2005. Available: <http://www.sciencedirect.com/science/article/pii/S0306452204007778>
- [16] O. S. Weihberger, J. E. Mikkonen, and U. Eger, "Quantitative examination of stimulus-response relations in cortical networks in vitro," *J. Neurophys.*, vol. 109 pp. 1764–1774, 2013. DOI: 10.1152/jn.00481.2012
- [17] H. Viertiö-Oja, V. Maja, M. Särkelä, P. Talja, N. Tenkanen, H. Tolvanen-Laakso, M. Paloheimo, J. E. Vakkuri, A. Yli-Hankala, P. Meriläinen, "Description of the entropy algorithm as applied in the Daxe-Ohmeda S/5 Entropy Module," *Acta Anaesthesiol. Scand.*, vol. 48, pp.154–161, 2004. DOI:10.1111/j.0001-5172.2004.00322.x
- [18] J. S. Richman and J. R. Moorman, "Physiological time-series analysis using approximate entropy and sample entropy," *Am. J. Physiol. Heart Circ. Physiol.*, vol. 278, no. 6, H2039–H2049. Available: <http://ajpheart.physiology.org/content/278/6/H2039>
- [19] S. M. Pincus, "Approximate entropy as a measure of system complexity," *Proc. Natl. Acad. Sci.*, vol. 88, pp. 2297–2301, 1991. DOI:10.1073/pnas.88.6.2297
- [20] J. M. Yentes, N. Hunt, K. K. Schmid, J. P. Kaipust, D. McGrath, and N. Stergiou, "The appropriate use of approximate entropy and sample entropy with short data sets," *Ann. Biomed. Eng.*, vol. 41, pp. 349–365, 2013. DOI:10.1007/s10439-012-0668-3

Kapucu F.E., Mäkinen, M.E.L., Tanskanen J.M.A., Ylä-Outinen L., Narkilahti S.,  
Hyttinen J.A.K.

**Joint analysis of extracellular spike waveforms and neuronal network  
bursts.**

*Journal of neuroscience methods 259 (2016): 143-155.*

Reprinted from Journal of Neuroscience Methods, 259, Kapucu F.E., Mäkinen,  
M.E.L., Tanskanen J.M.A., Ylä-Outinen L., Narkilahti S., Hyttinen J.A.K., Joint  
analysis of extracellular spike waveforms and neuronal network bursts, 143-155,  
Copyright (2016), with permission from Elsevier.





Contents lists available at ScienceDirect

## Journal of Neuroscience Methods

journal homepage: [www.elsevier.com/locate/jneumeth](http://www.elsevier.com/locate/jneumeth)

Computational Neuroscience

## Joint analysis of extracellular spike waveforms and neuronal network bursts

Fikret Emre Kapucu<sup>a,\*</sup>, Meeri E.-L. Mäkinen<sup>b</sup>, Jarno M.A. Tanskanen<sup>a</sup>,  
Laura Ylä-Outinen<sup>b</sup>, Susanna Narkilahti<sup>b</sup>, Jari A.K. Hyttinen<sup>a</sup><sup>a</sup> Tampere University of Technology, Department of Electronics and Communications Engineering, Computational Biophysics and Imaging Group, BioMediTech, Biokatu 6, FI-33520 Tampere, Finland<sup>b</sup> University of Tampere, NeuroGroup, BioMediTech, Biokatu 12, FI-33014 Tampere, Finland

## HIGHLIGHTS

- Spike and burst statistics give limited information on changes in networks.
- Here, spike sorting combined with burst detection.
- Spike waveform type participation in bursts revealed.
- Spike type compositions of bursts change under network modifications.
- New kind of information obtained on the changes in bursting networks.

## ARTICLE INFO

## Article history:

Received 2 June 2015

Received in revised form

23 November 2015

Accepted 24 November 2015

Available online 7 December 2015

## Keywords:

Neuronal network

Microelectrode array

Burst detection

Spike waveform

Spike sorting

Electrophysiological signal analysis

## ABSTRACT

**Background:** Neuronal networks are routinely assessed based on extracellular electrophysiological microelectrode array (MEA) measurements by spike sorting, and spike and burst statistics. We propose to jointly analyze sorted spikes and detected bursts, and hypothesize that the obtained spike type compositions of the bursts can provide new information on the functional networks.

**New method:** Spikes are detected and sorted to obtain spike types and bursts are detected. In the proposed joint analysis, each burst spike is associated with a spike type, and the spike type compositions of the bursts are assessed.

**Results:** The proposed method was tested with simulations and MEA measurements of *in vitro* human stem cell derived neuronal networks under different pharmacological treatments. The results show that the treatments altered the spike type compositions of the bursts. For example, 6-cyano-7-nitroquinoxaline-2,3-dione almost completely abolished two types of spikes which had composed the bursts in the baseline, while bursts of spikes of two other types appeared more frequently. This phenomenon was not observable by spike sorting or burst analysis alone, but was revealed by the proposed joint analysis.

**Comparison with existing methods:** The existing methods do not provide the information obtainable with the proposed method: for the first time, the spike type compositions of bursts are analyzed.

**Conclusions:** We showed that the proposed method provides useful and novel information, including the possible changes in the spike type compositions of the bursts due to external factors. Our method can be employed on any data exhibiting sortable action potential waveforms and detectable bursts.

© 2015 Elsevier B.V. All rights reserved.

\* Corresponding author. Tel.: +358 40 849 0023; fax: +358 3 364 1385 (departmental fax; +not at the corresponding author's location, usage discouraged).

E-mail addresses: [fikret.kapucu@tut.fi](mailto:fikret.kapucu@tut.fi) (F.E. Kapucu), [meeri.makinen@uta.fi](mailto:meeri.makinen@uta.fi) (M.E.-L. Mäkinen), [tanskanen@iee.org](mailto:tanskanen@iee.org) (J.M.A. Tanskanen), [laura.yla-outinen@uta.fi](mailto:laura.yla-outinen@uta.fi) (L. Ylä-Outinen), [susanna.narkilahti@uta.fi](mailto:susanna.narkilahti@uta.fi) (S. Narkilahti), [jari.hyttinen@tut.fi](mailto:jari.hyttinen@tut.fi) (J.A.K. Hyttinen).<sup>1</sup> Department of Electronics and Communications Engineering, Tampere University of Technology

## 1. Introduction

Regardless of decades of research, neuronal networks, and their development and functioning, are still not fully understood. The analysis of electrophysiological data is one of the methodologies for advancing our knowledge. Developing new methods to derive more information from the available measurement data is highly desirable. Here, we propose a new joint spike and burst analysis method for analyzing extracellular network electrophysiology data. We illustrate the method with simulated signals, and as the test bench we use human stem cell derived neuronal networks cultured on microelectrode arrays (MEAs). Such networks have been shown to develop spontaneous electrical activity and show histiotypic behavior (Buzańska et al., 2005, 2006; Heikkilä et al., 2009).

MEAs are commonly employed in the assessment of the electrical activity of neuronal networks both *in vitro* and *in vivo*. MEA recordings carry information on the electrical activity in tissues and cell cultures at network and cell levels (Gross et al., 1977; Thomas et al., 1972; Pine, 1980; Egert et al., 1998), e.g., from neurons in the vicinity of the MEA electrodes. Physically, MEAs record extracellular field potentials as voltage signals, which can exhibit contributions from both action potentials and lower frequency neuronal activity, in addition to noise. Here, we consider that an action potential is synonymous with a voltage spike over any area of neuronal cell membrane recorded via a MEA electrode. In the recordings, spikes may occur as individual spikes, or as trains or bursts manifesting network activity (Kandel and Spencer, 1961; Connors et al., 1982; Gray and McCormick, 1996).

To use neuronal networks on MEAs as biosensors was proposed by Gross and Rhoades (1995), who described the effects of several pharmacological agents on bursting, and also mentioned the possibility to measure average spike waveforms. Several studies have suggested various spike and burst related metrics to quantify neuronal network behavior (Bal-Price et al., 2008; Johnstone et al., 2010; Defranchi et al., 2011; Hogberg et al., 2011; Novellino et al., 2011; Alloisio et al., 2015). In previous studies, parameters such as spike count, the number of bursts, mean spike rate, mean burst rate, the number of spikes in bursts, burst duration, inter-burst interval, and the percentage of spikes in bursts have been commonly used (Johnstone et al., 2010; Novellino et al., 2011; Uchida et al., 2012). Furthermore, patterns and spatial distributions of activity are inherent and crucial aspects in network electrophysiology (Banerjee and Ellender, 2009; Uhlhaas et al., 2009; Crumiller et al., 2011).

Burst analysis is necessary in analyzing network activity and the network effects of different *in vitro* treatments (Johnstone et al., 2010). Previously, several different burst detection methods, mostly based on experimentally pre-defined parameters such as interspike interval (ISI) and the number of spikes in bursts (Chiappalone et al., 2005; Turnbull et al., 2005; Wagenaar et al., 2006; Pasquale et al., 2010), have been proposed, for example, to study rat cortical or hippocampal neuronal networks. Burst definitions which are more adaptive to the analyzed network have also been proposed (Pasquale et al., 2010; Kapucu et al., 2012). Such adaptability is called for in the analysis of maturing networks, such as human stem cell derived networks (Kapucu et al., 2012).

In spike analysis, spike waveform cut-outs are sorted, and the waveforms in each resulting class, or cluster, can be averaged to obtain the representative spike waveform types (Gibson et al., 2012). Despite its challenges, spike sorting is required for isolating or identifying single neuronal cell activities in a population firing in an orchestrated manner (Buzsáki, 2004), and different spike sorting algorithms have been utilized in various studies (Santhanam et al., 2006; Sun et al., 2010; Truccolo et al., 2011). Most related to our work, Illes et al. (2014) utilized raster plots of the sorted spikes.

In this paper, a novel joint analysis of sorted spike waveforms and detected bursts is proposed. The joint analysis provides information on the participation of the spike types in bursts for the particular data at hand. In other words, spike type compositions of the bursts, and their changes, e.g., in time or due to external effects, can be assessed using the proposed framework. To our best knowledge, such a joint analysis has not been proposed previously.

A motivation for the development of the joint analysis has been an earlier study on the relationship between single spike features and network bursting in hippocampal pyramidal cells (Harris et al., 2001), which indicated that conditions that cause high firing rates do not necessarily produce high bursting in pyramidal cells. Moreover, the relation between firing rate and bursting may change differently for bursts with different intraburst ISIs (Harris et al., 2001). This may also be the case with our cells, or with any other neuronal network. If this is the case, increase in the activity of a spike type would not guarantee a higher probability of its participation in bursts. Thus, joint analysis would be necessary to assess the burst participations of different spike types.

The joint analysis is illustrated with simulated data containing spikes with different waveforms, organized as individual spikes and bursts, and demonstrated with real MEA data from *in vitro* human neuronal networks undergoing a pharmacological experiment to alter the networks. We show that the proposed framework yields information on the networks and on the changes therein, which is not obtainable by spike and burst analysis nor by spike sorting alone.

The methods presented in this paper were implemented in Matlab and run in a standard laptop PC. The Matlab code for the proposed joint framework is publicly freely available in the Matlab Central File Exchange (<http://www.mathworks.com/matlabcentral/fileexchange/54277-joint-analysis-of-extracellular-spike-waveforms-and-neuronal-network-bursts>).

## 2. Materials and methods

In this paper we demonstrate our proposed joint analysis together with the conventional methods. The methods are organized in three sections: Section 2.1 Cell preparations and the pharmacological experiment; Section 2.2 MEA measurements; and Section 2.3 MEA measurement analysis, describing the spike count statistics, spike sorting, burst detection, the proposed joint analysis (Fig. 1) illustrated with simulated data, and mathematical considerations on the proposed joint analysis.

### 2.1. Cell preparations and the pharmacological experiment

#### 2.1.1. Cell culturing

Human stem cells were used as the starting material for neuronal cultures (Lappalainen et al., 2010). University of Tampere has ethical approval from Pirkanmaa Hospital District to derive, culture, and differentiate human embryonic stem cells (Skottman, R05116), and the permission from the National Authority for Medicolegal Affairs (1426/32/300/05) to conduct human stem cell research. After differentiation and subsequent plating on MEAs (Heikkilä et al., 2009), the cultures were grown on the MEAs for seven weeks. Each MEA well was considered as one cell culture.

#### 2.1.2. Pharmacological experiment

The proposed method is demonstrated by analyzing MEA data measured from 12 neuronal cell cultures which were pharmacologically manipulated for different effects on neuronal networks. The pharmacological experiment consisted of the following phases

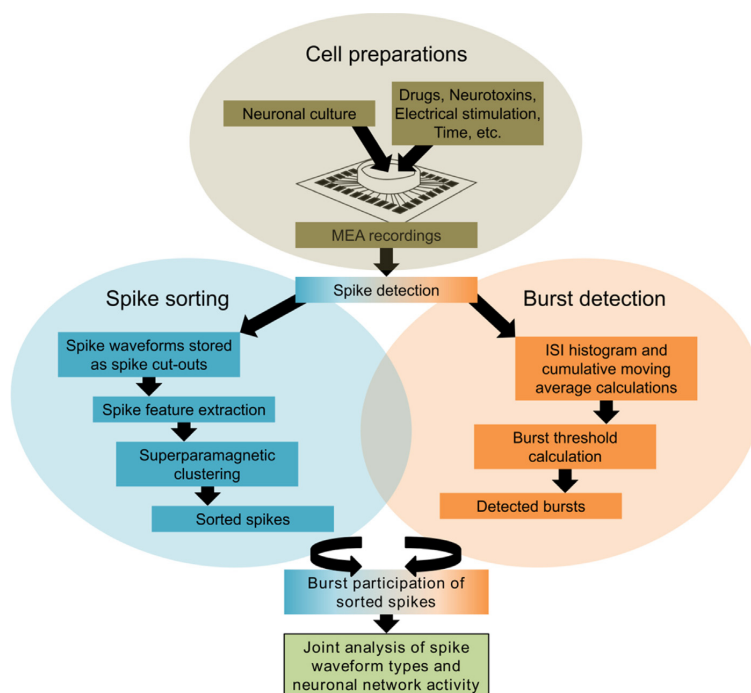


**Fig. 1.** A schematic presentation of the proposed joint analysis. The proposed framework consists of spike sorting and burst detection, followed by the analysis of the participation of the spikes of different types observed in bursts. Here, the spike sorting by Quiroga et al. (2004) and burst detection by Kapucu et al. (2012) were employed.

with MEA data acquired at each phase immediately after pharmacological manipulation or wash, and before any manipulations:

- (i) Baseline.
- (ii) 1st wash with fresh medium, to observe the effects of immediate medium change.
- (iii) CNQX (20  $\mu\text{mol}$ , AMPA/kainate receptor antagonist 6-cyano-7-nitroquinoxaline-2,3-dione, Abcam), to block AMPA/kainate mediated signaling.
- (iv) CNQX (20  $\mu\text{mol}$ , Abcam) + D-AP5 (30  $\mu\text{mol}$ , D(-)-2-amino-5-phosphonopentanoic acid, Abcam) AMPA/kainate and NMDA receptor antagonist, to block glutamatergic signaling.
- (v) 2nd wash with fresh medium.
- (vi) GABA (100  $\mu\text{mol}$ , Sigma), to boost GABAergic signaling.
- (vii) Bicuculline (30  $\mu\text{mol}$ , GABA<sub>A</sub> antagonist bicuculline methiodide, Sigma), to inhibit GABAergic signaling.

## 2.2. MEA measurements

MEA measurements were performed with the MEA wells sealed with semi-permeable membranes (ALA MEA-MEM, ALA Scientific Instruments, Westbury, NY, USA) or custom made PDMS blocks (Kreutzer et al., 2012). The signals from the MEAs were amplified with a preamplifier MEA1060-Inv-BC (Multi Channel Systems MCS GmbH, Reutlingen, Germany, MCS) and analog filtered and amplified with a filter amplifier FA60S-BC (MCS) (bandwidth: 1 Hz–8 kHz, total gain: 1100). The temperature was controlled with an external heater unit (TC02, MCS) set to +38 °C, and the cultures were allowed to settle for 1 min in the preamplifier before each 5-minute recording. Analog to digital conversion was performed at 20 kHz sampling frequency with MC.Card (MCS) in a PC computer, and the measurement was controlled via MC.Rack software (MCS). The digitized recordings were further processed with MC.Rack to obtain

cleaner high frequency spike information using a 50 Hz notch filter to remove mains noise, and a second order Butterworth highpass filter with 200 Hz cutoff frequency to alleviate baseline fluctuations and low frequency local field potential effects. MCS MEA data was imported to Matlab (MathWorks, Inc., Natick, MA, USA) using Neuroshare library (Neuroshare Library, 2003) for offline analysis.

## 2.3. MEA measurement analysis

At each phase of the pharmacological experiment (see Section 2.1.2), one 300 s recording was made from each culture (MEA well). The numbers of independent cultures included in the analyses are given in Table S1 along with the inclusion/exclusion criteria for the different analyses.

### 2.3.1. Spike count statistics

Traditional spike count (the total numbers of spikes in one recording) was calculated for each recording. Only the MEA wells which exhibited sufficient action potential activity were included in burst detection: It was required that at least 50 spikes were detected from an electrode of a MEA well in any 300 s recording of the baseline or at one of the pharmacological experiment phases. (See Table S2 for the numbers of channels fulfilling this criterion in each well at each phase of the experiment.) The same criterion has been used previously in burst analysis for human embryonic stem cell derived neuronal networks (Kapucu et al., 2012).

To obtain descriptive statistics for the spike counts at the different phases of the experiment, and to compare them with the respective spike counts in the baseline recordings, data from all electrodes of each well was pooled and medians were calculated over the wells. The upper and lower quartiles were calculated along with the differences between the upper and lower quartiles, *i.e.*, the interquartile ranges (IQRs) containing 50% of the data. In the sequel,

IQRs are shown in all relevant figures displaying the results. All the spike count statistics calculations were performed in GraphPad Prism 6 (GraphPad Software, Inc., La Jolla, CA, USA).

### 2.3.2. Spike detection and sorting

Data analysis was performed on data from a single channel and on data pooled from all electrodes. For the single channel analysis, we selected a channel whose firing rate at baseline was the closest to the average firing rate over all channels at the baseline. The average firing rate for the selected channel at the baseline was approximately 1.61 spikes/s, whereas the average firing rate for all baseline recordings per channel was 1.58 spikes/s with the maximum firing rate 14.04 spikes/s.

For the pooled data analysis, spike sorting was performed well for each phase of the pharmacological experiment. Spike sorting classifies spikes to classes corresponding to the neuronal action potential waveforms. First, spikes were detected by thresholding at five times the median of the baseline noise, and the spike time stamps and waveform cut-outs (spanning 1 ms prior and 2.2 ms after the maximum of the spike) were stored. The obtained spike waveform cut-outs were sorted using the Wave clus algorithm (Quiroga et al., 2004), which gave the average cluster waveforms and the associated lower and upper standard deviation waveforms. In Wave clus, the cluster size was initially set for the baseline according to the number of spikes to be sorted. All the detected spikes were included in the spike count and spike sorting analysis (the total of 172,750 spikes). Minimum cluster size for baseline recordings was five spikes for single electrode analysis (the total of 483 spikes were analyzed for the baseline) and 50 spikes for pooled data (the total of 51,230 spikes were analyzed for the baseline). However, the cluster sizes were altered for the different phases of the pharmacological experiment, since the activity and spike counts varied between the phases.

After automatic clustering, supervised tuning of the temperature was performed as suggested in the tutorial of Wave clus (Wave.clus., 2004), improving the spike sorting. Still, such spike sorting is less subjective than completely supervised spike sorting. Tuning the temperature was the only supervised correction performed. After unsupervised clustering, the temperature was tuned to observe if more clusters could be formed: If the average spike waveforms of the new clusters due to tuning could be considered as spike types different from those obtained without tuning, the new clusters were retained.

In this work, the effects of overlapping spikes are later discussed based on the analysis results. This matter has been wider addressed, e.g., by Quiroga et al. (2004). Performances of spike sorting algorithms, including Wave clus, have been addressed by Wild et al. (2012), also providing references to methods aimed at solving the spike overlapping problem.

### 2.3.3. Spike type identification and labeling

To track the occurrence of the spike types over the pharmacological experiment, it was necessary to identify the representative spike types, and label all the average waveforms observed at the different phases of the experiment with the spike types. This was done by selecting the representative average waveforms as spike types, as described below, and performing correlation analysis of the average waveforms and their respective standard deviation waveforms with those of the spike type waveforms. A simple operator-guided method was devised for the single electrode data analysis and a fully automated method for the full data analysis.

For the single electrode data analysis, the most prominent and distinguished average spike waveforms amongst all the average waveforms for the entire experiment were selected as the representative spike types by visual assessment. Thereafter, cross correlations between each of the remaining average waveforms

with all the spike type waveforms were calculated, and the waveforms were tentatively labeled with spike types according to the highest cross correlations. Thus, each cluster produced by Wave clus was assigned a tentative spike label. To take into account the waveform variability, analogous cross correlation analysis was also performed between the standard deviation waveforms: To confirm the tentative spike type labeling, the highest cross correlations had to be found between the standard deviation waveforms of the tentatively labeled cluster and the corresponding standard deviation waveforms of its tentative spike type. Otherwise, the average waveform was considered to represent a new spike type.

For the full data analysis, an automated version of the above cross correlation analysis was devised: Instead of visual identification of the spike types, the average waveforms given by Wave clus for the baseline measurements were used as the spike types. Thereafter, the cross correlation analysis to label the average waveforms with spike types, and the adoption of new spike types was performed alike described for the single electrode data analysis.

### 2.3.4. Burst detection

To analyze network activity, an adaptive burst detection algorithm, the cumulative moving average algorithm (CMA; Kapucu et al., 2012), was employed. CMA utilizes ISI statistics to objectively define and detect bursts. Here, CMA was employed with the same parameters as in (Kapucu et al., 2012). The exclusion/inclusion criterion was the same as for the spike count statistics (see Table S1).

### 2.3.5. The proposed joint analysis

In our proposed joint analysis (Fig. 1), first, spikes are detected and sorted. In parallel with spike sorting, burst detection is performed. After spike sorting and burst detection, every detected spike is labeled as either a burst spike or an individual spike, and carries a spike type label. Thus, the participation of different types of spikes in the network activity is unraveled. The wells which did not exhibit any bursting were excluded from the joint analysis of spike types and bursts (see Table S1).

Here, the joint analysis was implemented with the spike detection, spike sorting, and burst detection methods described earlier. To illustrate the proposed joint analysis, we simulated noisy single channel MEA data carrying spikes of three different waveforms (denoted as Asp 1, Asp 2, and Asp 3). The waveforms were modified from the data in the Wave clus distribution package (Wave.clus., 2004). The ISIs were set to at least 30 ms for the spikes in bursts and 300 ms for the individual spikes. Thus, no spike overlapping was introduced to concentrate on the joint analysis without having to consider the performances of spike detection and sorting for overlapping spikes. A 60 s simulation exhibited 10 bursts with seven Asp 1s and three Asp 2s in each burst. Four spikes (one Asp 1, one Asp 2 and two Asp 3s) were placed between all bursts. Background noise added to the formed spike signal was a random signal with uniformly distributed values between  $-3$  mV and  $3$  mV. The spike waveforms are shown in Fig. 2A, and a section of the simulated signal in Fig. 2C. From the simulated signal, spikes were detected and sorted, and burst and joint analysis were performed to illustrate the methodology.

In the results of this illustrative toy analysis, three average spike waveforms (Fig. 2A), i.e., the spike types, appeared as expected and were sorted with 100% accuracy. The burst detection result (Fig. 2B) shows that all the bursts were correctly detected. An exemplary burst shown in Fig. 2C illustrates the outcome of the proposed analysis framework: **the spike type composition of the burst**. The burst shown in Fig. 2C was composed of the spikes of types Asp 1 and Asp 2 as expected, with one individual Asp 3 types spike observed before the burst. The obtained numbers of spikes of different types in bursts and outside of the bursts are presented in Fig. 2D, from which it is seen that all the bursts were composed

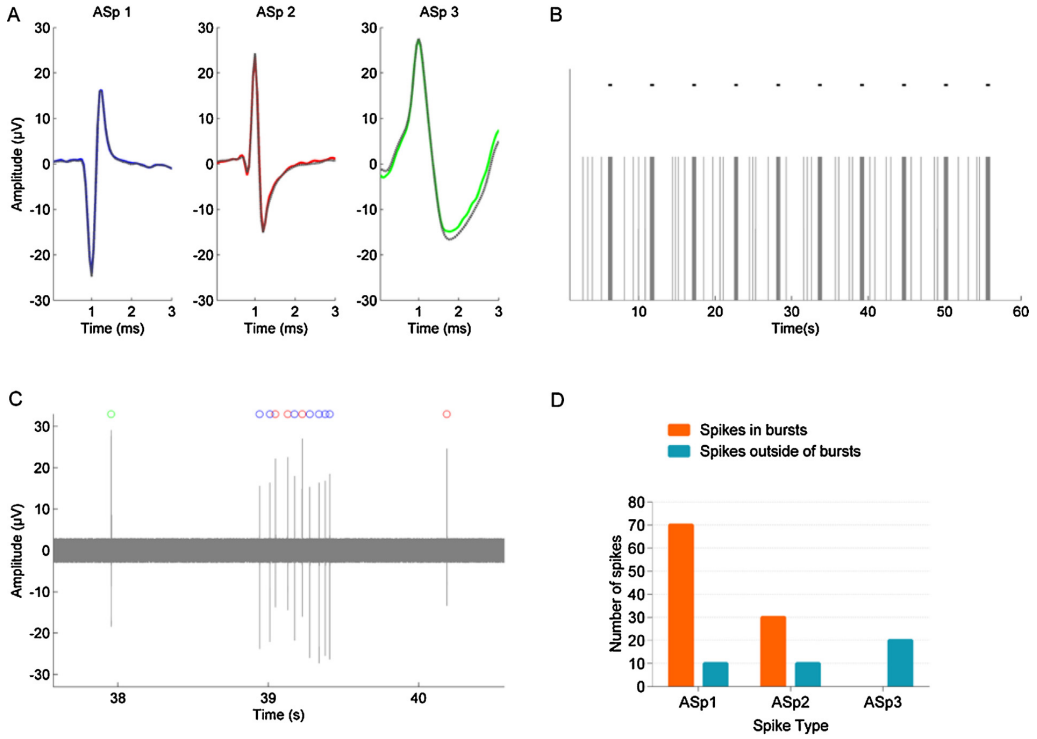


**Fig. 2.** Simulated toy data and its illustrative joint analysis results. (A) The simulated spike waveforms **ASp 1** (blue), **ASp 2** (red), and **ASp 3** (green), along with the corresponding average waveforms (grey dotted curves) calculated based on the detected and sorted noisy spikes. (B) The time points of the detected spikes (grey vertical bars), and the detected bursts (black horizontal lines). (C) A section of the simulated signal with sorted spikes indicated by circles with the colors indicating the particular waveforms as shown in (A). (D) The results of the joint analysis showing the counts of the different types of spikes participating in the bursts, along with those occurring outside of the bursts. (For interpretation of the references to color in this figure legend, the reader is referred to the web version of this article.)

solely of the spikes of types ASp 1 and ASp 2, whereas spikes of all spike types appeared as individual spikes outside of the bursts, which was 100% in accordance with the simulation setup.

### 2.3.6. Mathematical considerations regarding the proposed joint analysis

To formulate a mathematical expression of the spike compositions of the bursts in a measurement, a measured signal during a burst with the different identified spike type waveforms can be expressed as

$$s_t(t) = \sum_{j=1}^{J_i} W_{swt_{i,j}, t_{i,t}^o}(t) + n_i(t)$$

where,  $s_t(t)$  is the measured signal sample at discrete time  $t$  during the  $i$ th burst;  $J_i$  is the number of the detected spikes in the  $i$ th burst; and  $W_{swt_{i,j}, t_{i,t}^o}(t)$  is the sample of a spike waveform signal (of the length of the  $i$ th burst in samples) which is zero except for the period  $t_{i,t}^o \leq t \leq t_{i,t}^o + L - 1$  during which the  $L$  samples long  $swt_{i,j}$  type spike waveform occurs ( $swt_{i,j}$  denotes that the type of the  $j$ th spike of the  $i$ th burst is  $swt$ ).  $n_i(t)$  is the corresponding measured background noise sample accounting for all other signal components except for the identified spike type waveforms. This formulation effectively dissects the bursts in to their constituent spike types. The spike type compositions of the bursts in an entire measured signal is then given by all the pairs  $\{swt_{i,t}, t_{i,t}^o\}$ .

The information gain due to the proposed joint analysis compared to merely detecting the burst spikes corresponds to that of observing a string of letters formed from the alphabet of the size equal to the number of the spike types plus one (each letter corresponding to a spike type and a symbol '0' to denote 'no waveform') vs. a binary string ('1' corresponding to a detected spike). For example, with three detected spike waveform types denoted A, B, and C, the information gain would result from observing a burst as a string, for example, like '00A0B0000A0CC' (for illustrative purposes, only a few 0s are shown), as compared to observing the same burst with mere spike detection as '0010100001011'. Here, possible spike overlapping has not been considered. For the binary alphabet with equal symbol probabilities, the information content is  $\log_2(2) = 1$  bit per symbol, whereas an alphabet of size four with equal symbol probabilities results in the information content of  $\log_2(4) = 2$  bits per symbol (Shannon, 1948). Naturally the same amount of information per spike waveform is provided by spike sorting alone, but with the proposed joint analysis, this information is extracted specifically for each burst. For a real MEA measurement, the probability of an occurrence of the 'no waveform' symbol is much larger than that of a symbol denoting a spike; thus, the information contents of the spike symbols are larger than in the example, but the principal difference between the two approaches remains. Thereafter, the information gain achievable by the analyzes of the spike type waveforms themselves, their changes, and their occurrences in time, compared to the analysis of mere time stamps of the burst spikes, depends on the following neurobiological analysis,

and the associated information gain is not simply formally quantifiable.

### 3. Results

To demonstrate the proposed method and the obtainable results, we first present the analysis results for a signal measured via one electrode (Figs. 3 and 4); this example illustrates from phase to phase of the pharmacological experiment, what happened in a vicinity of one electrode, *i.e.*, in a local part of the neuronal network seen via one electrode. Next, we present the analysis results for the entire data set at every phase of the pharmacological experiment. See Table S1 for the number of the cultures at each phase.

#### 3.1. Results of single channel pharmacological experiment data analysis

In the analysis of single electrode data, spike sorting resulted in four different spike types (Fig. 3): one negative and one positive monophasic spike waveform (Spike-I, Fig. 3A, and Spike-II, Fig. 3B), and two biphasic spike waveforms (Spike-III, Fig. 3C, and Spike-IV, Fig. 3D).

Spike counts are shown in Fig. 4A: the total number of spikes detected decreased with the 1st wash compared to the baseline, and also with the application of CNQX. Application of CNQX + D-AP5 increased the number of spikes from that observed with CNQX alone. In the subsequent phases of the pharmacological experiment, the number of spikes did not change much. On the other hand, observing the numbers of spikes of particular types (Fig. 4B), and the changes in the numbers of spikes of different types relative to the baseline (Fig. 4C), different phenomena can be observed: In the baseline, most of the spikes were of the type Spike-I, which decreased in numbers at the 1st wash and further due to CNQX (Fig. 4B). The number of Spike-II type spikes exhibited a roughly similar trend (Fig. 4B). At the 2nd wash (Fig. 4B) and thereafter, spikes of types Spike-III and Spike-IV were the most prominent. In summary, with the near extinction of spikes of types Spike-I and Spike-II, spikes of types Spike-III and Spike-IV appeared (Fig. 4B).

Observing the numbers of spikes of the different types relative to the baseline (Fig. 4C), it is seen that as the pharmacological experiment progressed, the number spike of type Spike-III went through great changes. Since Spike-IV did not appear at baseline, its results cannot be shown relative to the baseline in Fig. 4C. It is clear that the information gained from the analysis of spike statistics for the different spike types (Fig. 4B and C) cannot be obtained from the mere total numbers of spikes (Fig. 4A).

Traditional burst analysis results presented as the relative number of bursts, relative average burst duration, and relative average numbers of spikes in a burst, all compared to their respective baselines, are shown in Fig. 4D–F, respectively. For example: The 1st wash greatly increased the number of bursts, duration, and the number of spikes in a burst (Fig. 4D–F, respectively). CNQX, compared to the previous experiment phase, decreased the relative number of bursts (Fig. 4D), but did not change the burst duration (Fig. 4E), and brought the number of spikes in a burst close to that at the baseline (Fig. 4F). The 2nd wash nearly extinguished bursting activity, whereas the subsequent application of GABA restored approximately half of the number of bursts compared to the baseline (Fig. 4D), and had a tremendous increasing effect on both the burst duration (Fig. 4E) and the number of spikes in a burst (Fig. 4F). Regarding the extreme increase in burst duration for GABA in Fig. 4E, the average burst duration at the baseline was 0.1 s, whereas after GABA application it was 67.3 s, resulting in the shown 67,300% increase in the average duration.

The results of the joint analysis of spike types and bursts are presented in Fig. 4G and H. For clarification, the results in Fig. 4G are presented in Fig. S1A in percentages relative to the total numbers of spikes. To compare the burst spike types and individual spike types for completeness, the different spike types seen in individual spikes are shown in Fig. S2A. To demonstrate the proposed joint analysis, for example, in the baseline the bursts were composed merely of spikes of types Spike-I and II (Fig. 4G), whereas later in the experiment, under CNQX + D-AP5, the bursts were composed far mostly of the spikes of type Spike-II, and the 2nd wash nearly abolished bursting (Fig. 4G and H). However, the picture is totally changed by the application GABA: Under the influence of GABA

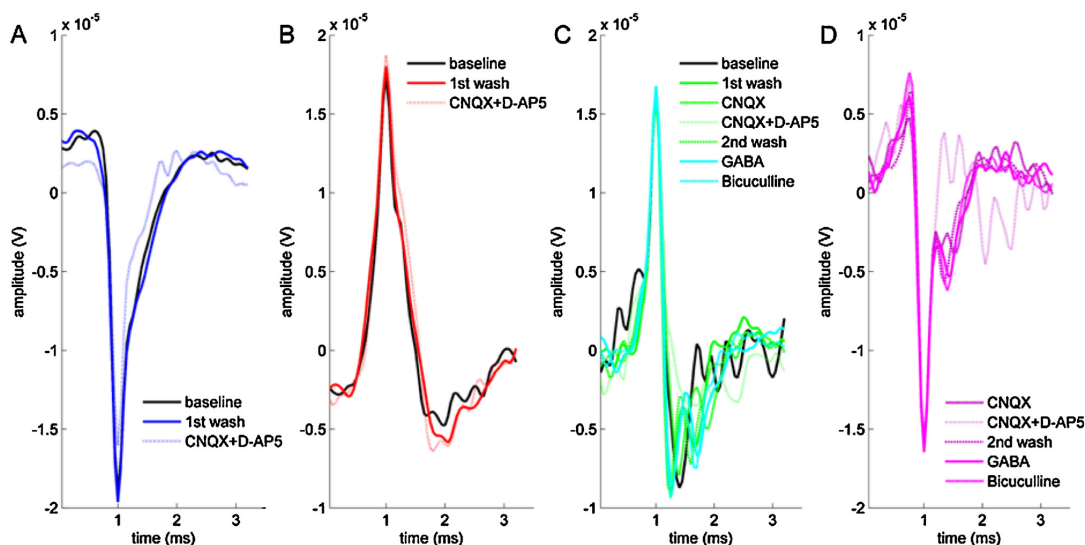


**Fig. 3.** The average spike waveforms observed in one channel in the pharmacological experiment, shown for the phases of the pharmacological experiment at which the particular waveforms were observed (see the legend in each panel). The spike types: (A) Spike-I (blue), (B) Spike-II (red), (C) Spike-III (green), and (D) Spike-IV (purple). (For interpretation of the references to color in this figure legend, the reader is referred to the web version of this article.)

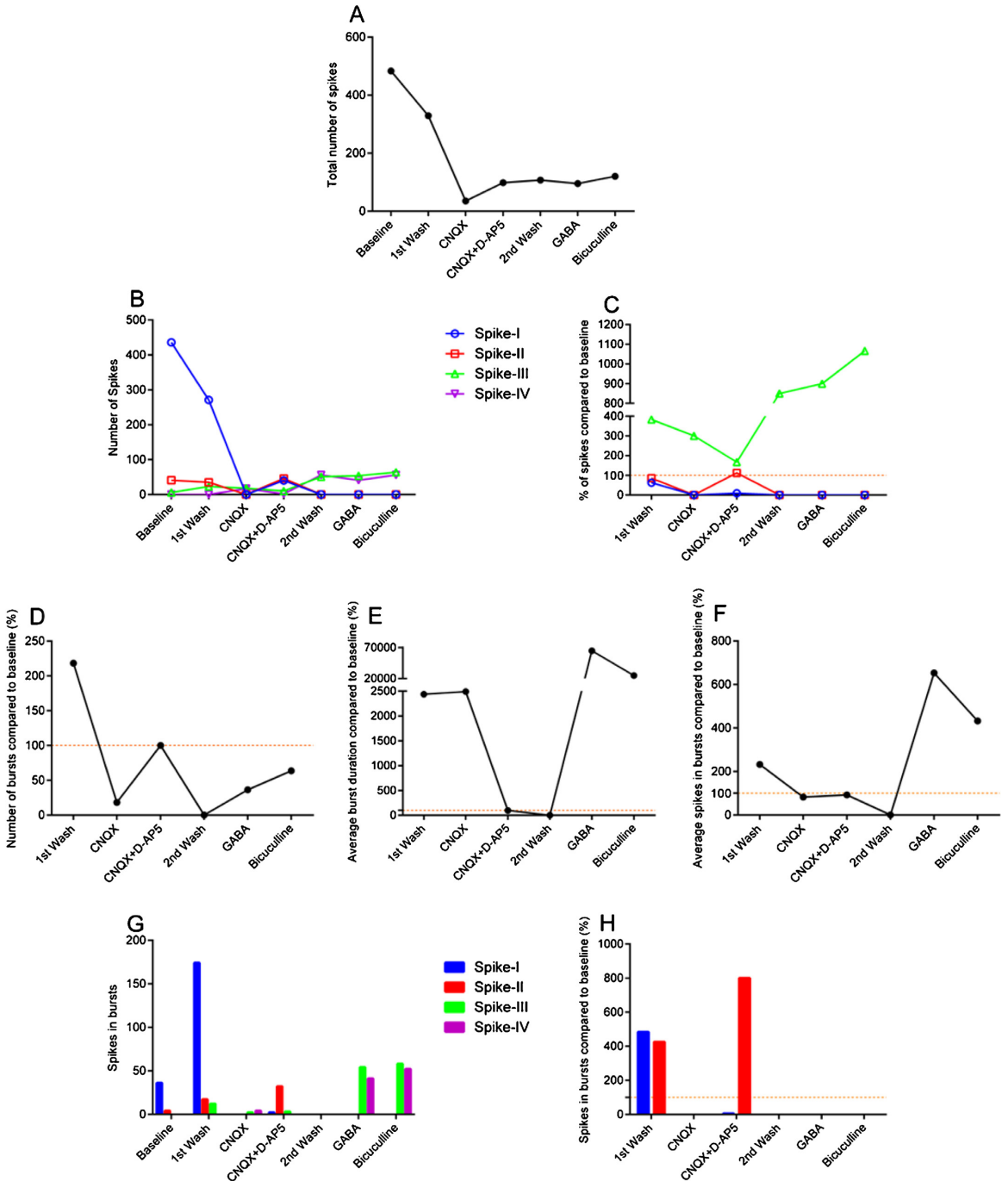


**Fig. 4.** The results of the traditional spike and burst analysis (A–F) and the joint analysis (G and H) at all phases of the pharmacological experiment for one MEA channel. (A) The total number of spikes. (B) and (C) The numbers of the different types of spikes, and their relative amounts, respectively. (D) The relative numbers of bursts. (E) The relative average durations of bursts. (F) The relative average numbers of spikes in a burst. (G) The numbers of spikes of each type in bursts. (H) The relative numbers of spikes of each type in bursts. The relative quantities are with respect the corresponding values at the respective baselines. The spike types: Spike-I (blue), Spike-II (red), Spike-III (green), and Spike-IV (purple). (For interpretation of the references to color in this figure legend, the reader is referred to the web version of this article.)

and thereafter of GABA and bicuculline, the bursts were composed merely of the spikes of types Spike-III and Spike-IV. Thus, the joint analysis of spike types and bursts (Fig. 4G and H) provided more information on the network effects of pharmacological than the traditional burst analysis alone (Fig. 4D–F).

Alike with the spike counts (Fig. 4B and C), also here observing the numbers of spikes in burst (Fig. 4G) and the same relative to the baseline (Fig. 4H), different views to the phenomena are obtained. For example, the increase in the number of Spike-I type spikes after the 1st wash was far greater than that of Spike-II type spikes, but the increase in percentages (Fig. 4H) is roughly equal.

To explicitly point out new information given by the proposed joint analysis, for example, in Fig. 4B it is seen that after the 1st wash, there was a notable decrease in the occurrence of Spike-I type spikes and a slight decrease in the number of Spike-II type spikes, whereas in Fig. 4D it is seen that simultaneously the number of bursts more than doubled compared to baseline. For this experiment phase, the joint analysis results in Fig. 4G show a notable increase in the burst participation of Spike-I type spikes and slight increase in the burst participation of Spike-II type spikes. This is also reflected in the percentual amounts of the spikes of these types appearing in bursts compared to the total spike counts (Fig. S1A), whereas individual spikes (Fig. S2A) of both types decreased. This information on the changes in the burst participation of the different types of spikes cannot be obtained by the traditional analysis results in Fig. 4B and D.

Also, new information provided by the joint analysis can be demonstrated by observing the activity in Fig. 4B after the CNQX + D-AP5 application when the number of Spike-II type spikes recovered to the approximately same level as it was at the baseline. Spike-I type spikes also recovered approximately to the same level as Spike-II type spikes, however remaining still greatly fewer than at the baseline. At this point of the experiment, the number of bursts, average burst durations, and the average numbers of spikes in bursts were close to what they had been at the baseline (Fig. 4D–F, respectively). The joint analysis results in Fig. 4G show that at this time, the bursts were mostly composed of Spike-II type spikes, whereas at the baseline, the burst spikes had been mainly Spike-I

type spikes. In conclusion, although the traditional burst characteristics (Fig. 4D–F) were approximately equal at base line and after the CNQX + D-AP5 application, the joint analysis revealed that the main burst spike type was different between these two experiment phases. This information on the burst composition change cannot be obtained from results of the traditional analyses in Fig. 4B and D, but only with the proposed joint analysis.

### 3.2. Results of full pharmacological experiment data analysis

In the analysis of the full data set, data from all the MEAs and MEA wells was pooled (see Table S1), and analyzed for each phase of the pharmacological experiment. The average spike waveforms (Fig. 5) obtained from the pooled data exhibited naturally more variation than the spike waveforms obtained from the signal measured via one electrode (Fig. 3). It is to be noted that the variability in the data was quite large, as seen from the IQRs in Fig. 6; therefore we chose not to draw biological conclusions. Nevertheless, the results clearly demonstrate the usability of the proposed joint analysis. In the analysis results in Fig. 6, the quantities shown are the medians over the analyzed wells with the whiskers covering the 50% IQRs. For burst durations (Fig. 6E) and the number of spikes in a burst (Fig. 6F), shown are the medians of the per-well averages (See the numbers of the analyzed wells in Table S1).

Spike sorting analysis of the pooled data resulted in five different spike types (Spike-I, Spike-II, Spike-III, Spike-IV, and Spike-V, seen in Fig. 5A–E, respectively). In Fig. 5, the average waveforms for each spike type are shown for the phases of the pharmacological experiment at which they were observable.

For this data, two monophasic (one negative (Spike-I, Fig. 5A), and one positive (Spike-II, Fig. 5B)) and two biphasic spike waveforms were obtained (Spike-III, Fig. 5C, and Spike-IV, Fig. 5D), but not all of them were observed at all phases of the pharmacological experiment. Also obtained was Spike-V (Fig. 5E), which appeared only at the 1st wash and under the influence of CNQX + D-AP5. Spike-V was composed of greatly varying individual spike waveforms which could not be clustered together.

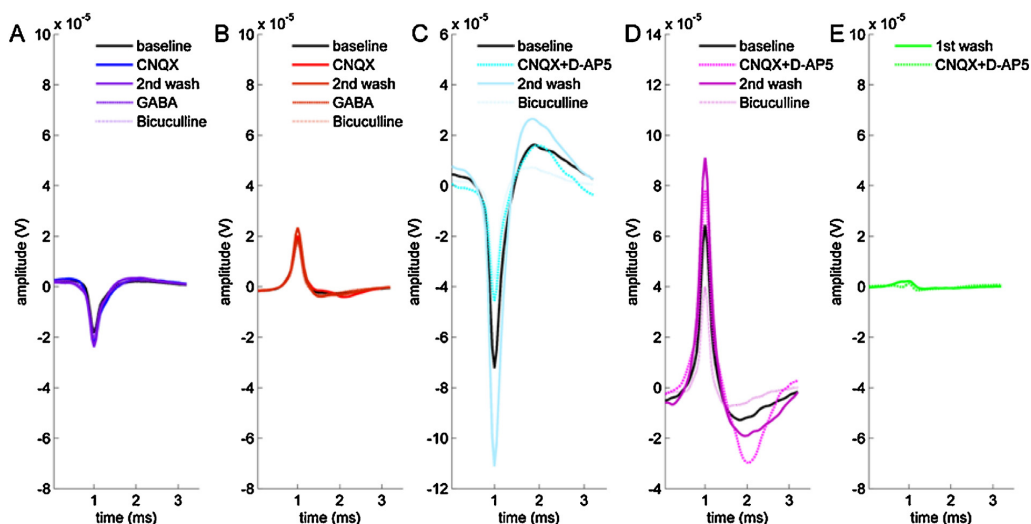


**Fig. 5.** The average spike waveforms observed in the entire pharmacological experiment data set, shown for the phases of the pharmacological experiment at which the particular waveforms were observed (see the legend in each panel). The spike types: (A) Spike-I (blue), (B) Spike-II (red), (C) Spike-III (cyan), (D) Spike-IV (purple), and (E) Spike-V (green). (For interpretation of the references to color in this figure legend, the reader is referred to the web version of this article.)

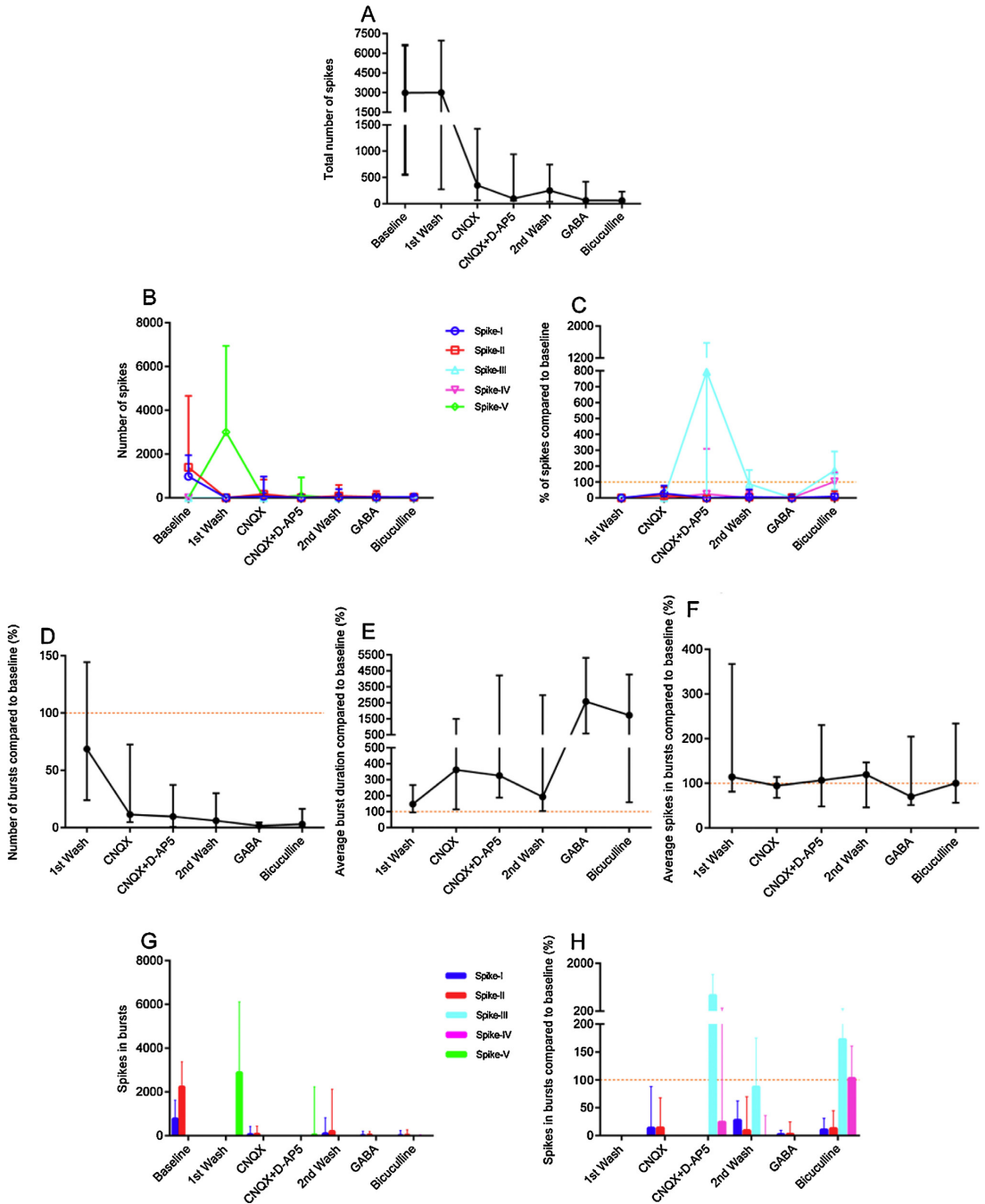


**Fig. 6.** The results of the traditional spike and burst analysis (A–F) and the joint analysis (G and H) at all the phases of the pharmacological experiment for the entire data set. (A) The total number of spikes. (B) and (C) The numbers of the different types of spikes, and their relative amounts, respectively. (D) The relative numbers of bursts. (E) The relative average durations of bursts. (F) The relative average numbers of spikes in a burst. (G) The numbers of spikes of each type in bursts. (H) The relative numbers of spikes of each type in bursts. The quantities shown are the medians over the number of analyzed wells (see Table S1) with the whiskers covering the 50% IQRs. The relative quantities are with respect to the corresponding values at the respective baselines. The spike types: Spike-I (blue), Spike-II (red), Spike-III (cyan), Spike-IV (purple), and Spike-V (green). (For interpretation of the references to color in this figure legend, the reader is referred to the web version of this article.)

In the spike count analysis (Fig. 6A), variability in the total number of spikes was high at the baseline and 1st wash. At the CNQX application, the median of the total number of spikes decreased drastically and remained low compared to the baseline through the rest of the pharmacological experiment. Alike for the single channel data, more information can be obtained by observing the numbers of spikes of different types (Fig. 6B and C). At baseline, Spike-I and II were observed in higher numbers than the other types of spikes. The 1st wash changed the situation drastically, making the Spike-V the most prominent; let us recall that Spike-V was composed of greatly varying spike waveforms which could not be clustered, *i.e.*, the 1st wash greatly disturbed the spike waveforms. Also, Spike-V did not appear at the baseline, and is thus not shown in Fig. 6C and H. CNQX caused some spikes of types Spike-I and II to reappear, whereas CNQX + D-AP5 caused an uprising of Spike-III type spikes (Fig. 6C), which dominated also at the 2nd wash and at the application of bicuculline. GABA nearly shut down spiking (Fig. 6C). Naturally, the spike-type specific phenomena (Fig. 6B and C) cannot be observed from the mere total number of spikes (Fig. 6A).

Traditional burst analysis results presented as the relative number of bursts, relative median of the well-wise average burst durations, and the relative median of the well-wise average number of spikes in a burst, all compared to their respective baselines, are shown in Fig. 6D–F. The relative number of bursts decreased through the pharmacological experiment (Fig. 6D). Burst duration (Fig. 6E) increased slightly at the 1st wash, and more prominently under the influence of CNQX, whereas the 2nd wash decreased the burst duration. GABA caused a large increase in the burst duration (Fig. 6E), to which bicuculline had little effect. Interestingly, the fraction of the total number of spikes appearing in burst remained approximately constant through the experiment (Fig. 6F).

The proposed joint analysis results (Fig. 6G) reveal that at the baseline, the bursts were composed almost completely composed of the spikes of types Spike-I and II, *i.e.*, the monophasic negative (Fig. 5A) and positive (Fig. 5B) spikes, respectively. (For clarification, the results in Fig. 6G are presented in Fig. S1B as the relative numbers of the burst spikes with respect to the total numbers of spikes in percentages. To compare the burst spike types and individual spike types for completeness, the different spike types seen in individual spikes are shown in Fig. S2B.) This means that the networks were operating with the spikes of types Spike-I and II. The 1st wash caused the burst to be composed of almost entirely of Spike-V type spikes (Fig. 6G) which did not represent a well-defined waveform (Fig. 5E). CNQX partially recovered Spike-I and II type spikes also in bursts, whereas CNQX + D-AP5 again removed them from bursts (Fig. 6G and H). The 2nd wash brought the spikes of types Spike-I and II partially back to the bursts, which were now composed of spikes of types Spike-I, II, III, and IV. Under the influence of GABA, there were almost no spikes in bursts (Fig. 6G and H), as there were almost no bursts (Fig. 6D). Nevertheless, the few remaining bursts had approximately the same number of spikes in a burst as at the baseline (Fig. 6F). Bicuculline caused the bursts to be composed mainly of the spikes of types Spike-I and II (Fig. 6G) with a few Spike-III and IV type spikes also present in the bursts (Fig. 6H).

Again, observing the results as counts (Fig. 6B and C) and in percentages (Fig. 6C and H) provided clearly different and complementary views to the results. Although in this pooled data experiment the spike type change trends (Fig. 6G and H) in the joint analysis in general followed those observed in the traditional analyses (Fig. 6B and C), the proposed joint analysis of spikes and bursts nevertheless provided the actual data on the spike type compositions of the bursts, which was naturally not obtainable by the means of the traditional analyses.

#### 4. Discussion and conclusions

In this paper, we have proposed a novel analysis method for the joint analysis of action potentials and network events observed in local field potential measurements. The main usage of the proposed method is to test a hypothesis that spike types in bursts and spikes in general have different dynamics, *e.g.*, in response to external effects. We have demonstrated that this hypothesis is worth testing, and that the tool developed will provide deeper information on the activity of neuronal networks and their alterations. The essence of the proposed joint analysis was illustrated by a simulation (Fig. 2C), in which a spike type composition of a burst was seen for the first time. The value of the method was demonstrated by analyzing the MEA measurements from a pharmacological experiment with several different chemical applications; the effects of the pharmacological agents were observed with both traditional spike and burst analysis, and with the proposed joint analysis of spikes and bursts, where we demonstrated that the proposed joint analysis reveals information on the network activity which is not obtainable by the traditional analyses, *i.e.*, **the burst participation of the different types of spikes**, and the changes of this by chemical modification of the neuronal activity.

In the analysis of the pooled data, the overall results were calculated in each phase of the pharmacological experiment per well and not per electrode. With this approach, we aimed to study the general behavior of the networks in the different experimental phases. We are confident that regardless of the variability in our data (Heikkilä et al., 2009; Kapucu et al., 2012), the function of the proposed method was described, and the new information obtainable by the method demonstrated. We observed that indeed there are different dynamics of spike waveform types contributing to the bursts and spikes in general.

To investigate the stability of the signals, especially motivated by the large deviation seen in Spike-V, we took a look at the stability of the spike waveforms during the 300-second measurement after the 1st wash when the Spike-V appeared (Fig. 6B and G). We analyzed each disjoint 100-second section separately. Especially the first and third 100-second sections of the recording had similar clustering results as the complete recording, exhibiting a cluster of highly varying spike waveforms. However, spike waveforms in the second 100-second section were different. This demonstrates that the network function was changing during the recording. In general, one possible disturbing effect may have been the relatively short 1-minute stabilizing period before the measurement after the MEAs were placed in the measurement device. However, due to the described observed behavior during the 100-second sections, we can assume that a longer stabilizing period would not have resulted in more stable networks.

Another issue is the effect of overlapping spikes. Especially for bursting action potentials, spike sorting has been always challenging (Lewicki, 1998; Quiroga et al., 2004; Wild et al., 2012). In our work, especially for the pooled data, spike sorting represents average waveform types obtained from large datasets. Waveform distortions caused by overlapping spikes can be expected to be seen as average and standard deviation waveforms which greatly differ from the general spike average and standard deviation waveforms. Here, highly distorted spikes which could not be assigned to any cluster during spike sorting, accounted for approximately 3.7% of all the analyzed spikes (3.36% for the burst spikes and 0.34% for the individual spikes). Additionally, average and standard deviation waveforms of the obtained spike types were consistent over the different phases of the experiment for both burst and individual spikes. In conclusion, even though the effects of overlapping could be seen in our analysis, they are not expected to change our results or conclusions.

Using the proposed method, here, we show that the burst spike types and the spikes in general may have different dynamics. By assessing the results both as percentual changes with respect to the baseline activity for each spike type, and as changes in the actual burst spike counts, different views were gained to the changes in the network activity. In the literature, either absolute counts, such as spike and burst counts (Gopal, 2003; Brewer et al., 2009; Hogberg et al., 2011) or changes of percentual values (Gramowski et al., 2000; Ylä-Outinen et al., 2010) are given. Keefer et al. (2001) and Johnstone et al. (2010) provided the results partially in both forms. However, simultaneous analysis of both quantities has not been common practice, and not utilized in drawing comparative conclusions. Here, we demonstrated the usefulness of utilizing both approaches simultaneously in the joint analysis.

The polarity of the measured waveforms has been described to depend on the location of the neuron relative to the electrode (Henze et al., 2000; Gold et al., 2006). Thus, the observed changes in the spike waveforms and the spike type compositions of the bursts may have resulted from chemical induced functional changes in the cells or networks, morphological effects on the cells, different cell compartments contributing to the measurements, or from any combination of these. Nevertheless, we conclude that the observable effects are not random, but consistent manifestations of the changes in the networks. In long-term experiments, cell movement may also affect spike waveforms, which should naturally be evident also in the controls. Here, the experiment was acute, spike sorting was equally successful in all phases of the pharmacological experiment, and the spike type formation and assignment worked consistently; thus, the observed changes in spike waveforms due to the pharmacological applications did not interfere with spike sorting. It is also to be noted that the number of spikes available for the analysis may also affect the spike sorting results. Here, spike sorting worked consistently.

The pharmacological effects observed in the joint analysis are clear and interesting. Joint analysis results do provide more information on the network changes. Unraveling the actual reasons for, and the consequences of the observed spike type compositions of the bursts, and their changes due to pharmacological and other treatments, call for detailed studies with in-depth neuronal network analysis providing information on the sources of spikes, including information on active neuronal types and cell compartments. This is naturally called for in any spike sorting based analysis.

#### 4.1. Further applicability

Here, the spike sorting by Quiroga et al. (2004) and burst detection by Kapucu et al. (2012) were employed. However, the proposed joint analysis framework (Fig. 1) can be implemented with any spike sorting and burst detection algorithms appropriate for the measurement data at hand. This is important to facilitate both different analysis approaches, and the different characteristics of spikes and bursts in the *in vitro* networks derived from different species and origins; the differences in network behavior have substantial influence on the applicability of different spike sorting and burst detection methods, and also call for more objective and automated methods (Kapucu et al., 2012). For spike sorting, the advantages and drawbacks of supervised and unsupervised algorithms can be argued: An automatic classification can be corrected or optimized by the user with unsupervised approaches in a final classification step which makes the approach still supervised but less subjective and less time consuming (Martínez and Quiroga, 2013). Certainly it would be preferable to have an accurate and fully unsupervised algorithm, which still remains a largely open question (Martínez and Quiroga, 2013). The only assumptions imposed by the proposed joint analysis framework itself are that there are

sortable action potential waveforms and detectable bursts present in the data.

To possibly alleviate the effects of high variability in the data, the single channel analysis used here merely to demonstrate the method, could also be employed in the analysis of the entire MEA by analyzing each channel separately. Thereafter, should the single channel analyses produce mutually corroborative results, overall conclusions could be drawn. However, combining the single channel analyses results to an overall result would require the development of a separate statistically valid method. Straighter forward, the analysis of single channel data can be employed to reveal the spatial distributions of the different types of spikes composing the bursts. This analysis technique would be promising, e.g., for tracking the spike waveforms and their network participations. Single electrode data analysis naturally considers the local network in the vicinity of the electrode, whereas the analysis pooled data provides a better view to the overall activity and allows statistical analysis, while possibly losing information on particular local network phenomena.

The proposed joint analysis can be performed on all detected spikes, or alternatively, separately on burst spikes and non-burst spikes. In applying the analysis on such different sets of spikes, one needs to consider the possibly different functions of spikes occurring in different circumstances, such as in bursts or individually (Valiante and Carlen, 2014). Here, our main aim was the analysis of bursts, which can be assumed to manifest actual network activity. Similarly, instead of bursts, spike trains can be analyzed with the proposed method providing the spike types and their changes in the spike trains. Naturally, the same can be done also with individual spikes, i.e., for the spikes not in bursts or trains as demonstrated in Fig. S2. Thus, complementary information on the different processes in the networks can be obtained by the selection of the data to be analyzed. Given spike sorting and burst and/or train detection methods appropriate for the data at hand, the framework is applicable in the analysis of any electrophysiological data, not only in the analysis of *in vitro* measurements.

#### 4.2. Conclusions

Currently, there is a great call for methods to analyze neuronal network function from *in vitro* MEA recordings in more detail, for example, for research on basic biological questions such as neuronal network development and learning, for the assessment of various culturing methods, and for drug research and neurotoxicology (Coecke and Price, 2007; LeFew et al., 2013). Here, we propose a new joint analysis method that provides the spike type compositions of the bursts. We showed that the spike type compositions of bursts may change subject to environmental effects. Specifically, based on the presented results, pharmacological substances may affect the spike type compositions of the bursts, which are not seen in traditional spike and burst analysis, including spike sorting as traditionally utilized. Thus, with our joint analysis, more detailed information on the network behavior and its changes can be obtained.

#### Acknowledgments

The work of F. E. Kapucu has been supported by the Finnish Cultural Foundation (the Central Fund and Pirkanmaa Regional Fund), by the Ella and Georg Ehrnrooth Foundation, by the Human Spare Parts Project funded by the Finnish Funding Agency for Technology and Innovation (Tekes), and by the 3DNeuroN project in the European Union's Seventh Framework Programme, Future and Emerging Technologies, grant agreement no. 296590. The works of M. E.-L. Mäkinen, L. Ylä-Outinen, and S. Narkilahti have been supported by the Human Spare Parts Project funded by the Finnish

Funding Agency for Technology and Innovation (Tekes). The work of J. M. A. Tanskanen has been supported by the 3DNeuroN project in the European Union's Seventh Framework Programme, Future and Emerging Technologies, grant agreement no. 296590.

## Appendix A. Supplementary data

Supplementary data associated with this article can be found in the online version at <http://dx.doi.org/10.1016/j.jneumeth.2015.11.022>.

## References

- Alloisio S, Nobile M, Novellino A. Multiparametric characterisation of neuronal network activity for *in vitro* agrochemical neurotoxicity assessment. *NeuroToxicology* 2015;48:152–65. <http://dx.doi.org/10.1016/j.neuro.2015.03.013>.
- Bal-Price AK, Suñol C, Weiss DG, van Vliet E, Westerink RHS, Costa LG. Application of *in vitro* neurotoxicity testing for regulatory purposes: symposium III summary and research needs. *NeuroToxicology* 2008;29(3):520–31. <http://dx.doi.org/10.1016/j.neuro.2008.02.008>.
- Banerjee A, Ellender TJ. Oscillations in the developing cortex: a mechanism for establishing and synchronizing an early network? *J Neurosci* 2009;29(48):15029–30. <http://dx.doi.org/10.1523/JNEUROSCI.4567-09.2009>.
- Brewer GJ, Boehler MD, Ide AN, Wheeler BC. Chronic electrical stimulation of cultured hippocampal neurons increases spontaneous spike rates. *J Neurosci Methods* 2009;184(1):104–9. <http://dx.doi.org/10.1016/j.jneumeth.2009.07.031>.
- Buzańska L, Jurga M, Stachowiak EK, Stachowiak MK, Domańska-Janik K. Neural stem-like cell line derived from a nonhematopoietic population of human umbilical cord blood. *Stem Cells Dev* 2006;15(3):391–406. <http://dx.doi.org/10.1089/scd.2006.15.391>.
- Buzańska L, Habich A, Jurga M, Sypecka J, Domańska-Janik K. Human cord blood-derived neural stem cell line—possible implementation in studying neurotoxicity. *Toxicol in vitro* 2005;19(7):991–9. <http://dx.doi.org/10.1016/j.tiv.2005.06.036>.
- Buzsáki G. Large-scale recording of neuronal ensembles. *Nat Neurosci* 2004;7(5):446–51. <http://dx.doi.org/10.1038/nn1233>.
- Chiappalone M, Novellino A, Vajda I, Vato A, Martinoia S, van Pelt J. Burst detection algorithms for the analysis of spatio-temporal patterns in cortical networks of neurons. *Neurocomputing* 2005;65–66:653–62. <http://dx.doi.org/10.1016/j.neucom.2004.10.094>.
- Coecke S, Price A. Why *in vitro* neurotoxicity approaches are not formally validated and used for regulatory purposes: The way forward. (<http://www.alttox.org/trc/toxicity-tests/neurotoxicity/way-forward/coecke-price/>); 2007 [updated 06.12.07; cited 01.11.13].
- Connors BW, Gutnick MJ, Prince DA. Electrophysiological properties of neocortical neurons *in vitro*. *J Neurophysiol* 1982;48(6):1302–20. <http://jn.physiology.org/content/48/6/1302>.
- Crumiller M, Knight B, Yu Y, Kaplan E. Estimating the amount of information conveyed by a population of neurons. *Front Neurosci* 2011;5:90. <http://dx.doi.org/10.3389/fnins.2011.00090>.
- Defranchi E, Novellino A, Whelan M, Vogel S, Ramirez T, van Ravenzwaay B, et al. Feasibility assessment of micro-electrode chip assay as a method of detecting neurotoxicity *in vitro*. *Front Neuroeng* 2011;4:6. <http://dx.doi.org/10.3389/fneng.2011.00006>.
- Egert U, Schlosshauer B, Fennrich S, Nisch W, Fejtl M, Knott T, et al. A novel organotypic long-term culture of the rat hippocampus on substrate-integrated multielectrode arrays. *Brain Res Protoc* 1998;2(4):229–42. [http://dx.doi.org/10.1016/S1385-299X\(98\)00013-0](http://dx.doi.org/10.1016/S1385-299X(98)00013-0).
- Gibson S, Jack WJ, Markovic D. Spike sorting: the first step in decoding the brain. *IEEE Signal Process Mag* 2012;29(1):124–43. <http://dx.doi.org/10.1109/MSP.2011.941880>.
- Gold C, Henze DA, Koch C, Buzsáki G. On the origin of the extracellular action potential waveform: a modeling study. *J Neurophysiol* 2006;95:3113–28. <http://dx.doi.org/10.1152/jn.00979.2005>.
- Gopal KV. Neurotoxic effects of mercury on auditory cortex networks growing on microelectrode arrays: a preliminary analysis. *Neurotoxicol Teratol* 2003;25(1):69–76. [http://dx.doi.org/10.1016/S0892-0362\(02\)00321-5](http://dx.doi.org/10.1016/S0892-0362(02)00321-5).
- Gramowski A, Schiffmann D, Gross GW. Quantification of acute neurotoxic effects of trimethyltin using neuronal networks cultured on microelectrode arrays. *NeuroToxicology* 2000;21(3):331–42. <http://europepmc.org/abstract/MED/10894123>.
- Gray CM, McCormick DA. Chattering cells: superficial pyramidal neurons contributing to the generation of synchronous oscillations in the visual cortex. *Science* 1996;274(5284):109–13. <http://dx.doi.org/10.1126/science.274.5284.109>.
- Gross GW, Rhoades BK. The use of neuronal networks on multielectrode arrays as biosensors. *Biosens Bioelectron* 1995;10(6–7):553–67. [http://dx.doi.org/10.1016/0956-5663\(95\)96931-N](http://dx.doi.org/10.1016/0956-5663(95)96931-N).
- Gross GW, Rieske E, Kreutzberg GW, Meyer A. A new fixed-array multi-microelectrode system designed for long-term monitoring of extracellular single unit neuronal activity *in vitro*. *Neurosci Lett* 1977;6(2–3):101–5. [http://dx.doi.org/10.1016/0304-3940\(77\)90003-9](http://dx.doi.org/10.1016/0304-3940(77)90003-9).
- Harris KD, Hirase H, Leinekugel X, Henze DA, Buzsáki G. Temporal interaction between single spikes and complex spike bursts in hippocampal pyramidal cells. *Neuron* 2001;32(1):141–9. [http://dx.doi.org/10.1016/S0896-6273\(01\)00447-0](http://dx.doi.org/10.1016/S0896-6273(01)00447-0).
- Heikkilä TJ, Ylä-Outinen L, Tanskanen JMA, Lappalainen RS, Skottman H, Suuronen R, et al. Human embryonic stem cell-derived neuronal cells form spontaneously active neuronal networks *in vitro*. *Exp Neurol* 2009;218(1):109–16. <http://dx.doi.org/10.1016/j.expneurol.2009.04.011>.
- Henze DA, Borhegyi Z, Csicsvari J, Mamiya A, Harris KD, Buzsáki G. Intracellular features predicted by extracellular recordings in the hippocampus *in vivo*. *J Neurophysiol* 2000;84(1):390–400. <http://jn.physiology.org/content/84/1/390>.
- Hogberg HT, Sobanski T, Novellino A, Whelan M, Weiss DG, Bal-Price AK. Application of micro-electrode arrays (MEAs) as an emerging technology for developmental neurotoxicity: evaluation of domoic acid-induced effects in primary cultures of rat cortical neurons. *NeuroToxicology* 2011;32(1):158–68. <http://dx.doi.org/10.1016/j.neuro.2010.10.007>.
- Illes S, Jakab M, Beyer F, Gelfert R, Couillard-Despres S, Schnitzler A, et al. Intrinsically active and pacemaker neurons in pluripotent stem cell-derived neuronal populations. *Stem Cell Rep* 2014;2(3):323–36. <http://dx.doi.org/10.1016/j.stemcr.2014.01.006>.
- Johnstone AFM, Gross GW, Weiss DG, Schroeder OH-U, Gramowski A, Shafer T. Microelectrode arrays: a physiologically based neurotoxicity testing platform for the 21st century. *NeuroToxicology* 2010;31(4):331–50. <http://dx.doi.org/10.1016/j.neuro.2010.04.001>.
- Kandel ER, Spencer WA. Electrophysiology of hippocampal neurons. II. After-potentials and repetitive firing. *J Neurophysiol* 1961;24(3):243–59. <http://jn.physiology.org/content/24/3/243>.
- Kapucu FE, Tanskanen JMA, Mikkonen JE, Ylä-Outinen L, Narkilahti S, Hyttinen JAK. Burst analysis tool for developing neuronal networks exhibiting highly varying action potential dynamics. *Front Comput Neurosci* 2012;6:38. <http://dx.doi.org/10.3389/fncom.2012.00038>.
- Keefe EW, Norton SJ, Boyle NAJ, Talsa V, Gross GW. Acute toxicity screening of novel AChE inhibitors using neuronal networks on microelectrode arrays. *NeuroToxicology* 2001;22(1):3–12. [http://dx.doi.org/10.1016/S0161-813X\(00\)00014-0](http://dx.doi.org/10.1016/S0161-813X(00)00014-0).
- Kreutzer J, Ylä-Outinen L, Kärnä P, Kaarela T, Mikkonen J, Skottman H, et al. Structured PDMS chambers for enhanced human neuronal cell activity on MEA platforms. *J Bionic Eng* 2012;9(1):1–10. [http://dx.doi.org/10.1016/S1672-6529\(11\)60091-7](http://dx.doi.org/10.1016/S1672-6529(11)60091-7).
- Lappalainen RS, Salomäki M, Ylä-Outinen L, Heikkilä TJ, Hyttinen JAK, Pihlajamäki H, et al. Similarly derived and cultured hESC lines show variation in their developmental potential towards neuronal cells in long-term culture. *Regen Med* 2010;5(5):749–62. <http://dx.doi.org/10.2217/rme.10.58>.
- LeFevre WR, McConnell ER, Crooks JL, Shafer TJ. Evaluation of microelectrode array data using Bayesian modeling as an approach to screening and prioritization for neurotoxicity testing. *NeuroToxicology* 2013;36:34–41. <http://dx.doi.org/10.1016/j.neuro.2013.02.006>.
- Lewicki MS. A review of methods for spike sorting: the detection and classification of neural action potentials. *Netw: Comput Neural Syst* 1998;9(4):R53–78. [http://dx.doi.org/10.1088/0954-898X\\_9\\_4\\_001](http://dx.doi.org/10.1088/0954-898X_9_4_001).
- Martínez J, Quiroga RQ. Spike sorting. In: Quiroga RQ, Panzeri S, editors. Principles of neural coding. London, UK: CRC Press; London, UK; 2013. p. 61–74. <http://dx.doi.org/10.1201/b14756-6>.
- Neuroshare Library. (<http://www.multichannelsystems.com/software/neuroshare-library/>); [September 2003, accessed March 2015].
- Novellino A, Scelfo B, Palosaari T, Price A, Sobanski T, Shafer TJ, et al. Development of micro-electrode array based tests for neurotoxicity: assessment of interlaboratory reproducibility with neurotoxic chemicals. *Front Neuroeng* 2011;4:4. <http://dx.doi.org/10.3389/fneng.2011.00004>.
- Pasquale V, Martinoia S, Chiappalone M. A self-adapting approach for the detection of bursts and network bursts in neuronal cultures. *J Comput Neurosci* 2010;29(1–2):219–29. <http://dx.doi.org/10.1007/s10827-009-0175-1>.
- Pine J. Recording action potentials from cultured neurons with extracellular microcircuit electrodes. *J Neurosci Methods* 1980;2(1):19–31. [http://dx.doi.org/10.1016/0165-0270\(80\)90042-4](http://dx.doi.org/10.1016/0165-0270(80)90042-4).
- Quiroga RQ, Nadasdy Z, Ben-Shaul Y. Unsupervised spike detection and sorting with wavelets and superparamagnetic clustering. *Neural Comput* 2004;16(8):1661–87. <http://dx.doi.org/10.1162/089976604774201631>.
- Santhanam G, Ryu SI, Yu BM, Afshar A, Shenoy KV. A high-performance brain-computer interface. *Nature* 2006;442(7099):195–8. <http://dx.doi.org/10.1038/nature04968>.
- Shannon CE. A mathematical theory of communication. *Bell Syst Tech J* 1948;XXVII(3):379–423. <http://dx.doi.org/10.1002/j.1538-7305.1948.tb01338.x>.
- Sun JJ, Kilb W, Luhmann HJ. Self-organization of repetitive spike patterns in developing neuronal networks *in vitro*. *Eur J Neurosci* 2010;32(8):1289–99. <http://dx.doi.org/10.1111/j.1460-9568.2010.07383.x>.
- Thomas CA Jr, Springer PA, Loeb GE, Berwald-Netter Y, Okun LM. A miniature microelectrode array to monitor the bioelectric activity of cultured cells. *Exp Cell Res* 1972;74(1):61–6. [http://dx.doi.org/10.1016/0014-4827\(72\)90481-8](http://dx.doi.org/10.1016/0014-4827(72)90481-8).
- Truccolo W, Donoghue JA, Hochberg LR, Eskandar EN, Madsen JR, Anderson WS, et al. Single-neuron dynamics in human focal epilepsy. *Nat Neurosci* 2011;14(5):635–41. <http://dx.doi.org/10.1038/nn.2782>.
- Turnbull L, Dian E, Gross G. The string method of burst identification in neuronal spike trains. *J Neurosci Methods* 2005;145(1–2):23–35. <http://dx.doi.org/10.1016/j.jneumeth.2004.11.020>.

- Uchida T, Suzuki S, Hirano Y, Ito D, Nagayama M, Gohara K. Xenon-induced inhibition of synchronized bursts in a rat cortical neuronal network. *Neuroscience* 2012;214:149–58, <http://dx.doi.org/10.1016/j.neuroscience.2012.03.063>.
- Uhlhaas PJ, Pipa G, Lima B, Melloni L, Neuenschwander S, Nikolić D, et al. Neural synchrony in cortical networks: history, concept and current status. *Front Integr Neurosci* 2009;3:17, <http://dx.doi.org/10.3389/fneuro.07.017.2009>.
- Valiante TA, Carlen PL. Electrophysiological mechanisms of network control: bursting in the brain—from cells to networks. In: Faingold C, Blumenfeld H, editors. *Neuronal networks in brain function, CNS disorders, and therapeutics*. London, UK: Academic Press; 2014. p. 121–33, <http://dx.doi.org/10.1016/B978-0-12-415804-7.00009-5>.
- Wagenaar DA, Pine J, Potter SM. An extremely rich repertoire of bursting patterns during the development of cortical cultures. *BMC Neurosci* 2006;7(7):11, <http://dx.doi.org/10.1186/1471-2202-7-11>.
- Waveclus. Unsupervised spike detection and sorting, (<http://www2.le.ac.uk/departments/engineering/research/bioengineering/neuroengineering-lab/spike-sorting/>; 2004 [accessed 11.12.15]).
- Wild J, Prekopcsak Z, Sieger T, Novak D, Jech R. Performance comparison of extracellular spike sorting algorithms for single-channel recordings. *J Neurosci Methods* 2012;203(2):369–76, <http://dx.doi.org/10.1016/j.jneumeth.2011.10.013>.
- Ylä-Outinen L, Heikkilä J, Skottman H, Suuronen R, Äänismaa R, Narkilahti S. Human cell-based micro electrode array platform for studying neurotoxicity. *Front Neuroeng* 2010;3:111, <http://dx.doi.org/10.3389/fneng.2010.00111>.

# Joint analysis of extracellular spike waveforms and neuronal network bursts

Fikret Emre Kapucu, Meeri E.-L. Mäkinen, Jarno M. A. Tanskanen, Laura Ylä-Outinen, Susanna Narkilahti, Jari A. K. Hyttinen

Journal of Neuroscience Methods

## Supplementary Material

**Table S1**

The experiment and analysis structure. The MEAs, MEA wells, and the numbers of wells (i.e., the numbers of separate cultures,  $n$ ) included in each test and analysis, along with the well inclusion criteria. The individual MEAs are identified by numbers. On each MEA chip, there were six wells with nine microelectrodes in each well.

Analysis method	Test	MEAs and MEA wells included in the analysis	Number of wells ( $n$ )	Well inclusion criteria
<i>Spike Sorting Based Analysis</i>	Baseline	MEA 1, all wells MEA 2, all wells	12	All wells (no exclusion criteria)
	1 <sup>st</sup> Wash	MEA 1, all wells MEA 2, all wells	12	
	CNQX	MEA 1, all wells MEA 2, all wells	12	
	CNQX+D-AP5	MEA 1, all wells MEA 2, all wells	12	
	2 <sup>nd</sup> Wash	MEA 1, all wells MEA 2, all wells	12	
	GABA	MEA 1, all wells MEA 2, all wells	12	
	Bicuculline	MEA 1, all wells MEA 2, all wells	12	
<i>Spike Activity Analysis</i>  <i>and</i> <i>Burst Detection</i>	Baseline	MEA 1, wells A, B, C, D, F MEA 2, wells A, B, C, E, F	10	Minimum of 50 spikes detected in a 300 s recording from an electrode of a well in at least one phase of the experiment (Kapucu et al., 2012)
	1 <sup>st</sup> Wash	MEA 1, wells A, B, C, D, F MEA 2, wells A, B, C, E, F	10	
	CNQX	MEA 1, wells A, B, C, D, F MEA 2, wells A, B, C, E, F	10	
	CNQX+D-AP5	MEA 1, wells A, B, C, D, F MEA 2, wells A, B, C, E, F	10	
	2 <sup>nd</sup> Wash	MEA 1, wells A, B, C, D, F MEA 2, wells A, B, C, E, F	10	
	GABA	MEA 1, wells A, B, C, D, F MEA 2, wells A, B, C, E, F	10	
	Bicuculline	MEA 1, wells A, B, C, D, F MEA 2, wells A, B, C, E, F	10	
<i>Burst Analysis</i>  <i>and</i> <i>Proposed Joint Analysis</i>	Baseline	MEA 1, wells A, B, C, D, F MEA 2, wells A, B, C, E, F	10	Minimum of 50 spikes, and at least one burst detected with the employed burst detection algorithm (Kapucu et al., 2012) in a 300 s recording from an electrode of a well
	1 <sup>st</sup> Wash	MEA 1, wells A, B, C, D, F MEA 2, wells A, B, C, E, F	10	
	CNQX	MEA 1, wells A, B, C, D, F MEA 2, wells A, B, C, E, F	10	
	CNQX+D-AP5	MEA 1, wells A, B, C, F MEA 2, wells A, B, C, E, F	9	
	2 <sup>nd</sup> Wash	MEA 1, wells A, B, C, F MEA 2, wells A, B, C, E	8	
	GABA	MEA 1, wells A, B, C, D, F MEA 2, wells A, B, C	8	
	Bicuculline	MEA 1, wells A, B, C, D, F MEA 2, wells A, B, E, F	9	

# Joint analysis of extracellular spike waveforms and neuronal network bursts

Fikret Emre Kapucu, Meeri E.-L. Mäkinen, Jarno M. A. Tanskanen, Laura Ylä-Outinen, Susanna Narkilahti, Jari A. K. Hyttinen

Journal of Neuroscience Methods

## Supplementary Material

**Table S2**

The numbers of channels in the wells which exhibited more than 50 spikes in 300 s for different experiment phases. The individual MEAs are identified by numbers whereas the individual wells are identified by capital letters. On each MEA chip, there were six wells with nine microelectrodes in each well.

Wells	Baseline	1 <sup>st</sup> Wash	CNQX	CNQX+D-AP5	2 <sup>nd</sup> Wash	GABA	Bicuculline
MEA 1, well A	7	6	3	3	1	0	2
MEA 1, well B	6	5	4	0	0	0	0
MEA 1, well C	9	7	8	8	7	5	5
MEA 1, well D	7	4	2	0	0	0	0
MEA 1, well E	0	0	0	0	0	0	0
MEA 1, well F	3	4	1	3	4	1	1
MEA 2, well A	9	6	1	0	4	3	0
MEA 2, well B	9	9	9	5	9	9	8
MEA 2, well C	7	3	0	1	0	0	0
MEA 2, well D	0	0	0	0	0	0	0
MEA 2, well E	5	4	1	0	2	0	0
MEA 2, well F	0	1	0	0	0	0	0

# Joint analysis of extracellular spike waveforms and neuronal network bursts

Fikret Emre Kapucu, Meeri E.-L. Mäkinen, Jarno M. A. Tanskanen, Laura Ylä-Outinen, Susanna Narkilahti, Jari A. K. Hyttinen

Journal of Neuroscience Methods

## Supplementary Material

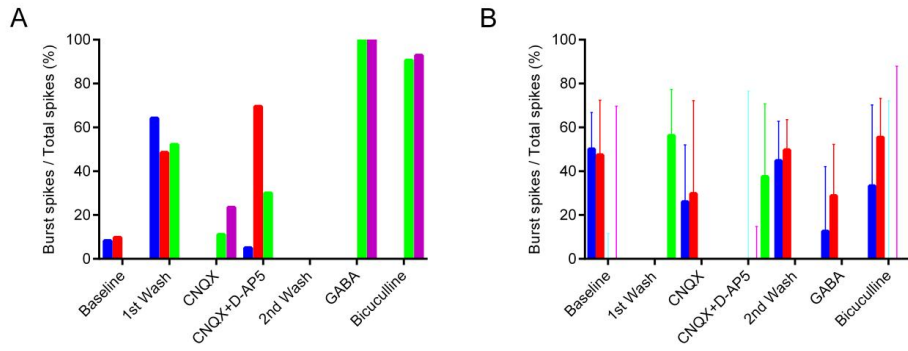


**Fig. S1.** The numbers of each type of spikes in bursts relative to the total numbers of spikes (A) for the single channel analysis (c.f. Fig. 4G), and (B) for the pooled data analysis (c.f. Fig. 6G).

# Joint analysis of extracellular spike waveforms and neuronal network bursts

Fikret Emre Kapucu, Meeri E.-L. Mäkinen, Jarno M. A. Tanskanen, Laura Ylä-Outinen, Susanna Narkilahti, Jari A. K. Hyttinen

Journal of Neuroscience Methods

## Supplementary Material

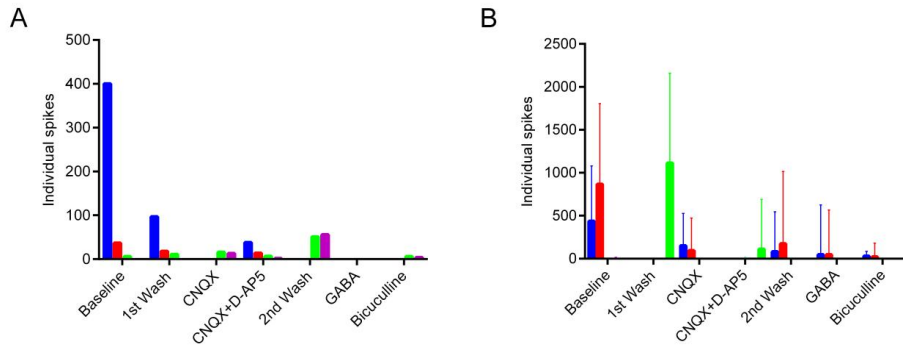


**Fig. S2.** The numbers of each type of spikes in individual spikes (A) for the single channel analysis (c.f. Fig. 4G), and (B) for the pooled data analysis (c.f. Fig. 6G).



Kapucu F.E., Mikkonen J.E., Tanskanen J.M.A., Hyttinen J.A.K.

**Analyzing the feasibility of time correlated spectral entropy for the  
assessment of neuronal synchrony.**

*In Proceedings of the 38th Annual International Conference of the IEEE  
Engineering in Medicine and Biology Society (EMBC), Orlando, FL, Aug.2016,  
pp. 1595-1598. IEEE, 2016.*

©2015 IEEE. Reprinted, with permission, from Kapucu F.E., Mikkonen J.E.,  
Tanskanen J.M.A., Hyttinen J.A.K., Analyzing the feasibility of time correlated  
spectral entropy for the assessment of neuronal synchrony, In Proceedings of the  
38th Annual International Conference of the IEEE Engineering in Medicine and  
Biology Society (EMBC), Aug, 2016.



# Analyzing the Feasibility of Time Correlated Spectral Entropy for the Assessment of Neuronal Synchrony \*

Fikret E. Kapucu, Jarno E. Mikkonen, Jarno M. A. Tanskanen, *Member, IEEE*, and Jari A. K. Hyttinen, *Member, IEEE*

**Abstract**—In this paper, we study neuronal network analysis based on microelectrode measurements. We search for potential relations between time correlated changes in spectral distributions and synchrony for neuronal network activity. Spectral distribution is quantified by spectral entropy as a measure of uniformity/complexity and this measure is calculated as a function of time for the recorded neuronal signals, i.e., time variant spectral entropy. Time variant correlations in the spectral distributions between different parts of a neuronal network, i.e., of concurrent measurements via different microelectrodes, are calculated to express the relation with a single scalar. We demonstrate these relations with *in vivo* rat hippocampal recordings, and observe the time courses of the correlations between different regions of hippocampus in three sequential recordings. Additionally, we evaluate the results with a commonly employed causality analysis method to assess the possible correlated findings. Results show that time correlated spectral entropy reveals different levels of interrelations in neuronal networks, which can be interpreted as different levels of neuronal network synchrony.

## I. INTRODUCTION

Neuronal synchrony can be expressed as the simultaneous activity of neuronal ensembles. There are several methods to analyze simultaneous activity. For example, it is very common to analyze neuronal synchrony by evaluating simultaneous occurrence of detected action potentials, i.e. spikes [1,2], or temporal occurrence of intense firing of spikes, i.e., neuronal bursts [3,4]. Other methods, for example, quantify frequency/phase coupling to assess the synchrony between sig-

nals in predefined frequency bands, particularly between the well-defined brain oscillation frequencies seen in electroencephalograms [5]. Techniques quantifying the spectral properties of neuronal ensembles are efficient for analyzing synchrony of neuronal populations if their effective frequency bands can be distinguished clearly. On the other hand, correlation effects on the spectral complexity of synchronous neuronal populations have not been studied to the best of our knowledge.

Previously, spectral entropy (SE) has been used to assess the complexity of signals based on their frequency dynamics, and used for analyzing particular neuronal events [6] and quantifying neuronal bursts [7]. Even though the latter study focused only on neuronal bursts, relations were also analyzed spatially, thus indicating possible spatial synchrony. Results obtained in Kapucu et al. [7] motivated us to investigate correlations of SE values of recordings from different regions of neuronal networks without considering only burst sequences. Since changes in the correlation structures of neuronal network activities would also be related with the changes in their functional connectivity [8], we can assume that we can observe the correlation dynamics, and thus gain more information on the network structure of neuronal populations.

In this paper, we first calculate time variant SE values for different spatial neuronal network locations. Next, we investigate the correlations for every pair of locations, and estimated pairwise interrelations according to the level of correlation. In addition, causality was estimated between the same locations, and the results were assessed jointly. In conclusion, we studied the potentials of the suggested analysis technique to be a valid method with further development to assess neuronal network synchrony.

## II. EXPERIMENTAL TEST DATA

The *in vivo* recordings were collected from anaesthetized rats. After placing anaesthetized rats in a stereotaxic instrument, holes were drilled on the skull above the target structures. Recordings were obtained by a silicon probe (courtesy of University of Michigan Center for Neural Communication Technology, MI, USA) with 16 microelectrodes on one shank and 100  $\mu\text{m}$  distance between the electrodes. Two of the topmost electrodes (channels 15 and 16) of the probe were omitted due to setup design and recording apparatus restrictions. Electrophysiological recordings were acquired after the probe was lowered into hippocampus. The location of the hippocampus, and thus the probe, was estimated based on CA1 pyramidal cell firing patterns to antidromical stimulation of the commissural efferents of the contralateral CA3 region. Three measurements were obtained one after the other, X, Y and Z. During a measurement session, stimulation de-

\* The works of F. E. Kapucu and J. M. A. Tanskanen have been supported by the 3DNeuroN project in the European Union's Seventh Framework Programme, Future and Emerging Technologies, grant agreement n°296590. The work of F. E. Kapucu has also been supported by the Academy of Finland under the project Bio-integrated Software Development for Adaptive Sensor Networks, project number 278882, by Human Spare Parts Project funded by Tekes – the Finnish Funding Agency for Innovation, and by Ella and Georg Ehrnrooth Foundation, Finland. The work of J. M. A. Tanskanen has also been supported by Jane and Aatos Erkkö Foundation, Finland, under the project Biological Neuronal Communications and Computing with ICT.

F. E. Kapucu (e-mail: fikret.kapucu@tut.fi, tel.: +358 40 849 0023) is with Tampere University of Technology, Department of Pervasive Computing, and Department of Electronics and Communications Engineering, Computational Biophysics and Imaging Group, BioMediTech, 33520 Tampere, Finland.

J. M. A. Tanskanen (e-mail: jarno.m.tanskanen@tut.fi) and J. A. K. Hyttinen (e-mail: jari.hyttinen@tut.fi) are with Tampere University of Technology, Department of Electronics and Communications Engineering, Computational Biophysics and Imaging Group, BioMediTech, 33520 Tampere, Finland.

J. E. Mikkonen (e-mail: jarno.e.mikkonen@jyu.fi) is with University of Jyväskylä, Department of Psychology and Centre for Interdisciplinary Brain Research, 40014 University of Jyväskylä, Finland.

scribed in [9] was repeated every 10 min. In this paper, we analyzed three sequential recordings from one rat to investigate the time course of the correlated locations. The data was collected previously for other research. The full description of the experimental setup can be found in [9].

The experimental procedures involving animal models described in this paper follow the international guidelines on the ethical use of experimental animals, and were approved by the Provincial Government of Eastern Finland (approval number 99-61).

The original recordings were sampled at the rate of 12.5 kHz. Signals were filtered with a 50 Hz notch filter and a 7 Hz high pass filter to eliminate AC noise and low frequency fluctuations, respectively.

### III. METHODS

To demonstrate the basic idea, we first analyzed on a small toy data set with assumed good and weak correlations. For that, we picked pairs of neighboring channels,  $(X_1, X_2)$ ,  $(Y_1, Y_2)$ , and  $(Z_1, Z_2)$  from each of three sequential recordings,  $X, Y$  and  $Z$  and pooled them together.

Next, we analyze the time variant SE and its correlation from entire recorded data, and present the relations illustratively according to the different levels of correlations. Finally, causality is calculated with a commonly used algorithm, partial granger causality (PGC), and the results evaluated jointly.

#### A. Calculation of time variant SE

SE is generally described as the application of Shannon's entropy algorithm on power spectrum. Shannon entropy is calculated from probability density function (PDF) values of a time sequence as

$$H = -\sum_i p_i \log p_i, \quad (1)$$

where  $p_i$  is the probability that an amplitude value occurs in the  $i$ th amplitude bin.

SE is calculated from the PDF values in a defined frequency range. First, power spectrum  $P(f_i)$  is calculated and normalized with a constant  $C_n$  in the defined frequency band  $[f_1, f_2]$  so that the sum of the normalized power spectrum over the frequency bands is equal to unity.

$$\sum_{f_i=f_1}^{f_2} P_n(f_i) = C_n \sum_{f_i=f_1}^{f_2} P(f_i) = 1 \quad (2)$$

Then SE is calculated from the normalized power spectrum, and normalized again with  $\log(N[f_1, f_2])$  to be within  $0 < S_N < 1$ , where  $N[f_1, f_2]$  is the total number of frequency components in the defined frequency band  $[f_1, f_2]$  so that

$$SE = \frac{1}{\log(N[f_1, f_2])} \sum_{f_i=f_1}^{f_2} P_n(f_i) \log\left(\frac{1}{P_n(f_i)}\right). \quad (3)$$

In this paper, spectral entropy is calculated in the Nyquist range since the effective bandwidths of the studied signals were not known.

SE is calculated for every 0.5 s time window with 50% overlapping windows to achieve time variant SE. Fig. 1 illustrates an exemplary time sequence from a recording and its

time variant SE. In the sequel, we only discuss the time variant SE.

#### C. Correlation of time variant SEs

After calculating time variant SEs, we search for the degree of temporal correlations between different pairs, e.g.  $X$  and  $Y$  of the time variant SE time series. For that, cross-covariance,  $C_{SE_X SE_Y}$  is estimated at the 0 lag of the previously calculated SEs for the same number of total time windows,  $M$ , where time variant SE is calculated (4).

$$C_{SE_X SE_Y} = \frac{1}{M} \sum_{i=1}^M \left( (SE_{X,i} - \overline{SE_X})(SE_{Y,i} - \overline{SE_Y}) \right), \quad (4)$$

where  $\overline{SE_X}$  and  $\overline{SE_Y}$  are the sample means of the corresponding SEs. Thereafter, cross-correlation at lag 0 is estimated as

$$r_{SE_X SE_Y} = \frac{C_{SE_X SE_Y}}{\sigma_{SE_X} \sigma_{SE_Y}}, \quad (5)$$

where  $\sigma_{SE_X}$  and  $\sigma_{SE_Y}$  are the standard deviations of the corresponding SEs.

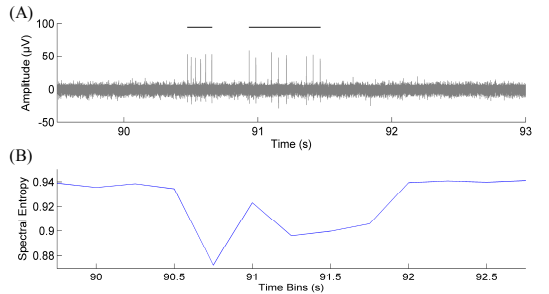


Figure 1. (A) A short sequence from a neuronal recording. The black lines indicate the neuronal bursts detected as described by Kapucu et al. [10]. (B) Time variant SE calculated from the recording in panel (A) with 50% overlapping 0.5 s long windows.

#### D. PGC

Granger Causality (GC) describes if a prediction error  $\varepsilon$  of the future values of  $Y$  by considering the past values of  $Y$  and the past values of  $X$  together (full model) is less than the prediction error  $\hat{\varepsilon}$  considering only the past values of  $Y$  (restricted model). If so, the time series  $X$  Granger causes the time series  $Y$ ,  $GC_{X \rightarrow Y}$  [11].  $GC_{X \rightarrow Y}$  is defined as

$$GC_{X \rightarrow Y} = \log \frac{\text{var}(\hat{\varepsilon})}{\text{var}(\varepsilon)}. \quad (6)$$

PGC was proposed by Guo et al. [12] by extending GC with the existence of common exogenous inputs and latent variables driven by  $Z$ ; thus defining the restricted and full models in (7) and (8), respectively.

$$\begin{cases} X_t = \sum_{i=1}^p a_{1i} X_{t-i} + \sum_{i=1}^p c_{1i} Z_{t-i} + \{u_{1t}\} \\ Y_t = \sum_{i=1}^p b_{1i} Y_{t-i} + \sum_{i=1}^p d_{1i} Z_{t-i} + \{u_{2t}\} \end{cases} \quad (7)$$

and

$$\begin{cases} X_t = \sum_{i=1}^p a_{2i} X_{t-i} + \sum_{i=1}^p b_{2i} Y_{t-i} + \sum_{i=1}^p c_{2i} Z_{t-i} + \{u_{3t}\} \\ Y_t = \sum_{i=1}^p d_{2i} X_{t-i} + \sum_{i=1}^p e_{2i} Y_{t-i} + \sum_{i=1}^p f_{2i} Z_{t-i} + \{u_{4t}\} \end{cases}, \quad (8)$$

where  $u_{kt}$  is defined as  $u_{kt} = \varepsilon_{kt} + \varepsilon_{kt}^E + B_k(L)\varepsilon_{kt}^E$ , where  $\varepsilon^E$  and  $B(L)\varepsilon_{kt}^E$  are the residuals of the exogenous inputs and latent variables, respectively. Covariance matrixes for the

indirect interactions, i.e., for the latent and exogenous inputs are defined for the restricted (9) and full (10) models as

$$S = \begin{bmatrix} \text{var}(u_{1t}) & \text{cov}(u_{1t}, u_{2t}) \\ \text{cov}(u_{2t}, u_{1t}) & \text{var}(u_{2t}) \end{bmatrix}, \quad (9)$$

and

$$\Sigma = \begin{bmatrix} \text{var}(u_{3t}) & \text{cov}(u_{3t}, u_{4t}) \\ \text{cov}(u_{4t}, u_{3t}) & \text{var}(u_{4t}) \end{bmatrix}, \quad (10)$$

respectively. Then, the  $PGC_{X \rightarrow Y|Z}$  is calculated as

$$PGC_{X \rightarrow Y|Z} = \log \left( \frac{S_{22} - S_{21} S_{11}^{-1} S_{12}}{S_{22} - S_{21} \Sigma_{11}^{-1} S_{12}} \right). \quad (11)$$

#### IV. RESULTS

Correlations of time variant SEs are presented in Fig. 2A and PGCs in Fig. 2B for the small scale toy data. Time variant SEs are strongly correlated for the neighboring channels picked from same recording sequence, as expected. Moreover, the causality values are higher for the same channel pairs, indicating a causal relation for those pairs.

Interrelation maps were formed according to the correlations of time variant SEs for the entire data set (Fig. 3). We demonstrated only the relations  $r_{SE_X SE_Y} > 0.8$  with relations  $r_{SE_X SE_Y} > 0.9$  indicated by red or blue, as also indicated on the measurement probe illustrations (Figs. 3A-3C). Probe and electrode locations in the hippocampus are illustrated in Fig. 3D. In each measurement (Figs. 3A-3C), two different groups were identified based on the strongest relations ( $r_{SE_X SE_Y} > 0.9$ ). However, these two strong groups have also

weak relations with each other. Actually, the time variant SE method based interrelation maps (Figs. 3A-3C) clearly indicate two separate connected groups, which correspond to the anatomical regions CA1 and CA3 of the hippocampus (Fig. 3D). Additionally, the analysis revealed that the strongly connected group in CA3 region was expanding as the experiment proceeded, which was probably due to the effects of electrical stimulation during the experiment: briefly, the strongest groups in the map ( $r_{SE_X SE_Y} > 0.9$ ) were seen to expand, where also the weaker correlations ( $r_{SE_X SE_Y} < 0.9$ ) were seen to get stronger.

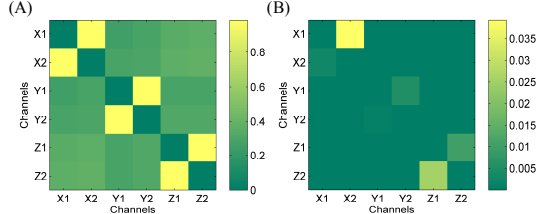


Figure 2. (A) Correlation results for the small data set calculated based on time variant SEs. (B) PGCs for the same data set. Channels from same recordings named with same variable names, i.e., X, Y, and Z.

The results of the PCG analysis for the first and third measurements are shown in Fig. 4. The PGC results of third measurement (Fig. 4B) with respect to first measurement exhibit a gradual increase in the PGC causalities between the channels, from channel 10 down to channel 1, which actually are included into the large network seen in the SE based analysis interrelation map in Fig. 3C. Additionally, for the first measurement, separate groups with interrelations

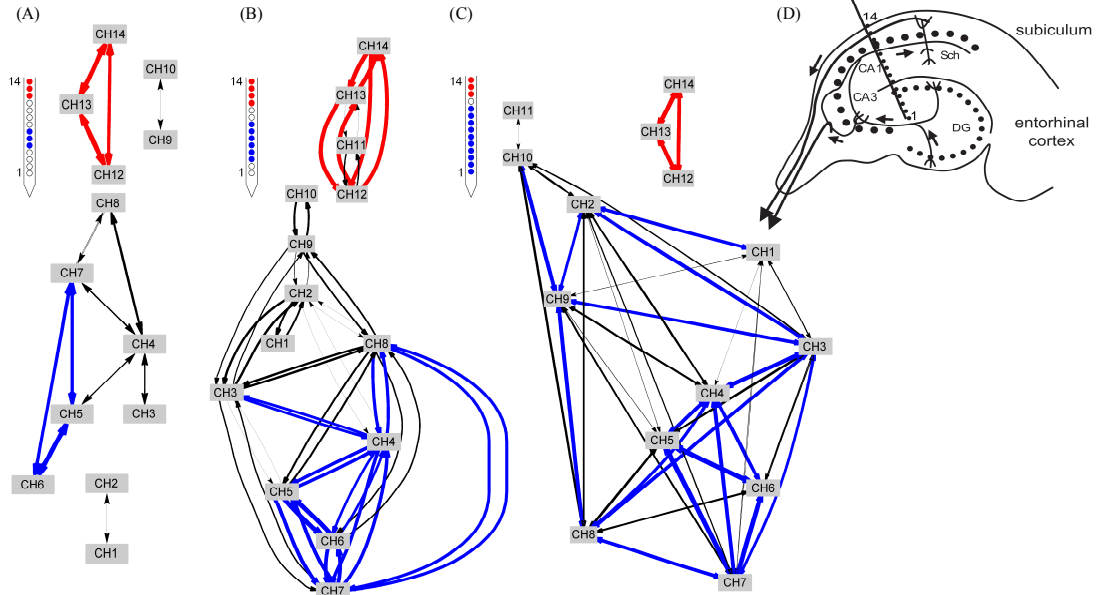


Figure 3. (A)-(C) The interrelation maps based on the strongest correlations found in the three *in vivo* measurements based on time variant SEs. Line width indicates correlation strength. The strongest correlations ( $r_{SE_X SE_Y} > 0.9$ ) indicated by blue or red, and the corresponding electrodes with the same colors on the schematic illustrations of the electrode shafts. Results for one measurement are presented in each panel correspondingly. (D) A schematic illustration of the rat hippocampus with the locations of the channels 1 and 14 with the hippocampal regions indicated. (Sch-Schaffer collaterals, DG- dentate gyrus).

$r_{SE_X SE_Y} > 0.8$ , e.g., the group formed by the channels 5, 6, and 7, the group formed by the channels 9 and 10 and the group formed by the channels 1 and 2 in Fig. 3A, are also highlighted in the PGC analysis spatially as channels with stronger causal relations (Fig. 4A). In these cases, the two methods yielded corroborative results.

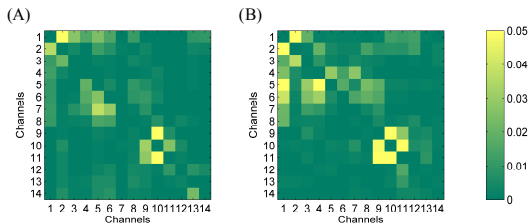


Figure 4. (A) PGC analysis results from the first measurement corresponding to the Fig. 3A for comparison. (B) PGC analysis results from the third measurement corresponding to the Fig. 3C for comparison.

## V. CONCLUSIONS AND DISCUSSION

We showed that the novel time variant correlation of spectral entropy has potential to assess neuronal interrelations. Outcomes of the analysis proposed in this paper produced corroborative findings with the PGC analysis. On the other hand, correlation analysis does not provide any information on causality, whereas PGC provides causal relations with an additional feature of eliminating exogenous inputs and latent variables.

The differences between our and the causality methods observed do not necessarily mean that either of the findings is wrong as such; on the contrary, the information derived can be complementary. If the time correlated spectral analysis studied here, implied synchrony between different locations of the hippocampus, the causality and synchronicity could be studied simultaneously. For example, the relations between synchrony and causality were studied by Battaglia et al. [13] and Buehlmann and Deco [14].

This work can be considered as a feasibility study for investigating the potential of the proposed analysis method. However, further validation studies e.g. with known neuronal networks or simulated data is needed. In any case our method has potential to provide new insights, e.g., in many applications of microelectrode array neuronal recordings. Especially the methods can be seen usable in developing neuronal populations, where synchrony cannot be determined in the early stages of their development by the means of synchronous bursts, since such burst appear only later in the development.

## REFERENCES

- [1] R. Q. Quiroga, T. Kreuz, and P. Grassberger, "Event synchronization: a simple and fast method to measure synchronicity and time delay patterns," *Physical Review E*, vol. 66, no. 4, article 041904, Oct. 2002. DOI:10.1103/PhysRevE.66.041904
- [2] S. Schreiber, J. M. Fellous, D. Whitmer, P. Tiesinga, and T. J. Sejnowski, "A new correlation-based measure of spike timing reliability," *Neurocomputing*, vol. 52–54, pp. 925–931, June 2003. DOI:10.1016/S0925-2312(02)00838-X
- [3] A. Zwanenburg, E. Meijer, W. Jennekens, C. van Pul, B. Kramer, and P. Andriessen, "Automatic detection of burst synchrony in preterm infants," *2012 annual international conference of the IEEE Engineering in medicine and biology society (EMBC)*, 2012. DOI: 10.1109/EMBC.2012.6347021
- [4] J. V. Selinger, J. J. Pancrazio, and G. W. Gross, "Measuring synchronization in neuronal networks for biosensor applications," *Biosensors and Bioelectronics*, vol. 19, no. 7, pp. 675–683, 2004. DOI:10.1016/S0956-5663(03)00267-7
- [5] J. M. Palva, S. Palva, and K. Kaila, "Phase synchrony among neuronal oscillations in the human cortex," *The Journal of Neuroscience*, vol. 25, no. 15, pp. 3962–3972, 2005.
- [6] H. Viertio-Oja, V. Maja, M. Särkelä, P. Talja, N. Tenkanen, H. Tolvanen-Laakso, M. Paloheimo, A. Vakkuri, A. Yli-Hankala, P. Meriläinen, "Description of the entropy algorithm as applied in the Datex-Ohmeda S/5 Entropy Module," *Acta Anaesthesiol. Scand.*, vol. 48, pp.154–161, 2004. DOI:10.1111/j.0001-5172.2004.00322.x
- [7] F. E. Kapucu, J. E. Mikkonen, J. Tanskanen, and J. A. Hyttinen, "Quantification and automatized adaptive detection of in vivo and in vitro neuronal bursts based on signal complexity," in *2015 37th Annual International Conference of the IEEE Engineering in Medicine and Biology Society (EMBC)*, pp. 4729–4732, 2015.
- [8] E. Salinas and T. J. Sejnowski, "Correlated neuronal activity and the flow of neural information," *Nat. Rev. Neurosci.*, vol. 2, pp. 539–550, 2001. DOI:10.1038/35086012.
- [9] J. E. Mikkonen and M. Penttonen, "Frequency bands and spatiotemporal dynamics of beta burst stimulation induced afterdischarges in hippocampus in vivo," *Neurosci.*, vol. 130, pp. 239–247, 2005. DOI:10.1016/j.neuroscience.2004.08.039
- [10] F. E. Kapucu, J. M. A. Tanskanen, J. E. Mikkonen, L. Ylä-Outinen, S. Narkilahti, and J. A. K. Hyttinen, "Burst analysis tool for developing neuronal networks exhibiting highly varying action potential dynamics," *Front. Comput. Neurosci.*, vol. 6, no. 38, 2012. DOI:10.3389/fncom.2012.00038.
- [11] C. W. J. Granger, "Investigating Causal Relations by Econometric Models and Cross-spectral Methods," *Econometrica* 37 (3), 424–438, 1969. DOI:10.2307/1912791.
- [12] S. Guo, A. K. Seth, K. M. Kendrick, C. Zhou, and J. Feng, "Partial Granger causality—eliminating exogenous inputs and latent variables," *J. Neurosci. Meth.*, vol. 172, no. 1, pp. 79–93, 2008. DOI: 10.1016/j.jneumeth.2008.04.011
- [13] D. Battaglia, A. Witt, and F. Wolf, T. Geisel, "Dynamic effective connectivity of inter-areal brain circuits," *PLoS Comput. Biol.* 8:e1002438, 2012. DOI:10.1371/journal.pcbi.1002438.
- [14] A. Buehlmann and G. Deco, "Optimal information transfer in the cortex through synchronization," *PLoS Comput. Biol.* 16:e1000934, 2010. DOI:10.1371/journal.pcbi.1000934

Kapucu F.E., Vornanen I., Mikkonen J.E., Leone C., Lenk K., Tanskanen J.M.A.,  
Hyttinen J.A.K.

**Spectral entropy based neuronal network synchronization analysis  
based on microelectrode array measurements.**

*Frontiers in Computational Neuroscience, 10:112, 2016.*

Open access. Authors retain the copyright to this publication.





# Spectral Entropy Based Neuronal Network Synchronization Analysis Based on Microelectrode Array Measurements

Fikret E. Kapucu<sup>1,2\*</sup>, Inkeri Vällki<sup>2</sup>, Jarno E. Mikkonen<sup>3</sup>, Chiara Leone<sup>4</sup>, Kerstin Lenk<sup>2</sup>, Jarno M. A. Tanskanen<sup>2</sup> and Jari A. K. Hyttinen<sup>2</sup>

<sup>1</sup> Department of Pervasive Computing, Tampere University of Technology, Tampere, Finland, <sup>2</sup> Computational Biophysics and Imaging Group, Department of Electronics and Communication Engineering, BioMediTech, Tampere University of Technology, Tampere, Finland, <sup>3</sup> Department of Psychology, Center for Interdisciplinary Brain Research, University of Jyväskylä, Jyväskylä, Finland, <sup>4</sup> Department of Management and Production Engineering, Politecnico di Torino, Torino, Italy

## OPEN ACCESS

### Edited by:

Ramon Guevara Erra,  
Laboratoire Psychologie de la  
Perception (CNRS), France

### Reviewed by:

John E. Lewis,  
University of Ottawa, Canada  
Diego Martin Mateos,  
Sick Kids Hospital, Canada

### \*Correspondence:

Fikret E. Kapucu  
fikret.kapucu@tut.fi

Received: 22 July 2016

Accepted: 05 October 2016

Published: 18 October 2016

### Citation:

Kapucu FE, Vällki I, Mikkonen JE,  
Leone C, Lenk K, Tanskanen JMA and  
Hyttinen JAK (2016) Spectral Entropy  
Based Neuronal Network  
Synchronization Analysis Based on  
Microelectrode Array Measurements.  
*Front. Comput. Neurosci.* 10:112.  
doi: 10.3389/fncom.2016.00112

Synchrony and asynchrony are essential aspects of the functioning of interconnected neuronal cells and networks. New information on neuronal synchronization can be expected to aid in understanding these systems. Synchronization provides insight in the functional connectivity and the spatial distribution of the information processing in the networks. Synchronization is generally studied with time domain analysis of neuronal events, or using direct frequency spectrum analysis, e.g., in specific frequency bands. However, these methods have their pitfalls. Thus, we have previously proposed a method to analyze temporal changes in the complexity of the frequency of signals originating from different network regions. The method is based on the correlation of time varying spectral entropies (SEs). SE assesses the regularity, or complexity, of a time series by quantifying the uniformity of the frequency spectrum distribution. It has been previously employed, e.g., in electroencephalogram analysis. Here, we revisit our correlated spectral entropy method (CorSE), providing evidence of its justification, usability, and benefits. Here, CorSE is assessed with simulations and *in vitro* microelectrode array (MEA) data. CorSE is first demonstrated with a specifically tailored toy simulation to illustrate how it can identify synchronized populations. To provide a form of validation, the method was tested with simulated data from integrate-and-fire model based computational neuronal networks. To demonstrate the analysis of real data, CorSE was applied on *in vitro* MEA data measured from rat cortical cell cultures, and the results were compared with three known event based synchronization measures. Finally, we show the usability by tracking the development of networks in dissociated mouse cortical cell cultures. The results show that temporal correlations in frequency spectrum distributions reflect the network relations of neuronal populations. In the simulated data, CorSE unraveled the synchronizations. With the real *in vitro* MEA data, CorSE produced biologically plausible results. Since CorSE analyses continuous data, it is not affected by possibly poor spike

or other event detection quality. We conclude that CorSE can reveal neuronal network synchronization based on *in vitro* MEA field potential measurements. CorSE is expected to be equally applicable also in the analysis of corresponding *in vivo* and *ex vivo* data analysis.

**Keywords:** synchronization, spectral entropy, correlation, mouse cortical cells, rat cortical cells, developing neuronal networks, MEA, microelectrode array

## INTRODUCTION

Temporally correlated activity between neurons or neuronal networks *in vivo* and *in vitro* has been vastly studied in terms of event based synchrony, or synchrony between oscillations or rhythmic activities in different frequency bands. Salinas and Sejnowski (2001) argued that the presence of correlations between the activities of pairs of neurons, or synchrony *per se*, is not important in general, since they may arise from common inputs or synaptic interactions, or from overlapping receptive fields, respectively; however, changes in the correlation structure of a neuronal network reflect changes in its functional connectivity. Previous studies have shown that the pattern of synchronization determines the pattern of neuronal interactions, and that the efficiency of transferred information is also modulated by synchrony (Buehlmann and Deco, 2010; Battaglia et al., 2012). Thus, assessing the relations of synchrony is essential not only for fully developed neuronal networks, such as in the brain, but also for the assessment of development and plasticity of cultured neuronal networks.

In the past years, several studies concentrated on quantifying and analyzing the network relations of cultured neuronal cells (Garofalo et al., 2009; Mack et al., 2014). Most of the studies utilized binary analysis based on events, particularly the occurrences of spikes and bursts. For example, in several studies, transfer entropy (TE), joint entropy, mutual information (MI), coincidence index, and event synchrony (ES) were employed on detected spikes to evaluate network relations (Quiroga et al., 2002; Garofalo et al., 2009; Ito et al., 2011); however, as stated by Buzsáki et al. (2012), network relations affect local field potentials (LFPs) as well.

For brain studies, synchronization, causality, phase and frequency coupling, or tracking previously defined rhythms, can reveal network interactions (Ginter et al., 2005; Buehlmann and Deco, 2010). A review of a few connectivity measures to assess neuronal activity has been presented by Bastos and Schoffelen (2016). The amount of propagating activity observed in different frequency bands (rhythmic activities) or associated with well-defined electroencephalogram (EEG) rhythms (delta, theta, alpha, beta, and gamma) is important in interpreting the results of such a study (Ginter et al., 2005). On the other hand,

generally in cultured neuronal networks, the different frequency bands are not as distinguishable as in the brain studies, or the absence of well-defined rhythms makes the analysis more challenging. Even though LFPs (or raw recordings that may include both spikes and LFPs) potentially carry information on network relations, they are not commonly used for the network analysis based on microelectrode array (MEA) measurement data from cultured cells. MEAs are usually used to measure extracellular field potentials from electrically active tissues and cell cultures at network and cell levels (Thomas et al., 1972; Gross et al., 1977; Pine, 1980; Egert et al., 1998). MEA electrodes record field potentials, e.g., from the neurons in their vicinity, which can carry contributions from both extracellular action potentials (EAPs) from individual neuronal cells and lower frequency contributions originating from neuronal population activity. Neurons may temporarily arrange themselves into synchronous functional ensembles to perform a given task. These ensembles may be volatile and only exist for short periods of time before new ensembles with partially different subsets of neurons are formed. Connected neuronal ensembles are thought to operate at certain frequencies (for general references, see Buzsáki and Chrobak, 1995; Penttonen and Buzsáki, 2003; Buzsáki and Draguhn, 2004). Consequently, frequency domain analysis has potential to obtain novel information also from cell cultures (Jarvis and Mitra, 2001; Brown et al., 2004). Frequency spectrum analysis may also be a good alternative in cases with unreliable spike detection either due to low amplitude spikes in noise or conflicting results from different spike detection algorithms.

Drawing from above, we have hypothesized that also temporal correlations of the frequency spectrum distributions could reflect the network relations of neuronal populations (Kapucu et al., 2016a). Intuitively, this is motivated by the possibility that measurements from functionally connected neuronal populations may be quite different if only time domain properties were considered. For analyzing the functional connectivity of a network, techniques quantifying the spectral properties of neuronal ensemble activity provide promising alternatives to the methods assessing the couplings or correlations between specific rhythms or frequencies. Spectral entropy (SE) quantifies the regularity, or complexity, of a signal based on its frequency dynamics. SE is a frequency based realization of Shannon's entropy algorithm (Shannon, 1948), which was previously used for analyzing certain neuronal events, such as burst suppression, and for the EEG based assessment of the depth of anesthesia (Viertiö-Oja et al., 2004). In our previous work (Kapucu et al., 2015), we utilized SE and sample entropy to quantify *in vivo* and *in vitro* neuronal bursts according to their complexities, and demonstrated similarities in the complexity values of bursts

**Abbreviations:** cES, corrected event synchronization; CorSE, correlated spectral entropy method; DIV, days *in vitro*; EAP, extracellular action potentials; EEG, electroencephalogram; ES, event synchronization; eSTD, thresholding at five times the standard deviation of the background noise; FN, false negative; LFP, local field potential; MEA, microelectrode array; MI, mutual information; SE, spectral entropy; STD, thresholding at five times the standard deviation of the signal; TE, transfer entropy; WGN, white Gaussian noise.

from neighboring channels. Also in Kapucu et al. (2016a), we tested the feasibility of SE for the assessment of synchronization. However, the method was never validated with simulations and its true applicability was not demonstrated with larger real measurement datasets. An earlier study of the relations between the synchronization and the activity level, as well as the relations between synchronization and connectivity levels (Chawla et al., 1999), was also a motivation for the evaluation of CorSE with different levels of connected networks.

In this paper, we expand the original idea proposed by Kapucu et al. (2016a) and investigate the benefits of SE time course correlation analysis as a tool for analyzing synchronization by analyzing a larger set of data. Here, we also name the proposed method CorSE. Firstly, we illustrate CorSE with a toy simulation of neuronal ensembles (Montgomery, 2014). Next, we validate our method with simulated MEA data produced with computational integrate-and-fire model based neuronal networks with known connectivity levels. The results of CorSE are compared to and assessed together with the results from three existing event based synchronization assessment algorithms, ES (Quiroga et al., 2002), MI (Gray, 1990), and TE (Schreiber, 2000). Finally, we demonstrate the applicability of CorSE with MEA data measured from cultured rat cortical neurons with different activity levels, and with MEA data measured from a developing network of mouse cortical neurons.

## MATERIALS AND METHODS

### Biological Data

*In vitro* MEA experiments were performed with dissociated rat and mouse cortical cell cultures. The data from dissociated rat cortical cells was originally collected for a previous study (see the details given by Weihberger et al., 2013); animal treatment was according to the Freiburg University (Freiburg, Germany) and German guidelines on the use of animals in research. Briefly, rat cortical cells were obtained from prefrontal cortical tissue of newborn Wistar rats and plated on MEA plates, which consist of 60 titanium nitride electrodes of 30  $\mu\text{m}$  diameter and 200  $\mu\text{m}$  interelectrode spacing on an 8  $\times$  8 rectangular grid with corner electrodes missing (model: 60MEA200/30iR, Multi-Channel Systems MCS GmbH, Reutlingen, Germany). Seeded cell density was approximately 1250 cells/ $\text{mm}^2$ . After 4 weeks of culturing, the cultures were considered mature (Wagenaar et al., 2006) and recordings were conducted inside a dry incubator.

To assess *in vitro* network development over time, commercially available mouse cortical cells (A15586, Gibco, Thermo Fisher) were plated on MEAs similar to those described above. Briefly, the MEAs were coated with poly-L-lysine and laminin, and the cells were sowed as droplets on to MEA plates for culturing (Wagenaar et al., 2006). Electrophysiological data were recorded three times a week starting from 4 days *in vitro* (DIV) until the 29th DIV. Every recording lasted for 5 min.

The recordings from rat cortical cell cultures were analyzed using the different synchronization assessment methods considered in this paper. All *in vitro* data was first filtered with a 50 Hz notch filter and 7 Hz high pass filter to alleviate the powerline noise and low frequency fluctuations, respectively.

For the analysis methods that are based on spike time stamps, spikes were detected using two thresholding methods to evaluate the effects of different spike detection methods on the results of the synchronization assessment algorithms: spike detection thresholds were set to five times the standard deviation of the signal, or at five times the estimated standard deviation of the background noise of the band pass filtered signal as proposed by Quiroga et al. (2004). Here, the different thresholding methods are denoted by STD and eSTD, respectively. CorSE was employed to demonstrate the tracking of network development in the mouse cortical cell cultures. Since CorSE operates on the measured signals themselves (either raw or filtered), spike detection was not performed.

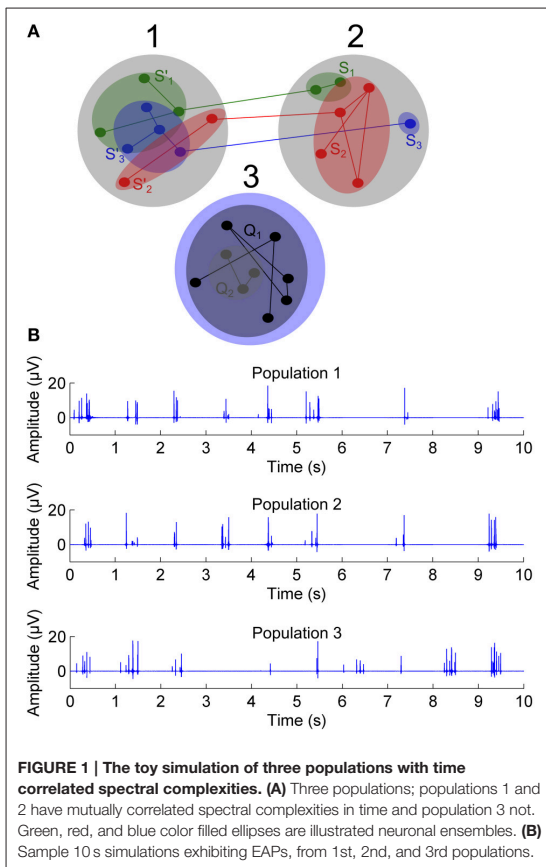
Two cultures were selected for the analysis according to the number of active locations where spiking activity was observed according to a house made rule of 50 spikes per 300 s (Kapucu et al., 2012, 2016b) so that the chosen MEAs had different numbers of active locations. The analyzed cultures are denoted by MEA1 and MEA2. The MEA1 had 32 or 37 active sites as calculated with STD and eSTD, respectively, and MEA2 had 15 or 12 active sites as calculated with STD and eSTD, respectively.

### Simulated Data

#### Toy Simulations of Correlated Time-Variant SEs

A toy simulation of a MEA signal was generated to illustrate and explain the proposed SE based synchronization assessment method CorSE. Here, MEA measured neuronal unit activities, i.e., EAPs, and the average activity of neuronal ensembles, i.e., LFPs, were simulated as cardinal *Sine*, i.e., *Sinc* waves, and oscillation of *Sines*, respectively (see Montgomery, 2014 for the *Sine* wave representation of LFPs), to generate a simulated population signal as seen via an electrode. In such a model, neuronal synchronization between two populations was defined as simultaneous activity of neuronal ensembles in a simple way: when a number of neuronal ensembles (illustrated with green, red, and blue color filled ellipses in **Figure 1A**) activated in a population, the same number of neuronal ensembles was also activated in the other population, i.e., the model assumes that all the active neuronal ensembles are connected to other ensembles in the other population. Three populations were simulated with two of them (populations 1 and 2) fully synchronous with each other, and the third population (population 3) independent of the other populations (**Figure 1A**).

Simulated signals were generated in 1 s sections which were simply concatenated to form a simulation of a 3 min measurement. For each 1 s section, a random number of constituent *Sine* signals, and a random number of *Sinc* signals, were generated and summed together. The sampling rate for the generated signals was 1 kHz. The number of constituent *Sine* signals was evenly distributed between 5 and 10, and the number of constituent *Sinc* signals evenly distributed between 0 and 10. The oscillation amplitudes, frequencies, and phases were randomly selected and evenly distributed. To generate the two connected populations, whenever a *Sine* or *Sinc* appeared in one of them, a *Sine* or *Sinc*, respectively, appeared also in the other population, both with independently random amplitudes, frequencies, and phases. The signals for the unconnected



population were generated independently of the other two populations.

The simulations were implemented in Matlab (MathWorks, Inc., Natick, MA, USA). A large data set of 1000 triplets of populations 1, 2, and 3 was generated, each simulated signal corresponding to a 3 min recording. To investigate the functioning of the methods with either LFPs or EAPs or both, signals with five different EAP-LFPs power ratios  $P_{EAPs/LFPs} = 0, 10, 20, 50,$  and  $100\%$  were generated ( $P_{EAPs}$  and  $P_{LFPs}$  denote the total estimated powers of the summed constituent *Sinc* and *Sine* signals, respectively).

Statistical validation was approached by calculating all pairwise synchronizations between all 1000 simulated recordings in all three populations, and by calculating statistics for the signals from the two connected populations to express detected synchronization vs. the synchronization between signals from the unconnected populations.

### Simulations with Integrate-and-Fire Model Based Neuronal Networks

The computational neuronal network simulation was based on the model introduced by Tsodyks et al. (2000). The networks

consisted of integrate-and-fire neurons with short-term plastic synapses, and exhibited clear population bursts. The parameters employed for neurons and synapses were the same as in Tsodyks et al. (2000). To introduce spontaneous activity in the network, the neurons were driven with white noise current. Three-minute MEA measurements were simulated.

The simulated networks consisted of two populations. Each population consisted of 50 neurons, of which 40 were excitatory and 10 inhibitory. Each population was internally fully connected, but without autapses. Simulations were conducted at five inter-population connectivity levels, 0, 10, 20, 50, and 100%, between the two populations. Hundred percent connected populations correspond to one population twice the size of the original populations. Here, the percentages give the probabilities for one neuron to be connected to another neuron in the other population. Hundred pairs of populations were simulated for each inter-population connectivity level. The weights of all connections were tuned so that the mean spike rate in a population would not vary highly between the simulations with different levels of connectivity, resulting in the mean spike rate of 39–45 spikes/second in a simulation.

The NEST simulator (Gewaltig and Diesmann, 2007) was used to provide spike time stamps of the EAPs of the individual neurons. From the time stamps, artificial MEA recordings were constructed to simulate raw MEA recordings: the time resolution of the simulation was 1 ms, and a single spike was recorded for a one-millisecond time bin if any number of individual spikes appeared during the bin (Figure 2A). Thereafter, a *Sinc* function with random parameters, similarly as in the toy simulation, was formed for each spike and located in time with the maximum at the spike time point. The generated *Sinc* signals, peaking in general at different points in time, were summed to generated an EAP signal. Basically, a *Sinc* kernel can be used to reconstruct a sampled signal (Blanche and Swindale, 2006) or a population activity (Nawrot et al., 1999), but here we intended not to reconstruct the original recording from its samples, but instead to obtain a continuous function based on the simulated spike time stamps. We call these simulated signals artificial raw recordings (c.f., Figure 2B).

Artificial LFPs were added to the EAP simulations as described in Section CorSE, SE Based Synchronization Analysis (c.f., Figure 2B). Simulations were conducted at  $P_{EAPs/LFPs} \approx 20\%$  and  $P_{EAPs/LFPs} \approx 50\%$ , to roughly correspond to two difference scenarios of background noise and activity levels vs. action potential amplitudes. Thereafter, to make the simulations more realistic, white Gaussian noise (WGN) was added to the generated artificial raw signals for all cases simulated. WGN was added to obtain signal to noise ratios (SNRs) of 50% and 20%, as calculated by  $SNR = 100 \cdot P_{EAPs}/P_{WGN}$ , where  $P_{EAP}$  is the estimated power of a generated artificial recording, and  $P_{WGN}$  is the estimated power of the added WGN.

### CorSE, SE Based Synchronization Analysis Shannon Entropy

Entropy in the context of information theory was introduced by Shannon as a measure of uncertainty (Shannon, 1948). Shannon entropy is defined as

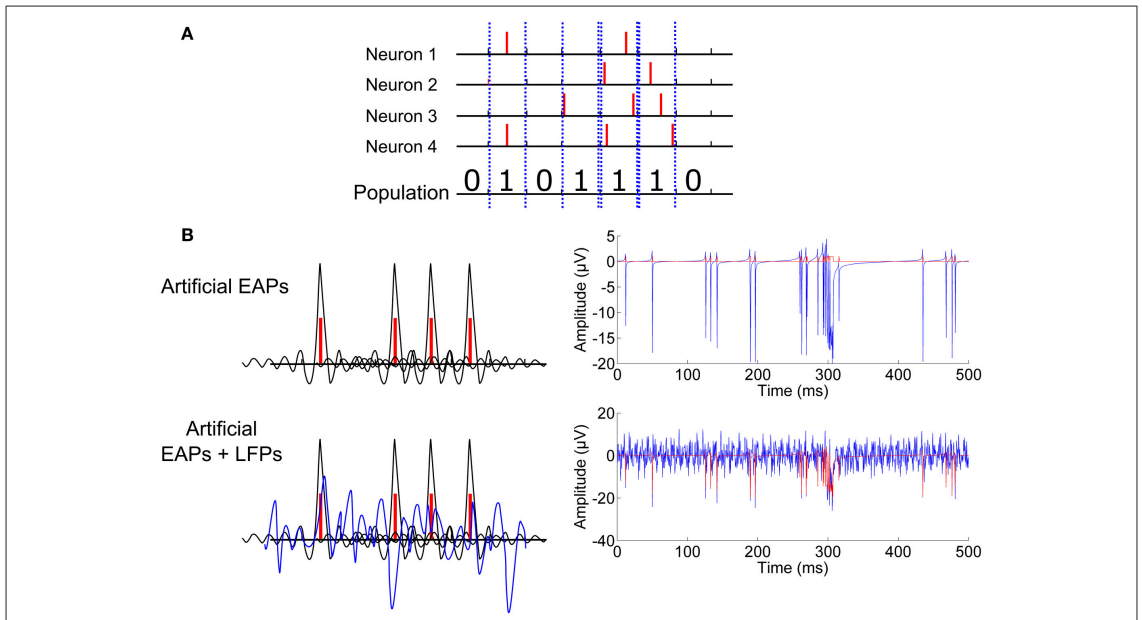


**FIGURE 2 | Computational neuronal network simulation. (A)** Any number of spikes in a time bin is counted as one population spike in that time bin. **(B)** A *Sinc* function with random parameters (black) is placed at each population spike (red) forming the EAPs. Thereafter, artificial LFPs are simulated by additive *Sine* functions with random parameters. Artificially created EAPs with and without LFPs for population signaling are plotted with blue. Illustrative signal construction and the resulting exemplary signals can be seen on the left and right-hand panels respectively.

$$H = -\sum_i p_i \log p_i, \tag{1}$$

where  $p_i$  is the probability that an amplitude value occurs in the  $i$ th amplitude bin, and is given by the probability density function of the time series.

**SE**

We calculated SE as Shannon’s entropy on power spectrum as described by Vartiö-Oja et al. (2004): SE was calculated by first obtaining the frequency spectrum of the time series  $x(n)$ , sampled at discrete time points  $n$ , by fast Fourier transform  $X(f)$  at frequency points  $f$  (2) with bold denoting a vector.

$$X(f) = \sum_n x(n)e^{-i2\pi fn} \tag{2}$$

The power spectrum is given by

$$P(f) = X(f) X^*(f), \tag{3}$$

where  $X^*(f)$  is the complex conjugate of  $X(f)$ . Here, power spectrum was estimated by Welch periodogram with a Hann window of a preset length of 0.5 s and 50% window overlap to provide a smoother transition between windows and to increase temporal resolution.

Power spectrum was normalized with a constant  $C$  for the Nyquist frequency range at  $K$  frequency points

$[f_1, \dots, f_k, \dots, f_K]$  so that the sum of the normalized power spectrum  $P_{norm}(f_k)$  equaled unity (4).

$$\sum_{f_k=f_1}^{f_K} P_{norm}(f_k) = C \sum_{f_k=f_1}^{f_K} P(f_k) = 1 \tag{4}$$

SE  $S$  was calculated from the normalized power spectrum as

$$S = \sum_{f_k=f_1}^{f_K} P_{norm}(f_k) \log \left( \frac{1}{P_{norm}(f_k)} \right), \tag{5}$$

and  $S$  was normalized to reside between 1 and 0 by

$$S_{norm} = \frac{S}{\log(K)} \tag{6}$$

In the sequel, SE is always considered to be the normalized SE  $S_{norm}$ .

**Correlation of SEs**

Here, we quantify the synchronization of signals by the correlation of the temporal changes of their spectral contents. This is obtained by calculating SEs in time windows, and the degree of common temporal changes for different sites in the neuronal network is assessed by calculating cross correlations:

the cross covariance  $C_{S_x S_y}(t, t + \tau)$  of the SEs  $S_x$  and  $S_y$  of the signals  $x$  and  $y$ , respectively, describes how well the SE of the signal  $y$  at time  $t + \tau$  is correlated with SE of the signal  $x$  at time  $t$ . Here, the sample cross correlations were estimated using the *crosscorr* function of Matlab (Chatfield, 2003). With  $O$  the number of time windows in which SEs were calculated, and  $i$  the index of a 0.5 s long time window,  $\{(S_{x,i}, S_{y,i}); i = 1, 2, \dots, O\}$ , cross covariance at the lag  $l = 0$  is given by

$$C_{S_x S_y} = \frac{1}{O} \sum_{i=1}^O ((S_{x,i} - \bar{S}_x)(S_{y,i} - \bar{S}_y)), \quad (7)$$

where  $\bar{S}_x$  and  $\bar{S}_y$  are the sample means of the corresponding SEs. The cross correlation  $r_{S_x S_y}$  at lag  $l = 0$  is then estimated as

$$r_{S_x S_y} = \frac{C_{S_x S_y}}{\sigma_{S_x} \sigma_{S_y}}, \quad (8)$$

where  $\sigma_{S_x}$  and  $\sigma_{S_y}$  are the standard deviations of the corresponding SEs. SE cross correlation (8) values at lag zero of the were used to assess the level of synchronization between pairs of channels, i.e., CorSE between signals  $x$  and  $y$  is given by  $CorSE_{xy} = r_{S_x S_y}$ .

### Known Event Based Methods Used for Comparison

For comparisons with CorSE, we implemented three commonly used event based synchronization assessment algorithms: ES (Quiroga et al., 2002), MI (Gray, 1990), and TE (Schreiber, 2000). Comparisons were made based on the results of all the algorithms considered for the computational neuronal network simulations and for the rat cortical cell recordings. EAPs detectable in these signals were taken as the events for the three event based algorithms considered. The spikes, i.e., EAPs, in both the artificial recordings and in real MEA recordings were detected with two different threshold based spike detection methods, STD and eSTD, as described in Section Biological Data, resulting in sets of binary strings as the inputs to algorithms. With the artificial recordings, the effects of added LFPs and WGN on the spike detection, and the consequences on the event based synchronization assessment algorithms, were also evaluated.

ES, introduced by Quiroga et al. (2002), measures synchronization based on quasi-simultaneous appearance of events. As an initial step, the ES algorithm finds from the time series  $x$  and  $y$  the maximum time period  $\tau_{i,j}$  between two consecutive spikes so that the two spikes occurring at times  $t_i^x$  and  $t_j^y$  in signals  $x$  and  $y$ , respectively, where  $i$  and  $j$  are spike indexes, can be considered simultaneous, by calculating the local spike appearances:

$$\tau_{i,j} = \frac{\min \left\{ t_{i+1}^x - t_i^x, t_i^x - t_{i-1}^x, t_{j+1}^y - t_j^y, t_j^y - t_{j-1}^y \right\}}{2}. \quad (9)$$

Then, cross covariance  $C_{x|y}$  is defined as the number of times a spike appears in  $x$  within  $\tau_{i,j}$  after a spike has appeared in  $y$ , as:

$$C_{x|y} = \sum_{i=1}^{M_x} \sum_{j=1}^{M_y} J_{i,j}, \quad (10)$$

where  $M_x$  and  $M_y$  are the total numbers of events for  $x$  and  $y$ , respectively, and

$$J_{i,j} = \begin{cases} 1, & 0 < t_i^x - t_j^y < \tau_{i,j} \\ \frac{1}{2}, & t_i^x = t_j^y \\ 0, & \text{otherwise.} \end{cases} \quad (11)$$

Finally, synchronization is given by

$$Q = \frac{C_{x|y} + C_{y|x}}{\sqrt{M_x M_y}}. \quad (12)$$

The algorithm in its original form did not have a requirement for the minimum number of events to consider; thus, two time series with even one simultaneous detectable event could be considered as fully synchronized. To circumvent this for MEA recordings, we employed the in-house criterion of minimum 50 spikes in 300 s, as in Kapucu et al. (2012) and Kapucu et al. (2016b), for the data to be analyzed. This eliminates unjustified synchronizations, which could be caused by coincidentally appearing rare events. We named the modified algorithm the corrected ES (cES) method.

The next method we used for comparisons was the well-known mutual information (MI) (Gray, 1990), which has been widely employed in many studies to quantify dependencies between time series or specifically for quantifying synchronization (Garofalo et al., 2009; Salazar et al., 2012). MI (13) is calculated by considering both single and joint probabilities of events in two time series  $x$  and  $y$ .

$$MI_{xy} = \sum_{e_i^y \in y} \sum_{e_i^x \in x} p(e_i^x, e_i^y) \log \left( \frac{p(e_i^x, e_i^y)}{p(e_i^x)p(e_i^y)} \right), \quad (13)$$

where  $e_i^x$  and  $e_i^y$  are  $i$ th single events occurring in the signals  $x$  and  $y$ , respectively,  $p(e_i^x, e_i^y)$  is the joint probability density function, and  $p(e_i^x)$  and  $p(e_i^y)$  are the single probabilities. Mutual information is a symmetric measure, i.e.,  $MI_{xy} = MI_{yx}$ .

The last algorithm is transfer entropy (TE), which extends the concept of MI to conditional properties by considering the history of the influenced information (Schreiber, 2000). In other words,  $TE_{y \rightarrow x}$  measures the increase in predictability of knowing the future and the past of  $x$ , once  $y$  is known. TE can be calculated as

$$TE_{y \rightarrow x} = \sum_{e_i^x, e_i^y} p(e_{i+1}^x, e_i^x, e_i^y) \log \left( \frac{p(e_{i+1}^x | e_i^x, e_i^y)}{p(e_{i+1}^x | e_i^x)} \right), \quad (14)$$

where in addition to the parameters defined above,  $p(e_{i+1}^x | e_i^x)$  denotes the conditional probability of observing the state  $e_{i+1}^x$  after  $e_i^x$ .

TE (15) was calculated in one-millisecond signal bins for delays up to three bins, and the maximum value of TE was considered as given in Ito et al. (2011).

$$TE_{y \rightarrow x} = \sum_{e_i^x, e_i^y} p(e_{i+1}^x | e_i^x, e_{i+1-d}^y) \log \left( \frac{p(e_{i+1}^x | e_i^x, e_{i+1-d}^y)}{p(e_{i+1}^x | e_i^x)} \right), \tag{15}$$

where  $d$  is the time delay. Since TE is asymmetric and we did not consider the directionality, we considered the maximum TE value obtained between the channel pairs, i.e.,  $TE = \max(TE_{y \rightarrow x}, TE_{x \rightarrow y})$ .

### Assessment of the Toy Simulations

To present the results of the toy simulation, it is necessary to define the detection of correct synchronization, false positive synchronization, and false negative synchronization, and to calculate their rates. Here, synchronization is detected correctly if CorSE between populations 1 and 2 is larger than CorSE between populations 2 and 3, and larger than between populations 1 and 3, i.e., when  $CorSE_{XY} > CorSE_{XZ}$  and  $CorSE_{XY} > CorSE_{YZ}$ . In this case, populations 1 and 3, and populations 2 and 3 are not deemed synchronized. False negative synchronization is detected when the true synchronization is missed, i.e., when either CorSE between populations 1 and 3, or between populations 2 and 3, is greater than or equal to CorSE between populations:  $CorSE_{XY} \leq CorSE_{XZ}$  and/or  $CorSE_{XY} \leq CorSE_{YZ}$ . False positive synchronization is detected when either populations 1 and 3, or populations 2 and 3 are deemed synchronized. In all cases of false positive detection, the true synchronization is also missed. Vice versa, in all cases of false negative synchronization, a false positive synchronization is detected. Thus, due to the system of populations in **Figure 1**, and the synchronization criterion applied, the false positive and false negative rates are equal.

### Comparative Assessment of the Analysis Methods for MEA Recording Analysis

For comparing the synchronization values obtained with the different methods considered, we first calculated the synchronization between each electrode pair, and thereafter created adjacency matrixes of the synchronization values. In **Figures 5, 6**, the matrixes are arranged for better visualization according to the ascending channel numbers on a MEA plate, e.g., channel 12 is located at (1,2) on an  $8 \times 8$  MEA layout. In each matrix, the values were normalized respect to the maximum of the matrix to form a color scale. This was done to make the locations of the maximally synchronized electrode pairs more easily comparable between the different methods.

Since the signals were recorded from unguided neuronal cells that freely form networks on the MEA plates, there was no ground truth available on the actual connections or synchronization between the neuronal populations. However, we compared the results from the different algorithms based on a fixed number of most synchronized channel pairs according to each algorithm, i.e., the strongest synchronizations; to illustrate the differences in the results of difference algorithms, the 40

strongest synchronizations were found using each algorithm for MEA1, and the 20 strongest synchronizations for MEA2.

Also, we evaluated the similarity of the synchronization based functional connectivity results of the algorithms. Here, we considered the measurement channels as nodes and synchronized channel pairs as links. The results are presented as the numbers of links and nodes common between the results from the different methods, when considering only 10, 20, ..., or 50 strongest synchronizations found with each algorithm, i.e., synchronization maps were drawn with each method, and similar findings between pairs of methods were reported by plotting the numbers of the found common nodes and the numbers of common links as functions of the number of the strongest synchronizations considered.

## RESULTS

### Toy Simulation Analysis Results

The Results from the analysis of the toy simulations with 1000 triplets indicate that CorSE was able to clearly distinguish the two populations with time correlated frequency distributions from the population pairs that did not have the correlated frequency distributions by design. In **Table 1**, results are shown for the model with LFPs, with EAPs, and for a model with both LFPs and EAPs with different  $P_{EAPs/LFPs}$  s (see Section SE). It is seen from **Table 1** that over 96% of the cases were correctly identified as synchronized, and the results show consistent performance regardless of the EAP-LFP power ratio considered. In summary, the results in **Table 1** demonstrate that the method can detect synchronization in the case simulated.

### Integrate-and-Fire Model Simulation Analysis Results

We assessed the simulated integrate-and-fire model based computational neuronal networks with CorSE and compared the results with the three different event based synchronization assessment algorithms described in Section Known Event Based Methods Used for Comparison. Firstly, in **Table 2**, we present the spike detection results employing two different spike detection methods, i.e., STD and eSTD, and with respect to the different

**TABLE 1 | Synchronization detection rates based on 1000 simulation of the toy model signal analysis with different EAP-LFP power ratios.**

Simulated EAP-LFP power ratio	Synchronization detection rate (%)	False positive rate; false negative rate (%)
$P_{EAPs/LFPs} \approx 100\%$ (EAPs only)	99.8	0.2
$P_{EAPs/LFPs} \approx 504\%$	97.9	2.1
$P_{EAPs/LFPs} \approx 20\%$	97.1	2.9
$P_{EAPs/LFPs} \approx 10\%$	96.7	3.3
$P_{EAPs/LFPs} \approx 0\%$ (LFPs only)	99.5	0.5

$X$ ,  $Y$ , and  $Z$ , denote the recorded signals from the populations 1, 2, and 3 respectively, with only  $X$  and  $Y$  with mutually correlated frequency distributions. For this analysis system, false positive rate is equal to false negative rate.

**TABLE 2 | Spike detection performances using STD and eSTD for the artificially generated MEA signals.**

Spike detection method	Added signal	$P_{EAPs/LFPs}$ (for LFPs); SNR (for WGNs) (%)	False negative rate (%)
STD	LFP	~50	64
		~20	97
	WGN	50	90
		20	99
eSTD	LFP	~50	45
		~20	96
	WGN	50	87
		20	99

EAP-LFPs power ratios considered, as well as different with levels of added WGN. **Table 2** shows the approximate mean values in percentages for false negative (FN) detections, i.e., the missed spikes for all 1000 artificial recordings created from 100 simulations for each five connectivity levels. False positive detection, i.e., detected spurious spikes, were observed very rarely and could be considered negligible in all cases. Results are given for the both spike detection methods for  $P_{EAPs/LFPs} \approx 20$  and 50%, as well as for SNRs of 20 and 50%. The results in **Table 2** indicate that both additive LFPs and WGN greatly affect spike detection, which is natural; the phenomenon occurs in all thresholding based spike detection systems, since with increasing LFP and/or WGN power, more and more spikes fall below overall noise level and cannot be detected by thresholding, and subsequent analysis is done based on only the detectable spikes. In practice in general, the FN detections correspond to the action potentials from neurons far away from the measurement electrode, so that the action potential amplitudes fall below the general noise level; such neurons are naturally more abundant than the neurons in the close vicinity of the electrode.

Next, we evaluated the synchronization values obtained by the different algorithms for the different connectivity levels. Exemplary raster plots for individual neurons and their corresponding artificial population activity for different connectivity levels are presented on the left-hand and right-hand panels of **Figure 3**, respectively. By visual inspection, inter- and intra-population synchronization can be observed in the left-hand panels of **Figure 3**. In **Figure 4**, we present the calculated synchronicities from the artificial recordings in the left-hand panels, and the corresponding sample signals in the right-hand panels. **Figure 4A** presents the synchronicities calculated from the artificial recordings with only EAPs (see the right-hand panel for an exemplary 2 s signal segment). Synchronization values calculated by all the algorithms increase with the increasing connectivity, except for the connectivity levels 50 and 100% for all other methods than CorSE. CorSE was the only method showing monotonous increase in the synchronization when the connectivity increased for the considered connectivity values.

**Figures 4B,C** presents the synchronicities calculated from the artificial recordings with EAPs and added fully synchronized

LFPs. Comparisons between the results with the EAP-LFP power ratios  $P_{EAPs/LFPs} \approx 20\%$  vs. 50%, and  $P_{EAPs/LFPs} \approx 20\%$  vs. 20% can be seen in **Figures 4B,C**, respectively. With the added artificial LFPs (see **Figures 4B,C** right-hand panels for exemplary 2 s signal segments with  $P_{EAPs/LFPs} \approx 50$  and 20%, respectively), the synchronization levels detected with the event based algorithms were noticeably smaller than those detected with CorSE as predictable from the FN spike detection rates shown in **Table 1**. With LFPs or WGN (**Figures 4B–E**), it is observed that the increased connectivity did not always lead to increased observed synchronization. Results indicate that the spike detection performances have a strong influence on the synchronization results of the event based algorithms, as expected. In contrary, although synchronization values of the artificial recordings measured with CorSE changed with the superimposed LFPs, the correlation between the increased synchronization and the increased level of connectivity is somewhat preserved and the behavior between simulations remained similar.

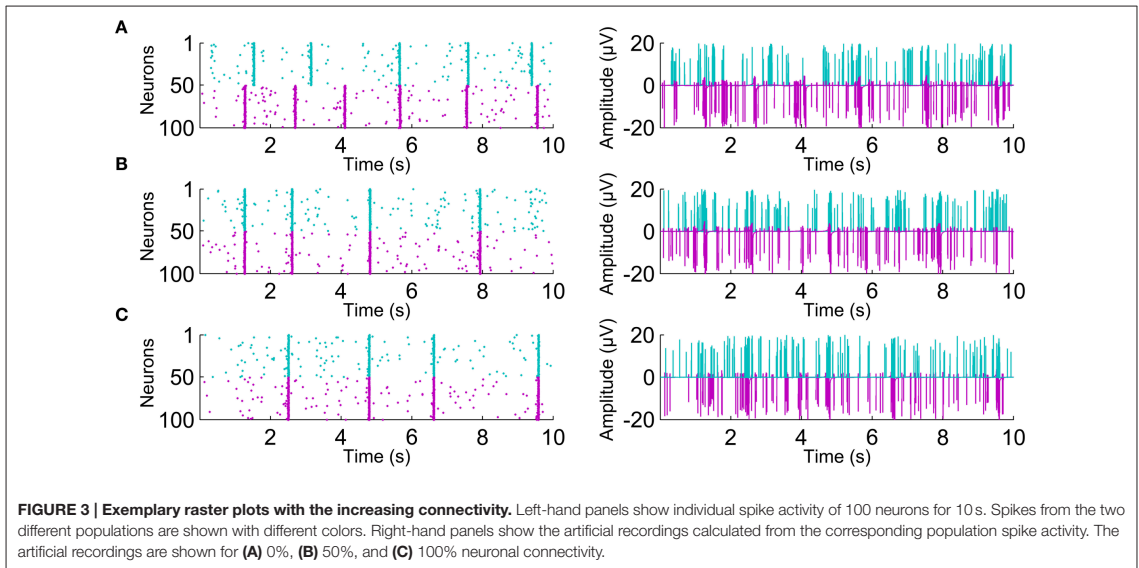
**Figures 4D,E** shows the synchronicities calculated from the artificial recordings with EAPs and added WGN. The results from the different SNR values, 50 and 20%, are presented in **Figures 4D,E**, respectively, whereas right-hand panels again show corresponding exemplary 2 s signal segments. Adding WGN greatly decreased the synchronization detected by the event based algorithms (c.f., **Figures 4D,E**). On the other hand, to compare, cES presented better performance in distinguishing the relation between the increasing levels of connectivity and synchronization. Synchronization values calculated by CorSE changed much less due to WGN than those for the event based methods. Even though CorSE was still able to distinguish the unconnected (0% level connectivity) populations from the connected populations, it cannot distinguish the different levels of connectivity; especially with the lower SNR.

In conclusion, CorSE was applicable in determining the level of synchronization according to the level of population connectivity not only for the simulated recordings which solely consisted of EAPs, but also in presence of LFPs. CorSE was also usable for functional connectivity assessment to distinguish the connected and unconnected populations in low SNR conditions caused by high WGN power.

## MEA Recordings

We present the results of different synchronization assessment algorithms applied on rat cortical network measurement data (MEA1 and MEA 2) in different forms: First, we demonstrate the obtained synchronization values for the different methods as adjacency matrices (**Figures 5, 6**). Then, the most synchronized channel pairs found with different methods are presented (**Figures 7, 8**) on the MEA layout. Finally, we compare the most synchronized channel pairs found by different algorithms (**Figures 9, 10**). To see the effects of the different spike detection methods, the results employing both spike detection methods (STD and eSTD) are presented for the event based algorithms (**Figures 5–10**).

Adjacency matrices present an overview of the found synchronicities. For MEA1, the highest synchronization was



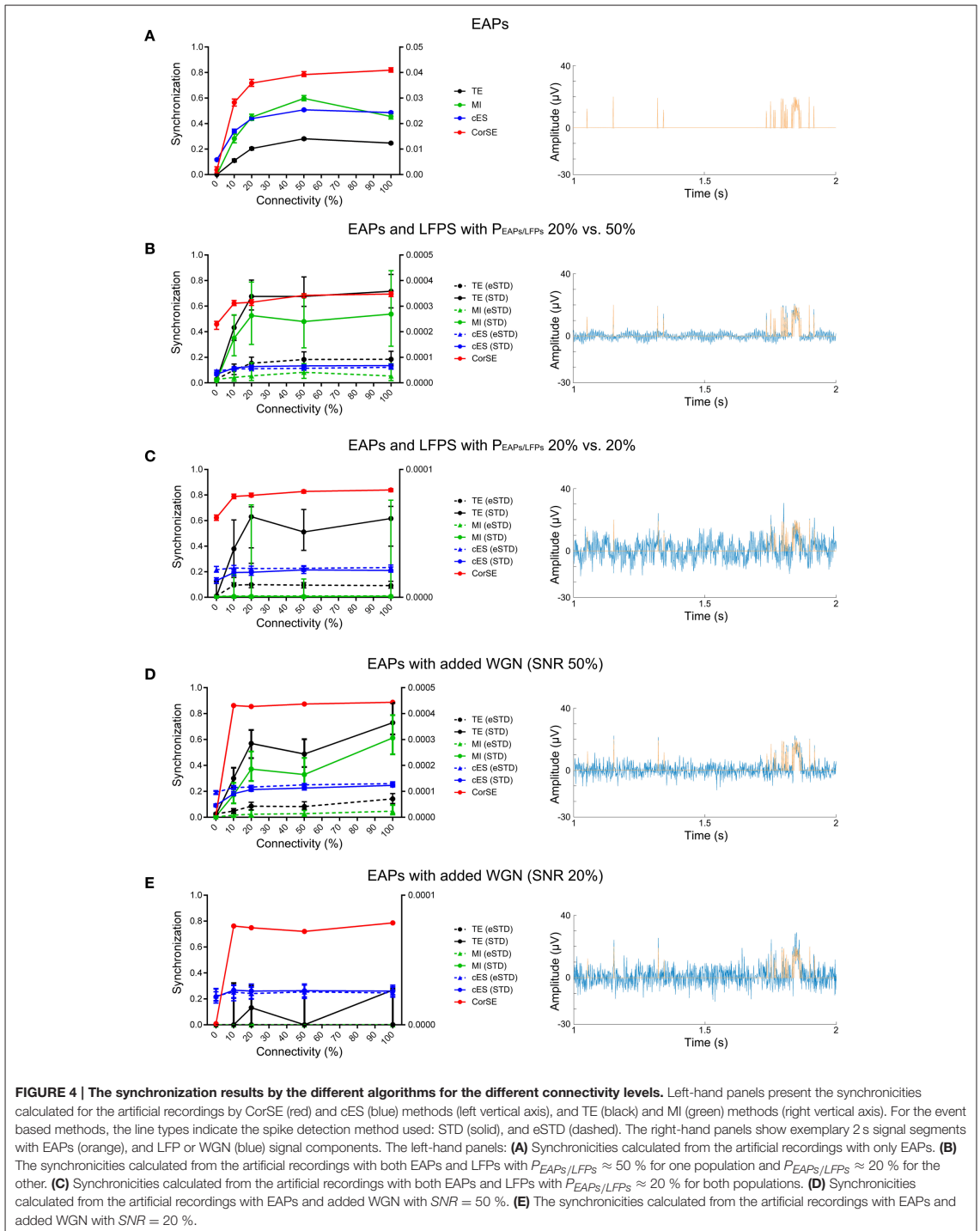
found between the channels 56 and 67 (represented in **Figure 5** as (5,6) and (6,7), respectively, in the sequel similarly) by CorSE, and the TE (with eSTD) and MI (with eSTD) methods (**Figures 5B–D**). The rest of the methods resulted in different maximally synchronized culture locations. For MEA2, the highest synchronization was found between the channels 73 (7,3) and 83 (8,3) by CorSE, and the MI (with STD and eSTD) and cES (with STD and eSTD) methods (**Figures 6B,D,E**).

For further comparisons between the algorithms and to demonstrate the most synchronized channel pairs (strongest synchronizations), the 40 strongest synchronizations for MEA1, and the 20 strongest synchronizations for MEA2, are shown in **Figures 7, 8**, respectively. The different algorithms found most synchronized channel pairs differently. Moreover, the different spike detection methods change the results of the event based synchronization assessment algorithms as can be seen also from **Figures 5, 6**. Among all algorithms considered, the results of the TE and MI methods are most similar where CorSE has more common outputs with both the TE and MI methods compared to the output of the cES method. For example, there are channels with more links than the others; in other words, network locations acting as hubs (see **Figures 7, 8**), such as channels 56 and 67 found by the TE and MI methods (with both spike detection methods) and CorSE as the top two channels with the highest numbers of links for MEA1. The cES method found channels 55 and 27 (with eSTD), and 83 and 51 (with STD) as the top two hub channels. For MEA2, channel 75 was a channel that could be considered a hub found by the TE and MI methods (with both spike detection methods) and CorSE, but again not by the cES method.

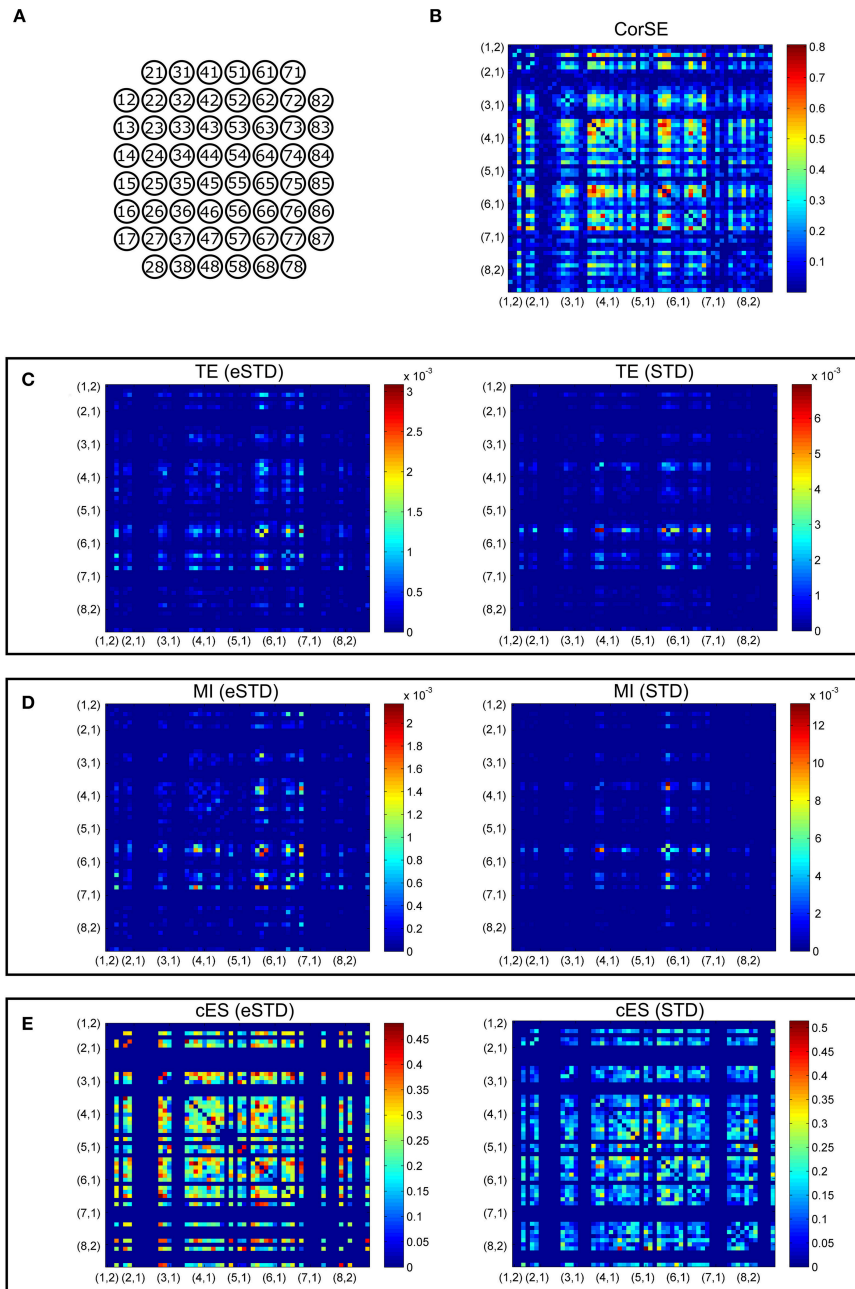
To assess the common aspects of the results produced with the difference algorithms in more detail, the number of common nodes (channels) and common links (pairwise

synchronizations) are plotted according to the number of strongest synchronizations (**Figures 9, 10**). The results show that for MEA1 and using eSTD, all the algorithms found approximately a similar number of common nodes (**Figure 9C**), alike for MEA2 with either STD or eSTD (**Figures 10C,D**). However, the numbers of found common links between the common nodes show more dependence on the method used (**Figures 10A,B**). The results from the TE and MI methods had the most common links, and CorSE found more common links with these two algorithms than the cES algorithm did.

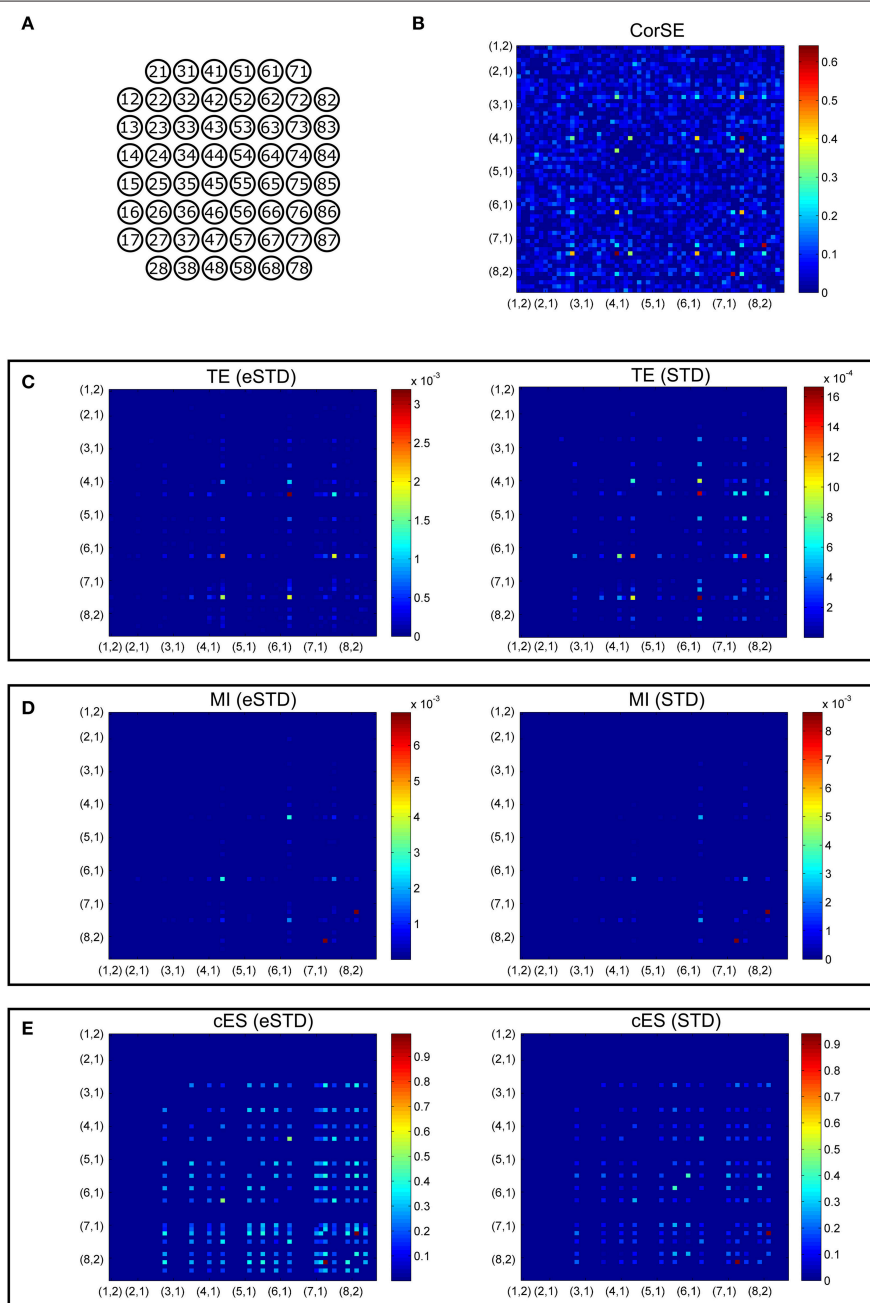
Finally, we present the results of CorSE in unraveling a developing mouse cortical neuron network. **Figure 11** presents the development of a network between the 13th and 29th DIV. Channel pairs with synchronizations exceeding an arbitrary threshold ( $CorSE > 0.5$ , selected for illustrative purposes) are illustrated. The first links were seen on the 13th DIV, and thereafter the network gradually expanded while also synchronizations between all the channels were getting stronger, with the strongest network synchronizations found on the 22nd DIV (see **Figure 12**). The mean values of synchronizations between all the channel pairs (in total 1770 links) were calculated during the development of the network (see **Figure 12**). The results show that the mean values of all the synchronizations were also correlated with the number of channel pairs with synchronizations greater than  $CorSE > 0.5$ ; in other words, the overall network synchronization strength followed the same trend with the observed channel pairs. Synchronization between some channels varied for different measurement days. A noteworthy example for this case is the smaller network that appeared on the 25th DIV, could not be observed on the 27th DIV, and reappeared on the 29th DIV with a stronger synchronization (**Figure 11**).



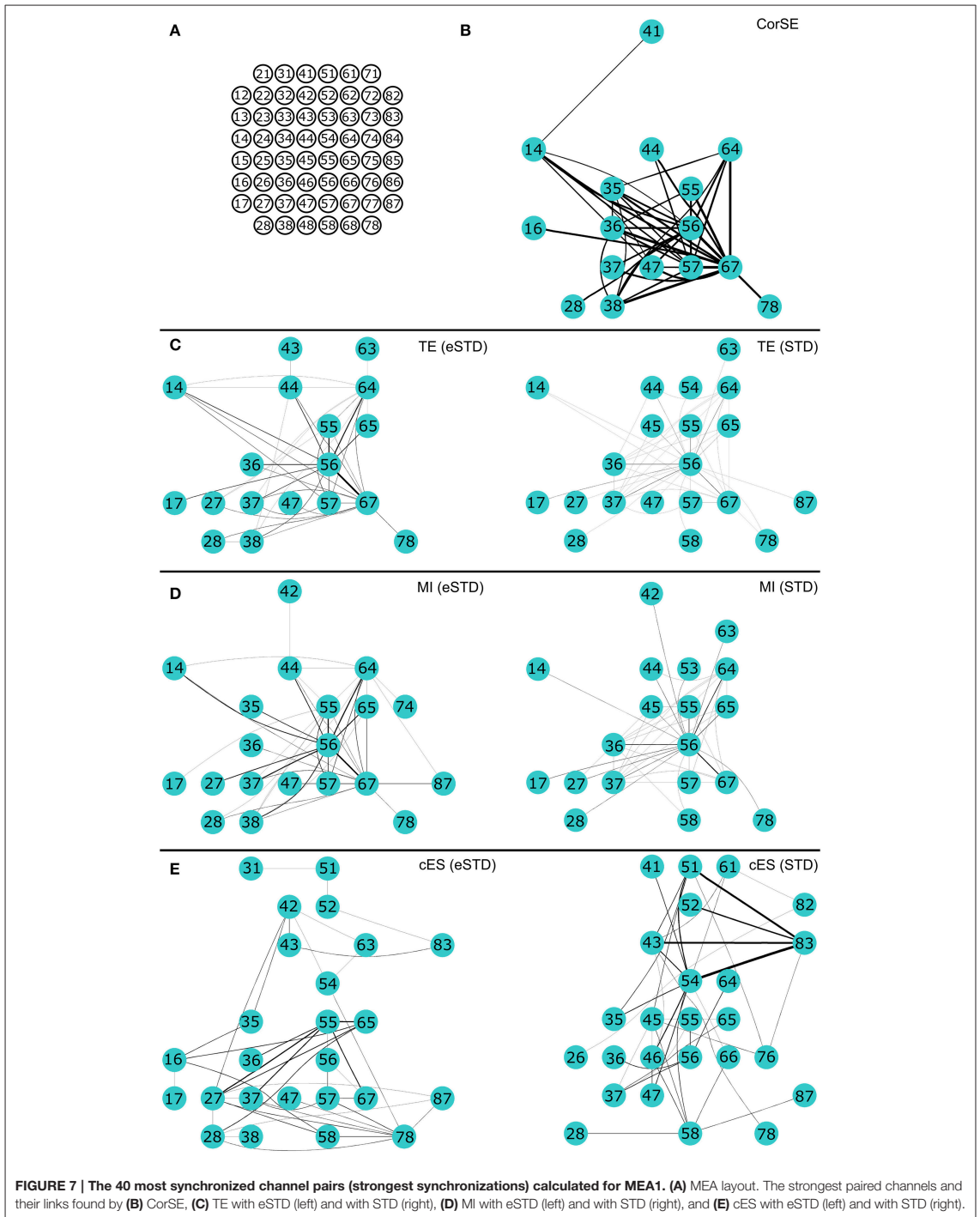
**FIGURE 4 | The synchronization results by the different algorithms for the different connectivity levels.** Left-hand panels present the synchronicities calculated for the artificial recordings by CorSE (red) and cES (blue) methods (left vertical axis), and TE (black) and MI (green) methods (right vertical axis). For the event based methods, the line types indicate the spike detection method used: STD (solid), and eSTD (dashed). The right-hand panels show exemplary 2 s signal segments with EAPs (orange), and LFP or WGN (blue) signal components. The left-hand panels: **(A)** Synchronicities calculated from the artificial recordings with only EAPs. **(B)** The synchronicities calculated from the artificial recordings with both EAPs and LFPs with  $P_{EAPs/LFPs} \approx 50\%$  for one population and  $P_{EAPs/LFPs} \approx 20\%$  for the other. **(C)** Synchronicities calculated from the artificial recordings with both EAPs and LFPs with  $P_{EAPs/LFPs} \approx 20\%$  for both populations. **(D)** Synchronicities calculated from the artificial recordings with EAPs and added WGN with  $SNR = 50\%$ . **(E)** The synchronicities calculated from the artificial recordings with EAPs and added WGN with  $SNR = 20\%$ .

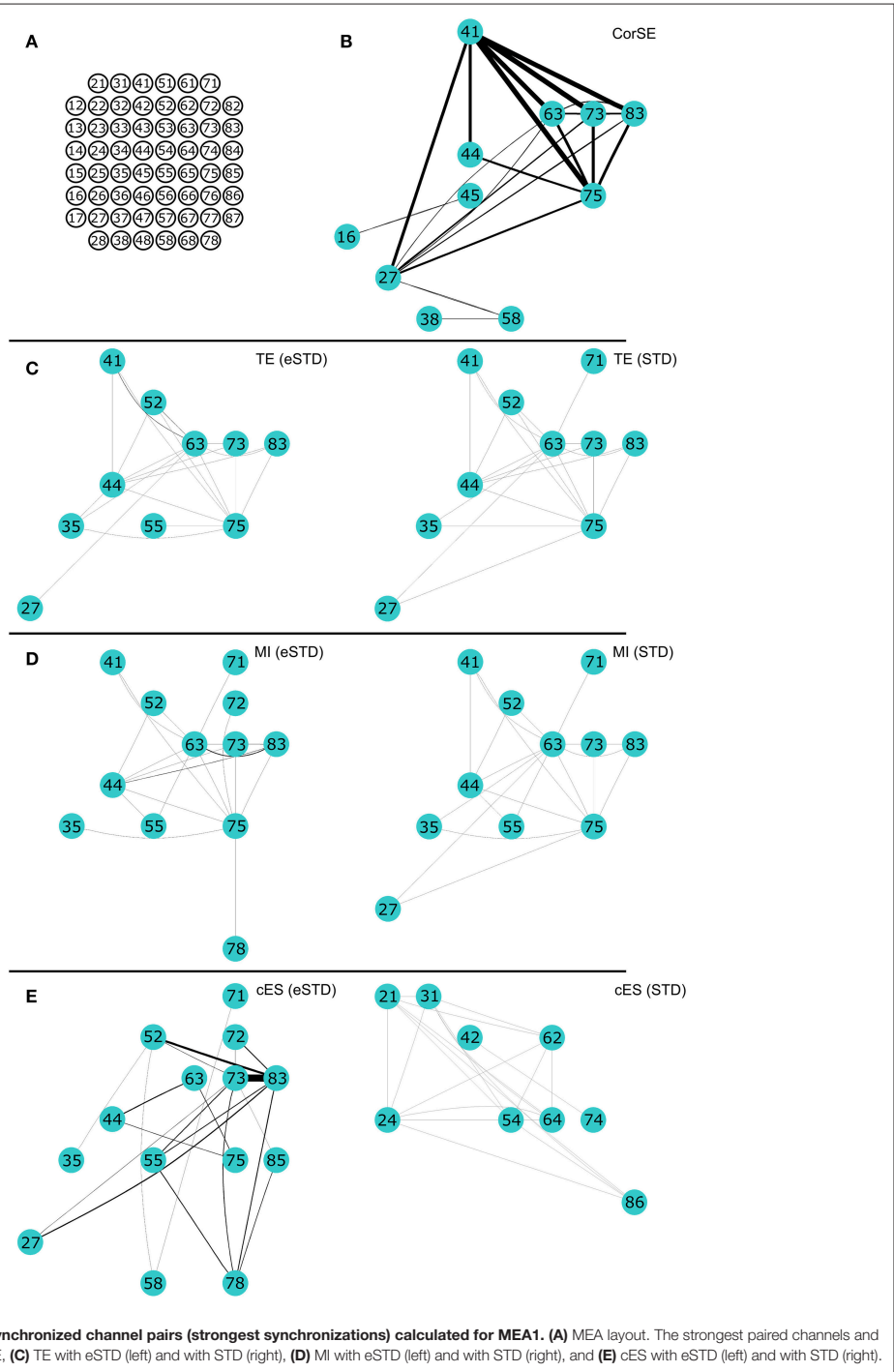


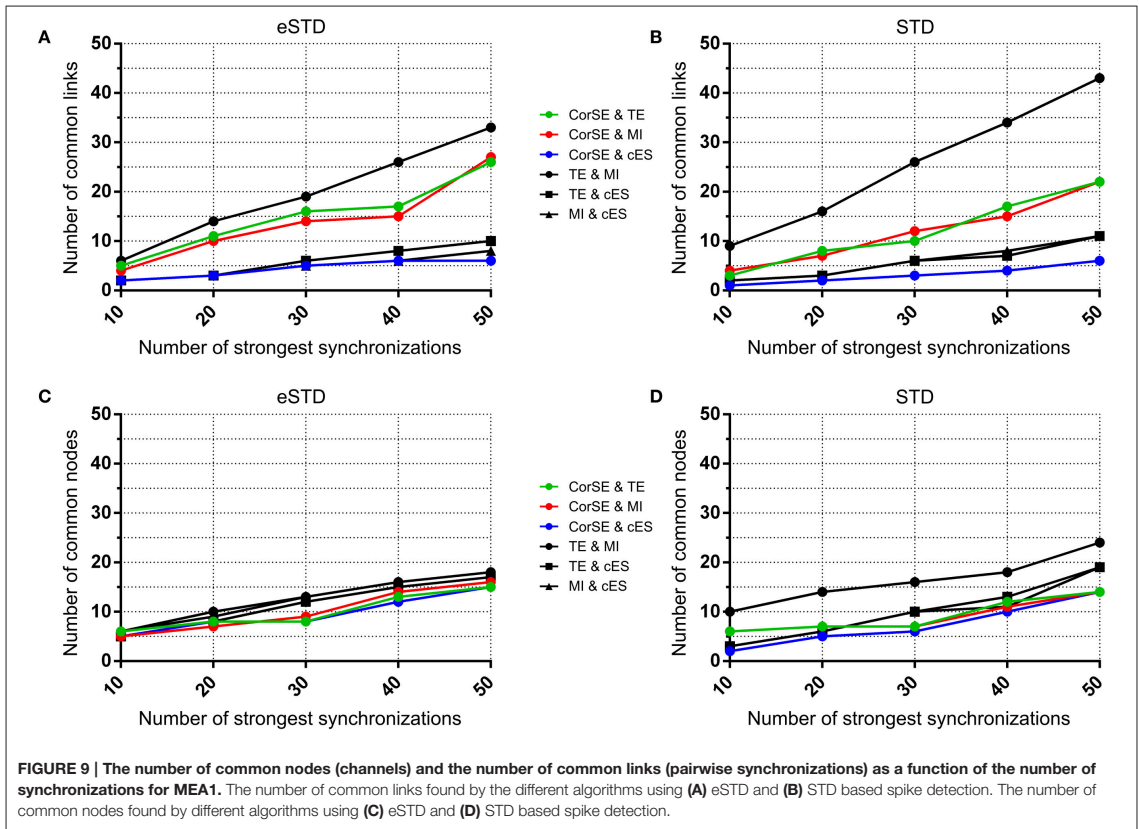
**FIGURE 5 | Adjacency matrixes of the synchronization values given by the different algorithms for MEA1. (A)** MEA layout. The synchronization values calculated with **(B)** CorSE, **(C)** TE with eSTD (left) and with STD (right), **(D)** MI with eSTD (left) and with STD (right), and **(E)** cES with eSTD (left) and with STD (right). The color scales are normalized for each matrix separately regarding to the maximum value obtained.



**FIGURE 6 | Adjacency matrixes of the synchronization values given by the different algorithms for MEA2. (A)** MEA layout. The synchronization values calculated with **(B)** CorSE, **(C)** TE with eSTD (left) and with STD (right), **(D)** MI with eSTD (left) and with STD (right), and **(E)** cES with eSTD (left) and with STD (right). The color scales are normalized for each matrix separately regarding to the maximum value obtained.





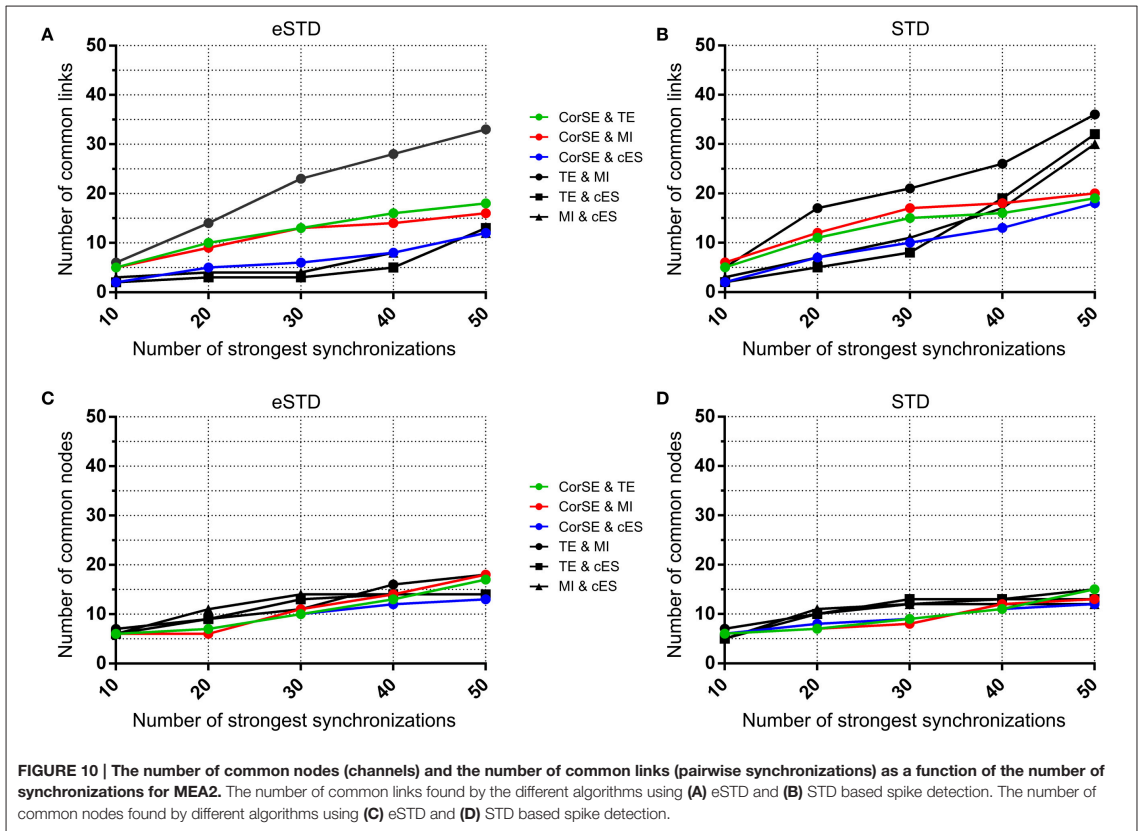


## DISCUSSION

We have previously shown the feasibility of our correlated spectral entropy method CorSE for the assessment of synchronization (Kapucu et al., 2016a). In this paper, we have not only presented the usability of the method with larger real data, but we have made simulations justifying our concept and algorithm. For that, we realized both a toy simulation and simulations based on a widely used computation neuronal network model. The results of the simulations showed that it was possible to distinguish and assess the synchronization and connectivity strengths in neuronal populations by assessing the synchronization via the time correlated complexity measure CorSE.

In practice, in addition to biological sources, many other sources contribute to the measured electrophysiological signals. Any sources of noise that are not biological, e.g., artifacts and electrical interference, might influence the results of the algorithms employed. To assess this, we also performed the simulations with additive white Gaussian noise. Increasing the level of noise naturally had a negative effect on the results, as expected. Clearly, with the increasing noise level, more

spikes were missed during spike detection, and the employed event based synchronization measures were more likely to fail. Concerning CorSE, increasing the level of noise had an effect on the uniformity of the spectral distribution, and thus on the synchronization measure. However, simulations showed that even with the increasing noise, it was still possible to distinguish between the connected and unconnected populations, even though the level of connectivity strength was not distinguishable anymore. Here, it may be noted that in all the event based synchronization assessment algorithms in the literature, anything other than detectable spikes is generally considered as biological “noise” (Obien et al., 2015), and a reasonable amount of information from LFPs is omitted. CorSE takes also LFPs into account in synchronization assessment. Thus, we observed the effects of different power ratios of EAPs and LFPs on the detected synchronization: the results showed that CorSE can assess the level of connectivity under the effects of synchronized LFPs. In contrary, since LFPs are considered as biological “noise” by the event based analysis, signals with different power ratios of EAPs and LFPs affect the spike detection accuracy, and thus the results of these algorithms.

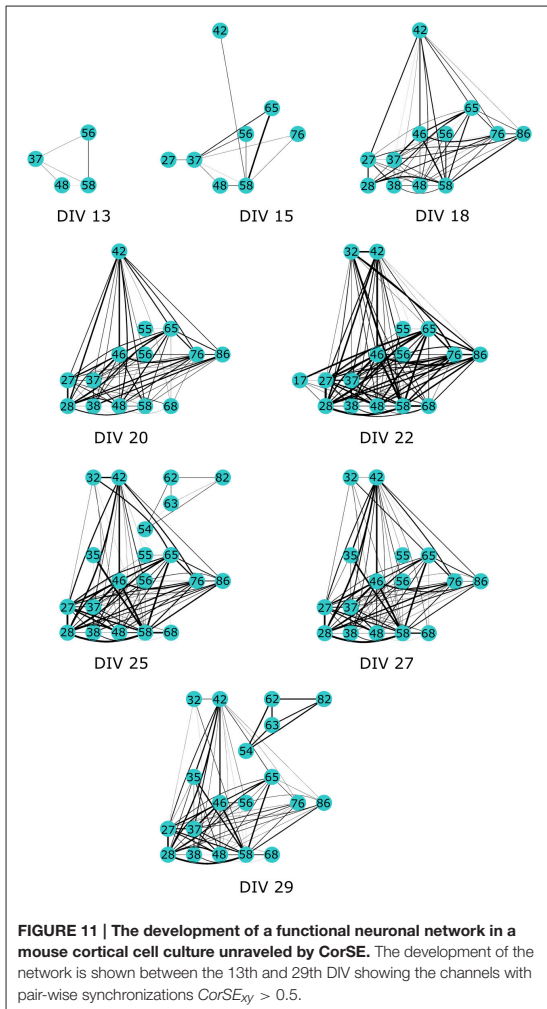


For the rat cortical cells used in this study, the mutual information and transfer entropy algorithms showed the most corroborative results, as expected, since the two methods are based on the same theoretical grounds. CorSE exhibited common findings with the mutual information and transfer entropy algorithms, but the results from the corrected event synchronization method were generally different from the results by the rest of the algorithms. Since the corrected event synchronization method is spike rate adaptive by its nature, one possible explanation could be that its results were significantly affected by spike detection.

The similarities and differences of the considered algorithms can be summarized by joint evaluation of adjacency matrices (Figures 5, 6), by observing the differences in the most synchronized MEA channel pairs (Figures 7, 8), and in the common links and nodes (Figures 9, 10): CorSE, and the mutual information and transfer entropy algorithms all found the same link as the most synchronized link for MEA1, whereas for MEA2, the same most synchronized link was found by CorSE, and the mutual information and corrected event synchronization methods. Additionally, channels which had the highest number of links (hub-channels) were identified similarly

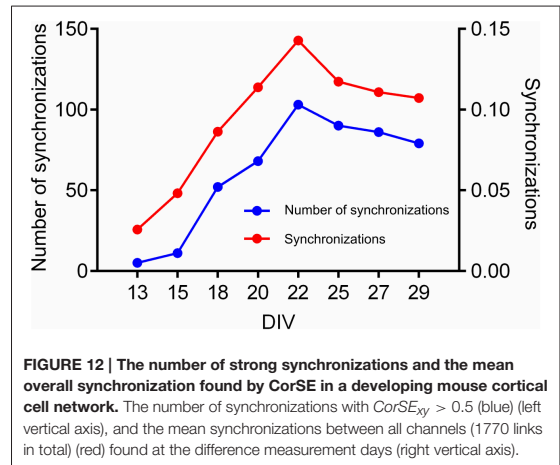
by CorSE, the mutual information and transfer entropy methods. Consequently, it may well be that the most synchronized links could be found similarly by the different algorithms employed in this work, whereas the most differences might be found in the weaker synchronized links. In fact, the numbers of common links and nodes presented in Figures 9, 10 show similar results for the strongest 10 synchronizations, whereas the difference grows with the increasing number of strongest synchronizations. It is to be noted that since we assessed unguided neuronal cells which developed freely on the MEA plates, there is no ground truth about the network structures which the cell cultures formed. Thus, actual validation of the synchronies measured by different algorithms was impossible with the real data, but has been to an extent provided by the simulations. Still, the comparisons of the findings from the real data give an idea of the general usability of the algorithm, and of its biological plausibility.

Also the feasibility of CorSE to track neuronal development by means of synchronization is studied in this paper. We tracked developing network synchronization for several measurement days using an arbitrary synchronization detection threshold, here,  $CorSE > 0.5$ . This provided a clear view to the appearance of the functional network (Figure 11), although setting such



a clear-cut threshold might have the effect of the temporary appearance and disappearance of some channels close to the detection threshold in the network development map (see **Figure 11**, 22–27 days *in vitro*). The results also correlated with the overall network synchronization behavior (**Figure 12**).

In conclusion, we have shown that CorSE is a promising tool to assess synchronization in neuronal networks. The method does not possess the shortcomings of event based methods resulting from possible poor event, e.g., spike, detection performance. Moreover, CorSE does not need specified effective frequency bands for the analysis. Our method would be useful especially for the acute analysis of possibly noisy recordings collected with MEAs for the experiments where fast processing is necessary: since it is based on the efficient fast Fourier transform and simple cross correlation, it can be used even for



online processing (Semmlow and Griffel, 2014). In fact, for more than a decade, spectral entropy has been utilized in real-time electroencephalogram monitoring to quickly assess the depth of anesthesia (Viertiö-Oja et al., 2004). We believe that methods not based on events, i.e., methods using all data recorded from the electrodes, such as CorSE, can help us in obtaining more information from the valuable neuronal network measurements, and provide robust synchrony measures, both *in vitro* and *in vivo*.

The Matlab code for CorSE has been developed to be applied straight forward on any time series data, and is publicly freely available in the Matlab Central File Exchange (<https://se.mathworks.com/matlabcentral/fileexchange/59626-spectral-entropy-based-neuronal-network-synchronization-analysis-corse>).

## AUTHOR CONTRIBUTIONS

FK developed the method, implemented the program code, designed and made the simulations, contributed to the culturing of mouse cortical cells, analyzed the data, and wrote the manuscript. IV made the computational neuronal network simulations, contributed to culturing of mouse cortical cells, and to the writing of the manuscript. JM cultured rat cortical cells, collected the data, and contributed to writing of the manuscript. CL contributed to method development and implementation. KL contributed to culturing of mouse cortical cells and writing of manuscript. JT contributed to method development and to the writing of the manuscript. JH contributed to method development and to the writing of the manuscript. All the authors approved the final version to be published.

## FUNDING

The work of FK has been supported by the 3DNeuroN project in the European Union’s Seventh Framework Programme, Future and Emerging Technologies, grant agreement no. 296590; by the

Academy of Finland under the project Bio-integrated Software Development for Adaptive Sensor Networks, project number 278882; by the Human Spare Parts Project funded by Tekes—The Finnish Funding Agency for Innovation; and by the Ella and Georg Ehrnrooth Foundation, Finland. The work of IV has been supported by the 3DNeuroN project in the European Union's Seventh Framework Programme, Future and Emerging Technologies, grant agreement no. 296590; by the Human Spare Parts Project funded by Tekes—The Finnish Funding Agency for Innovation; and by the Jane and Aatos Erkkö Foundation, Finland, under the project Biological Neuronal

Communications and Computing with ICT. The work of KL has been supported by the 3DNeuroN project in the European Union's Seventh Framework Programme, Future and Emerging Technologies, grant agreement no. 296590, and by the Human Spare Parts Project funded by Tekes—The Finnish Funding Agency for Innovation. The work of JT has been supported by the 3DNeuroN project in the European Union's Seventh Framework Programme, Future and Emerging Technologies, grant agreement no. 296590; and by the Jane and Aatos Erkkö Foundation, Finland, under the project Biological Neuronal Communications and Computing with ICT.

## REFERENCES

- Bastos, A. M., and Schoffelen, J.-M. (2016). A tutorial review of functional connectivity analysis methods and their interpretational pitfalls. *Front. Syst. Neurosci.* 9:75. doi: 10.3389/fnsys.2015.00175
- Battaglia, D., Witt, A., Wolf, F., and Geisel, T. (2012). Dynamic effective connectivity of inter-areal brain circuits. *PLoS Comput. Biol.* 8:e1002438. doi: 10.1371/journal.pcbi.1002438
- Blanche, T. J., and Swindale, N. V. (2006). Nyquist interpolation improves neuron yield in multiunit recordings. *J. Neurosci. Methods* 155, 81–91. doi: 10.1016/j.jneumeth.2005.12.031
- Brown, E. N., Kass, R. E., and Mitra, P. P. (2004). Multiple neural spike train data analysis: state-of-the-art and future challenges. *Nat. Neurosci.* 7, 456–461. doi: 10.1038/nn1228
- Buehlmann, A., and Deco, G. (2010). Optimal information transfer in the cortex through synchronization. *PLoS Comput. Biol.* 16:e1000934. doi: 10.1371/journal.pcbi.1000934
- Buzsáki, G., Anastassiou, C. A., and Koch, C. (2012). The origin of extracellular fields and currents—EEG, ECoG, LFP and spikes. *Nat. Rev. Neurosci.* 13, 407–420. doi: 10.1038/nrn3241
- Buzsáki, G., and Chrobak, J. J. (1995). Temporal structure in spatially organized neuronal ensembles: a role for interneuronal networks. *Curr. Opin. Neurobiol.* 5, 504–510. doi: 10.1016/0959-4388(95)80012-3
- Buzsáki, G., and Draguhn, A. (2004). Neuronal oscillations in cortical networks. *Science* 304, 1926–1929. doi: 10.1126/science.1099745
- Chatfield, C. (2003). *The Analysis of Time Series: An Introduction*. Boca Raton, FL: Chapman and Hall/CRC Press.
- Chawla, D., Lumer, E. D., and Friston, K. J. (1999). The relationship between synchronization among neuronal populations and their mean activity levels. *Neural Comput.* 11, 1389–1411. doi: 10.1162/089976699300016287
- Egert, U., Schlosshauer, B., Fennrich, S., Nisch, W., Fejt, M., Knott, T., et al. (1998). A novel organotypic long-term culture of the rat hippocampus on substrate-integrated multielectrode arrays. *Brain Res. Protocols* 2, 229–242. doi: 10.1016/S1385-299X(98)00013-0
- Garofalo, M., Nieuws, T., Massobrio, P., and Martinoia, S. (2009). Evaluation of the performance of information theory-based methods and cross-correlation to estimate the functional connectivity in cortical networks. *PLoS ONE* 4:e6482. doi: 10.1371/journal.pone.0006482
- Gewaltig, M.-O., and Diesmann, M. (2007). NEST (NEural Simulation Tool). *Scholarpedia* 2, 1430. doi: 10.4249/scholarpedia.1430
- Ginter, J. Jr., Blinowska, K. J., Kamin, M., Durka, P. J., Pfurtscheller, G., and Neuper, C. (2005). Propagation of EEG activity in the beta and gamma band during movement imagination in humans. *Methods Inf. Med.* 44, 106–113.
- Gray, R. M. (1990). *Entropy and Information Theory*. New York, NY: Springer.
- Gross, G. W., Rieske, E., Kreuzberg, G. W., and Meyer, A. (1977). A new fixed-array multi-microelectrode system designed for long-term monitoring of extracellular single unit neuronal activity *in vitro*. *Neurosci. Lett.* 6, 101–105. doi: 10.1016/0304-3940(77)90003-9
- Ito, S., Hansen, M. E., Heiland, R., Lumsdaine, A., Litke, A. M., and Beggs, J. M. (2011). Extending transfer entropy improves identification of effective connectivity in a spiking cortical network model. *PLoS ONE* 6:e27431. doi: 10.1371/journal.pone.0027431
- Jarvis, M. R., and Mitra, P. P. (2001). Sampling properties of the spectrum and coherency of sequences of action potentials. *Neural Comput.* 13, 717–749. doi: 10.1162/089976601300014312
- Kapucu, F. E., Mäkinen, M. E. L., Tanskanen, J. M. A., Ylä-Outinen, L., Narkilahti, S., and Hyttinen, J. A. K. (2016b). Joint analysis of extracellular spike waveforms and neuronal network bursts. *J. Neurosci. Methods* 259, 143–155. doi: 10.1016/j.jneumeth.2015.11.022
- Kapucu, F. E., Mikkonen, J. E., Tanskanen, J. M. A., and Hyttinen, J. A. K. (2015). “Quantification and automatized detection of *in vivo* and *in vitro* neuronal bursts based on signal complexity,” in *2015 37th Annual International Conference of the IEEE Engineering in Medicine and Biology Society (EMBC)* (Milan), 4729–4732.
- Kapucu, F. E., Mikkonen, J. E., Tanskanen, J. M. A., and Hyttinen, J. A. K. (2016a). “Analyzing the feasibility of time correlated spectral entropy for the assessment of neuronal synchrony,” in *2016 38th Annual International Conference of the IEEE Engineering in Medicine and Biology Society (EMBC)* (Orlando, FL).
- Kapucu, F. E., Tanskanen, J. M. A., Mikkonen, J. E., Ylä-Outinen, L., Narkilahti, S., and Hyttinen, J. A. K. (2012). Burst analysis tool for developing neuronal networks exhibiting highly varying action potential dynamics. *Front. Comput. Neurosci.* 6:38. doi: 10.3389/fncom.2012.00038
- Mack, C. M., Lin, B. J., Turner, J. D., Johnstone, A. F., Burgoon, L. D., and Shafer, T. J. (2014). Burst and principal components analyses of MEA data for 16 chemicals describe at least three effects classes. *Neurotoxicology* 40, 75–85. doi: 10.1016/j.neuro.2013.11.008
- Montgomery E. B. Jr. (2014). *Intraoperative Neurophysiological Monitoring for Deep Brain Stimulation: Principles, Practice and Cases*. New York, NY: Oxford University Press.
- Nawrot, M., Aertsen, A., and Rotter, S. (1999). Single-trial estimation of neuronal firing rates: from single-neuron spike trains to population activity. *J. Neurosci. Methods* 94, 81–92. doi: 10.1016/S0165-0270(99)00127-2
- Obien, M. E. J., Deligkaris, K., Bullmann, T., Bakkum, D. J., and Frey, U. (2015). Revealing neuronal function through microelectrode array recordings. *Front. Neurosci.* 8:423. doi:10.3389/fnins.2014.00423
- Penttonen, M., and Buzsáki, G. (2003). Natural logarithmic relationship between brain oscillators. *Thalamus Relat. Syst.* 2, 145–152. doi: 10.1016/S1472-9288(03)00007-4
- Pine, J. (1980). Recording action potentials from cultured neurons with extracellular microcircuit electrodes. *J. Neurosci. Methods* 2, 19–31. doi: 10.1016/0165-0270(80)90042-4
- Quiroga, R. Q., Kreuz, T., and Grassberger, P. (2002). Event synchronization: a simple and fast method to measure synchronicity and time delay patterns. *Phys. Rev. E* 66:041904. doi: 10.1103/PhysRevE.66.041904
- Quiroga, R. Q., Nadasdy, Z., and Ben-Shaul, Y. (2004). Unsupervised spike detection and sorting with wavelets and superparamagnetic clustering. *Neural Comput.* 16, 1661–1687. doi: 10.1162/089976604774201631
- Salazar, R. F., Dotson, N. M., Bressler, S. L., and Gray, C. M. (2012). Content-specific fronto-parietal synchronization during visual working memory. *Science* 3, 1097–1100. doi: 10.1126/science.1224000
- Salinas, E., and Sejnowski, T. J. (2001). Correlated neuronal activity and the flow of neural information. *Nat. Rev. Neurosci.* 2, 539–550. doi: 10.1038/35086012
- Schreiber, T. (2000). Measuring information transfer. *Phys. Rev. Lett.* 85, 461–464. doi: 10.1103/PhysRevLett.85.461

- Semmlow, J. L., and Griffel, B. (2014). *Biosignal and Medical Image Processing*. Boca Raton, FL: CRC press.
- Shannon, C. E. (1948). A mathematical theory of communication. *Bell Syst. Tech. J.* 27, 379–423. doi: 10.1002/j.1538-7305.1948.tb01338.x
- Thomas, C. A. Jr., Springer, P. A., Loeb, G. E., Berwald-Netter, Y., and Okun, L. M. (1972). A miniature microelectrode array to monitor the bioelectric activity of cultured cells. *Exp. Cell Res.* 74, 61–66. doi: 10.1016/0014-4827(72)90481-8
- Tsodyks, M., Uziel, A., and Markram, H. (2000). Synchrony generation in recurrent networks with frequency-dependent synapses. *J. Neurosci.* 20, RC50.
- Viertiö-Oja, H., Maja, V., Särkelä, M., Talja, P., Tenkanen, N., Tolvanen-Laakso, H., et al. (2004). Description of the Entropy<sup>TM</sup> algorithm as applied in the Datex-Ohmeda S/5<sup>TM</sup> Entropy Module. *Acta Anaesthesiol. Scand.* 48, 154–161. doi: 10.1111/j.0001-5172.2004.00322.x
- Wagenaar, D. A., Pine, J., and Potter, S. M. (2006). An extremely rich repertoire of bursting patterns during the development of cortical cultures. *BMC Neurosci.* 7:11. doi: 10.1186/1471-2202-7-11
- Weihberger, O., Okujeni, S., Mikkonen, J. E., and Egert, U. (2013). Quantitative examination of stimulus-response relations in cortical networks *in vitro*. *J. Neurophysiol.* 109, 1764–1774. doi: 10.1152/jn.00481.2012

**Conflict of Interest Statement:** The authors declare that the research was conducted in the absence of any commercial or financial relationships that could be construed as a potential conflict of interest.

Copyright © 2016 Kapucu, Vätkki, Mikkonen, Leone, Lenk, Tanskanen and Hyttinen. This is an open-access article distributed under the terms of the Creative Commons Attribution License (CC BY). The use, distribution or reproduction in other forums is permitted, provided the original author(s) or licensor are credited and that the original publication in this journal is cited, in accordance with accepted academic practice. No use, distribution or reproduction is permitted which does not comply with these terms.

Tampereen teknillinen yliopisto  
PL 527  
33101 Tampere

Tampere University of Technology  
P.O.B. 527  
FI-33101 Tampere, Finland

ISBN 978-952-15-3857-5  
ISSN 1459-2045